Scuola Superiore Meridionale
University of Naples Federico II

Doctoral Thesis
in Cosmology, Space Science & Space Technology

Quantum Communication in Cosmological Settings: Theoretical and Phenomenological Implications

Internal Supervisor:
Prof. Salvatore Capozziello

Author:
Alessio Lapponi

External Supervisors:
Profs. Orlando Luongo and Stefano Mancini

Submitted in fulfilment of the requirements for the degree of Doctor of Philosophy in Cosmology, Space Science & Space Technology.
Coordinator: Prof. Salvatore Capozziello.

December 2025

Abstract

The application of gravitational physics to quantum information theory offers a promising framework for addressing some of the most profound open questions in modern science. This thesis investigates how gravity influences quantum systems through the lens of quantum communication protocols, and how these effects can, in turn, be exploited to face open challenges in cosmology and general relativity.

By using both a semiclassical and a quantum theory of gravity, two communication protocols are developed and analyzed in a variety of relativistic and cosmological settings. The first involves the transmission of quantum and classical information via well-defined single-mode bosonic channels, where gravitational curvature and expansion act as sources of signal degradation. The second protocol employs localized quantum detectors - effectively, quantum antennas - revealing how gravitational and cosmological effects can enhance, rather than hinder, information exchange.

These studies demonstrate that quantum communication provides a concrete operational tool to investigate fundamental gravitational phenomena such as cosmological particle production, curvature coupling, and even self-gravitational decoherence. Beside that, the results suggest that information loss and signal fidelity can serve as sensitive indicators of spacetime properties, giving the opportunity to experimental test gravitational features via quantum information protocols.

Acknowledgements

First of all, I'd like to thank the PhD coordinator and supervisor Prof. Salvatore Capozziello for guiding me not only scientifically speaking, but also through the opportunities that the Scuola Superiore Meridionale gave me.

Secondly, my main mentors, Prof. Orlando Luongo and Prof. Stefano Mancini from the University of Camerino, who always sustained me since I was applying for the PhD program, and who made me fall in love with the world of Cosmology and Quantum Information.

A special acknowledgement to the Scuola Superiore Meridionale, which allowed me to travel around all the parts of the world, giving me new experiences, friends and collaborators during conferences and period abroads. Among them, a special thank to David Edward Bruschi - collaborator, friend and Wegweiser zu Schnitzel, Brezeln und Bier in den kalten Landen Deutschlands. Beside him, I thank Prof. Jorma Louko and the rest of the Gravity Laboratory Group (the best research group ever) for gifting me an amazing period abroad in UK.

My acknowledgements also extend to my family (or whatever is left of it), which allowed me to study in the first place. I hope you can be proud of me despite my future chosen path.

Last but not least, my PhD collegues - with whom I'm sure we will stay in contact forever, my dear Universitary friends in Camerino - who accompanied and sustained me over the first 2 years of this route - all the ESN people in Naples and finally, my future wife Carolina, who supported and tolerated me during the writing of this thesis.

It was a pleasure to share these years with you. I wish you the best.

I take the opportunity to dedicate this thesis to my father and wish him good luck for the battle he faces everyday. Don't give up, you are a warrior!

Contents

Chapter 1

Introduction

General Relativity currently stands as the most successful and comprehensive description of gravitation [1, 2]. From it, gravity is described as the dynamics of spacetime geometry, encoded in Einstein's field equations [3]. With these premises, General Relativity has passed precision tests from solar-system scales to strong-field observations (light deflection, perihelion precession, gravitational waves and black-hole imaging) [4]. The application of General Relativity to our Universe is also known as *cosmology*, describing the hot Big Bang, the formation of large-scale structures (e.g. galaxies) and the measured expansion history [5, 6, 7].

Despite these successes, many mysteries and open problems remain in gravitation and cosmology. Current observations require the dominant presence of unseen components, such as *dark matter*, to explain galactic dynamics and *dark energy*, to account for accelerated expansions [8, 7, 9]. Beside particle physics candidates [10, 11], proposed solutions involve modifications of General Relativity on cosmological scales [12, 13, 14, 15, 16] or the presence of more complete and alternative and realistic cosmological fluids for dark energy [17, 18, 19]. However, testing these solutions is notoriously hard [20, 21]. In fact, alternative theories must be consistent with local observations (i.e. in the Solar System). In this way, eventual departures from General Relativity prediction are often too small to be detected with actual means or present into currently not-achievable energy regimes [22].

The most fundamental conceptual tension, however, is on the incompatibility with quantum mechanics, whose validity was corroborated in microscopic scales (i.e. atomic scales and below) [23]. This problem led scientists to also question about the nature or gravity itself - i.e. if it can be described by a classical field (following General Relativity), or rather if this field is quantized in microscopic scales. Many attempts were done so far to provide a consistent *quantum gravity theory*, recovering General Relativity in the macroscopic world [24, 25, 26, 27].

As a first step in this direction, *Quantum field theory in curved spacetime* explores quantum systems in presence of an external classical gravitational field [28, 29]. The theoretical predictions of this theory are outstanding, challenging the concept of quantum particle itself and bringing up unitarity problems on the evolution of macroscopic objects [30, 31]. Many attempts were done to test the predictions of quantum field theory in curved spacetime, leading to their confirmation in analog gravity systems [32, 33, 34]. Despite this, a direct observation of these phenomena by actually gravitating systems is compromised because of utterly small effects [35], usually covered by background radiation [36]. Effective field theories involving quantum gravity, such *linearized* *quantum gravity*, have the same observational problem despite the intriguing theoretical predictions [37, 38].

A recent approach to test these effects, relying on the use of quantum information tools - such as entanglement, metrology and information protocols, is called *relativistic quantum information* [39, 40]. In particular, this field studies how motion, acceleration and spacetime curvature affect quantum correlations and information flow [41, 42]. Several operational probes (detectors, channels, communication/estimation protocols) which can both reveal and exploit relativistic quantum effects, were proposed so far [43, 44, 45, 46]. This approach offers a concrete and operational way to probe particle production [47], decoherence induced by horizons/curvature [48], and possible signatures of new gravitational physics [49].

Within the quantum information framework, *quantum communication* provides the natural setting to explore how quantum information can be transmitted, encoded and preserved across space and time. By exploiting non-classical resources such as entanglement and quantum coherence, communication schemes allow distant parties to exchange information in ways that outperform any classical protocol [50, 51, 52]. The study of how such channels behave under relativistic motion or gravitational fields thus offers an operational route to probe the interplay between quantum mechanics and spacetime structure [42, 41, 53].

In line with this view, the study of quantum communication schemes in relativistic contexts could not only be used to test the gravitational physics, but also to predict eventual noisy effects or amplifications of quantum signals due to gravity, which can be used in future space and quantum technologies. To this perspective, quantum communication (and, more generally, quantum networks) has matured considerably in the past two decades, from theoretical proposals to experimental platforms [54, 55]. In the terrestrial setting, for example, a recent experiment demonstrated entanglement distribution and teleportation over a 14.4 Km dark-fiber urban link [56]. However, many factors still provide major technological constraints towards long-distance quantum networks [54] (e.g. fiber loss, phase drift, coupling inefficiencies and the no-cloning theorem limiting classical amplification).

To face these limitations on terrestrial links, space-based quantum communication has to scale up quantum networks globally. Early space experiments have already demonstrated feasibility: the Micius satellite performed satellite-to-ground Quantum Key Distribution and entanglement distribution over distances of thousands of Kilometers [57, 58]; micro-satellite experiments have successfully transmitted polarization-encoded qubits from a 50 kg LEO satellite down to Earth with acceptable quantum bit error rates [59].

To build reliable and testable quantum communication in space settings, it is necessary to study how the information stored in quantum systems is modified by relativistic effects. In so doing, one may predict eventual noisy effects and/or find ways to exploit gravity to enhance the quality of communication protocols. The main purpose of this thesis is precisely to investigate this aspects, while also assessing the possibility to test the currently unknown features of gravitational physics via quantum communication protocols. A secondary objective has a more theoretical foundation, relying on knowing how quantum states behave in presence of gravity in a more complete, general and operational way. Moreover, when possible, application in space technology are addressed as well. In this framework, the research aims to know whether a space-based quantum communication protocol can increase or decrease its communication capabilities, due to gravitational effects.

To achieve these objectives, two protocols are analyzed in details and applied in a plethora of iconic and useful relativistic scenarios: the first one involves the communication of a single-mode bosonic state, emulating uni-directional signals lacking of information loss over long distances; the second involves the communication between a pair localized quantum systems, interacting uniformly and isotropically with its surroundings.

The ability of these protocols to amplify the small effects of gravity in quantum systems is demonstrated in several contexts. This opens the possibility to: i) detect the particles produced in a cosmological expansion [60] or from a black hole [61]; ii) test the value of the coupling between curvature and scalar field [28]; iii) test gravity modifications [13]; iv) probe cosmological fluids proposed as alternatives to dark energy [62]; v) investigate the nature of gravity itself [37].

A secondary objective has a more theoretical foundation, knowing how quantum systems behaves in presence of gravitational field in a more general and operational way.

Beside those operational applications, the results obtained also provide many theoretical implications. Gravitational effects are always found to provide noisy contributions in the communication of unidirectional signals. However, this is no longer true when the communication is performed via quantum antennas: in this case, the quality of communication of classical information is proved to be enhanced by a cosmological expansion. Furthermore, the limits of those antennas to communicate quantum information reliably is addressed by using the no-cloning theorem. In so doing, highly anisotropic situations turn out to be the only ones which may allow a reliable quantum key distribution. Finally, a mechanism inducing a self-gravitational decoherence is discovered in quantum gravity context, which becomes more "testable" when recast to the loss of quantum information in a protocol.

The structure of the thesis is the following.

- Chapter 2 introduces the theoretical foundations where the protocols are applied - i.e. quantum field theory in curved spacetime and linearized quantum gravity. This chapter surveys the most relevant phenomena predicted by those theories - cosmological particle production [60], Hawking radiation [61], dynamical Casimir effect [63], Unruh effect [35] - providing the background needed for later chapters. Without being intended as a comprehensive review, it also introduces elements of General Relativity and modern cosmology required for the application studied in this thesis.

- Chapter 3 presents the first of the two protocols under consideration. After reviewing key tools from quantum information theory - particularly *continuous-variable quantum communication theory* - the chapter analyzes a protocol based on the communication of particles with well-defined momentum in a specific direction. In other words, the focus here is on the preservation of classical and quantum information stored into single-mode bosons. While these particle perfectly preserve information in special relativity setups, some gravitational features may disrupt this perfect conservation. Despite challenges associated with causality and the uncertainty principle, this protocol remains physically realistic if the two parts communicate over large distances and time intervals, and it provides simple and intuitive results.

- In Chapter 4 turns to more realistic scenarios involving spatially localized senders and receivers. The investigation here focuses both on the communication between distant parts and on the conservation of localized information in time. In this last scenario, by using a superposition of two different localizations, decoherence is proved also in absence of any source of gravity.

- Chapter 5 summarizes the main results and highlights the future directions of this research.

Throughout the thesis, the signature $(-,+,+,+)$ is used. Regarding the units, the reduced Planck one $c=\hbar=k_{\mathrm{B}}=8\pi G=1$ are mostly considered, unless otherwise specified.

List of papers this thesis is based on

- [P1] Michael R. R. Good, Alessio Lapponi, Orlando Luongo, and Stefano Mancini. Quantum communication through a partially reflecting accelerating mirror. *Physical Review D*, 104(10), November 2021.
- [P2] Salvatore Capozziello, Rocco D'Agostino, Alessio Lapponi, and Orlando Luongo. Black hole thermodynamics from logotropic fluids. *The European Physical Journal C*, 83(2), February 2023.
- [P3] Michael R. R. Good, Alessio Lapponi, Orlando Luongo, and Stefano Mancini. Modeling black hole evaporative mass evolution via radiation from moving mirrors. *Physical Review D*, 107(10), May 2023.
- [P4] Alessio Lapponi, Dimitris Moustos, David Edward Bruschi, and Stefano Mancini. Relativistic quantum communication between harmonic oscillator detectors. *Physical Review D*, 107(12), June 2023.
- [P5] Alessio Lapponi, Jorma Louko, and Stefano Mancini. Making two particle detectors in flat spacetime communicate quantumly. *Physical Review D*, 110(2), July 2024.
- [P6] Salvatore Capozziello, Alessio Lapponi, Orlando Luongo, and Stefano Mancini. Preserving quantum information in $f(Q)$ non-metric gravity cosmology. *The European Physical Journal C*, 84(10), October 2024.
- [P7] Alessio Lapponi, Orlando Luongo, and Stefano Mancini. How cosmological expansion affects communication between distant quantum systems. *Phys. Rev. D*, 111:044040, Feb 2025.
- [P8] Alessio Lapponi, Alessandro Ferreri, and David Edward Bruschi. Gravitational redshift via quantized linear gravity, 2025. *arXiv:2504.03956*
- [P9] Alessio Lapponi, David Edward Bruschi, Stefano Mancini and Frank Wilhelm-Mauch. Self-gravity affects quantum states. *Soon in arXiv*.

Chapter 2

Quantum field theory in curved spacetime and perturbative gravity

Contents

The following chapter wants to introduce the physics background where the thesis research is developed. Wondering how information travels in relativistic setups, a description of how gravitational fields may affect the behaviour of quantum particles - according to quantum field theory - is here provided. To do that, two physical theories are mainly used, i.e. *Quantum field theory in curved spacetime* and *Linearized quantum gravity*.

Despite some common qualities, the two theories have a fundamental difference relying on the nature of gravity. In fact, in quantum field in curved spacetime, gravity is considered *classical* - i.e. non-quantum. Therefore, according to *General Relativity* [3, 4] a gravitational field manifests itself as the curvature of the background spacetime. The theory is then focused on the behaviour of quantum particles in the spacetime curved by gravitational effects [28, 29].

On the contrary, linearized quantum gravity considers gravity to have a *quantum* nature [37, 38]. The gravitational field is quantized as the other quantum fields. The quantum particles - i.e. the field excitations - are then traveling in a flat spacetime but interacting with the gravitational field quanta - called *gravitons*.

Only the information relevant to develop the results of this thesis are here resumed. Interested readers could refer to [28, 31] for a complete description of quantum field theory in curved spacetime, and to [37] for the linearized quantum gravity theory.

The chapter is structured as follows, Sec. 2.1 introduces quantum field theory in curved spacetime and the possibility to produce particles from vacuum. As a first application of this theory, in Sec. 2.2 the creation of particle given by the expansion of the universe is discussed. The most studied phenomenon arising from quantum field theory in curved spacetime, i.e. Hawking radiation, is instead discussed in Sec. 2.3, where the dynamical Casimir effect and the thermodynamics of black holes are discussed as well. Unruh effect is briefly described in Sec. 2.4, with the purpose of introducing Unruh-deWitt detectors and localized quantum systems. Finally, in Sec. 2.5, a brief description of linearized quantum gravity is provided.

2.1 Quantum field theory in curved spacetime

The behaviour of quantum particles in special relativity is fully described by *quantum field theory* [64, 65]. The key concept of it stands on particles considered as excitations of a field, which is properly quantized to become an operator.

2.1.1 The case of a flat spacetime

The theory of quantum fields is briefly sketched in a flat, Minkowski spacetime, characterized by the metric tensor $\eta_{\mu\nu} = \mathrm{diag}(-1, 1, 1, 1)$. For the sake of simplicity, the behaviour of a non-interacting scalar particle - characterized by its mass m - is addressed. This particle can be considered as an excitation of a scalar field $\Phi(\mathbf{x}, t)$ whose Lagrangian density reads[1]

$$\mathcal{L}_\Phi = -\frac{1}{2}\partial^\mu\Phi\partial_\mu\Phi - \frac{m^2}{2}\Phi^2\,, \tag{2.1}$$

leading to the Klein-Gordon equation

$$(\Box - m^2)\Phi(\mathbf{x}, t) = 0\,, \tag{2.2}$$

where $\Box$ is the D'Alembert operator, equivalent to $\eta_{\mu\nu}\partial^\mu\partial^\nu$ in a Minkowski background. The field Φ can be promoted to an operator $\hat{\Phi}$. From canonical quantization [64] $\hat{\Phi}$ can be written as

$$\hat{\Phi}(\mathbf{x}, t) = \int \mathrm{d}\mathbf{k}\left(\hat{a}_\mathbf{k} u_\mathbf{k}(\mathbf{x}, t) + \hat{a}^\dagger_\mathbf{k} u^*_\mathbf{k}(\mathbf{x}, t)\right)\,, \tag{2.3}$$

where $\hat{a}_\mathbf{k}$ is the annihilation operator relative to a scalar particle with momentum $\mathbf{k}$, satisfying the algebra

$$\left[\hat{a}_\mathbf{k}, \hat{a}^\dagger_{\mathbf{k}'}\right] = \delta^3(\mathbf{k} - \mathbf{k}')\,; \quad [\hat{a}_\mathbf{k}, \hat{a}_{\mathbf{k}'}] = 0\,. \tag{2.4}$$

The functions $u_\mathbf{k}$ in Eq. (2.3) are called *normal modes* of the scalar field. They represent the *positive frequency solutions* of the Klein-Gordon equation $(\Box - m^2)u_\mathbf{k} = 0$ normalized so that

[1] Notice that the minus in the first term on the r.h.s. of Eq. (2.1) is due to the choice of the metric signature and not due to the presence of ghost fields.

$(u_{\mathbf{k}}, u_{\mathbf{k}'})_{\mathrm{KG}} = \delta^{(3)}(\mathbf{k}-\mathbf{k}')$ according to the scalar product $(\dots,\dots)_{\mathrm{KG}}$, reading

$$(u_{\mathbf{k}}, u_{\mathbf{k}'})_{\mathrm{KG}} \coloneqq -i\int_{\Sigma_t} d\mathbf{x}\,(u_{\mathbf{k}}(\mathbf{x},t)\partial_t u^*_{\mathbf{k}'}(\mathbf{x},t) - u^*_{\mathbf{k}'}(\mathbf{x},t)\partial_t u_{\mathbf{k}}(\mathbf{x},t))\ , \tag{2.5}$$

where Σ_t is the Cauchy surface $t = \text{const}$.

As $\{u_{\mathbf{k}}\}_{\mathbf{k}}$ represent the set of positive frequency solutions of the Klein-Gordon equation (2.2), $\{u^*_{\mathbf{k}}\}_{\mathbf{k}}$ represent the respective negative frequency solution. The set $\{u_{\mathbf{k}}\}_{\mathbf{k}} \cup \{u^*_{\mathbf{k}}\}_{\mathbf{k}}$ is required to be complete and orthonormal w.r.t. the scalar product (2.5). In a flat, Minkowski spacetime, the normal modes $u_{\mathbf{k}}$ can be easily calculated as

$$u_{\mathbf{k}}(\mathbf{x},t) = \frac{e^{i\mathbf{k}\cdot\mathbf{x}-i\omega_{\mathbf{k}}t}}{\sqrt{(2\pi)^3 2\omega_{\mathbf{k}}}}\,, \tag{2.6}$$

where $\omega_{\mathbf{k}} \coloneqq \sqrt{|\mathbf{k}|^2+m^2}$.

Both in a flat and in a curved spacetime, quantum fields are effective mathematical instruments to describe quantum particles. In opposition to classical particles, those particles cannot have well-defined position and momentum together, because of the uncertainty principle. This fact is well enclosed in quantum field theory. In fact, by considering a flat background and a scalar field, a field operator $\hat{\Phi}(\mathbf{x})$ effectively creates a particle at the position $\mathbf{x}$ from vacuum. However, by computing the probability amplitude that the particle at $\mathbf{x}$ has a momentum $\mathbf{k}$, from Eqs. (2.3) one gets

$$\langle 0|\,\hat{a}_{\mathbf{k}}\hat{\Phi}(\mathbf{x})\,|0\rangle = u_{\mathbf{k}}(\mathbf{x},t)\,, \tag{2.7}$$

Corresponding to the probability $P(\mathbf{k}) = \frac{N}{(2\pi)^3 2\omega_{\mathbf{k}}}$ where the normalization constant N turns out to be infinite, meaning that the momentum of the particle localized precisely at $\mathbf{x}$ is completely undefined, as expected from the Heisenberg principle.

As a consequence, to have a particle with a valid momentum distribution, one must not define the particle in a single well-defined position - i.e. a *point-like particle* - but rather assume the particle to follow a probability amplitude $f(\mathbf{x})$ for its position, called - also called *smearing function*. The field operator creating such a particle is the *smeared field operator*, reading

$$\hat{\Phi}_f(t) = \int \mathrm{d}\mathbf{x} f(\mathbf{x})\hat{\Phi}(\mathbf{x},t)\,. \tag{2.8}$$

The point-like field operator (2.3) is recovered from Eq. (2.8) when $f(\mathbf{x})$ has a delta-like form. From Eq. (2.8), one can compute the momentum probability amplitude of the smeared particle, achieving

$$\langle 0|\,\hat{a}_{\mathbf{k}}\hat{\Phi}_f(\mathbf{x})\,|0\rangle =: g(\mathbf{k}) = \frac{\tilde{f}(\mathbf{k})}{\sqrt{2\omega_{\mathbf{k}}}}\,, \tag{2.9}$$

where $\tilde{f}$ is the Fourier transform of f, for which the following convention was used

$$\tilde{f}(\mathbf{k}) = \frac{1}{(2\pi)^3}\int \mathrm{d}\mathbf{x} f(\mathbf{x}) e^{-i\mathbf{k}\cdot\mathbf{x}}\,. \tag{2.10}$$

Notice that, to describe a scalar particle, $f(\mathbf{x})$ must be real valued to make $\hat{\Phi}_f$ an Hermitian operator. As a consequence, for the momentum amplitude, one has $g(\mathbf{k}) = g^*(-\mathbf{k})$ and therefore, the smeared scalar field $\hat{\Phi}_f$ in Eq. (2.8) can be rewritten as

$$\Phi_f(t) = \int \mathrm{d}\mathbf{k}\left(g(-\mathbf{k})e^{-i\omega_{\mathbf{k}}t} + g(\mathbf{k})e^{i\omega_{\mathbf{k}}t}\right)\,. \tag{2.11}$$

2.1.2 Generalization to a curved background

The quantum field theory formalism can be generalized when the background is described by a generic metric tensor $g_{\mu\nu}$ in place of the Minkowski one $\eta_{\mu\nu} = \mathrm{diag}(-1,1,1,1)$. According to *general relativity* [3, 4], the metric $g_{\mu\nu}$ is the solution of the Einstein field equations, giving a one-on-one relation between the spacetime curvature and the distribution of matter in space and time, encoded in the stress energy tensor $T_{\mu\nu}$. In their tensorial form, the Einstein field equations can be written as

$$R_{\mu\nu} - \frac{1}{2} R g_{\mu\nu} + \Lambda g_{\mu\nu} = T_{\mu\nu}\,, \tag{2.12}$$

where $R_{\mu\nu}$ is the *Ricci curvature*, $R = R^{\mu}_{\mu}$ the *scalar curvature* and Λ the *cosmological constant*. Remarkably, Eq. (2.12) is obtained by variating the Einstein-Hilbert action S_{GR} w.r.t. the metric tensor $g_{\mu\nu}$. This object reads [66]

$$S_{\mathrm{GR}} = \frac{1}{2}\int d^4x (R - 2\Lambda)\sqrt{-g} + \int d^4x \mathcal{L}_{\mathrm{m}} \sqrt{-g}\,, \tag{2.13}$$

where $g \coloneqq \det g_{\mu\nu}$ and $\mathcal{L}_{\mathrm{m}}$ is the matter Lagrangian density scalar, related to the stress energy tensor through

$$T_{\mu\nu} = -\frac{2}{\sqrt{-g}} \frac{\delta(\sqrt{-g}\mathcal{L}_{\mathrm{m}})}{\delta g^{\mu\nu}}\,. \tag{2.14}$$

Since the scalar curvature R is in general non-null, then the possibility of its coupling with the scalar field Φ has to be taken into account. Therefore, the Lagrangian density (2.1) can be generalized to

$$\mathcal{L}_{\Phi} = -\frac{1}{2} g_{\mu\nu} \partial^{\mu}\Phi \partial^{\nu}\Phi - \frac{m^2}{2}\Phi^2 - \frac{1}{2}\xi R \Phi^2\,, \tag{2.15}$$

where ξ is a coupling constant. From Eq. (2.15), the corresponding Klein-Gordon equation can be found as

$$(\Box - m^2 - \xi R)\Phi = 0\,. \tag{2.16}$$

where the d'Alembert operator now reads $\Box = \frac{1}{\sqrt{-g}}\partial_{\mu}\left(\sqrt{-g} g^{\mu\nu}\partial_{\nu}\right)$.

At this point, the scalar field Φ can be quantized and expanded again as in Eq. (2.3), being $u_{\mathbf{k}}$ ($u^*_{\mathbf{k}}$) the positive frequency (negative frequency) solutions of the generalized Klein-Gordon equation (2.16). The set of modes $\{u_{\mathbf{k}}\}_{\mathbf{k}}$ are now required to be orthonormal w.r.t. to the following scalar product, generalization of the one in Eq. (2.5), i.e.

$$(u_{\mathbf{k}}, u_{\mathbf{k}'})_{\mathrm{KG}} = -i \int d\Sigma^{\mu} \left(u_{\mathbf{k}} \partial_{\mu} u^*_{\mathbf{k}'} - u^*_{\mathbf{k}'} \partial_{\mu} u_{\mathbf{k}}\right)\,, \tag{2.17}$$

where $d\Sigma^{\mu} := d\Sigma n^{\mu}$, $d\Sigma$ is the volume element of a spacelike Cauchy surface Σ and n^{μ} a time-like vector unit orthogonal to Σ.

The localization of particles via smeared quantum fields, as done in Sec. 2.1.1, can be done also in curved spacetime. However, one has to be aware of the coordinates chosen, since different observers may see different smearing functions for the same particle. Moreover, the parameter $\mathbf{k}$, in a curved spacetime, does not necessarily indicate the momentum of the mode, so that $g(\mathbf{k})$ from Eq. (2.9) is not necessarily a momentum distribution amplitude - despite related to it.

2.1.3 Bogoliubov transformation of the field normal modes

In the definition of the scalar product (2.17) lies a crucial problem of quantum field theory in a curved spacetime, challenging the univoque definition of *particle*. In a Minkowski spacetime, a Cauchy surface Σ_t can be naturally defined as $t = \text{const}$, as done in Eq. (2.5). In fact, since ∂_t is a global timelike Killing vector, there is a global time translation symmetry so that every inertial observer have the same, unambiguous definition of positive and negative frequency modes.

In a curved spacetime, however, such a global timelike Killing vector does not always exist. Therefore, by choosing two different Cauchy surfaces for the scalar product (2.17) - i.e. two different time foliations - one may end up with different decompositions between positive and negative frequency modes.

For the sake of clarity, a toy model example is now presented. In particular, two observers - called A and B by convention - are considered in a curved spacetime, with proper times τ_{A} and τ_{B}, respectively. A Cauchy surface for A can be $\tau_{\mathrm{A}} = \text{const}$. Therefore, the observer A finds a set of complete and orthonormal modes w.r.t. the scalar product (2.5) by choosing $\tau_{\mathrm{A}} = \text{const}$ as Σ. The observer B does the same, but choosing the Cauchy surface as $\tau_{\mathrm{B}} = \text{const}$. However, since the scalar product (2.17) is coordinate-dependent, the decomposition between positive frequency and negative frequency modes is observer-dependent. What the observer A interprets as a positive frequency mode, the observer B may see as a mix between positive and negative frequency modes.

To see that, the sets of orthonormal positive frequency normal modes found respectively by A and B are called respectively $\{u_{\mathbf{k}}\}_{\mathbf{k}}$ and $\{v_{\mathbf{k}}\}_{\mathbf{k}}$. The normal mode decomposition of a scalar field follows Eq. (2.3) for the observer A. For the observer B, instead, one can write

$$\hat{\Phi}(\mathbf{x}, t) = \int \mathrm{d}\mathbf{k} \left(\hat{b}_{\mathbf{k}} v_{\mathbf{k}}(\mathbf{x}, t) + \hat{b}^\dagger_{\mathbf{k}} v^*_{\mathbf{k}}(\mathbf{x}, t) \right) , \tag{2.18}$$

where $\hat{b}_{\mathbf{k}}$ is the annihilation operator relative to the mode $v_{\mathbf{k}}$ and it follows the same algebra (2.4) of $a_{\mathbf{k}}$. Since both the sets $\{u_{\mathbf{k}}\}_{\mathbf{k}} \cup \{u^*_{\mathbf{k}}\}_{\mathbf{k}}$ and $\{v_{\mathbf{k}}\}_{\mathbf{k}} \cup \{v^*_{\mathbf{k}}\}_{\mathbf{k}}$, must be complete and orthonormal, one can write the modes $v_{\mathbf{k}}$ in terms of the modes $u_{\mathbf{k}}$ through a completeness relation, also called *Bogoliubov transformation* of the modes, reading

$$v_{\mathbf{k}}(\mathbf{x}, t) = \int \mathrm{d}\mathbf{k}' \left(\alpha_{\mathbf{k}\mathbf{k}'} u_{\mathbf{k}'} + \beta_{\mathbf{k}\mathbf{k}'} u^*_{\mathbf{k}'} \right) , \tag{2.19}$$

where $\alpha_{\mathbf{k}\mathbf{k}'} := (v_{\mathbf{k}}, u_{\mathbf{k}'})_{\mathrm{KG}}$ and $\beta_{\mathbf{k}\mathbf{k}'} := (v_{\mathbf{k}}, u^*_{\mathbf{k}'})_{\mathrm{KG}}$ are called *Bogoliubov coefficients*. By putting Eq. (2.19) into Eq. (2.18) and by comparing the results with Eq. (2.3), one achieves a relation between the bosonic operators $a_{\mathbf{k}}$ and $b_{\mathbf{k}}$, i.e.

$$\hat{b}_{\mathbf{k}} = \int \mathrm{d}\mathbf{k}' \left(\alpha^*_{\mathbf{k}\mathbf{k}'} \hat{a}_{\mathbf{k}'} - \beta^*_{\mathbf{k}\mathbf{k}'} \hat{a}^\dagger_{\mathbf{k}'} \right) . \tag{2.20}$$

To make the operators $b_{\mathbf{k}}$ satisfy the same algebra of $a_{\mathbf{k}}$, i.e. the one in Eq. (2.4), the Bogoliubov coefficients must satisfy the following canonical realtions, i.e.

$$\int \mathrm{d}\mathbf{k}'' \left(\alpha_{\mathbf{k}\mathbf{k}''} \alpha^*_{\mathbf{k}'\mathbf{k}''} - \beta_{\mathbf{k}\mathbf{k}''} \beta^*_{\mathbf{k}'\mathbf{k}''} \right) = \delta^3(\mathbf{k} - \mathbf{k}') ; \tag{2.21a}$$

$$\int \mathrm{d}\mathbf{k}'' \left(\alpha_{\mathbf{k}\mathbf{k}''} \beta_{\mathbf{k}'\mathbf{k}''} - \beta_{\mathbf{k}\mathbf{k}''} \alpha_{\mathbf{k}'\mathbf{k}''} \right) = 0 . \tag{2.21b}$$

Since the two observers A and B use different bosonic operators for their normal modes ($\hat{a}_{\mathbf{k}}$ and $\hat{b}_{\mathbf{k}}$, respectively), then they also have a different notion of vacuum. In fact, A (B) defines the vacuum

$|0_{\rm A}\rangle$ ($|0\rangle_{\rm B}$) as the state satisfying $\hat{a}_{\mathbf{k}}\,|0_{\rm A}\rangle = 0$ ($\hat{b}_{\mathbf{k}}\,|0_{\rm B}\rangle = 0$). Therefore, what the observer A considers a vacuum state is not vacuum for the observer B. If B counts the average number of particles on A's vacuum - by using the number operator $\hat{b}^{\dagger}_{\mathbf{k}}\hat{b}_{\mathbf{k}}$ - then he obtains

$$N_{\mathbf{k}} = \langle 0_{\rm A}|\, b^{\dagger}_{\mathbf{k}} b_{\mathbf{k}}\, |0_{\rm A}\rangle = \int \mathrm{d}\mathbf{k}' |\beta_{\mathbf{k}\mathbf{k}'}|^2 \,. \tag{2.22}$$

This means that, differently to what is known from quantum field theory in Minkowski spacetime, the number of particles is an observer-dependent quantity in curved spacetimes.

More generally, from Eq. (2.22), a different particle content is measured when the Bogoliubov coefficients $\beta_{\mathbf{k}\mathbf{k}'}$ are non-zero. This happens when the "unphysical modes" (i.e. the negative frequency modes) are seen as "physical modes" (the positive frequency ones) by another observer. In general, this feature occurs when two observers A and B are non-inertial w.r.t. each other[2].

Another notable case where this "mode discrepancy" occurs is when a single observer measures the number of particles at different times while the background spacetime geometry is time-evolving. For example, in presence of a dynamical gravitational field, different time foliations occur throughout the background evolution. Therefore, different normal mode decomposition may occur depending on "when" the modes are observed. If an observer experiences a vacuum state before the spacetime evolves, the same observer could experience a number of particles different than zero once the spacetime completes its evolution. In this context, one can say that particles are produced from vacuum by the gravitational field dynamics. In other words, an evolving background geometry - or, analogously, an evolving gravitational field - causes a *particle production* from vacuum.

2.1.4 The field stress energy tensor

From the matter Lagrangian density $\mathcal{L}_{\rm m}$ in Eq. (2.13), one can derive a stress-energy tensor through Eq. (2.14). Since also a quantum scalar field has a Lagrangian density (2.15), then the presence of this field induces a stress-energy tensor as well. In particular, by quantizing Φ into $\hat{\Phi}$ and by putting Eq. (2.15) in place of $\mathcal{L}_m$ in Eq. (2.14), the quantum stress energy tensor induced by the scalar field reads

$$\hat{T}^{\Phi}_{\mu\nu} = (1-2\xi)\nabla_\mu\hat{\Phi}\nabla_\nu\hat{\Phi} - \left(\frac{1}{2} - 2\xi\right) g_{\mu\nu}\nabla^\rho\hat{\Phi}\nabla_\rho\hat{\Phi} - 2\xi\nabla_\mu\nabla_\nu\hat{\Phi} + 2\xi g_{\mu\nu}\hat{\Phi}\Box\hat{\Phi} + \xi G_{\mu\nu}\hat{\Phi}^2 \,, \tag{2.23}$$

where $G_{\mu\nu} := R_{\mu\nu} - \frac{1}{2}g_{\mu\nu}R$ is called *Einstein tensor* and ∇_μ is a covariant derivative w.r.t. the coordinate labeled by μ.

Because of the vacuum contribution, $\langle\phi|\,\hat{T}^{\Phi}_{\mu\nu}\,|\phi\rangle$ in Eq. (2.23) diverges - even in the Minkowski spacetime case [67]. This divergence can be removed through various renormalization techniques [68, 28], which set the vacuum energy into arbitrary values.

In a curved spacetime, as stated before, two non-inertial observers A and B have two different vacuum definition, respectively $|0_{\rm A}\rangle$ and $|0_{\rm B}\rangle$. Therefore, $\langle 0_{\rm A}|\,\hat{T}^{\Phi}_{\mu\nu}\,|0_{\rm A}\rangle \neq \langle 0_{\rm B}|\,\hat{T}^{\Phi}_{\mu\nu}\,|0_{\rm B}\rangle$ and so, the following can be associated to the stress energy tensor relative to the particles produced by the modes Bogoliubov transformation, i.e.

$$T^{\Phi}_{\mu\nu}(\mathrm{A}\to\mathrm{B}) = \langle 0_{\rm B}|\,\hat{T}^{\Phi}_{\mu\nu}\,|0_{\rm B}\rangle - \langle 0_{\rm A}|\,\hat{T}^{\Phi}_{\mu\nu}\,|0_{\rm A}\rangle \,. \tag{2.24}$$

[2] Instead, when they are inertial and in a flat spacetime, it is trivial to prove that each physical normal mode for A corresponds to a physical normal mode for B up to a frequency shift.

From Eq. (2.24), further information on what the observer B sees from A's vacuum is obtained. In particular, from $T^{\Phi}_{\mu\nu}(\mathrm{A} \to \mathrm{B})$, one achieves the distribution on space and time of the particles created by the mode discrepancy as well as the energy fluxes - while no information regarding the spectrum is obtained, according to the Heisenberg principle.

At this point, one may wonder if the field stress energy tensor (2.23) affects the spacetime curvature. The short answer is yes, because Eq. (2.23) contributes on the r.h.s. of the Einstein equations (2.12), providing a stress-energy tensor. However, since vacuum is not expected to produce gravity at a first glance, renormalization techniques often involve a zero vacuum stress energy tensor in a flat spacetime[3]. By doing this choice, the right hand side of Eq. (2.23) gives a non-null contribute only in presence of particles. This would effectively contribute on the spacetime curvature, but its contribute is expected to be negligible w.r.t. classical gravitational sources, often involved in quantum field theory in curved spacetime. Therefore, when using this theory, the presence of scalar particles are considered not to affect the spacetime curvature further. In other words, the *backreaction* of the quantum fields on the metric is neglected.

2.2 Particle production in cosmological domains

The first example of an evolving spacetime, producing particles according to Sec. 2.1.3 is provided by the Universe itself, which, according to General Relativity, is currently undergoing a cosmological expansion. Therefore, a particle creation by a universe expansion - called *cosmological particle production* - is expected and here investigated. In so doing, all the concepts of modern cosmology used in the thesis are introduced as well - with no intentions to give a complete overview of the subject, for which Refs. [5, 6, 7] are left to interested readers.

At very large scales, the Universe can be considered with good approximation as homogeneous and isotropic. The background metric describing such a flat universe expansion is known as the Friedmann-Lemaitre-Robertson-Walker metric, reading

$$ds^2 = -dt^2 + a^2(t)(d\mathbf{x} \cdot d\mathbf{x}) \,, \tag{2.25}$$

where $a(t)$ is the cosmological scale factor, giving the expansion rate.

By putting the metric (2.25) in the left hand side of the Einstein field equations (2.12), with $\Lambda = 0$, one obtains a non-null stress energy tensor

$$T_{\mu\nu} = \mathrm{diag}(\varrho(t), a^2(t)p(t), a^2(t)p(t), a^2(t)p(t)) \,, \tag{2.26}$$

indicating that the universe expansion is justified by the presence of an homogeneous and isotropic fluid, with density ϱ and pressure p, pervading the universe. The magnitude of ϱ and p are related to $a(t)$ and its derivatives through the Friedmann equations, reading

$$H^2 = \frac{1}{3}\varrho \,; \tag{2.27a}$$

$$\dot{H} = -\frac{1}{2}\left(\varrho + p\right) \,, \tag{2.27b}$$

[3]Eventual non-null vacuum contributions of the stress-energy tensor could be canceled out by the third term in the l.h.s. of Eq. (2.12), i.e. the cosmological constant term. However, the expected vacuum energy from quantum field theory turns out to be ~ 120 orders higher than the observed Λ from standard cosmology. This discrepancy leads to the famous *cosmological constant problem* [68, 69, 70]

where $H := \frac{\dot{a}}{a}$ is the Hubble function. The cosmological fluid, characterized by an equation of state $p = p(\varrho)$, cannot be arbitrary, but it must satisfy some *energy conditions*, to rule out exotic matter or unphysical situations. In particular:

- The *null-energy condition* $\varrho + p \geq 0$ ensures that no negative flux of energy is ever flowing along null rays.
- The *weak energy condition* ensures that no time-like observer could see a negative energy density. For a perfect fluid, this condition is satisfied if $\varrho + p \geq 0$ and $\varrho \geq 0$, implying automatically the null-energy condition.
- The *dominant energy condition* $\varrho \geq |p|$ implies that energy flows causally. Its violation suggests the presence of tachyonic matter in the fluid.
- The *strong energy condition* $\varrho + p \geq 0$ and $\varrho + 3p \geq 0$ imposes that gravity is always attractive. Notably, the Friedmann equations (2.27a) and (2.29b) tell us that an accelerating universe expansion, i.e. $\ddot{a} > 0$ is possibly only provided that $\varrho + 3p < 0$, i.e. only by violating the strong energy condition. Since there are evidences that the Universe is currently accelerating - and also of other accelerating phases in past eras [7] - this condition is often dropped in these scenarios.

A generic cosmological constant $\Lambda \neq 0$ is now considered in the Einstein equation (2.12). In so doing, the stress energy tensor (2.26) becomes

$$T_{\mu\nu} = \mathrm{diag}\left(\rho + \Lambda, (p - \Lambda)\, a^2(t), (p - \Lambda)\, a^2(t), (p - \Lambda) a^2(t)\right) , \tag{2.28}$$

and the Friedmann equations become

$$H^2 = \frac{1}{3}\varrho + \frac{\Lambda}{3} \,; \tag{2.29a}$$

$$\dot{H} = -\frac{1}{2}\,(\varrho + p) + \frac{\Lambda}{3} \,. \tag{2.29b}$$

Remarkably, the cosmological constant term in the left hand side of Eq. (2.12) contributes with a fluid with a constant energy density Λ and a pressure $-\Lambda$. This fluid is often associated with *dark energy* and its presence is mandatory to match current cosmological observations. In fact, the Λ-CDM model - including the presence of a positive Λ - is currently considered as the standard model for modern Big Bang cosmology, describing effectively the majority of the current cosmological observations [7, 71] - despite challenged by a minority of them [72].

2.2.1 Cosmological particle production

For convenience, it is useful to write the metric (2.25) in its *conformal* form, i.e. by defining the *conformal time* η so that $d\eta = a^{-1}(t)dt$ and Eq. (2.25) becomes

$$ds^2 = a^2(\eta)(-d\eta^2 + d\mathbf{x} \cdot d\mathbf{x}) \,. \tag{2.30}$$

At this point, one has to find a set of normal modes $u_{\mathbf{k}}(\mathbf{x}, \eta)$ solution of Eq. (2.16) and satisfying the normalization condition (2.17).

From Eq. (2.30), a homogeneous and isotropic cosmological expansion breaks only the time translational symmetry, while the spatial ones are conserved and the same of a Minkowski spacetime. Therefore, one expects the modes $u_{\mathbf{k}}(\mathbf{x},\eta)$ to be proportional to the spatial plane waves $e^{i\mathbf{k}\cdot\mathbf{x}}$. In this way, the normal modes can be written as i.e.

$$u_{\mathbf{k}}(\mathbf{x},\eta)=\frac{e^{i\mathbf{k}\cdot\mathbf{x}}}{a(\eta)(2\pi)^{3/2}}\chi_k(\eta)\,, \tag{2.31}$$

where $\{\chi_k(\eta)\}_k$ are function dependent only on the conformal time η and on $k:=|\mathbf{k}|$. By putting Eq. (2.31) into the Klein-Gordon equation, χ_k satisfies the differential equation

$$\frac{d^2\chi_k}{d\eta^2}+(k^2+M^2_{\text{eff}}(\eta))\chi_k=0\,, \tag{2.32}$$

where $M_{\text{eff}}(\eta)$ is a time-dependent effective mass [73], reading

$$M_{\text{eff}}(\eta)=a^2(\eta)\left(m^2+\left(\xi-\frac{1}{6}\right)R(\eta)\right)\,, \tag{2.33}$$

The scalar curvature R relative to the metric (2.25) is

$$R=6\frac{a''}{a^3}\,, \tag{2.34}$$

where the prime $'$ indicates a first derivative w.r.t. η - while the derivative w.r.t. is indicated with the upper dot, as usual.

The normalization condition $(u_{\mathbf{k}},u_{\mathbf{k}'})=\delta^3(\mathbf{k}-\mathbf{k}')$, according to the scalar product (2.17), gives the following condition for $\chi_{\mathbf{k}}$, called *Wronskian condition*, namely

$$(\chi_k(\chi_k^*)'-\chi_k^*\chi_k')=i\,. \tag{2.35}$$

If the effective mass (2.33) is constant then Eq. (2.32) gives $\chi_k=\frac{e^{-i\eta\Omega_k}}{\sqrt{2\Omega_k}}$, where $\Omega_k:=\sqrt{k^2+M^2_{\text{eff}}}$, ending up with a Minkowski mode (2.6) describing a particle with momentum $\mathbf{k}$ and energy Ω_k, which clearly satisfies the Wronskian condition (2.35). If the effective mass M_{eff} is constant at infinity past and infinite future, one can identify the input modes $\phi^{\text{in}}_{\mathbf{k}}$ as the modes satisfying the Wronskian condition (2.35) at $\eta\to-\infty$ and the output modes $\phi^{\text{out}}_{\mathbf{k}}$ as the ones satisfying Eq. (2.35) at $\eta\to+\infty$. This condition is always verified if $a(\eta)$ is asymptotically constant at infinite past and infinite future.

Therefore, this simple scenario is considered - discussing its implications at the end of this section. The sets of modes $\{\phi^{\text{in}}_{\mathbf{k}}\}_{\mathbf{k}}$ and $\{\phi^{\text{out}}_{\mathbf{k}}\}_{\mathbf{k}}$ are related through a Bogoliubov transformation as in Eq. (2.19). The fact that each momentum $\mathbf{k}$ is conserved from infinite past to infinite future - while the energy Ω_k is not - implies the Bogoliubov coefficients to have the form

$$\alpha_{\mathbf{k}\mathbf{k}'}=\alpha_k\delta^3(\mathbf{k}-\mathbf{k}')\,;\quad \beta_{\mathbf{k}\mathbf{k}'}=\beta_k\delta^3(\mathbf{k}+\mathbf{k}')\,. \tag{2.36}$$

The particle production (2.22) becomes trivially $N_{\mathbf{k}}=|\beta_k|^2$ and the canonical relation (2.21a) becomes

$$|\alpha_k|^2-|\beta_k|^2=1\,. \tag{2.37}$$

2.2.2 Perturbative solutions for the particle production

The explicit expressions for the coefficients α_k and β_k in Eq. (2.36) depend on the particular expansion chosen. Analytic solutions for them are provided by some toy models - see e.g. [74, 75, 60]. However, to have more freedom on the cosmological expansion to chose, a perturbative method is here presented - proposed in Ref. [76, 77, 60], with the aim to find a compact form for the Bogoliubov coefficients (2.36).

For simplicity, $a_{\text{in}} \coloneqq a(\eta \to -\infty) = 1$ is considered. Since $R(\eta \to \pm\infty) = 0$, from Eq. (2.33) one has $M_{\text{eff}}(\eta \to -\infty) = m$ and $\Omega_k(\eta \to -\infty) = \omega_{\text{in}}$ corresponds to the frequency of the initial mode $\mathbf{k}$. The equation (2.32) can be conveniently rewritten in terms of the initial frequency ω_{in} as

$$\chi_k'' + (\omega_{\text{in}}^2 + U(\eta))\chi_k = 0\,, \tag{2.38}$$

where $U(\eta) \coloneqq M_{eff}^2 - m^2$. By choosing a time η_0 when $\dot{a}(\eta_0) = 0$ - eventually, η_0 can be $-\infty$ - an implicit solution for Eq. (2.38) is provided by

$$\chi_k^{(0)}(\eta) = \left(\hat{\text{Id}} + \hat{\mathcal{U}}_k\right)\chi_k(\eta)\,, \tag{2.39}$$

where $\chi_k^{(0)}(\eta) \coloneqq \frac{e^{-i\omega_{\text{in}}\eta}}{\sqrt{2\omega_{\text{in}}}}$ providing the Minkowski mode, $\hat{\text{Id}}$ is the identity operator and $\hat{\mathcal{U}}_k$ is an operator acting on a test function $f(\eta)$ as

$$\hat{\mathcal{U}}_k[f(\eta)] = \frac{1}{k}\int_{\eta_0}^{\eta} d\eta_1 \sin(\omega_{\text{in}}(\eta - \eta_1))U(\eta_1)f(\eta_1)\,. \tag{2.40}$$

Now, Eq. (2.39) can be inverted to obtain

$$\chi_k(\eta) = \left(\hat{\text{Id}} + \hat{\mathcal{U}}_k\right)^{-1}\chi_k^{(0)}(\eta) = \left(\sum_{l=0}^{\infty}(-1)^l\hat{\mathcal{U}}_k^l\right)\chi_k^{(0)}(\eta)\,. \tag{2.41}$$

To Eq. (2.41) an n-order perturbation theory can be applied by truncating the sum at the r.h.s. of Eq. (2.41) at $l = n$. For example, up to second order, one has

$$\begin{aligned}\chi_k(\eta) \sim{}& \chi_k^{(0)}(\eta) - \frac{1}{k}\int_{\eta_0}^{\eta} d\eta_1 \sin(k(\eta-\eta_1))U(\eta_1)\chi_k^{(0)}(\eta_1)\\ &+ \frac{1}{k^2}\int_{\eta_0}^{\eta} d\eta_1 \int_{\eta_0}^{\eta_1} d\eta_2 \sin(k(\eta-\eta_1))\sin(k(\eta_1-\eta_2))U(\eta_1)U(\eta_2)\chi_k^{(0)}(\eta_2)\,.\end{aligned} \tag{2.42}$$

This approximation holds if the function U is small enough in the interval $[\eta_0, \eta]$. In particular, the relative error given by using perturbation theory up to the n-th order can be estimated to be [78]

$$\mathcal{E}_{\text{P}} = \max_k \frac{\hat{\mathcal{U}}_k^{n+1}\chi_k(\eta)}{\chi_k^{(0)}(\eta)}\,. \tag{2.43}$$

At this point, the input modes $\phi_{\mathbf{k}}^{\text{in}}$ are obtained by putting Eq. (2.39) into Eq. (2.31). Once done that, one can invert the Bogoliubov transformation (2.19) and compare the result with Eq. (2.39). Up to second order, one gets

$$\alpha_k = \frac{a_{\text{out}}}{a_{\text{in}}}\left(1 + \frac{i}{2\omega_{\text{in}}}\int_{-\infty}^{+\infty} d\eta_1 U(\eta_1) + \frac{1}{4\omega_{\text{in}}^2}\int_{-\infty}^{+\infty}\int_{-\infty}^{+\infty} d\eta_1 d\eta_2 U(\eta_1)U(\eta_2)(e^{2\omega_{\text{in}} i(\eta_1-\eta_2)} - 1)\right)\,; \tag{2.44a}$$

$$\beta_k = -\frac{a_{\text{out}}}{a_{\text{in}}}\left(\frac{i}{2\omega_{\text{in}}}\int_{-\infty}^{+\infty} d\eta_1 e^{-2i\omega_{\text{in}}\eta_1}U(\eta_1) + \frac{1}{4\omega_{\text{in}}^2}\int_{-\infty}^{+\infty}\int_{-\infty}^{+\infty} d\eta_1 d\eta_2 e^{2\omega_{\text{in}} i(\eta_2-\eta_1)}U(\eta_1)U(\eta_2)\right)\,, \tag{2.44b}$$

where $a_{\text{out}} = a(\eta \to +\infty)$.

The cosmological particle production can be studied via Bogoliubov transformations provided the spacetime flatness at infinite past and infinite future. This obviously provides a major limitation on the possible cosmological models to be taken, requiring $a(\eta \to \pm\infty) = \text{const}$. More importantly, from the Friedmann equations (2.27a) and (2.27b), it turns out that the fluid giving such cosmological models violate the null-energy condition [60]. Therefore, from a physical cosmological perspective, the situations were the Bogoliubov coefficients can be strictly calculated are not realistic. Nevertheless, mathematical approximations can be employed to approximate $a(\eta)$ as approximately constant over a limited time interval. This allows to relax the condition of the existence of a time η_0 so that $\dot{a}(\eta_0) = 0$. In fact, as shown by several authors, the approach of considering an adiabatic transformation of the vacuum state enables a definition of the particle number even during a universe expansion [79, 80, 74]. Moreover, algebraic approaches to quantum field theory have been recently proven to provide an unambiguously definition of vacuum during certain cosmological expansions [81, 82, 83].

By using such methods, the cosmological particle predicted by the Bogoliubov coefficient formalism introduced in this section can be used also in more coherent and realistic expansions. For example, those approaches were used to exploring the possibility of a particle creation during the reheating period [84]. In this regard, several cosmological models have been proposed as responsible to the creation of WIMP dark matter [85, 86, 87] and gamma ray bursts [88, 89, 90].

2.3 Particle production by black holes

One of the most mysterious and fascinating objects in the universe is a black hole [91]. Predicted by general relativity and confirmed by recent astronomical observations, black holes are regions of space where gravity is so intense that nothing - not even light - can escape from their pull. They form through the collapse of very massive stars, whose matter shrinks into incredibly small and dense points, called *singularities*. The region of space where nothing can escape from is called *event horizon*, since the matter inside it becomes causally disconnected with the outside.

According to general relativity, black holes can be considered as a cosmic vacuum cleaners. Therefore, the prediction that black holes can also emit particles, from quantum field theory in curved spacetime, was a groundbreaking discovery [92]. There are currently various mechanisms predicting the emission of particles by black holes (such as pair creation on the horizon [93, 30] or tunnel effect [94]). However, this section focuses on the first, historical one, predicted by Stephen Hawking in Ref. [61], involving the star gravitational collapse as the radiation primer. In fact, the collapse of a massive object into a black hole represents a situation where the background spacetime evolves in time, so that a different particle content is expected between past infinity and future infinity, as for a cosmological expansion.

In Refs. [61, 28], a simplified model for a collapsing ball mimicking a star gravitational collapse is provided. At past infinity, the collapsing star in considered to be so large that the spacetime can be approximated as flat. A Bogoliubov transformation arises between the modes normalized at infinite past and the ones normalized at infinite future - also called *input modes* $\phi^{\text{in}}_{\mathbf{k}}$ and *output modes* $\phi^{\text{out}}_{\mathbf{k}}$, respectively.

By considering the standard Planck units $c = \hbar = k_{\text{B}} = G = 1$, the metric at infinite future is the one describing a static black hole of mass M, called *Schwarzschild metric* [95] and reading

$$ds^2 = -\left(1 - \frac{2M}{r}\right) dt^2 + \left(1 - \frac{2M}{r}\right)^{-1} dr^2 + r^2(d\theta^2 + \sin^2\theta d\varphi^2)\,, \tag{2.45}$$

where r is the radial coordinate from the singularity (at $r = 0$) and θ and φ are angular coordinates. Remarkably, Eq. (2.45) is a static and spherically symmetric solution of Eq. (2.12) in vacuum (i.e. $T_{\mu\nu} = 0$) and with $\Lambda = 0$. The event horizon is given by a sphere of radius $r_\mathrm{S} = 2M$, called *Schwarzschild radius.*

The explicit computation of the input and output modes is very long and left to the reader at the references [61, 28]. The Bogoliubov coefficients linking the input and output modes are

$$\alpha_{\omega lm,\omega' l' m'} = -\frac{\delta_{ll'}\delta_{mm'}}{\sqrt{4\pi^2\omega\omega'}} e^{2\pi M\omega'} (4M\omega)^{4iM\omega'} 4iM\omega'\Gamma\left(-4iM\omega\right)\,; \tag{2.46a}$$

$$\beta_{\omega lm,\omega' l' m'} = (-1)^m \frac{\delta_{ll'}\delta_{mm'}}{\sqrt{4\pi^2\omega\omega'}} e^{-2\pi M\omega'} (4M\omega)^{-4iM\omega'} 4iM\omega'\Gamma\left(4iM\omega\right)\,. \tag{2.46b}$$

Where Γ is the Euler-Gamma function and l, m are the angular momentum quantum numbers, dropped from now on for simplicity. From Eq. (2.46b) one has immediately

$$|\beta_{\omega\omega'}|^2 = \frac{2M}{\pi\omega'}\frac{1}{e^{8\pi M\omega} - 1}\,; \quad N_\omega = A\frac{1}{e^{8\pi M\omega} - 1}\,. \tag{2.47}$$

Therefore, a star collapsing into a black hole produces a thermal spectrum of particles with temperature $T_\mathrm{H} = \frac{1}{8\pi M}$, called *Hawking temperature*. The radiation arising from this process is called *Hawking radiation* and its important implications will be further discussed in this section.

The constant $A := \int_0^\infty d\omega \frac{2M}{\pi\omega}$ is divergent. However, since N_ω from Eq. (2.47) refers to a global particle, the divergence of A is not unphysical and it is actually suggesting that the black hole radiation continues to be emitted indefinitely as long as the black hole exists[4]. Notably, the divergence of A is also consistent with Eq. (2.21a). Indeed, by using the Bogoliubov coefficients (2.46a) and (2.46b) in Eq. (2.21a) and by putting $\mathbf{k} = \mathbf{k}'$ (i.e. $l = l'$, $m = m'$ and $\omega = \omega'$), one obtains $A \simeq \delta(0)$.

To better understand *when* Hawking radiation is produced during the star collapse, one can give a time dependence on the black holes particle production. First of all, a set of complete and orthonormal family of wave packets for the output normal modes must be defined. For example, one could take

$$\phi^\mathrm{out}_{jn} := \frac{1}{\sqrt{\epsilon}}\int_{j\epsilon}^{(j+1)\epsilon} d\omega e^{2\pi i\omega\frac{n}{\epsilon}}\phi^\mathrm{out}_\omega\,, \tag{2.48}$$

where j and n are discrete quantum numbers indicating respectively the frequency window - going from $j\epsilon$ to $(j+1)\epsilon$ - and the time window - going from $\left(n - \frac{1}{2}\right)/\epsilon$ to $\left(n + \frac{1}{2}\right)/\epsilon$ (from the Heisenberg principle, the largest the width of the frequency windows - i.e. the largest ϵ - the smallest the width of the time windows). One can easily verify that the localized modes (2.48) are orthonormal w.r.t. each other, i.e. $(\phi^\mathrm{out}_{jn}, \phi^\mathrm{out}_{j'n'}) = \delta_{jj'}\delta_{nn'}$.

The scalar product between the input modes ϕ^in_ω and the localized output modes ϕ^out_{jn} can be computed to obtain the Bogoliubov coefficients $\alpha_{jn\omega'} = \left(\phi^\mathrm{out}_{jn}, \phi^\mathrm{in}_{\omega'}\right)$ and $\beta_{jn\omega'} = \left(\phi^\mathrm{out}_{jn}, \phi^{\mathrm{in}*}_{\omega'}\right)$ related with the old ones through

$$\beta_{jn\omega'} = \frac{1}{\sqrt{\epsilon}}\int_{j\epsilon}^{(j+1)\epsilon} d\omega e^{2\pi i\omega\frac{n}{\epsilon}}\beta_{\omega\omega'}\,, \tag{2.49}$$

[4] In general, divergences like the one in Eq. (2.47) are common when dealing with Bogoliubov coefficients with continuous modes.

and the same for $\alpha_{jn\omega'}$ by substituting β with α. From $\beta_{jn\omega'}$ a localized particle production can be derived as

$$N_{jn} = \int_0^\infty d\omega' |\beta_{jn\omega'}|^2 \,. \tag{2.50}$$

By putting Eq. (2.46b) into Eq. (2.49) and by using Eq. (2.50), for the Hawking radiation one obtains

$$N_{jn} = \frac{1}{8\pi M\epsilon} \ln\left(\frac{e^{8\pi M(j+1)\epsilon} - 1}{e^{8\pi Mj\epsilon} - 1}\right) - 1 \,. \tag{2.51}$$

For $\epsilon/M \ll 1$, one recovers the thermal spectrum with temperature T_{H}, as expected. Remarkably, Eq. (2.51) implies that N_{jn} is independent from n. Henceforth, Hawking radiation is constant during all the collapsing process. More interestingly, Hawking radiation continues to be emitted indefinitely even when the star has completely collapsed into a black hole.

The fact that Hawking radiation occurs also during the ball collapses is intriguing. However, the collapse model used to compute the Bogoliubov coefficients (2.46a) and (2.46b) is very approximate - for example, the massive ball is considered to shrink at the speed of light. However, some others physically consistent collapsing models were studied. For example, in Ref. [96] the collapsing star is considered as a thin spherical shell of light - in this case, M refers to the energy of the shell. In this case, the Bogoliubov coefficients between the modes before and after the collapse, occurring at a time $t = 0$ by ansatz, are

$$\alpha_{\omega\omega'} = \frac{2M}{\pi} \frac{\sqrt{\omega\omega'}}{\omega - \omega'} \left(-4iM(\omega - \omega')\right)^{-4iM\omega} \Gamma(4iM\omega) \,; \tag{2.52a}$$

$$\beta_{\omega\omega'} = \frac{2M}{\pi} \frac{\sqrt{\omega\omega'}}{\omega + \omega'} \left(-4iM(\omega + \omega')\right)^{-4iM\omega} \Gamma(4iM\omega) \,. \tag{2.52b}$$

For such Bogoliubov coefficients, numerical calculations (see e.g. Fig. 4 of Ref. [97]) show that the localized particle production N_{jn} is very close to zero for negative n and turns on around $n \sim 0$ to reach the expected Hawking thermal spectrum (2.47) when $n \gg 1$. Therefore, the result for N_{jn} indicates that Hawking radiation turns on when the black hole is formed.

Despite the Schwarzschild spacetime describing a black hole is static, a radiation of particles is produced as well. Therefore, this particle production is attributed not to the spacetime dynamics but to the presence of an event horizon, whose formation switches the radiation on[5]. This fact is intuitive by considering the Hawking radiation as the product of the pair creation of virtual particles, from vacuum fluctuations, near the horizon [93]. In fact, as schematized in Fig. 2.1, while normally a pair of virtual particles immediately reannihilate after their creation, if near a black hole event horizon, one particle will be swallowed by the black hole while the other escapes as part of Hawking radiation.

2.3.1 Black hole thermodynamics

From the picture shown in Fig. 2.1, the event horizon of a black hole emits a thermal spectrum with temperature $T_{\mathrm{H}} = \frac{1}{8\pi M}$. Therefore this horizon behaves exactly as a black body with temperature T_{H}. For this reason, it comes natural to assign other thermodynamical quantities to a black hole

[5]This fact holds for every event horizon, not only black hole ones. For example, the Unruh radiation studied in Sec. 2.4 can be associated with the presence of a Rindler horizon as the cosmological particle production by accelerating universe expansions can be associated to the presence of a cosmological horizon.

Figure 2.1: Schematization of the production of Hawking radiation from a black hole event horizon.

- e.g. an entropy S. By studying the thermodynamics of a black hole, one is in fact capable to describe the interaction between a black hole and its surrounding universe via few thermodynamical parameters.

The first step is to find an entropy S for the black hole, for which the second law of thermodynamics $\frac{\mathrm{d}S}{\mathrm{d}t} \geq 0$ holds. To do that, the *Hawking area law* is invoked [98], stating that, for the event horizon area A, one has $\frac{\partial A}{\partial t} \geq 0$[6], to assume $S \propto A$ [101]. This assumption was verified in Ref. [61] to obtain the so-called *Bekenstein-Hawking formula* for the black hole entropy, i.e.

$$S = \frac{A}{4}\,. \tag{2.53}$$

From Eq. (2.53), the second law of thermodynamics simply becomes the Hawking area law. For a Schwarzschild black hole with no external pressure, the first law of thermodynamics $dE = TdS - PdV$ gives instead

$$dE = T_{\mathrm{H}} dS = \frac{\kappa}{8\pi} dA\,, \tag{2.54}$$

where $\kappa = 2\pi T_{\mathrm{H}}$ is the *surface gravity* of the black hole, i.e. the acceleration an observer feels at the event horizon. Finally, the third law of thermodynamics ensures that no black hole has $\kappa = 0$ and the zeroth law that κ is constant along all the event horizon.

2.3.1.1 Thermodynamics of Anti-deSitter black holes

Until now, the focus was only on Schwarzschild black holes, coming from Eq. (2.12) with $T_{\mu\nu} = \Lambda = 0$. However, it is interesting to see what happens for non-null values of the cosmological constant Λ.

As seen in Sec. 2.2, a positive Λ induces the presence of a dark energy fluid (with density $\frac{\Lambda}{8\pi}$ and pressure $p = -\frac{\Lambda}{8\pi}$ in our unities) which is responsible for an accelerating universe expansion - called *de Sitter phase*. By considering Eq. (2.12) with $\Lambda > 0$, asymptotic black hole solutions in de Sitter space can be derived [102, 103]. As expected, the surface gravity of the black hole horizon determines the temperature of the particles it emits. However, since the universe is accelerating, one has another event horizon, similar to the Rindler horizon studied in Sec. 2.4, called *cosmological event horizon*. Therefore, thermal equilibrium is only possible when the temperatures at both horizons match — that is, when the two surfaces coincide [104, 105].

[6]This result was verified by observing the merging of two different black holes. In particular, it was observed that two black holes, with areas A_1 and A_2 respectively, merge together into a black hole with area $A_{\mathrm{tot}} \geq A_1 + A_2$ [99, 100].

A negative Λ, instead, leads to an asymptotically contracting universe. The associated spacetime is called *anti-de Sitter space*. Despite models predicted by $\Lambda < 0$ are less realistic from a cosmological perspective - the fluid arising from it violates the weak energy condition - anti-de Sitter spaces are mostly used because of the *AdS/CFT correspondence*, providing a non-perturbative definition of quantum gravity and tools to study strongly coupled quantum field theories using classical gravity [106, 107, 108]. Similar to the case of asymptotically flat space, the entropy and temperature of anti-de Sitter black holes are proportional to 1/4 of the event horizon area. However, unlike in flat space, AdS black holes can exist in stable thermal equilibrium with surrounding radiation at a given temperature, owing to their positive specific heat [109]. In recent years, interest in the physics of asymptotically AdS black holes has grown significantly due to the development of the AdS/CFT correspondence. Within this framework, considerable focus has been placed on studying thermal field theories defined on the AdS boundary, as well as on the rich variety of phase transitions exhibited by black holes in the bulk [110].

For the reasons above, the focus is now in the thermodynamics of asymptotically anti-de Sitter black holes. Let us consider the Einstein field equations (2.12) with a generic $T_{\mu\nu} \neq 0$. From recent studies, in the extended phase space, Λ can be considered as a thermodynamic pressure [111, 112]. In particular, a black solution of Eq. (2.12) with $\Lambda \neq 0$ is undergoing a pressure

$$P = -\frac{\Lambda}{8\pi} . \tag{2.55}$$

The pressure P is considered to be due to a presence of an homogeneous and isotropic fluid, with density ϱ and Eq. of state $P = P(\varrho)$. The black hole solutions in presence of such a fluid is now explored. The fluid induces a thermodynamical pressure $P = P(\varrho)$ - corresponding to Eq. (2.55) - on the black hole.

A generic static and spherically symmetric line element is given by

$$ds^2 = -f(r,\varrho)dt^2 + \frac{dr^2}{f(r,\varrho)} + r^2 d\Omega^2 , \tag{2.56}$$

for a function $f(r,\varrho)$ to determine. To impose the presence of a black hole horizon, one can ansatz

$$f(r,\varrho) = -\frac{2M}{r} + \frac{8}{3}\pi r^2 P - h(r,\varrho) . \tag{2.57}$$

The Schwarzschild case is recovered for $h(r,\varrho) = -1$ and $P = 0$, while the limit $h(r,\varrho) \to 0$ corresponds to the asymptotic anti-de Sitter black hole solution [109, 107]. The event horizon radius $r_{\rm h}$ is given by solving the equation $f(r_{\rm h},\varrho) = 0$. This allows to write the black hole mass M in terms of the horizon radius $r_{\rm h}$ through

$$M = \frac{4}{3}\pi r_{\rm h}^3 P - \frac{r_{\rm h}}{2} h(r_{\rm h},\varrho) . \tag{2.58}$$

The entropy S of the black hole is supposed to follow again Eq. (2.53).

From the first law of thermodynamics, the energy of a black hole with volume V under a pressure P is $E = M - PV$. Since the enthalpy B of a thermodynamic system reads $B = E + PV$, then one naturally has $B(S,P) = M$. In other words, the enthalpy of a black hole corresponds to its mass. Other thermodynamic quantities are derived from the enthalpy, such as $V = \left(\frac{\partial B}{\partial P}\right)_S$ and $T = \left(\frac{\partial B}{\partial S}\right)_P$. By using those relations and Eq. (2.58), one obtains

$$V = \frac{4}{3}\pi r_{\rm h}^3 - \frac{r_{\rm h}}{2} \frac{\partial h(r_{\rm h},\varrho)}{\partial \varrho} \left(\frac{\partial P}{\partial \varrho}\right)^{-1} ; \tag{2.59}$$

$$T = -\frac{1}{4\pi r_{\mathrm{h}}}\left(\frac{\partial(rh(r,\varrho))}{\partial r}\right)_{r=r_{\mathrm{h}}} + 2r_{\mathrm{h}}P\,. \tag{2.60}$$

Therefore, Eqs. (2.59) and (2.60), together with Eq. (2.58) for the black hole mass and Eq. (2.53) for the entropy, provide a generalization on the black hole thermodynamics when an external pressure, given e.g. by a cosmological fluid, is applied to it.

2.3.1.2 Black hole evaporation

Since a black hole emits energy in form of Hawking radiation, one can invoke the Stephan-Boltzmann law [113] to study the energy emitted by a black hole per unit time, i.e.

$$-\frac{dE}{dt} = A\sigma_n T^n\,. \tag{2.61}$$

where n is the spacetime dimension and $\sigma_n = \frac{\Gamma(n)\zeta(n)}{(2\pi)^{n-1}}$, being Γ and ζ the Euler-Gamma and Riemann-zeta function, respectively.

For the sake of simplicity, a Schwarzschild black hole lying in vacuum in a $(3+1)$-D spacetime is considered. Then, Eq. (2.61) becomes

$$-\frac{dE}{dt} = \frac{1}{15360\pi M^2}\,. \tag{2.62}$$

From energy conservation, the emission of Hawking radiation should drain the black hole internal energy, i.e. its mass M. Therefore, by associating E with M in Eq. (2.62) one ends up with a first order differential equation for M, leading to the solution

$$M(t) = \sqrt[3]{M_0^3 - \frac{t}{5120\pi}} \tag{2.63}$$

where M_0 is the initial black hole mass. This means that a black hole, lying static in a vacuum, slowly evaporates in time. The greatest is the black hole mass, the slowest is the evaporation.

At the time $t_{\mathrm{ev}} = 5120\pi M_0^3$, the black hole should completely evaporate according to this theory. Nevertheless, when the black hole reaches Planck-like dimensions, the semiclassical theory of quantum field theory in curved spacetime is expected to fail in favor of a complete quantum gravity theory. The ultimate fate of a black hole is then uncertain and cannot be addressed by quantum field theory in curved spacetime [114].

2.3.2 Mirrors as a black hole analog

A very simple and fascinating scenario where particles are produced from vacuum occurs in a Minkowski flat spacetime in presence of moving mirrors [115, 116, 63]. Even if the background spacetime is static, an object like a mirror provides a boundary for the field normal modes. Therefore, if the mirror moves non-inertially, the input and output modes would have a different structure, causing the production of particles as occurring from the creation of black holes or for a cosmological expansion. This effect is also called *dynamical Casimir effect*, reflecting the possibility to obtain it with two moving mirrors in a cavity [117]. Remarkably, this is the first quantum field theory in curved spacetime-experimentally confirmed phenomenon [118]. After a short review or their properties, their properties to mimick black hole radiation properties are explored as well [97, 119].

A perfectly reflecting mirror moving in a $(1+1)$-dimensional spacetime[7] with a trajectory $z(t)$ is considered. It is convenient to work with the null variables $u = t - x$ and $v = t + x$. In terms of them, the mirror trajectory can be written as $v_m = p(u)$ or $u_m = f(v)$. Without boundaries, the left-traveling modes $\{\phi^{\mathrm{L}}_\omega\}_\omega$ are proportional to $e^{-i\omega v}$. However, a perfectly reflecting mirror induces the boundary condition $\phi^{\mathrm{L}}_\omega(v = v_m) = 0$. These modes are

$$\phi^{\mathrm{L}}_\omega = \frac{1}{\sqrt{4\pi\omega}} \left(e^{-i\omega v} - e^{-i\omega p(u)} \right) . \tag{2.64}$$

Instead, the right-travelling modes are

$$\phi^{\mathrm{R}}_\omega = \frac{1}{\sqrt{4\pi\omega}} \left(e^{-i\omega u} - e^{-i\omega f(v)} \right) . \tag{2.65}$$

The observer is considered at the right of the mirror and infinitely distant from it. In this way, the left-travelling modes ϕ^{L}_ω can be seen as *input modes*, since they are going towards the mirror from the observer and they are normalized at the right infinite past. On the contrary, the modes ϕ^{R}_ω are the one reflected by the mirror and going towards the observer and they can be considered as *output modes* - normalized at the right infinite future. The Bogoliubov coefficients linking the input and output modes are [97]

$$\alpha_{\omega\omega'} = \frac{1}{2\pi}\sqrt{\frac{\omega}{\omega'}} \int_{-\infty}^{+\infty} du\, e^{-i\omega u + i\omega' p(u)} ; \tag{2.66a}$$

$$\beta_{\omega\omega'} = -\frac{1}{2\pi}\sqrt{\frac{\omega}{\omega'}} \int_{-\infty}^{+\infty} du\, e^{-i\omega u - i\omega' p(u)} . \tag{2.66b}$$

The particles produced towards the right of the mirror are then given by putting Eq. (2.66b) into Eq. (2.22). The computation of the coefficients (2.66a) and (2.66b) often involves integrals $\int_{-\infty}^{+\infty} du e^{-i\omega u}$ - required for the scalar product (2.17) - which need to be regularized with the parameter ϵ, i.e. by considering $u - i\epsilon$ in place of u and then take the limit $\epsilon \to 0$.

The energy radiated by moving mirrors can be studied from the stress energy tensor variation in Eq. (2.24). In a $(1+1)$-D dimensional spacetime, the component $\langle \hat{T}_{uu} \rangle$ of the stress energy tensor corresponds to the flux of energy going towards the right of the mirror. For a mirror with a trajectory $p(u)$, it was computed to be [115]

$$F := \langle \hat{T}_{uu} \rangle = \frac{1}{24\pi} \left(\frac{3}{2} \left(\frac{p''}{p'} \right)^2 - \frac{p'''}{p'} \right) , \tag{2.67}$$

where the prime $'$ here indicates a derivative w.r.t. u. By using the coordinates t and x, and by indicating the time derivative with the upper dot, one has

$$F = \frac{\dddot{z}\,(\dot{z}^2 - 1) - 3\dot{z}\ddot{z}^2}{12\pi(\dot{z} - 1)^4(\dot{z} + 1)^2} . \tag{2.68}$$

A specific mirror trajectory, called the *Carlitz-Willey trajectory* is now chosen, namely [63]

$$p(u) = -\frac{1}{\kappa} e^{-\kappa u} \quad \text{or} \quad z(t) = -t - \frac{1}{\kappa} W(e^{-2\kappa t}) , \tag{2.69}$$

[7] The $(1+1)$-D model is considered because it provides the black hole radiation analogy. The reader is led to Ref. [120] for $(3+1)$-D models.

where κ is a parameter proportional to the mirror's proper acceleration and W is the Lambert function - satisfying $W(x)e^{W(x)} = x$. By putting Eq. (2.69) into Eq. (2.66b), one has

$$|\beta_{\omega\omega'}|^2 = \frac{1}{2\pi\kappa\omega'}\frac{1}{e^{2\pi\kappa\omega} - 1}\,. \tag{2.70}$$

Remarkably, Eq. (2.70) coincides with Eq. (2.47) for the black hole radiation by choosing the parameter κ of the trajectory (2.69) to be equal to $1/(4M)$, i.e. the surface gravity of a black hole. A mirror with the trajectory (2.69) with $\kappa = 1/(4M)$ emits exactly as a black hole with mass M. This is true not only by considering the spectrum of the particles produced, but also by considering the flux of particles emitted. In fact, by putting the trajectory (2.69) into Eq. (2.68), one gets

$$F = \frac{\kappa^2}{48\pi}\,. \tag{2.71}$$

The energy emitted by a black hole, given by the Stephan-Boltzmann law, correspond to the flux of Hawking particles outgoing to infinity and can be called F. For a $(1+1)$-D black hole - or, analogously, a $(3+1)$-D black holes where only radial particles are emitted - the Stephan-Boltzmann law (2.61) gives

$$F = -\frac{dE}{dt} = \frac{1}{768\pi M^2}\,. \tag{2.72}$$

Again, if $\kappa = 1/(4M)$, then Eqs. (2.71) and (2.72) coincide. Then, one concludes that a mirror with the Carlitz-Willey trajectory is a black hole analog, at least by considering the emission of Hawking radiation.

This analogy was now shown for static, Schwarzschild black holes. However, in the literature, mirror analogs of Kerr [121], Reissman-Nordstrom [122] and de Sitter/anti-de Sitter black holes [123] are provided as well. Noticeably, a mirror trajectory can also emulate the radiation of Schwarzschild black hole coming from a null-shell collapse, providing the Bogoliubov coefficients (2.52a) and (2.52b) whose particle production turns on after the creation of the horizon. The trajectory implying this radiation reads [97]

$$z(t) = -t - \frac{1}{2\kappa}W(2e^{-2\kappa t})\,. \tag{2.73}$$

As shown in Ref. [97], the flux obtained by putting Eq. (2.73) into Eq. (2.68) drops exponentially in time for negative values of t. For positive t instead the trajectory (2.73) comes closer and closer to the Carlitz-Willey trajectory (2.69) and the relative flux deviates from the one in Eq. (2.71) by a term $\propto e^{-t/M}$. Therefore, the radiation can be considered to be effectively completely turned on at a time $t \sim 4M$.

2.4 Unruh effect

As a last historical example of particle production, two non-inertial observers are now considered [35]. In particular, the observer A is considered to be static in a $(3+1)$-D Minkowski spacetime, whose line-element is $ds^2 = -dt^2 + dx^2 + dy^2 + dz^2$. The observer B is instead uniformly accelerating along the x-axis, hence following the trajectory

$$\begin{cases} t(\tau) = \frac{1}{\alpha}\sinh(\alpha\tau) \\ x(\tau) = \frac{1}{\alpha}\cosh(\alpha\tau) \\ y(\tau) = 0 \\ z(\tau) = 0\,, \end{cases} \tag{2.74}$$

where α is the proper acceleration of the observer B and τ a trajectory parameter. A convenient coordinate choice for the accelerating observer is given by the *Rindler coordinates* (η, ξ, y, z), where η and ξ are related to t and x through [124]

$$t(\eta,\xi) = \left(\frac{1}{\alpha} + \xi\right)\sinh(\alpha\eta)\,; \quad x(\eta,\xi) = \left(\frac{1}{\alpha} + \xi\right)\cosh(\alpha\eta)\,. \tag{2.75}$$

In Rindler coordinates, the line element reads

$$ds^2 = -(1+\alpha\xi)^2 d\eta^2 + d\xi^2 + dy^2 + dz^2\,. \tag{2.76}$$

From Eq. (2.76), the Rindler metric has an horizon at $\xi = -\alpha^{-1}$, called *Rindler horizon*, as expected from a uniformly accelerated observer.

Inside the Rindler horizon, i.e. whenever $\xi > -\alpha^{-1}$, and $\alpha > 0$, ∂_η is a time-like Killing vector field, which can be used to define the Cauchy surface Σ in Eq. (2.17). In this way, one can compute the Rindler modes from the Klein-Gordon equation (2.16), using the metric (2.76). These modes are the ones the accelerated observer B works with, while the static observer A works with the usual Minkowski modes (2.6). By using the scalar product defined below Eq. (2.19), a technical calculation (see e.g. Ref. [125]) leads to the Bogoliubov coefficients

$$\alpha_{\mathbf{k}\mathbf{k}'} = \delta(k_y - k'_y)\delta(k_z - k'_z)\frac{e^{\frac{\pi\omega_{\mathbf{k}}}{2\alpha}}}{\sqrt{4\pi\omega_{\mathbf{k}'}\alpha\sinh\left(\frac{\pi\omega_{\mathbf{k}}}{\alpha}\right)}}\left(\frac{\omega_{\mathbf{k}'} + k'_z}{\omega_{\mathbf{k}'} - k'_z}\right)^{-i\frac{\omega_{\mathbf{k}}}{2\alpha}}\,. \tag{2.77a}$$

$$\beta_{\mathbf{k}\mathbf{k}'} = -\delta(k_y - k'_y)\delta(k_z - k'_z)\frac{e^{\frac{-\pi\omega_{\mathbf{k}}}{2\alpha}}}{\sqrt{4\pi\omega_{\mathbf{k}'}\alpha\sinh\left(\frac{\pi\omega_{\mathbf{k}}}{\alpha}\right)}}\left(\frac{\omega_{\mathbf{k}'} + k'_z}{\omega_{\mathbf{k}'} - k'_z}\right)^{-i\frac{\omega_{\mathbf{k}}}{2\alpha}}\,. \tag{2.77b}$$

From Eq. (2.77b), the spectrum of particles produced is

$$N_{\mathbf{k}} = B\frac{1}{e^{\frac{\pi\omega_{\mathbf{k}}}{2\alpha}} - 1}\,, \tag{2.78}$$

where B is a function specified later on. From Eq. (2.78), one obtains a particle production $N_{\mathbf{k}}$ proportional to a thermal spectrum with the temperature $T_{\mathrm{U}} = \frac{2\pi}{\alpha}$. Therefore, an accelerated observer undergoes a thermal radiation which is proportional to its proper acceleration. This effect is well known in the literature as the *Unruh effect* from the author of the concept in Ref. [35]. In the same way, the temperature T_{U} in called *Unruh temperature*. Remarkably, this temperature can be associated with the black hole temperature T_{H} when $\alpha = \kappa$, i.e. the surface gravity of the black hole. Therefore, Hawking radiation can be viewed as an Unruh-like effect due to the horizon seen by an observer hovering just outside the black hole.

The proportionality constant in Eq. (2.78) is

$$B := \frac{\delta^2(0)}{2\pi\alpha}\int_{-\infty}^{+\infty}\frac{dk}{\sqrt{m^2 + k^2}}\,, \tag{2.79}$$

which is divergent, similarly to the constant A in Eq. (2.47) when studying the Hawking radiation. Again, this tells us that the "total" amount of particles produced from past infinity to future infinity is indefinitely high, simply because the acceleration of B continues indefinitely.

2.4.1 Unruh-deWitt detectors

At this point, one may wonder if the particles produced by dynamical spacetimes or non-inertial observers could actually be seen to extract information about them - or if they are just a mathematical construct given by a mode discrepancy. This puzzle was solved by deWitt and by Unruh itself [35, 126], who developed a theoretical model of a particle detector - called *Unruh-deWitt detector* - to know if a quantum system actually reacts to the particles produced by the afore mentioned situation - in particular, by the Unruh effect.

An Unruh-deWitt detector is a quantum system interacting with a quantum field in the background. This system is initially considered in its ground state, so that the detection of a particle from the field is associated to the excitation of the quantum system. The interaction with the field occurs through an observable proper of the detector, called $\hat{O}$, coupled with the field operator of the background quantum field. In our case, for simplicity, a massless scalar field $\hat{\Phi}$ is chosen as background field. In this way, the coupling occurs via the Hamiltonian density $\hat{h}_{\mathrm{I}} = \hat{O} \otimes \hat{\Phi}$, giving the Hamiltonian

$$\hat{H}_{\mathrm{I}} = \int d\mathbf{x} F(\mathbf{x},t) \hat{O}(t) \otimes \hat{\Phi}(\mathbf{x},t)\,. \tag{2.80}$$

The function $F(\mathbf{x},t)$ in Eq. (2.80) indicates how the interaction is distributed in space and time. Ideally, one has $F(\mathbf{x},t) = f(\mathbf{x})\lambda(t)$, so that $f(\mathbf{x})$ is the smearing function defined in Sec. 2.1.1 and $\lambda(t)$ is the *switching-in* function, indicating how the interaction switches on and off in time. The smearing function $f(\mathbf{x})$, indicating an amplitude for the position probability of a particle, can be associated with the shape of the detector itself. Notice that, by using the from $F(\mathbf{x},t) = f(\mathbf{x})\lambda(t)$, Eq. (2.80) becomes

$$\hat{H}_{\mathrm{I}}(t) = \lambda_{\mathrm{i}}(t) \hat{O}(t) \otimes \hat{\Phi}_f(t_{\mathrm{i}})\,. \tag{2.81}$$

From Eq. (2.81), a detector with a shape $|f(\mathbf{x})|^2$ effectively interacts with the smeared scalar field (2.8) with a strength given by the switching-in function $\lambda(t)$.

For the sake of simplicity, Unruh-deWitt detectors are usually modeled by non-relativistic quantum systems [127, 128, 129]. However, to consider a such a detector in a curved spacetime, one must define a set of non-relativistic coordinates along the detector size (i.e. along the support of the smearing f). Such locally non-relativistic coordinates are the *Fermi-normal coordinates*. One can define the *Fermi length* L_{F} as the size of the region around the detector where Fermi-normal coordinates can be used. An estimation of this length is provided in Ref. [46], giving

$$L_{\mathrm{F}} \sim \frac{1}{\alpha + \sqrt{\lambda_R}}\,, \tag{2.82}$$

where α is the proper acceleration of the detector and λ_R is the greatest eigenvalue of the Riemann tensor component $R_{0\mathrm{i}0\mathrm{j}}$ computed in the detector's center of mass (i,j indicate spatial coordinates). If a detector can be locally described by Fermi-normal coordinates, then - by using these coordinates - the amplitude of momenta distribution can be found as in the flat case with Eq. (2.9).

The ability of Unruh-deWitt detectors to achieve Unruh radiated particles is now proven. The quantum system playing the detector role is chosen to be a two-level system - i.e. a quantum system with two energetic levels $|0\rangle$ and $|1\rangle$ - with energy gap ω. Moreover, for it, a Lorentzian smearing function is considered, namely

$$f(\mathbf{x}) = \frac{1}{\pi^2} \frac{\epsilon}{(|\mathbf{x} - \boldsymbol{\xi}|^2 + \epsilon^2)^2}\,, \tag{2.83}$$

where $\boldsymbol{\xi}$ is the position of the detector center of mass, ϵ can be considered as the *effective size* of the detector. The limit $\epsilon \to 0$ gives $f(\mathbf{x}) = \delta^3(\mathbf{x} - \boldsymbol{\xi})$, i.e. a point-like detector.

The probability of excitation of the detector, once interacting with the field, is given by the Fermi golden rule and reads

$$P_e = |\langle 1|\hat{O}(-\infty)|0\rangle|^2 \int_{-\infty}^{+\infty} dt\lambda(t) \int_{-\infty}^{+\infty} dt'\lambda(t')e^{-i\omega(t-t')} \langle\phi|\hat{\Phi}_f(t)\hat{\Phi}_f(t')|\phi\rangle \,, \tag{2.84}$$

where $|\phi\rangle$ is the initial state of the field and $\hat{\Phi}(t)$ is the smeared scalar field operator (2.8). In a Minkowski vacuum $|\phi\rangle = |0\rangle$, if the detector follows a trajectory $(t(\tau), \boldsymbol{\xi}(\tau))$, the quantity $\langle\phi|\hat{\Phi}_f(t)\hat{\Phi}_f(t')|\phi\rangle$ reads [47]

$$\langle 0|\hat{\Phi}_f(\tau)\hat{\Phi}_f(\tau')|0\rangle = -\frac{\Big((t(\tau) - t(\tau') - i\epsilon(\dot{t}(\tau) + \dot{t}(\tau')))^2 + |\boldsymbol{\xi}(\tau) - \boldsymbol{\xi}(\tau') - i\epsilon(\dot{\boldsymbol{\xi}}(\tau) + \dot{\boldsymbol{\xi}}(\tau'))|^2\Big)^{-2}}{4\pi} \,, \tag{2.85}$$

where the dot denotes a time derivative w.r.t. τ.

If the interaction with the field is constant in time, i.e. $\lambda(t) = \text{const}$, then the time derivative of P_e is effectively an excitation rate - or *transition rate*, namely[8]

$$R(\omega, t) = \int_{-\infty}^{t} \mathrm{d}s e^{-i\omega s} \langle 0|\hat{\Phi}_f(t)\hat{\Phi}_f(t-s)|0\rangle \,. \tag{2.86}$$

By putting the static observer trajectory - i.e. $(t(\tau), \boldsymbol{\xi}(\tau)) = (t, \mathbf{0})$ - in Eq. (2.85), and in the point-like limit $\epsilon \to 0$, the transition rate (2.86) becomes

$$R(\omega, t) = \frac{1}{2\pi}\omega\theta(-\omega) \,, \tag{2.87}$$

where θ is the Heaviside step function. Clearly, the r.h.s. of Eq. (2.87) is null, meaning that no transition can spontaneously occur in a vacuum for a static detector is static. Obviously, this is expected since no particles are created from a static observer point of view. The same is valid for every inertial trajectory, from which an analog result of Eq. (2.87) arises with a shifted energy gap.

For a Rindler accelerated detector, the transition rate (2.86) can be obtained as well by putting the trajectory (2.74) into Eq. (2.85), with $\boldsymbol{\xi} = (x, y, z)$, obtaining for $\epsilon \to 0$[9]

$$R(\omega, t) = \frac{1}{2\pi} \frac{\omega}{e^{\frac{2\pi\omega}{\alpha}} - 1} \,. \tag{2.88}$$

The transition rate (2.88) is exactly the one expected from a two-level system in a thermal bath with temperature $T_{\mathrm{U}} = \frac{\alpha}{2\pi}$. Therefore, an accelerating quantum system actually detects the particles created by the Unruh effect and it can extract information from them.

This fact opens the possibility to detect the particles created not only by Unruh effect, but also by the other effects studied in this Chapter. To this purpose, the Unruh-deWitt detector provides a particle detector model that also quantifies the probability of detection of these particles. For this reason, these detector models has recently become a central topic in relativistic quantum information [130, 44, 131].

Since Unruh effect is practically impossible to detect with today's means - an Unruh temperature of $1\,K$ is reached up to a proper acceleration $\sim 10^{20}$ m/s^2 - the possibility the obtain an analog Unruh effect has been recently studied with systems more easy to build in a laboratory. This is done, for example, by choosing stationary trajectories for Unruh-deWitt detectors, such as circular trajectories, producing a similar effect to the accelerating trajectories [132, 133, 134].

[8] The contribute $|\langle 1|\hat{O}(-\infty)|0\rangle|^2$ is not taken into account since it is independent from the detector trajectory.

[9] The results in Eqs. (2.87) and (2.88) are obtained by considering $\epsilon \ll \frac{1}{\omega}$, i.e. the point-like detector limit. However, as reported in chapter in Chapter 4, this limit often creates ultraviolet divergences.

2.5 Linearized quantum gravity

This chapter is concluded by introducing another physical theory attempting to describe the behaviour of quantum particles in presence of gravitational sources. Linearized quantum gravity basically consists on the quantization of gravitational fields in a weak field regime. In this limit, the gravitational field can be treated as a small perturbation of a flat Minkowski spacetime, enabling a perturbative quantization approach.

Despite giving a first definition of gravitational quanta, i.e. gravitons, this theory presents some limitations. Among all, the fact that gravitational interaction is not renormalizable [28]. Nevertheless, as an effective field theory - valid at energies way lower than the Planck mass - linearized quantum gravity leads to finite and predictive results for quantum corrections to classical gravity [38].

In weak field regimes, gravitational effects are expected to be so small that curvature is a small perturbation of flatness. For the metric tensor $g_{\mu\nu}$, one can write

$$g_{\mu\nu} \simeq \eta_{\mu\nu} + h_{\mu\nu}\,. \tag{2.89}$$

where $\eta_{\mu\nu}$ is the Minkowski metric and $|h_{\mu\nu}| \ll 1$ for each component μ, ν. In other words, gravitational masses are assumed to affect the metric tensor only perturbatively.

By putting Eq. (2.89) into Eq. (2.12) - with no stress energy tensor and cosmological constant - one has

$$\Box\left(h_{\mu\nu} - \frac{1}{2}\eta_{\mu\nu}h\right) = \Box\gamma_{\mu\nu} = 0\,. \tag{2.90}$$

where $h = h_\mu^{\ \mu}$. As a consequence, the tensor $\gamma_{\mu\nu} \coloneqq h_{\mu\nu} - \frac{1}{2}\eta_{\mu\nu}h$ propagates as a wave in vacuum.

To remove some unphysical degrees of freedom, one may employ the *harmonic gauge* [37], i.e. $\partial^\mu\gamma_{\mu\nu} = 0$. In so doing, by putting Eq. (2.89) into the Einstein-Hilbert action (2.13) a Lagrangian density for $\gamma_{\mu\nu}$ was obtained as [37]

$$\mathcal{L}_{\mathrm{G}} = -\frac{1}{4}\left(\partial_\rho\gamma_{\mu\nu}\partial^\rho\gamma^{\mu\nu} - \frac{1}{2}\partial_\rho\gamma\partial^\rho\gamma\right)\,. \tag{2.91}$$

The variables $\gamma_{\mu\nu}$ and $\gamma \coloneqq \gamma_\mu^{\ \mu}$ can be considered as independent w.r.t. each other. In so doing, Eq. (2.91) leads to

$$\Box\gamma_{\mu\nu} = 0\,; \quad \Box\gamma = 0\,. \tag{2.92}$$

Now, $\gamma_{\mu\nu}$ and γ can be promoted to operators, namely $\hat{\gamma}_{\mu\nu}$ and $\hat{\gamma}$, representing spin-2 and spin-0 graviton fields, respectively [37, 135]. From canonical quantization, one has

$$\hat{\gamma}_{\mu\nu} = \int \frac{d\mathbf{k}}{\sqrt{(2\pi)^3 2|\mathbf{k}|}}\left(\hat{P}_{\mu\nu}(\mathbf{k})e^{i\mathbf{k}\cdot\mathbf{x}-i|\mathbf{k}|t} + \hat{P}^\dagger_{\mu\nu}(\mathbf{k})e^{-i\mathbf{k}\cdot\mathbf{x}+i|\mathbf{k}|t}\right)\,; \tag{2.93a}$$

$$\hat{\gamma} = 2\int \frac{d\mathbf{k}}{\sqrt{(2\pi)^3 2|\mathbf{k}|}}\left(\hat{P}(\mathbf{k})e^{i\mathbf{k}\cdot\mathbf{x}-i|\mathbf{k}|t} + \hat{P}^\dagger(\mathbf{k})e^{-i\mathbf{k}\cdot\mathbf{x}+i|\mathbf{k}|t}\right)\,. \tag{2.93b}$$

where $\hat{P}_{\mu\nu}$ and $\hat{P}$ are the annihilation operators of spin-2 and spin-0 gravitons, satisfying the algebra

$$\left[\hat{P}_{\mu\nu}(\mathbf{k}), \hat{P}^\dagger_{\mu'\nu'}(\mathbf{k})\right] = (\eta_{\mu\mu'}\eta_{\nu\nu'} + \eta_{\mu\nu'}\eta_{\mu'\nu})\delta^3(\mathbf{k}-\mathbf{k}')\,; \quad \left[\hat{P}(\mathbf{k}), \hat{P}^\dagger(\mathbf{k})\right] = -\delta(\mathbf{k}-\mathbf{k}')\,, \tag{2.94}$$

while the other commutators vanish.

With the approximation (2.89), Eq. (2.14) gives the following for the matter Lagrangian density in terms of the stress-energy tensor, i.e.

$$\mathcal{L}_{\rm m} = -\frac{1}{2} h_{\mu\nu} T^{\mu\nu} \,. \tag{2.95}$$

where $h_{\mu\nu} = \gamma_{\mu\nu} - \frac{1}{2}\eta_{\mu\nu}\gamma$ from the definition below Eq. (2.90). In linearized quantum gravity, $\hat{h}_{\mu\nu}$ is quantized and then the Lagrangian $\mathcal{L}_{\rm m}$ becomes an interaction Lagrangian between the gravitons and the matter. If $T_{\mu\nu}$ represents classical matter, then the Lagrangian (2.95) indicates that the matter is non-other than a classical source of gravitons.

The interaction between gravitons and a quantum field is given again by Eq. (2.95) by considering the renormalized quantum stress energy tensor $\hat{T}_{\mu\nu}$, associated with the field, in place of the classical $T_{\mu\nu}$. Since $h_{\mu\nu}$ is promoted to be an operator $\hat{h}_{\mu\nu}$, the classical background where the particles travel becomes simply $\eta_{\mu\nu}$ and gravitational effects on the particle are just given by the quantum interaction it has with gravitons. Therefore, the stress energy tensor given e.g. by a quantum scalar field, in Eq. (2.23), becomes

$$\hat{T}^{\Phi}_{\mu\nu} = \partial_\mu \hat{\Phi} \partial_\nu \hat{\Phi} - \frac{1}{2}\eta_{\mu\nu}\left(\partial^\rho \hat{\Phi} \partial_\rho \hat{\Phi} + m^2 \hat{\Phi}^2\right) \,. \tag{2.96}$$

By removing the divergences on the stress energy tensor (2.96), the energy vacuum can be set to zero for each inertial observer at any time. Both those things could be done by simply applying the normal ordering operation to $\hat{T}_{\mu\nu}$ in Eq. (2.96). The normal ordered stress energy tensor is noted as $:\hat{T}_{\mu\nu}:$.

Is so doing, the field-graviton interaction is easily obtained by quantizing both $h_{\mu\nu}$ and the renormalized stress energy tensor in Eq. (2.95), giving the interaction Lagrangian density

$$\mathcal{L}_{\rm I} = -\frac{1}{2}\hat{h}_{\mu\nu} :\hat{T}^{\mu\nu}: \,. \tag{2.97}$$

To take into account both the presence of classical sources and the presence of quantum particles, in general one has

$$:\hat{T}_{\mu\nu}: = T^{\odot}_{\mu\nu} + :\hat{T}^{\Phi}_{\mu\nu}: \,, \tag{2.98}$$

where $T^{\odot}_{\mu\nu}$ is the stress energy tensor associated to a classical source, while $\hat{T}^{\Phi}_{\mu\nu}$ is the "field" stress energy tensor (2.96).

The complete Lagrangian density of linearized quantum gravity theory is then $\mathcal{L}_\Phi + \mathcal{L}_{\rm G} + \mathcal{L}_{\rm I}$, where the three terms are given respectively by Eqs. (2.1), (2.91) and (2.97), which is the starting point for calculations performed later on.

Chapter 3

Quantum communication via single bosonic modes

Contents

The effects of horizons and dynamical gravitational fields on the vacuum state of a quantum field were extensively addressed in Chapter 2. These effects are usually very small and their detection often require instrument whose precision are beyond our current capabilities or probes close to the speed of light.

This chapter aims to address this problem by considering, instead of the vacuum state, a generic bosonic input state. In particular, a bosonic state is considered as the input of a quantum channel, whose output includes the gravitational effects to analyze. Several situations are considered, such as the ones involving a Bogoliubov transformation of bosonic modes, studied in Chapter 2, and also additive noise of the background predicted by General Relativity. In all of them, the quality of the communication protocol is expected to be dependent on the properties of the examined gravitational phenomenon. Therefore, the possibility to use these protocol as a mean to see the small effects of quantum field theory in curved spacetime is addressed, as well as distinguish between different theories of gravity of different background cosmological fluids.

To study the evolution of bosonic modes, quantum information theory is used. In so doing, the focus is on the amount of information and entanglement stored in remote past and preserved up to gravitational effect [52]. In particular, *quantum communication theory* is addressed to study mappings between different quantum states, called *quantum communication channels* [136, 137, 138]. Their quality is quantified by the so-called *quantum channel capacities* [139, 140, 141], whose computation is the main goal.

The analysis has been restricted to bosonic communication. The reason for this choice relies on the arbitrary high amount of particles that a bosonic state can have[1] For example, this property always allows classical information to be reliably transmitted, unless a limit on the energy of the state is imposed [142, 143]. On the other side of the coin, bosonic states are way harder to be represented than fermionic state. In fact, a bosonic system is always an infinite dimensional quantum system and its representation involves infinite dimensional density matrices. Therefore, to represent those state compactly, alternative methods may be invoked, according to *continuous variable quantum information theory* [144]. The analysis is restricted also to one-mode bosonic states which, besides addressing the mathematical complexity, offer a simple effective way to study the evolution of the stored information.

The structure of the chapter is the following. In Sec. 3.1 continuous variable quantum information theory is introduced, as well as the mathematical tools from quantum communication used in this and the next chapter. In Sec. 3.2 each Bogoliubov transformation acting on bosons is related to a quantum channel. The properties of such a channel in terms of the Bogoliubov coefficients are found consequently. In Sec. 3.3 the effects of a cosmological expansion on single-mode bosonic states is explored, as well as the preservation of entanglement between two opposite bosonic modes. The modified $f(\mathsf{Q})$-theories of gravity are introduced as well, to investigate which one of them gives the most reliable quantum channel and to open the possibility to discern between the different gravity theories from the quality of the communication channel. In Sec. 3.4 the transmission of a signal through semitransparent moving mirrors is addressed, to see if particle production gives a noisy contribution even to a non-perfect quantum channel. The transmission through evaporating black hole is addressed in Sec. 3.5 and finally, in Sec. 3.6, an additive noise on the background is considered and well as its effect on quantum channels' capacities. In this last section, the focus is in particular to the noise created by asymptotic anti-de Sitter black holes.

This chapter is mainly based on the peer-reviewed papers [P1, P2, P3, P6]

3.1 Bosonic Gaussian channels in a nutshell

A quantum system made by a non-definite number of indistinguishable particles is represented by a *Fock space*. By supposing the particles to have a number of modes N, labeled by the discrete index

[1] Instead, from the Pauli principle, no more than one fermion can occupy the same quantum state. Therefore, the information that can be stored by a fermionic state is limited, while this is not true for a bosonic state, whose information stored can be arbitrarily increased by simply adding more bosons in the same state.

i - N may be eventually infinite - then the Fock space $\mathcal{F}$ can be written as

$$\mathcal{F} = \text{span}\left\{ \bigotimes_{\mathrm{i}=1}^{N} |n_{\mathrm{i}}\rangle \right\}_{n_{\mathrm{i}}} , \tag{3.1}$$

where n_{i} indicates the number of particles in the mode i.

If the particles are fermions, then n_{i} can be equal to 0 or 1, from the Pauli principle. In other words, no more than one fermion can occupy the same mode. The Fock space $\mathcal{F}$ is then isomorphic to $\left(\mathbb{C}^2\right)^{\otimes N}$ and can therefore be represented by an N-qubit system.

By considering bosons n_{i} can be a whatever natural number from 0 to $+\infty$. In this way, even a single mode bosonic system (i.e. $N = 1$) turns out to be an infinite-dimensional Hilbert space. Therefore, a bosonic state cannot be represented compactly by a finite dimensional density matrix.

From *continuous variable quantum information* [144], an N-modes bosonic system is conventionally through a function $\chi : \mathbb{C}^N \to \mathbb{R}$ called *characteristic function*, and related to the density operator of the state $\hat{\rho}$ through

$$\chi(\mathbf{z}) := \mathrm{Tr}\left(\hat{\rho}\hat{D}(\mathbf{z})\right), \tag{3.2}$$

where $\mathbf{z} = (z_1, \dots, z_N) \in \mathbb{C}^N$ and $\hat{D}$ is the N-mode displacement operator

$$\hat{D}(z_1, \dots, z_N) = \prod_{\mathrm{i}=1}^{N} \exp\left(z_{\mathrm{i}}\hat{a}_{\mathrm{i}}^{\dagger} - z_{\mathrm{i}}^{*}\hat{a}_{\mathrm{i}}\right) . \tag{3.3}$$

From the definition in Eq. (3.2), the characteristic function is the expectation value of the operator $\hat{D}$ in the state $\hat{\rho}$.

3.1.1 Bosonic Gaussian states

Among all the bosonic states, the ones with a Gaussian like characteristic function are considered. Such states are called *bosonic Gaussian states* and they are of paramount importance in quantum optics, computing and sensing [145, 146, 147, 148, 149]. According to many conjectures, these states are the ones supposedly conserving better classical and quantum information up to a quantum channel [150]. Moreover, bosonic Gaussian states include a great part of physically useful bosonic states, such as the vacuum state, thermal states and coherent states [151].

The characteristic function of a bosonic Gaussian state is

$$\chi(\mathbf{z}) = \exp\left(-\frac{1}{4}\mathbf{z}^T \cdot \sigma \cdot \mathbf{z} + i\mathbf{d}^T \cdot \mathbf{z}\right), \tag{3.4}$$

where $\mathbf{d}$ and σ are respectively the *first momentum vector* and the *covariance matrix*, reading

$$\mathbf{d} := \begin{pmatrix} \langle \hat{Q}_1 \rangle \\ \langle \hat{P}_1 \rangle \\ \vdots \\ \langle \hat{Q}_N \rangle \\ \langle \hat{P}_N \rangle \end{pmatrix} ; \quad \sigma = \left(\begin{array}{c|c|c} \sigma_{11} & \dots & \sigma_{1N} \\ \hline \vdots & \ddots & \vdots \\ \hline \sigma_{N1} & \dots & \sigma_{NN} \end{array}\right) . \tag{3.5}$$

The operators $\hat{Q}_{\mathrm{i}} := \frac{1}{\sqrt{2}}\left(\hat{a}_{\mathrm{i}} + \hat{a}_{\mathrm{i}}^{\dagger}\right)$ and $\hat{P}_{\mathrm{i}} := \frac{1}{\sqrt{2}i}\left(\hat{a}_{\mathrm{i}} - \hat{a}_{\mathrm{i}}^{\dagger}\right)$ are the *quadrature operators* and

$$\sigma_{\mathrm{ij}} = \frac{1}{2}\begin{pmatrix} \langle\left\{\hat{Q}_{\mathrm{i}}, \hat{Q}_{\mathrm{j}}\right\}\rangle - 2\langle\hat{Q}_{\mathrm{i}}\rangle\langle\hat{Q}_{\mathrm{j}}\rangle & \langle\left\{\hat{Q}_{\mathrm{i}}, \hat{P}_{\mathrm{j}}\right\}\rangle - 2\langle\hat{Q}_{\mathrm{i}}\rangle\langle\hat{P}_{\mathrm{j}}\rangle \\ \langle\left\{\hat{P}_{\mathrm{i}}, Q_{\mathrm{j}}\right\}\rangle - 2\langle\hat{P}_{\mathrm{i}}\rangle\langle\hat{Q}_{\mathrm{j}}\rangle & \langle\left\{\hat{P}_{\mathrm{i}}, \hat{P}_{\mathrm{j}}\right\}\rangle - 2\langle\hat{P}_{\mathrm{i}}\rangle\langle\hat{P}_{\mathrm{j}}\rangle \end{pmatrix} . \tag{3.6}$$

The uncertainty principle implies $\left[\hat{Q}_{\rm i}, \hat{P}_{\rm i}\right] > i$ for each mode i, leading to the following bound for the covariance matrix σ, i.e.

$$\sigma + i\Omega \geq 0\,; \quad \Omega = \bigoplus_{k=1}^{N} \begin{pmatrix} 0 & 1 \\ -1 & 0 \end{pmatrix} . \tag{3.7}$$

To quantify the quantum information encoded in a quantum state represented by $\hat{\rho}$, one uses the *Von Neumann entropy* $S_{\rm vN}$, namely

$$S_{\rm vN}(\hat{\rho}) := -{\rm Tr}\left(\hat{\rho}\log\hat{\rho}\right) , \tag{3.8}$$

where log refers to the base 2 logarithm. The Von Neumann entropy (3.8) is the degree of uncertainty of a quantum state and therefore, the amount of information about the quantum system one learns by observing it multiple times.

For a Bosonic Gaussian state, characterized by the pair $(\mathbf{d}, \sigma)$, the Von Neumann entropy reads [144]

$$\mathsf{S}_{\rm vN}(\mathbf{d}, \sigma) := \sum_{\rm i=1}^{N} h(\nu_{\rm i})\,, \tag{3.9}$$

where $\nu_1, \ldots, \nu_N$ are the symplectic eigenvalues of the matrix σ and

$$h(x) := \left(x + \frac{1}{2}\right)\log\left(x + \frac{1}{2}\right) - \left(x - \frac{1}{2}\right)\log\left(x - \frac{1}{2}\right) . \tag{3.10}$$

Remarkably, the Von Neumann entropy - and therefore, the information content - of a bosonic Gaussian state depends solely on its covariance matrix σ, while it is independent from $\mathbf{d}$. Since this thesis focus more on the quantum information content of a state, the procedure can be simplified by considering $\mathbf{d} = \mathbf{0}$ without loss of generality. In this way, Eq. (3.6) simplifies to

$$\sigma_{\rm ij} = \frac{1}{2}\begin{pmatrix} \langle\left\{\hat{Q}_{\rm i}, \hat{Q}_{\rm j}\right\}\rangle & \langle\left\{\hat{Q}_{\rm i}, \hat{P}_{\rm j}\right\}\rangle \\ \langle\left\{\hat{P}_{\rm i}, \hat{Q}_{\rm j}\right\}\rangle & \langle\left\{\hat{P}_{\rm i}, \hat{P}_{\rm j}\right\}\rangle \end{pmatrix} . \tag{3.11}$$

The submatrices $\sigma_{\rm ii}$ on the diagonal blocks of σ from Eq. (3.5) represents the state of the subsystem made only by the mode i. The off-diagonal matrix elements $\sigma_{\rm i\neq j}$ express the correlations between the modes i and j. Both of them can be compactly written through the parameters $n_{\rm i} := \langle\hat{a}_{\rm i}^\dagger\hat{a}_{\rm i}\rangle$, $m_{\rm i} := \langle\hat{a}_{\rm i}\hat{a}_{\rm i}\rangle$, $\gamma_{\rm ij} := \langle\hat{a}_{\rm i}^\dagger\hat{a}_{\rm j}\rangle$ and $\chi_{\rm ij} = \langle\hat{a}_{\rm i}\hat{a}_{\rm j}\rangle$ respectively as

$$\sigma_{\rm ii} = \begin{pmatrix} \frac{1}{2} + n_{\rm i} + \Re m_{\rm i} & \Im m_{\rm i} \\ \Im m_{\rm i} & \frac{1}{2} + n_{\rm i} - \Re m_{\rm i} \end{pmatrix} ; \tag{3.12}$$

$$\sigma_{\rm i\neq j} = \begin{pmatrix} \Re\gamma_{\rm ij} + \Re\chi_{\rm ij} & \Im\gamma_{\rm ij} + \Im\chi_{\rm ij} \\ -\Im\gamma_{\rm ij} + \Im\chi_{\rm ij} & \Re\gamma_{\rm ij} - \Re\chi_{\rm ij} \end{pmatrix} . \tag{3.13}$$

3.1.2 One-mode Gaussian channels

A generic *Gaussian channel* is non-other than a quantum channel mapping a Gaussian state into another Gaussian state. A map from an N-modes Gaussian state into another N-modes Gaussian state is called N-modes Gaussian channel.

The properties of such channels are very hard to explore due to the large number of free parameters involved (i.e. $(N-1)!$ more or less). To date, a complete classification of bosonic Gaussian channels is provided only when $N = 1$ [152], despite many recent progresses for $N \gtrsim 1$ [153, 154]. Therefore, the analysis mostly focuses on the information preserved in one-mode Gaussian states (i.e. $N = 1$), while two-modes Gaussian states ($N = 2$) are later employed to study the evolution of pre-existing entanglement.

Let us consider a channel $\mathcal{N}$ whose input is one-mode Gaussian state characterized by a 2×2 covariance matrix σ_{in} and a first momentum vector $\mathbf{d}_{\text{in}}$. If $\mathcal{N}$ is a one-mode Gaussian channel, then its output would be another one-mode Gaussian state with first momentum vector $\mathbf{d}_{\text{out}}$ and covariance matrix σ_{out}. In general one can prove that [155, 156]

$$\mathbf{d}_{\text{out}} = \mathbb{T}\mathbf{d}_{\text{in}} + \mathbf{v}\,, \quad \sigma_{\text{out}} = \mathbb{T}^T \sigma_{\text{in}} \mathbb{T} + \mathbb{N}\,, \tag{3.14}$$

where $\mathbf{v}$ is a 2-dimensional vector and $\mathbb{T}$ and $\mathbb{N}$ are 2×2 matrices. To ensure the output covariance matrix σ_{out} satisfies the uncertainty principle (3.7) one needs

$$\sqrt{\det \mathbb{N}} \geq \frac{1}{2} \left|1 - \det \mathbb{T}\right| \,. \tag{3.15}$$

A one-mode Gaussian channel $\mathbb{N}$ is then entirely characterized from the triad $(\mathbf{v}, \mathbb{T}, \mathbb{N})$. Since the Von Neumann entropy - and all the other entropic quantities - is unaffected by $\mathbf{d}$, one can consider for simplicity $\mathbf{v} = \mathbf{0}$ without affecting the information-related properties of the quantum channel.

At this point, the channel $\mathcal{N}$ is characterized only by the matrices $\mathbb{T}$ and $\mathbb{N}$. One can go further and reduce $\mathcal{N}$ to its canonical form *canonical form* $\mathcal{N}_{\text{c}}$ through a pair of unitary transformations $\mathcal{U}_{\text{in}}$ and $\mathcal{U}_{\text{out}}$ - called respectively *pre-processing* and *post-processing* - applied before and after the channel application, namely

$$\mathcal{N}_c := \mathcal{U}_{\text{out}} \circ \mathcal{N} \circ \mathcal{U}_{\text{in}}\,. \tag{3.16}$$

Since unitary transformations leaves the Von Neumann entropy unaltered, there are no differences about the information-related properties between the channels $\mathcal{N}$ and $\mathcal{N}_c$.

A one-mode Guassian state, with density operator $\hat{\rho}$ is affected by a unitary transformation $\mathcal{U} : \hat{\rho} \mapsto \hat{U}\hat{\rho}\hat{U}^\dagger$, where $\hat{U}$ is a unitary operator. Up to this transformation, the covariance matrix σ representing $\hat{\rho}$ is mapped as becomes $S\sigma S^\dagger$, where S is a symplectic matrix. Therefore, by calling S_{in} and S_{out} the 2×2 symplectic matrices corresponding to $\mathcal{U}_{\text{in}}$ and $\mathcal{U}_{\text{out}}$, respectively, then the action of $\mathcal{N}_c$ on the input covariance matrix reads

$$\mathcal{N}_c : \sigma_{\text{in}} \mapsto \sigma_{\text{out}} = \mathbb{T}_c^T \sigma_{\text{in}} \mathbb{T}_c + \mathbb{N}_c\,; \quad \mathbb{T}_c = S_{\text{in}} \mathbb{T} S_{\text{out}}\,; \quad \mathbb{N}_c = S_{\text{out}}^T \mathbb{N} S_{\text{out}}\,. \tag{3.17}$$

Remarkably, both $\mathbb{T}_c$ and $\mathbb{N}_c$ become diagonal for an appropriate choice of S_{in} and S_{out} [157]. In particular, by noting the elements of the matrices $\mathbb{T}$ and $\mathbb{N}$ as $T_{\text{ij}} := (\mathbb{T})_{\text{ij}}$ and $N_{\text{ij}} := (\mathbb{N})_{\text{ij}}$, respectively, the following matrices

$$S_{\text{in}} = \frac{\sqrt[4]{W}}{\sqrt{N_{11}\tau}} \begin{pmatrix} \frac{N_{11}T_{22} - N_{12}T_{12}}{\sqrt{W}} & -T_{12} \\ \frac{N_{12}T_{11} - N_{11}T_{21}}{\sqrt{W}} & T_{11} \end{pmatrix}; \tag{3.18}$$

$$S_{\text{out}} = \frac{\sqrt[4]{W}}{\sqrt{N_{11}}} \begin{pmatrix} 1 & 0 \\ -\frac{N_{12}}{\sqrt{W}} & \frac{N_{11}}{\sqrt{W}} \end{pmatrix}, \tag{3.19}$$

allow a canonical form for $\mathcal{N}_{\mathrm{c}}$ so that[2]

$$\mathbb{T}_c = \sqrt{|\tau|}\mathbb{I}\,; \quad \mathbb{N}_c = \sqrt{W}\mathbb{I}\,. \tag{3.20}$$

Since one has $\det S = \pm 1$ for each symplectic matrix S, one has

$$\tau = \det \mathbb{T}\,, \quad W = \det \mathbb{N}\,. \tag{3.21}$$

The application of the canonical form of the original channel then reads

$$\mathcal{N}_{\mathrm{c}} : \sigma_{\mathrm{in}} \mapsto \sigma_{\mathrm{out}} = \tau\sigma_{\mathrm{in}} + \sqrt{W}\mathbb{I}. \tag{3.22}$$

The parameter τ, called *transmissivity*, indicates the fraction of input signal present on the output. If $0 \leq \tau \leq 1$, then τ is effectively a transmission coefficient. However, one can also have $\tau > 1$, in case of a *linear amplifier channel* or even $\tau < 0$ if the channel is a conjugate of the amplifier. The parameter W is instead related to the additive noise present on the output. In particular, one can identify $\overline{n}$ with the average number of noisy particles in the output state and it is related to W as

$$\overline{n} = \begin{cases} \frac{\sqrt{W}}{|1-\tau|} - \frac{1}{2} & \text{if} \quad \tau \neq 1\,, \\ \sqrt{W} & \text{otherwise}\,. \end{cases} \tag{3.23}$$

The requirement (3.15) to preserve the uncertainty principle on the output leads to $\overline{n} \geq 0$.

A one-mode Gaussian channel $\mathcal{N}$ is then characterized by just two parameters i.e.τ and W - alternatively τ and $\overline{n} \geq 0$. The communication properties of the channel are then expected to be proportional to only these two parameters.

3.1.3 Communication capacities of a quantum channel

In this section, the aim is to quantify how well a channel $\mathcal{N} : \hat{\rho}_{\mathrm{in}} \mapsto \hat{\rho}_{\mathrm{out}}$ transmits information. In fact, apart from the ideal situation where $\mathcal{N} = \mathrm{Id}$ and $\hat{\rho}_{\mathrm{in}} = \hat{\rho}_{\mathrm{out}}$, the channel becomes noisy and the information contained in $\hat{\rho}_{\mathrm{in}}$ is compromised while passing through the channel $\mathcal{N}$. In such cases, the conservation of information from $\hat{\rho}_{\mathrm{in}}$ to $\hat{\rho}_{\mathrm{out}}$ is now quantified.

The *capacities* of a channel $\mathcal{N}$ are quantities indicating the maximum rate of information that the channel can reliably transmit with a certain protocol. By taking into account that a quantum channel can transmit both classical and quantum information, one defines the *classical capacity* (resp. *quantum capacity*) of a channel $\mathcal{N}$ as the maximum rate of classical (quantum) information that $\mathcal{N}$ can transmit with arbitrarily low error. If a channel $\mathcal{N}$ has zero classical (quantum) capacity, then $\mathcal{N}$ cannot reliably transmit classical (quantum) information. As long as the capacity of $\mathcal{N}$ is non-zero, then $\mathcal{N}$ is potentially capable to transmit information reliably. However, to this purpose, more channel uses are required the less is the capacity - in practice, a reliable communication requires more time with a channel with a lower capacity. Therefore, the channel capacities measure the "quality" of the channel, i.e. its capabilities to transmit information.

[2]Some peculiar situations may involve $\mathbb{T}$ or $\mathbb{N}$ to have rank 1, so that $\mathbb{T} = \mathrm{diag}(0, \tau)$ or $\mathbb{N} = \mathrm{diag}(0, W)$. However, this situation is never met throughout the examined problems, so that this possibility is not taken into account.

3.1.3.1 Classical capacity

The classical capacity of a one-mode Gaussian channel $\mathcal{N}$, characterized by the parameters τ and $\overline{n}$, is now computed.

To send a classical message through a quantum channel, the sender (also called *Alice*) must first encode this message into a quantum state. A classical message x^n consists on n-realizations of a random variable X which may assume values $(x_1, \ldots, x_N)$ according to a probability distribution $(p_1, \ldots, p_N)$. In other words, a message is a sequence of letters $x^n = x_{\mathrm{i}_1} x_{\mathrm{i}_2} \ldots x_{\mathrm{i}_n}$ picked up with a probability $p_{x^n} = \prod_{\mathrm{j}=1}^{n} p_{\mathrm{i_j}}$. By performing the encoding procedure, Alice associates each message x^n to a quantum state $\hat{\rho}_{x^n}$ which is sent to the receiver (also called *Bob*) through n uses of the quantum channel. The receiver Bob, once achieved the output $\hat{\rho}_{y^n} = \mathcal{N}^{\otimes n}(\hat{\rho}_{x^n})$, decodes it to achieve the message y^n. The mutual information between the messages x^n and y^n - i.e. the information about a message one has by reading the other - depends on the encoding and decoding procedure. However, this mutual information is upper bounded by the Holevo information $\mathcal{X}$, reading [140]

$$\mathcal{X}(\{\hat{\rho}_{x^n}, p_{x^n}\}_{x^n}, \mathcal{N}^{\otimes n}) = S_{\mathrm{vN}}\left(\mathcal{N}^{\otimes n}\left(\sum_{x^n} p_{x^n}\hat{\rho}_{x^n}\right)\right) - S_{\mathrm{vN}}\left(\sum_{x^n} p_{x^n}\mathcal{N}^{\otimes n}(\hat{\rho}_{x^n})\right) . \tag{3.24}$$

The Holevo information (3.24) represents the maximum information about Alice's classical message achievable to Bob once passing through n uses of the channel $\mathcal{N}$. The classical capacity C is therefore obtained by considering whatever quantum channel uses and maximizing over the possible ensembles of states $\{\hat{\rho}_{x^n}, p_{x^n}\}_{x^n}$, namely

$$C(\mathcal{N}) = \lim_{n\to\infty} \frac{1}{n} \max_{\{\hat{\rho}_{x^n}, p_{x^n}\}} \mathcal{X}(\{\hat{\rho}_{x^n}, p_{x^n}\}, \mathcal{N}^{\otimes n}) \tag{3.25}$$

From Eq. (3.25), to optimize the rate of transmission one needs to use the channel $\mathcal{N}$ the more as possible. That is because the entanglement between different channels' inputs can be exploited to increase the rate of reliable information transmitted. If the states $\{\hat{\rho}_{x^n}\}_{x^n}$ are separable among all the channel uses input, then the classical capacity (3.25) simplifies to

$$C^{(1)}(\mathcal{N}) = \max_{\{p_x, \hat{\rho}_x\}} \mathcal{X}\left(\{p_x, \hat{\rho}_x\}, \mathcal{N}\right) , \tag{3.26}$$

which is called *product state classical capacity*, for the reasons just explained. Notice that Eq. (3.26) also corresponds to the classical capacity C by restricting ourselves to a single channel use. In this chapter, and in the next one, all the communication protocols studied involve situations where many channel uses are unrealistic or without any meaning in that context[3]. Therefore, the study is restricted to a single use of the quantum channel. The capacity of a channel to transmit classical information is evaluated via the product state classical capacity $C^{(1)}$ from (3.26). In general, one has $C^{(1)} \leq C$, where the equality holds if the channel is *entanglement-breaking*, i.e. if any entangled state becomes separable while passing through $\mathcal{N}^{\otimes 2}$.

A one-mode Gaussian channel $\mathcal{N}$ is now considered. As input, only one-mode Gaussian states are considered, which are the ones preserving better classical information according to a widely verified

[3]For example, in this chapter, the protocol consists on Alice sending her message from the remote past and Bob receives it in the remote future. In Chapter 4, instead, the channels used are not memoriless - i.e. each channel application would affect future channel applications. Therefore, studying the communication capacities of this channel over many channel uses effectively means to study a different channel than the one before.

conjecture [152, 150, 154]. Hence, by restricting to Gaussian inputs, the channel classical capacity is not affected.

According to Ref. [142], the single-letter random variable X preserving better its classical information, up to a Gaussian channel, is the one with a Gaussian probability distribution p_{i}, characterized by a classical covariance matrix σ_{enc} (*classical* means that the bound (3.7) is not applied to σ_{enc}). Moreover, the optimal encoding associates each realization of the random variable X, i.e. x_{i}, to one-mode Gaussian states with the same covariance matrix σ_{in} but different first moment $\mathbf{d}_{\mathrm{i}}$.

With this optimal setup, the Holevo information (3.24), relative to a channel $\mathcal{N}$ characterized with the matrices $\mathbb{T}$ and $\mathbb{N}$ becomes

$$\mathcal{X}(\sigma_{\mathrm{in}},\sigma_{\mathrm{enc}},\mathcal{N}) = \mathsf{S}_{\mathrm{vN}}\left(\mathbb{T}(\sigma_{\mathrm{in}}+\sigma_{\mathrm{enc}})\mathbb{T}^T+\mathbb{N}\right) - \mathsf{S}_{\mathrm{vN}}\left(\mathbb{T}\sigma_{\mathrm{in}}\mathbb{T}^T+\mathbb{N}\right) . \tag{3.27}$$

The Holevo information (3.27) can be arbitrarily high by increasing arbitrarily the diagonal elements of σ_{enc}. The classical capacity of a bosonic Gaussian channel is then always infinite[4]. However, a realistic scenario involves a limited number of resources at our disposal for the encoding. For example, one usually provides an upper bound $\overline{N}$ on the number of particles a bosonic mode can have. This leads to the condition

$$\frac{1}{2}\mathrm{Tr}\left(\sigma_{\mathrm{in}}+\sigma_{\mathrm{enc}}\right) - \frac{1}{2} \leq \overline{N} . \tag{3.28}$$

Another realistic limit would be on the energy E used for the encoding procedure. In this case, the condition the covariance matrices should respect is

$$\frac{1}{2}\mathrm{Tr}\left(\sigma_{\mathrm{in}}+\sigma_{\mathrm{enc}}\right) \leq \frac{E}{\omega_{\mathrm{i}}} , \tag{3.29}$$

where ω_{i} is the frequency associated with the mode i. The bounds (3.28) and (3.29) are analog by imposing

$$E = \omega_{\mathrm{i}}\left(\frac{1}{2}+\overline{N}\right) . \tag{3.30}$$

By optimizing the Holevo information (3.27) while respecting the bound (3.28) (resp. the bound (3.29)) one obtains the so called *bounded classical capacity* $C_{\overline{N}}$ (resp. C_E).

By reducing the channel in its canonical form (3.16), the input of the channel now becomes $S_{\mathrm{in}}(\sigma_{\mathrm{in}}+\sigma_{\mathrm{enc}})S_{\mathrm{in}}^T$ instead of $\sigma_{\mathrm{in}}+\sigma_{\mathrm{enc}}$. The particle and energy bounds (3.28) and (3.29), respectively, are then modified by performing an analog substitution[5]. The Holevo information (3.27) from the canonical reduction, becomes

$$\mathcal{X} = \mathsf{S}_{\mathrm{vN}}(\mathbb{T}_{\mathrm{c}}S_{\mathrm{in}}(\sigma_{\mathrm{in}}+\sigma_{\mathrm{enc}})S_{\mathrm{in}}^T\mathbb{T}_{\mathrm{c}}+\mathbb{N}_{\mathrm{c}}) - \mathsf{S}_{\mathrm{vN}}(\mathbb{T}_{\mathrm{c}}S_{\mathrm{in}}\sigma_{\mathrm{in}}S_{\mathrm{in}}^T\mathbb{T}_{\mathrm{c}}+\mathbb{N}_{\mathrm{c}}) . \tag{3.31}$$

To proceed with the optimization of Eq. (3.31), the *input purity theorem*, telling us that a pure input state maximizes the Holevo information [143], is invoked. Therefore, for the preprocessed input one has $S_{\mathrm{in}}\sigma_{\mathrm{in}}S_{\mathrm{in}}^T = 1/2\,\mathrm{diag}(J,J^{-1})$, with $J>0$. Moreover, for the preprocessed classical covariance matrix analogously $S_{\mathrm{in}}\sigma_{\mathrm{in}}S_{\mathrm{enc}}^\dagger = \mathrm{diag}(X,Y)$ with $X,Y>0$. In this way (3.31) becomes

$$\begin{aligned}\mathcal{X}(J,X,Y) =& h\left(\frac{1}{2}\sqrt{\left(\tau J+2\sqrt{W}+2\tau X\right)\left(\frac{\tau}{J}+2\sqrt{W}+2\tau Y\right)}\right)\\ &- h\left(\frac{1}{2}\sqrt{\left(\tau J+2\sqrt{W}\right)\left(\frac{\tau}{J}+2\sqrt{W}\right)}\right) .\end{aligned} \tag{3.32}$$

[4] This is a consequence of the bosonic statistics allowing each bosonic mode to host an infinite number of particles.

[5] This was not done in previous references for the computation of the bounded classical capacities [142, 143], where the optimization of the Holevo information was done by considering the pre-processing as part of the channel.

The energy bound (3.29) is used for the pre-processed input of the channel which reads - knowing that Eq. (3.30) is sufficient to switch to the bound (3.28) - together with the conditions on the parameters X and Y

$$\begin{cases} \frac{J}{2} + X + \frac{1}{2J} + Y \leq 2\frac{E}{\omega_{\mathrm{i}}}, \\ X > 0, \\ Y > 0. \end{cases} \tag{3.33}$$

Eq. (3.33) represent the conditions on the parameters X, Y and J required to optimize the Holevo information (3.32). To the first, the equality is imposed, so that as much energy as possible would be used. In this way, Y can be expressed in terms of X and J with the following

$$Y = 2\frac{E}{\omega_{\mathrm{A}}} - \frac{1}{2J} - \frac{J}{2} - X\,. \tag{3.34}$$

By putting Eq. (3.34) into Eq. (3.32), the maximization for X can be performed to obtain

$$X = \begin{cases} 0, & \text{if} \quad 2\frac{E}{\omega_{\mathrm{A}}} < J < 2\frac{E}{\omega_{\mathrm{A}}} + \sqrt{4\frac{E^2}{\omega_{\mathrm{A}}^2} - 1} \\ \frac{E}{\omega_{\mathrm{A}}} - \frac{J}{2}, & \text{if} \quad \frac{\omega_{\mathrm{A}}}{2E} < J < 2\frac{E}{\omega_{\mathrm{A}}}. \end{cases} \tag{3.35}$$

By putting Eq. (3.35) into Eq. (3.32), the latter is finally maximized by $J = 1$. In this way, the constrained classical capacity C_E can finally be written as

$$C_E(\mathcal{N}) = h\left(\frac{E}{\omega_{\mathrm{i}}}|\tau| + \sqrt{W}\right) - h\left(\frac{|\tau|}{2} + \sqrt{W}\right)\,. \tag{3.36}$$

3.1.3.2 Quantum capacity

The maximum amount of quantum information a channel $\mathcal{N}$ is able to reliably send is now investigated. To do that, a precise meaning to "quantum information" should be given first. By calling with $\mathcal{S}(\mathcal{H})$ the set of density operators on the Hilbert space $\mathcal{H}$, the *purification theorem* states that, for each quantum state $\hat{\rho} \in \mathcal{S}(\mathcal{H})$, another quantum state $\hat{\rho}_{\mathrm{R}} \in \mathcal{S}(\mathcal{H}_{\mathrm{R}})$ exists so that the state $|\Psi\rangle\langle\Psi| \coloneqq \hat{\rho} \otimes \hat{\rho}_{\mathrm{R}} \in \mathcal{S}(\mathcal{H} \times \mathcal{H}_{\mathrm{R}})$ is pure. The Hilbert space $\mathcal{H}_{\mathrm{R}}$ is called *reference system* and its dimension is the of $\mathcal{H}$. Therefore, if $\hat{\rho}$ is mixed, then the state $|\Psi\rangle$ is a maximally entangled state, whose entanglement entropy is given by $S_{\mathrm{vN}}(\hat{\rho})$. In other words, the amount of quantum information a state $\hat{\rho}$ has corresponds to the amount of entanglement it has with its purification $\hat{\rho}_R$.

To know how much entanglement with the reference is conserved after the application of a channel $\mathcal{N}$, the *coherent information* I_c is used, namely

$$I_c(\hat{\rho}, \mathcal{N}) = S_{\mathrm{vN}}(\mathcal{N}(\hat{\rho})) - S_{\mathrm{vN}}((\mathcal{N} \otimes \mathrm{Id})(|\Psi\rangle\langle\Psi|)) \tag{3.37}$$

By maximizing Eq. (3.37), one obtains the one-shot version of the quantum capacity $Q^{(1)}$. In particular, one has

$$Q^{(1)}(\mathcal{N}) = \max\{0, \max_{\hat{\rho}} I_c(\hat{\rho}, \mathcal{N})\}\,. \tag{3.38}$$

As for the case of the classical capacity, $Q^{(1)}$ from Eq. (3.38) can be generalize to consider arbitrary uses of the channel $\mathcal{N}$, to obtain the quantum capacity Q. However, for the reasons explained in Sec. 3.1.3.1, the focus is restricted exclusively on $Q^{(1)}$. Notice that, since $Q > Q^{(1)}$, proving that $Q^{(1)} > 0$ is sufficient to prove the possibility of communication of quantum messages.

In Sec. 3.1.3.1 it was found how the classical capacity of a one-mode Gaussian channel $\mathcal{N}$ is always infinite unless an upper bound for the amount of resources used for the state preparation (i.e. the encoding procedure) is not imposed. The same is not true for the quantum capacity: even by considering an infinite amount of particles on the input, the quantum capacity is usually finite - even null in some cases. In Refs. [141, 158], the coherent information (3.37) increases together with the amount of input particles, to reach a finite asymptotic value which, for a one-mode Gaussian channel $\mathcal{N}$ with transmissivity τ and average noisy particles $\overline{n}$, reads

$$\max_{\sigma} I_c(\sigma, \mathcal{N}) = \begin{cases} \theta(\tau) \log \frac{\tau}{|1-\tau|} - h\left(\frac{1}{2} + \overline{n}\right) & \text{if} \quad \tau \neq 1\,, \\ -1 - \log(\overline{n}) & \text{otherwise}\,. \end{cases} \tag{3.39}$$

The one-shot quantum capacity $Q^{(1)}$ is obtained by putting Eq. (3.39) into Eq. (3.38). In this way, $Q^{(1)} > 0$ if I_c is positive.

By comparing the one-shot quantum capacity, from Eq. (3.39) and (3.38), with the constrained classical capacity C_E in Eq. (3.36). While the classical capacity is zero only for *erasure channels* - namely with $\tau = 0$ - the quantum capacity has more restrictive conditions to be greater than zero. This expresses the fact that, while classical information could always be sent reliably by putting enough energy on the input, the possibility of reliably transmitting quantum information has more profound and intrinsic limitations.

For example, since h is definite positive, from Eq. (3.39) a necessary - but not sufficient - condition to have $Q^{(1)} \neq 0$ is that $\tau > 1/2$. This is an implication of the *no-cloning theorem* [159]. In fact, if $\mathcal{N}$ has $\tau < 1/2$ and can reliably transmit quantum information to the receiver Bob, then a third part - called *Eve* - would extract the rest of the signal which did not arrive to Bob. The transmissivity of the channel from Alice to Eve - i.e. the *complementary channel* of $\mathcal{N}$ - would have $\tau > 1/2$. Since Eve would receive more portion of the signal than Bob, Alice's quantum state is transmitted reliably also to Eve, meaning that this state has been cloned.

3.1.4 Two-modes Gaussian states

To define the entanglement entropy between two different bosonic modes, then the properties of two-modes Gaussian states are briefly explained.

By labeling the two modes with i and j and by invoking the parameters defined before Eq. (3.12), the generic covariance matrix for a two-modes Gaussian state reads

$$\sigma = \begin{pmatrix} \frac{1}{2} + n_{\mathrm{i}} + \Re m_{\mathrm{i}} & \Im m_{\mathrm{i}} & \Re\gamma_{\mathrm{ij}} + \Re\chi_{\mathrm{ij}} & \Im\gamma_{\mathrm{ij}} + \Im\chi_{\mathrm{ij}} \\ \Im m_{\mathrm{i}} & \frac{1}{2} + n_{\mathrm{i}} - \Re m_{\mathrm{i}} & -\Im\gamma_{\mathrm{ij}} + \Im\chi_{\mathrm{ij}} & \Re\gamma_{\mathrm{ij}} - \Re\chi_{\mathrm{ij}} \\ \Re\gamma_{\mathrm{ij}} + \Re\chi_{\mathrm{ij}} & -\Im\gamma_{\mathrm{ij}} + \Im\chi_{\mathrm{ij}} & \frac{1}{2} + m_{\mathrm{j}} + \Re m_{\mathrm{j}} & \Im m_{\mathrm{j}} \\ \Im\gamma_{\mathrm{ij}} + \Im\chi_{\mathrm{ij}} & \Re\gamma_{\mathrm{ij}} - \Re\chi_{\mathrm{ij}} & \Im m_{\mathrm{j}} & \frac{1}{2} + m_{\mathrm{j}} - \Re m_{\mathrm{j}} \end{pmatrix}. \tag{3.40}$$

The two symplectic eigenvalues ν_+ and ν_- of the covariance matrix (3.40) are provided in literature (see e.g. [160]) and they read

$$\nu_{\pm} = \frac{1}{\sqrt{2}} \sqrt{\Gamma \pm \sqrt{\Gamma^2 - 4 \det \sigma}}\,. \tag{3.41}$$

where $\Gamma := \nu_{\mathrm{i}}^2 + \nu_{\mathrm{j}}^2 + 2\left(|\gamma_{\mathrm{ij}}|^2 - |\chi_{\mathrm{ij}}|^2\right)$, and ν_{i} (ν_{j}) is the symplectic eigenvalue of the 2×2 covariance matrix of the single mode i (j), which simply reads

$$\nu_{\mathrm{i}} = \sqrt{\det \sigma_{\mathrm{ii}}}\,. \tag{3.42}$$

The Von Neumann entropy of the two mode Gaussian state is hence given by

$$\mathsf{S}_{\mathrm{vN}}(\sigma) = h(\nu_-) + h(\nu_+)\,. \tag{3.43}$$

If a state is maximally entangled, then its entropy (3.43) is zero and a straightforward measurement for the entanglement is the entropy of the entangled substates, also called *entanglement entropy.* A maximally entangled two-modes Gaussian state occurs when $n_{\mathrm{i}} = n_{\mathrm{j}}$, $m_{\mathrm{i}} = m_{\mathrm{j}} = 0$, $\gamma_{\mathrm{ij}} = 0$ and $|\chi_{\mathrm{ij}}| = \sqrt{n_{\mathrm{i}}(n_{\mathrm{i}}+1)}$. Its covariance matrix reads

$$\sigma = \left(\begin{array}{c|c} \left(\frac{1}{2}+n_{\mathrm{i}}\right)\mathbb{I}_{2\times 2} & \sqrt{n_{\mathrm{i}}(n_{\mathrm{i}}+1)}R(\theta) \\ \hline \sqrt{n_{\mathrm{i}}(n_{\mathrm{i}}+1)}R(\theta) & \left(\frac{1}{2}+n_{\mathrm{i}}\right)\mathbb{I}_{2\times 2} \end{array}\right) \tag{3.44}$$

where θ is the phase of χ_{ij} and

$$R(\theta) = \begin{pmatrix} \cos\theta & \sin\theta \\ \sin\theta & -\cos\theta \end{pmatrix}\,. \tag{3.45}$$

The entanglement entropy S_{E} of a state represented by the covariance matrix (3.44) corresponds to the Von Neumann entropy of the one-mode subsystem i (or j). From Eqs. (3.42) and (3.9) one has

$$\mathsf{S}_{\mathrm{E}}(\sigma) = h\left(\frac{1}{2}+n_{\mathrm{i}}\right)\,, \tag{3.46}$$

and it is proportional on the average number of entangled particles n_{i}.

3.2 Information and entanglement under a Bogoliubov transformation

From the definition of Eq. (3.6), a covariance matrix is defined via expectation values of coupled bosonic operators. Since a Bogoliubov transformation changes the set of bosonic operators from $\{\hat{a}_{\mathbf{k}}, \hat{a}^\dagger_{\mathbf{k}}\}_{\mathbf{k}}$ to $\{\hat{b}_{\mathbf{k}}, \hat{b}^\dagger_{\mathbf{k}}\}_{\mathbf{k}}$ - according to Eq. (2.20) - then also the covariance matrix is expected to change as well. Moreover, since a Bogoliubov transformation (2.20) is linear, the Gaussianity of the characteristic function of a bosonic state is preserved. A Bogoliubov transformation then acts as a Gaussian channel, whose properties are studied in this section.

In this framework, $\mathbf{k}$ is initially considered to be a discrete index instead of a vector of continuous variables, for the sake of simplicity. In this case, the expressions provided in chapter 2 still hold by replacing the integral in $d\mathbf{k}$ with sums over $\mathbf{k}$ and the Dirac deltas like $\delta^{(3)}(\mathbf{k}-\mathbf{k}')$ with Kronecker deltas $\delta_{\mathbf{k}\mathbf{k}'}$.

Up to Bogoliubov transformation, a covariance matrix (3.5) will stay the same up to the substitution of the operators $\{\hat{b}_{\mathbf{k}}, \hat{b}^\dagger_{\mathbf{k}}\}_{\mathbf{k}}$ replacing the old ones $\{\hat{a}_{\mathbf{k}}, \hat{a}^\dagger_{\mathbf{k}}\}_{\mathbf{k}}$. In particular, by using the discrete mode version of Eq. (2.20) the elements $\langle \hat{a}^\dagger_{\mathbf{k}}\hat{a}_{\mathbf{k}'}\rangle$ and $\langle \hat{a}_{\mathbf{k}}\hat{a}_{\mathbf{k}'}\rangle$ appearing of the covariance matrix (3.5), up to a Bogoliubov transformation, become

$$\langle \hat{b}^\dagger_{\mathbf{k}}\hat{b}_{\mathbf{k}'}\rangle = \sum_{\mathbf{pq}} \left(\alpha_{\mathbf{kp}}\alpha^*_{\mathbf{k}'\mathbf{q}}\langle \hat{a}^\dagger_{\mathbf{p}}\hat{a}_{\mathbf{q}}\rangle - \alpha_{\mathbf{kp}}\beta^*_{\mathbf{k}'\mathbf{q}}\langle \hat{a}^\dagger_{\mathbf{p}}\hat{a}^\dagger_{\mathbf{q}}\rangle - \beta_{\mathbf{kp}}\alpha^*_{\mathbf{k}'\mathbf{q}}\langle \hat{a}_{\mathbf{p}}\hat{a}_{\mathbf{q}}\rangle + \beta_{\mathbf{kp}}\beta^*_{\mathbf{k}'\mathbf{q}}\langle \hat{a}_{\mathbf{p}}\hat{a}^\dagger_{\mathbf{q}}\rangle\right)\,. \tag{3.47}$$

$$\langle \hat{b}_{\mathbf{k}}\hat{b}_{\mathbf{k}'}\rangle = \sum_{\mathbf{pq}} \left(\alpha^*_{\mathbf{kp}}\alpha^*_{\mathbf{k}'\mathbf{q}}\langle \hat{a}_{\mathbf{p}}\hat{a}_{\mathbf{q}}\rangle - \alpha^*_{\mathbf{kp}}\beta^*_{\mathbf{k}'\mathbf{q}}\langle \hat{a}_{\mathbf{p}}\hat{a}^\dagger_{\mathbf{q}}\rangle - \beta^*_{\mathbf{kp}}\alpha^*_{\mathbf{k}'\mathbf{q}}\langle \hat{a}^\dagger_{\mathbf{p}}\hat{a}_{\mathbf{q}}\rangle + \beta^*_{\mathbf{kp}}\beta^*_{\mathbf{k}'\mathbf{q}}\langle \hat{a}^\dagger_{\mathbf{p}}\hat{a}^\dagger_{\mathbf{q}}\rangle\right)\,. \tag{3.48}$$

The parameters $n_{\mathbf{k}}$, $m_{\mathbf{k}}$, $\gamma_{\mathbf{kk}'}$ and $\chi_{\mathbf{kk}'}$, defined above Eq. (3.12) become

$$\begin{aligned}\tilde{n}_{\mathbf{k}} := \langle \hat{b}_{\mathbf{k}}^{\dagger}\hat{b}_{\mathbf{k}}\rangle = & \sum_{\mathbf{p}}\left(|\alpha_{\mathbf{kp}}|^2 n_{\mathbf{p}} - 2\Re\left(\alpha_{\mathbf{kp}}^*\beta_{\mathbf{kp}}m_{\mathbf{p}}\right) + |\beta_{\mathbf{kp}}|^2(1+n_{\mathbf{p}})\right) \\ & + \sum_{\mathbf{p}\neq\mathbf{q}}\left(\alpha_{\mathbf{kp}}\alpha_{\mathbf{kq}}^*\gamma_{\mathbf{pq}} - \alpha_{\mathbf{kp}}\beta_{\mathbf{kq}}^*\chi_{\mathbf{pq}}^* - \beta_{\mathbf{kp}}\alpha_{\mathbf{kq}}^*\chi_{\mathbf{pq}} + \beta_{\mathbf{kp}}\beta_{\mathbf{kq}}^*\gamma_{\mathbf{pq}}^*\right)\,;\end{aligned} \tag{3.49}$$

$$\begin{aligned}\tilde{m}_{\mathbf{k}} := \langle \hat{b}_{\mathbf{k}}\hat{b}_{\mathbf{k}}\rangle = & \sum_{\mathbf{p}}\left(\alpha_{\mathbf{kp}}^{*2} m_{\mathbf{p}} - \alpha_{\mathbf{kp}}^*\beta_{\mathbf{kp}}^*(1+2n_{\mathbf{p}}) + \beta_{\mathbf{kp}}^{*2}m_{\mathbf{p}}^*\right) \\ & + \sum_{\mathbf{p}\neq\mathbf{q}}\left(\alpha_{\mathbf{kp}}^*\alpha_{\mathbf{kq}}^*\chi_{\mathbf{pq}} - \alpha_{\mathbf{kp}}^*\beta_{\mathbf{kq}}^*\gamma_{\mathbf{pq}}^* - \beta_{\mathbf{kp}}^*\alpha_{\mathbf{kq}}^*\gamma_{\mathbf{pq}} + \beta_{\mathbf{kp}}^*\beta_{\mathbf{kq}}^*\chi_{\mathbf{pq}}^*\right)\,;\end{aligned} \tag{3.50}$$

$$\begin{aligned}\tilde{\gamma}_{\mathbf{kk}'} := \langle \hat{b}_{\mathbf{k}}^{\dagger}\hat{b}_{\mathbf{k}'}\rangle = & \sum_{\mathbf{p}}\left(\alpha_{\mathbf{kp}}\alpha_{\mathbf{k}'\mathbf{p}}^* n_{\mathbf{p}} - \alpha_{\mathbf{kp}}\beta_{\mathbf{k}'\mathbf{p}}^* m_{\mathbf{p}}^* - \alpha_{\mathbf{kp}}^*\beta_{\mathbf{k}'\mathbf{p}}m_{\mathbf{p}} + \beta_{\mathbf{kp}}\beta_{\mathbf{k}'\mathbf{p}}^*(1+n_{\mathbf{p}})\right) \\ & + \sum_{\mathbf{p}\neq\mathbf{q}}\left(\alpha_{\mathbf{kp}}\alpha_{\mathbf{k}'\mathbf{q}}^*\gamma_{\mathbf{pq}} - \alpha_{\mathbf{kp}}\beta_{\mathbf{k}'\mathbf{q}}^*\chi_{\mathbf{pq}}^* - \beta_{\mathbf{kp}}\alpha_{\mathbf{k}'\mathbf{q}}^*\chi_{\mathbf{pq}} + \beta_{\mathbf{kp}}\beta_{\mathbf{k}'\mathbf{q}}^*\gamma_{\mathbf{pq}}^*\right)\,;\end{aligned} \tag{3.51}$$

$$\begin{aligned}\tilde{\chi}_{\mathbf{kk}'} := \langle \hat{b}_{\mathbf{k}}\hat{b}_{\mathbf{k}'}\rangle = & \sum_{\mathbf{p}}\left(\alpha_{\mathbf{kp}}^*\alpha_{\mathbf{pk}'}^* m_{\mathbf{p}} - \alpha_{\mathbf{kp}}^*\beta_{\mathbf{k}'\mathbf{p}}^*(1+n_{\mathbf{p}}) - \beta_{\mathbf{kp}}^*\alpha_{\mathbf{k}'\mathbf{p}}^* n_{\mathbf{p}} + \beta_{\mathbf{kp}}^*\beta_{\mathbf{k}'\mathbf{p}}^* m_{\mathbf{p}}^*\right) \\ & + \sum_{\mathbf{p}\neq\mathbf{q}}\left(\alpha_{\mathbf{kp}}^*\alpha_{\mathbf{k}'\mathbf{q}}^*\chi_{\mathbf{pq}} - \alpha_{\mathbf{kp}}^*\beta_{\mathbf{k}'\mathbf{q}}^*\gamma_{\mathbf{pq}}^* - \beta_{\mathbf{kp}}^*\alpha_{\mathbf{k}'\mathbf{q}}^*\gamma_{\mathbf{pq}} + \beta_{\mathbf{kp}}^*\beta_{\mathbf{k}'\mathbf{q}}^*\chi_{\mathbf{pq}}^*\right)\,.\end{aligned} \tag{3.52}$$

By considering the vacuum as initial state, i.e. $n_{\mathbf{k}} = m_{\mathbf{k}} = \gamma_{\mathbf{kk}'} = \chi_{\mathbf{kk}'} = 0$ for each $\mathbf{k}$ and $\mathbf{k}'$, then the state created by a Bogoliubov transformation is

$$\tilde{n}_{\mathbf{k}} = \sum_{\mathbf{p}} |\beta_{\mathbf{kp}}|^2\,; \tag{3.53}$$

$$\tilde{m}_{\mathbf{k}} = -\sum_{\mathbf{p}} \alpha_{\mathbf{kp}}^*\beta_{\mathbf{kp}}^*\,; \tag{3.54}$$

$$\tilde{\gamma}_{\mathbf{kp}} = \sum_{\mathbf{q}} \beta_{\mathbf{kq}}\beta_{\mathbf{pq}}^*\,; \tag{3.55}$$

$$\tilde{\chi}_{\mathbf{kp}} = -\sum_{\mathbf{q}} \alpha_{\mathbf{kq}}^*\beta_{\mathbf{pq}}^*\,. \tag{3.56}$$

3.2.1 Bogoliubov transformation as one-mode Gaussian channel

The evolution of an N-mode Gaussian state up to a Bogoliubov transformation is entirely given by the modification of the parameters $n_{\mathbf{k}}$, $m_{\mathbf{k}}$, $\gamma_{\mathbf{kk}'}$ and $\chi_{\mathbf{kk}'}$ given by Eqs. (3.49), (3.50), (3.51) and (3.52), respectively.

The Bogoliubov transformation of one-mode Gaussian states is now addressed, whose general properties were examined in Sec. 3.1.2. By calling $\mathbf{k}$ the single mode whose evolution is studied, the other modes $\mathbf{k}' \neq \mathbf{k}$ - also called *environment modes* - are supposed to be in the vacuum. Up to a Bogoliubov transformation, the output covariance matrix σ_{out} is related to σ_{in} through Eq. (3.14). One can explicitly compute the matrices $\mathbb{T}$ and $\mathbb{N}$ to get

$$\mathbb{T} = \begin{pmatrix} \Re\left(\alpha_{\mathbf{kk}} - \beta_{\mathbf{kk}}\right) & \Im\left(\alpha_{\mathbf{kk}} + \beta_{\mathbf{kk}}\right) \\ -\Im\left(\alpha_{\mathbf{kk}} - \beta_{\mathbf{kk}}\right) & \Re\left(\alpha_{\mathbf{kk}} + \beta_{\mathbf{kk}}\right)\end{pmatrix}\,. \tag{3.57}$$

$$\mathbb{N} = \begin{pmatrix} \frac{1}{2}\sum_{\mathbf{k}'\neq\mathbf{k}} |\alpha_{\mathbf{kk}'}^* - \beta_{\mathbf{kk}'}|^2 & \sum_{\mathbf{k}'\neq\mathbf{k}} \Im(\alpha_{\mathbf{kk}'}\beta_{\mathbf{kk}'}) \\ \sum_{\mathbf{k}'\neq\mathbf{k}} \Im(\alpha_{\mathbf{kk}'}\beta_{\mathbf{kk}'}) & \frac{1}{2}\sum_{\mathbf{k}'\neq\mathbf{k}} |\alpha_{\mathbf{kk}'}^* + \beta_{\mathbf{kk}'}|^2\end{pmatrix}\,. \tag{3.58}$$

The transmissivity τ and the noise $\overline{n}$ follow as

$$\tau = |\alpha_{\mathbf{kk}}|^2 - |\beta_{\mathbf{kk}}|^2 \,. \tag{3.59}$$

$$\overline{n} = \begin{cases} \sqrt{B^2 - C^2} & \text{if} \quad \tau = 1\,; \\ \frac{1}{2}\left(-1 + \sqrt{1 + 4\frac{B}{1-\tau} + 4\frac{B^2-C^2}{(1-\tau)^2}}\right) & \text{otherwise}\,, \end{cases} \tag{3.60}$$

where $B := (N_{\mathbf{k}} - |\beta_{\mathbf{kk}}|^2)$ and $C := \left|\sum_{\mathbf{k}'\neq\mathbf{k}} \alpha_{\mathbf{kk}'}\beta_{\mathbf{kk}'}\right|$ and $N_{\mathbf{k}} := \sum_{\mathbf{k}'} |\beta_{\mathbf{k}'\mathbf{k}}|^2$ is the number of particles created from vacuum.

3.2.2 Continuous modes limit

Instead of considering $\mathbf{k}$ as a discrete index, the case where $\mathbf{k} \in \mathbb{R}^n$ is now investigated. In particular, in an $(n+1)$D spacetime, $\mathbf{k}$ can represent the momentum of a normal mode in absence of curvature - as in Chapter 2 for $n = 3$.

As in the discrete case, only particles in the mode $\mathbf{k}$ are present while all the others - i.e. the environment modes - are in vacuum. To represent this situation in the continuous limit one has

$$\langle \hat{a}^\dagger_{\mathbf{p}}\hat{a}_{\mathbf{q}}\rangle = \nu_{\mathbf{k}}\delta^n(\mathbf{k}-\mathbf{p})\delta^n(\mathbf{k}-\mathbf{q})\,; \quad \langle \hat{a}_{\mathbf{p}}\hat{a}_{\mathbf{q}}\rangle = \mu_{\mathbf{k}}\delta^n(\mathbf{k}-\mathbf{p})\delta^n(\mathbf{k}-\mathbf{q})\,. \tag{3.61}$$

By putting Eq. (3.61) into Eq. (3.11), the one-mode input covariance matrix turns out to be

$$\sigma_{\mathbf{kk}} = \begin{pmatrix} \frac{\delta^n(0)}{2} + \nu_{\mathbf{k}}\delta^{2n}(0) + \Re\mu_{\mathbf{k}}\delta^{2n}(0) & \Im\mu_{\mathbf{k}}\delta^{2n}(0) \\ \Im\mu_{\mathbf{k}}\delta^{2n}(0) & \frac{\delta^n(0)}{2} + \nu_{\mathbf{k}}\delta^{2n}(0) - \Re\mu_{\mathbf{k}}\delta^{2n}(0) \end{pmatrix}\,. \tag{3.62}$$

After a Bogoliubov transformation, $\langle \hat{a}^\dagger_{\mathbf{k}}\hat{a}_{\mathbf{k}}\rangle = \delta^{2n}(0)\nu_{\mathbf{k}}$ and $\langle \hat{a}_{\mathbf{k}}\hat{a}_{\mathbf{k}}\rangle = \delta^{2n}(0)\mu_{\mathbf{k}}$, from Eqs. (3.47) and (3.48) in the continuous case, become respectively

$$\langle \hat{b}^\dagger_{\mathbf{k}}\hat{b}_{\mathbf{k}}\rangle = \nu_{\mathbf{k}}|\alpha_{\mathbf{kk}}|^2 - \Re(\alpha^*_{\mathbf{kk}}\beta_{\mathbf{kq}}\mu_{\mathbf{k}}) + \nu_{\mathbf{k}}|\beta_{\mathbf{kk}}|^2 + N_{\mathbf{k}}\,. \tag{3.63}$$

$$\langle \hat{b}_{\mathbf{k}}\hat{b}_{\mathbf{k}}\rangle = \alpha^{*2}_{\mathbf{kk}}\mu_{\mathbf{k}} - \int d\mathbf{p}\alpha^*_{\mathbf{kp}}\beta^*_{\mathbf{kp}} - 2\alpha^*_{\mathbf{kk}}\beta^*_{\mathbf{kk}}\nu_{\mathbf{k}} + \beta^{*2}_{\mathbf{kk}}\mu_{\mathbf{k}}\,. \tag{3.64}$$

By repeating the same calculations of Sec. 3.2.1, the Bogoliubov transformation of a one-mode continuous bosonic mode is still a one-mode Gaussian channel with transmissivity

$$\tau = \frac{|\alpha_{\mathbf{kk}}|^2 - |\beta_{\mathbf{kk}}|^2}{\delta^{2n}(0)}\,. \tag{3.65}$$

and additive noise still given by Eq. (3.60) but where the parameters B and C become respectively

$$B = \frac{N_{\mathbf{k}}}{\delta^n(0)} - \frac{\beta_{\mathbf{kk}}}{\delta^{2n}(0)}\,; \quad C = \frac{1}{\delta^n(0)}\int d\mathbf{k}'\alpha_{\mathbf{kk}'}\beta_{\mathbf{kk}'} - \frac{\alpha_{\mathbf{kk}}\beta_{\mathbf{kk}}}{\delta^{2n}(0)}\,. \tag{3.66}$$

Despite the many divergences on Eqs. (3.65) and (3.66), those often cancel out with other divergences appearing on the Bogoliubov coefficients - which, as proved in Chapter 2, are pretty common in the continuous limit.

3.3 Information and entanglement under a cosmological expansion

The machinery introduced in Sec. 3.2 is now applied to cosmological expansions, whose particle production was extensively studied in Sec. 2.2. The capacity of the resulting channel tells how much information is preserved from particles existing in an epoch prior to the expansion. This could be crucial for the investigation of the *early Universe* whose observations done in the current epoch could provide vital information and boundaries to early Universe's models, leading to a wider and clearer vision on the history of our Universe year by year [161].

The protocol involves an input one-mode Gaussian state represented by σ_{in}, with momentum $\mathbf{k}$, prepared before a cosmological expansion. After it, the state's covariance matrix is σ_{out}, related to σ_{in} through Eq. (3.14). By putting Eq. (2.36) into Eqs. (3.65) and (3.66), the parameters τ and $\overline{n}$ are

$$\tau = 1 + N_k\,; \quad \overline{n} = 0\,. \tag{3.67}$$

Therefore, when acting on a single mode, a cosmological expansion is an *amplifier quantum channel.* The amplification is provided by the particle production N_k and proportional to it. Interestingly, the particles produced by a cosmological expansion do not simply add to the pre-existing particles. In fact, from n_k initial particles, after the expansion, from Eq. (3.63), one has a number of particles given by

$$\tilde{n}_k = N_k + (1 + N_k) n_k\,. \tag{3.68}$$

Therefore, after the expansion, new $(1 + n_k)N_k$ are added to the pre-existing mode. This has a profound mathematical implication on the non-additivity of the particle production. In other words, the particles produced by Bogoliubov transformation do not simply add to pre-existing particles, but they could interact with them by affecting their number and their behaviour.

To this perspective, the number of particles created by a cosmological expansion could be way higher than expected, if particles in the same mode are present also before the expansion. This fact can open the possibility of an observation of the cosmological particle production, even if N_k is usually infinitesimal [60].

The particle-bounded classical capacity C_E and the quantum capacity Q of a cosmological expansion, producing N_k particles from vacuum, are respectively

$$C_{\overline{N}} = h\left(\frac{1}{2} + \overline{N} + N_k + \overline{N} N_k\right) - h\left(\frac{1}{2} + N_k\right) \tag{3.69}$$

$$Q = \log\left(\frac{N_k + 1}{N_k}\right) \tag{3.70}$$

Their plots is shown in Fig. 3.1. When $N_k = 0$, $C_{\overline{N}}$ becomes $h(\frac{1}{2} + E)$ and decreases to $\log(1 + E)$ as $N_k \to \infty$. Instead, from Fig. 3.1, the quantum capacity Q is infinite when $N_k = 0$ - with no surprise, since $\mathcal{N}$ becomes the identity Id in that case - and drops to zero as N_k^{-1} as $N_k \to \infty$.

The two capacities have a distinct behaviour when the cosmological particle production N_k is high. Namely, the quantum capacity becomes very small while the classical one approaches a finite value. This difference lies in how particle production affects information transmission: while it amplifies the input signal rather than adding noise, the classical information (bit content) of the signal remains recoverable under amplification. Conversely, quantum information - i.e. the correlations

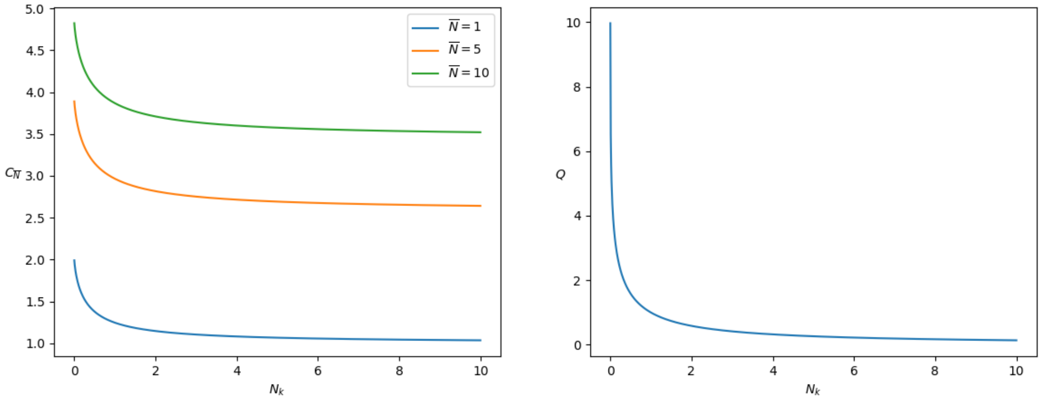

Figure 3.1: The channel capacities of a cosmological expansion in terms of the particles produced N_k. The left figure shows the particle-bounded classical capacity, obtained by putting Eq. (3.30) into Eq. (3.69). The right figure shows the quantum capacity, obtained from Eq. (3.70).

between the input and reference systems - is entirely lost, overwhelmed by the amplification of the input state [160].

Since cosmological particle production is usually very small - i.e. $N_k \sim 10^{-25}$ [60], one also expects the loss of information to be negligible. This is true when considering classical information. In fact, from Eq. (3.69) if $N_k \ll 1$, the bounded classical capacity deviates by the term $N_k \log N_k$ from its value when $N_k \to 0$. The capabilities of transmitting classical information are then practically unaffected by the cosmological particle production as long as $N_k \ll 1$.

Regarding the transmission of quantum information, instead, even an infinitesimal particle production N_k can provide a considerable bound on the amount of qubits reliably transmissible. From Fig. 3.2, even a particle production $\sim 10^{-30}$ involves a limited quantum capacity Q, i.e. a limited number of qubits, i.e. ~ 96 one can reliably transmit. If future technologies allows the communication of hundred of qubits via spatial probes, the limit given by the particle production would constitute a fundamental upper bound one has to take into account [162].

From an cosmological perspective, this model constrains the retrievable information from the recombination epoch encoded in the Cosmic Microwave Background [163], as well as information about the early universe accessible via primordial gravitational waves from inflation [164]. From this perspective, recent observational results are particularly promising for testing the model's predictions [36]

Finally, it is worth comparing this result with the case studied in Ref. [165], where qubit states are communicated through an expanding universe instead of bosonic states. There, the transmissivity turned out to be $\tau < 1$, giving an amplitude damping channel. This is probably due to the different statistics involving bosonic systems and qubit systems, since a qubit cannot be "amplified". However, the damping of a qubit with momentum k - i.e. its information loss - is proportional to the amount of particles produced in the mode k by the cosmological expansion. Therefore, as in the bosonic case, also qubit systems' information is better preserved by minimizing particle production.

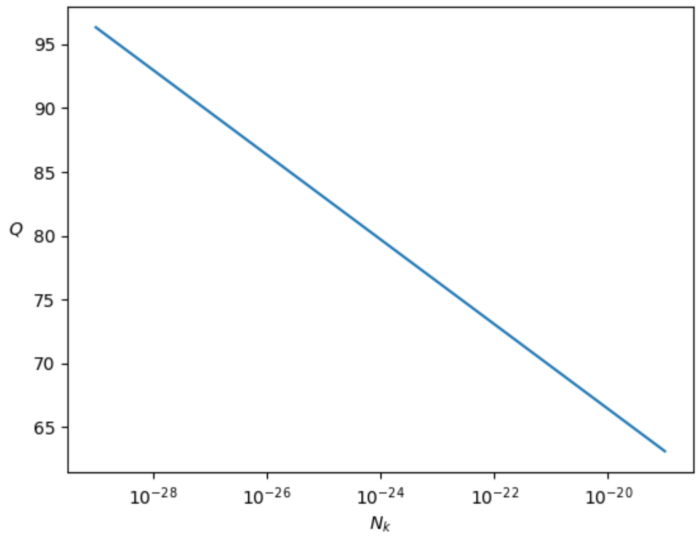

Figure 3.2: Quantum capacity of a cosmological expansion for a very small cosmological particle production, namely $N_k \ll 1$.

3.3.1 Preserving information in a modified theory of gravity

While General Relativity stands as an elegant and experimentally successful theory of gravitation, a variety of theoretical arguments and observational challenges motivate efforts to extend or modify Einstein's framework [12, 13, 14, 15]. Such modifications are particularly relevant when exploring regimes of extremely strong gravitational fields—where the predictions of General Relativity may no longer hold [166, 167]—and in cosmology, where the nature of dark energy and dark matter remains unresolved [168, 169].

Among these alternatives, a recently developed approach, called *symmetric teleparallel gravity* (or STEGR, for brevity), describes cosmic dynamics without imposing the metricity condition [170]. In other words, the connection described by the covariant derivatives ∇_α should no more satisfy the condition $\nabla_\alpha g_{\mu\nu} = 0$, but more generally

$$\nabla_\alpha g_{\mu\nu} = \mathsf{Q}_{\alpha\mu\nu} \,, \tag{3.71}$$

where $\mathsf{Q}_{\alpha\mu\nu}$ is called *non-metricity tensor*. In particular, with a peculiar choice for $\mathsf{Q}_{\alpha\mu\nu}$, one can obtain a STEGR theory equivalent to General Relativity even by neglecting the spacetime curvature. In other words, gravity as predicted by a curved spacetime can predicted as well by a flat, torsionless but non-metric spacetime. To reproduce a curved background with scalar curvature R, the non-metricity tensor must follow [171, 172]

$$R = -\mathsf{Q} - \mathcal{D}_\alpha(\mathsf{Q}^\alpha - \tilde{\mathsf{Q}}^\alpha) \,, \tag{3.72}$$

where ∇_α is the covariant derivative w.r.t. the Levi-Civita connection - i.e. the one leading to $\mathcal{D}_\alpha g_{\mu\nu} = 0$, $\mathsf{Q}^\alpha = \mathsf{Q}^{\alpha\lambda}_\lambda$ and $\tilde{\mathsf{Q}}^\alpha = \mathsf{Q}^{\lambda\alpha}_\lambda$, having

$$\mathsf{Q} = \frac{1}{4}\mathsf{Q}_{\alpha\beta\gamma}\mathsf{Q}^{\alpha\beta\gamma} - \frac{1}{2}\mathsf{Q}_{\alpha\beta\gamma}\mathsf{Q}^{\beta\alpha\gamma} - \frac{1}{4}\mathsf{Q}_\alpha\mathsf{Q}^\alpha + \frac{1}{2}\tilde{\mathsf{Q}}_\alpha\tilde{\mathsf{Q}}^\alpha \,, \tag{3.73}$$

In this way, the Einstein-Hilbert action (2.13) - with no matter or cosmological constant - becomes

$$S_{\text{STEGR}} = -\frac{1}{2}\int d^4x\sqrt{-g}\mathsf{Q}\,. \tag{3.74}$$

Lastly, it is worth reminding that the covariant derivative ∇_α defining $\mathsf{Q}_{\alpha\mu\nu}$ from Eq. (3.71) is not unique. Then, there is a gauge freedom on the connections. Among all, the so-called *coincident gauge* is particularly useful for our purposes. With this gauge choice, the connection vanishes globally and therefore the non-metricity tensor can be expressed via partial derivatives, i.e. [173, 174] through

$$\frac{1}{2}g^{\alpha\lambda}\left(g_{\lambda\nu,\mu}+g_{\mu\lambda,\nu}-g_{\mu\nu,\lambda}\right)=\frac{1}{2}g^{\alpha\lambda}\left(\mathsf{Q}_{\mu\alpha\nu}+\mathsf{Q}_{\nu\alpha\mu}-\mathsf{Q}_{\alpha\mu\nu}\right)\,. \tag{3.75}$$

The non-metricity scalar Q, with this gauge choice reads [175, 176, 177]

$$\mathsf{Q}=-g^{\mu\nu}\left(\left\{{}^{\alpha}_{\beta\mu}\right\}\left\{{}^{\beta}_{\nu\alpha}\right\}-\left\{{}^{\alpha}_{\beta\alpha}\right\}\left\{{}^{\beta}_{\mu\nu}\right\}\right)\,. \tag{3.76}$$

In the coincident gauge, the non-metricity scalar Q assumes a very simple form in the FLRW metric. In particular, by putting Eq. (2.25) into Eq. (3.76), one has

$$\mathsf{Q}=6\left(\frac{\dot a}{a}\right)^2=6H^2\,. \tag{3.77}$$

The behaviour of a scalar field $\hat\Phi$ in the STREGR theory of gravity is now investigated. To do that, a Yukawa-like interaction between the field and the non-metricity scalar Q is assumed (as occurs in general relativity with the scalar curvature R - see Eq. (2.15)), i.e.

$$\mathcal{L}_\Phi=-\frac{1}{2}\left(g^{\mu\nu}\partial_\mu\Phi\partial_\nu\Phi+m^2\Phi^2+\zeta\mathsf{Q}\Phi^2\right)\,, \tag{3.78}$$

where ζ is a dimensionless coupling constant. The Klein-Gordon equation (2.16) now reads

$$(\Box-m^2)\Phi-\zeta\mathsf{Q}\Phi=0\,. \tag{3.79}$$

At this point, one can proceed as done in Sec. 2.2 to obtain a Klein-Gordon Eq. (2.32) but with an effective mass

$$M_{\text{eff}}=a^2(\eta)\left(m^2+2(3\zeta+1)H^2(\eta)-\frac{H'(\eta)}{a(\eta)}\right)\,. \tag{3.80}$$

The Bogoliubov coefficients can be obtained via perturbation theory as done in Sec. 2.2.2. In so doing one obtains the same results found in Sec. 2.2.2 but the effective mass is now the one in Eq. (3.80) instead of the one in Eq. (2.33).

3.3.1.1 Modified symmetric teleparallel gravity

Now, some generalizations of STEGR are exproled. In particular, the so-called $f(\mathsf{Q})$-theories are now considered. They basically consist on replacing Q on the action (3.74) with a generic function $f(\mathsf{Q})$ of it [178, 175, 179], namely

$$S_{f(\mathsf{Q})}=-\frac{1}{2}\int\sqrt{-g}f(\mathsf{Q})d^4x\,. \tag{3.81}$$

Of course, by using the action (3.81), the resulting gravitational theory is no more equivalent to General Relativity, making new terms appearing on the Einstein field equations. In fact, the models involving *modified theories of gravity* seek to explain some phenomena which cannot be explained by general relativity and/or removing the dark energy and dark matter degrees of freedom [16].

Among the various extensions of gravity, $f(\mathsf{Q})$ models have found successful application in a wide range of fields, including astrophysical structure modeling [180, 181], gravitational-wave phenomenology [182, 183], and the study of cosmological evolution [176, 177, 184, 185, 186]. Across these domains, they have provided observationally consistent descriptions without invoking dark energy [187, 188].

With the above requirements, the aim is to know if an $f(\mathsf{Q})$ gravity modification can improve the preservation of information up to a cosmological expansion. The Friedmann equations (2.27a) and (2.27b), by using the coincident gauge and the action (3.81), become [171, 176, 184]

$$H^2 = \frac{\varrho + \frac{1}{2}f(\mathsf{Q})}{6f_{\mathsf{Q}}}\,, \tag{3.82a}$$

$$\frac{H'}{a} = -\frac{1}{2}\frac{\varrho + p}{12H^2 f_{\mathsf{QQ}} + f_{\mathsf{Q}}}\,, \tag{3.82b}$$

The standard Friedmann equations (2.27a) and (2.27b) are clearly recovered as $f(\mathsf{Q}) \to \mathsf{Q} = 6H^2$.

From Eq.(3.82), the presence of an $f(\mathsf{Q})$-modification leads to an altered evolution of the Hubble parameter $H(\eta)$. As a consequence, according to Eqs. (2.44b) and (3.80), this modification results in a different particle production. By fixing the parameters ϱ and p, Eq. (3.82) yields a new expression for $H(\eta)$. The change in $H(\eta)$ also affects the scale factor $a(\eta)$, whose evolution depends on the particular $f(\mathsf{Q})$ model considered, giving

$$a_{\text{mod}}(\eta) = \left(\frac{1}{a_{\text{in}}} - \frac{1}{\sqrt{6}}\int_{-\infty}^{\eta}\sqrt{\frac{\rho(\eta') + \frac{1}{2}f(\mathsf{Q})}{f_{\mathsf{Q}}}}d\eta'\right)^{-1}\,. \tag{3.83}$$

In turn, the function $U(\eta)$ introduced in Eq. (2.38) becomes

$$U(\eta) = m^2(a^2_{\text{mod}}(\eta) - a^2_{\text{in}}) + a^2_{\text{mod}}(\eta)\left((3\zeta - 1)\frac{\varrho + \frac{1}{2}f(\mathsf{Q})}{3f_{\mathsf{Q}}} + \frac{f_{\mathsf{Q}}}{2}\frac{\varrho + p}{2\rho f_{\mathsf{QQ}} + f(\mathsf{Q})f_{\mathsf{QQ}} + f^2_{\mathsf{Q}}}\right)\,. \tag{3.84}$$

By putting $U(\eta)$ from Eq. (3.84) into Eq. (2.44b), with a_{out} now given by $a_{\text{mod}}(\eta \to +\infty)$, one gets the cosmological particle production for the particular $f(\mathsf{Q})$ theory considered.

Within the family of modified $f(\mathsf{Q})$ theories, only certain subclasses yield a finite amount of particle production from the remote past to future infinity. In particular, to require the finiteness of N_k, i.e. $|\beta_k|^2$, it is required, from Eq. (2.44b), that a_{mod} is constant at infinite future so that H^2 vanishes in this limit. Since $\mathsf{Q} = 6H^2$, it follows that $f(\mathsf{Q})$ must be well-behaved in the limit $\mathsf{Q} \to 0$.

Another restriction on the $f(\mathsf{Q})$-theories is given by local observations of the gravitational constant G equal to $(8\pi)^{-1}$ in the units chosen. In fact, a modified gravity theory $f(\mathsf{Q})$ implies an effective gravitational constant G_{eff}, reading [171, 188]

$$G_{\text{eff}} \equiv \frac{1}{8\pi f_{\mathsf{Q}}(\mathsf{Q})}\,. \tag{3.85}$$

Obviously, G_{eff} should deviate from 1 only by an infinitesimal amount, to match the Solar system observations.

Resuming, to have a finite particle production and to avoid disrupting local observations, $f(\mathsf{Q} = 0) = \text{const}$ and $|f_{\mathsf{Q}}(\mathsf{Q} \to 0) - 1| \ll 1$ are needed conditions. These requirements allow to select suitable $f(\mathsf{Q})$ models involving a small particle production, similarly to what was done in Ref. [73] for $f(R)$ modified gravity theories.

3.3.1.2 Power-law gravity modification

The following specific model for $f(\mathsf{Q})$ is now considered [175, 187, 177],

$$f(\mathsf{Q}) = \mathsf{Q} + \epsilon A \left(\frac{\mathsf{Q}}{A}\right)^d , \tag{3.86}$$

where $A > 0$. This scenario recovers the standard ΛCDM model when $d = 0$ and remains consistent with constraints from Big Bang Nucleosynthesis [189, 190, 191]. In the asymptotic future, $f(\mathsf{Q})$ remains finite for $d \geq 0$, and the effective gravitational coupling G_{eff} follows the equation

$$8\pi G_{\text{eff}} = \frac{1}{f_{\mathsf{Q}}(\mathsf{Q} \to 0)} \begin{cases} \frac{1}{1+\epsilon} \quad \text{if} \quad d = 1\,; \\ 1 \quad \text{if} \quad d = 0 \quad \text{or} \quad d > 1\,; \\ 0 \quad \text{otherwise}\,. \end{cases} \tag{3.87}$$

Then, the parameter d in Eq. (3.86) is restricted to be zero or strictly greater than 1, while $d = 1$ is possible only if $\epsilon \ll 1$.

These results can be compared with known experimental bounds, confirming the reliability of our estimated range for d. In particular, when incorporating constraints from model-independent approaches based on cosmography [192, 193, 194, 195], the deviations from the standard cosmological model are minimal at late times but become more pronounced in the early Universe. By following the analyses of Refs. [196, 184, 185], the found constraints on d are consistent with scenarios that reproduce slight departures from the ΛCDM paradigm. Moreover, observations at intermediate redshifts imply $d \leq 2$ [197], which is consistent with our bounds for d.

3.3.1.3 A practical example

To have cosmological particle production, one has to take toy models for the cosmological expansion involving flatness at far future. At the end of Sec. 2.2, it was discussed how, despite the violations of some energy conditions, such expansions may model realistic situations under certain approximations.

Therefore, the model presented in Ref. [75], known as *Bernard-Duncan model*, is considered, involving

$$a(\eta) = \frac{1}{\sqrt{2}} \sqrt{1 + a_{\text{in}}^2 + (1 - a_{\text{in}}^2) \tanh(r\eta)}\,. \tag{3.88}$$

The free parameters of Eq. (3.88) - r in particular - can be constrained with upper limits as done in Ref. [198] to consider the late time evolution as adiabatic and overcome the violations of the energy conditions when the expansion decelerates.

By considering the second order perturbation theory, the relative error is expected to be proportional to $\mathcal{E}_{\text{P}}$ from Eq. (2.43) with $n = 2$. For it, one has $\mathcal{E}_{\text{P}} \ll 1$ as long as $1 - a_{in}^2 \ll \omega_{in}^2 / m^2$ and $r^2 \ll \omega_{in}^2$. To satisfy those conditions, massless particles are chosen $m = 0$. Moreover, the parameters are set up to be $\omega = 0.1$ and $r = 0.01$. In this way, from Eq. (2.43), one has $\mathcal{E}_{\text{P}} \simeq 5 \cdot 10^{-5}$. With these parameters, the Bogoliubov coefficients α_ω and β_ω can be easily found with Eqs. (2.44a) and (2.44b), respectively. From them, the particle production $N_\omega = |\beta_\omega|^2$, the bounded classical capacity (3.36) with $\overline{N} = 10$ and the quantum capacity (3.70), were numerically computed, obtaining the results shown in Table 3.1 for different values of the coupling ζ between the field and the non-metricity. As expected, the cosmological particle production is very low and the amount of

ζ	$N_{\omega=0.1}$	$C_{\overline{N}=10}$	Q
0	$1.5831 \cdot 10^{-25}$	4.8345	82.3854
1/3	$1.5833 \cdot 10^{-25}$	4.8345	82.3853
2/3	$4.7439 \cdot 10^{-25}$	4.8345	80.8021

Table 3.1: The table presents the massless particle production $N_{\omega=0.1} = |\beta_{\omega=0.1}|^2$ (Eq. (2.44b)), the constrained classical capacity $C_{\overline{N}}$ (Eq. (3.69)) and the quantum capacity Q (Eq. (3.70)) for a Bernard-Duncan cosmological expansion (3.88) with $r = 0.01$ and $a_{\text{in}} = 0.5$, evaluated for different values of the coupling ζ between the scalar field and the non-metricity scalar Q.

classical information lost by the cosmological expansion is completely negligible. On the contrary, the quantum capacity Q slightly changes for different N_ω even if $N_\omega \ll 1$. Moreover, in General Relativity, there is a peculiar value for the field-curvature coupling ξ giving no particle production in the massless case - namely, the *conformal coupling* $\xi = 1/6$ from Eq. (2.33). This is not the case in STEGR, i.e. there is no value for ζ implying no particle production. This offers a scenario where cosmological particle production can play a pivotal role on the history of the Universe [199].

The power-law $f(\mathsf{Q})$ modification given in Eq. (3.86) is examined. The particle production is computed by inserting Eq. (3.84) into Eq. (2.44b) in place of the potential $U(\eta)$ defined below Eq. (2.38). Conventionally, it was set $A \propto Q$ and set $A = \max_\eta\{2\rho(\eta)\} \simeq 1.418 \cdot 10^{-4}$. Fig 3.3 displays the results for various values of ζ, d, and ϵ, where the unmodified case from Eq. (3.86) corresponds to $\epsilon = 0$. As expected, the behavior of particle production depends on the sign of ϵ. For $\zeta = 1/3$ or $\zeta = 2/3$, the production N_ω is smaller than in General Relativity only when $\epsilon < 0$ and d lies within a bounded interval. In contrast, if $\epsilon > 0$, the particle production N_ω is always greater than in the unmodified case $\epsilon = 0$.

An opposite trend emerges in the minimal coupling case $\zeta = 0$, where particle production N_ω is minimized for $\epsilon > 0$. When $\epsilon < 0$, the production still decreases w.r.t. the unmodified case, but the reduction is much smaller than that achieved for $\epsilon > 0$.

Since Table 3.1 shows that the classical capacity is essentially unaffected by very low particle production, the focus is now only on the quantum capacity. In Table 3.1 the quantum capacities, for the modified theories of gravity presented in Fig. 3.3 $f(Q)$ modifications, are shown and compared with their General Relativity values. For each coupling ζ, the maximum quantum capacity occurs at $d = d_{\min}$, where particle production reaches its minimum $N_\omega^{\min}$. This allows us to quantify the maximum possible gain in quantum capacity as

$$\Delta Q = \frac{Q(N_\omega = N_\omega^{\min}) Q(\epsilon = 0)}{Q(\epsilon = 0)} \,. \tag{3.89}$$

The values of ΔQ are reported in Tab. 3.2, as well as the numerically computed values of $d_{\min}$.

As a result, for each coupling ζ, there exists a polynomial $f(\mathsf{Q})$ model, with parameters given in Table 3.2, that preserves quantum information from the remote past more effectively than the unmodified case. A direct comparison with General Relativity can be made for the minimal coupling $\xi = \zeta = 0$, where the scalar field Lagrangian (2.15) coincides with the STEGR one. In this setting, the $f(\mathsf{Q})$ model of Eq. (3.86) with $d \simeq 1.59$ and $\epsilon = 0.004$ enhances the quantum capacity (i.e., the amount of conserved information from the early Universe) by up to 4.23%. This model also preserves the gravitational coupling G in the far future, ensuring consistency with local observations.

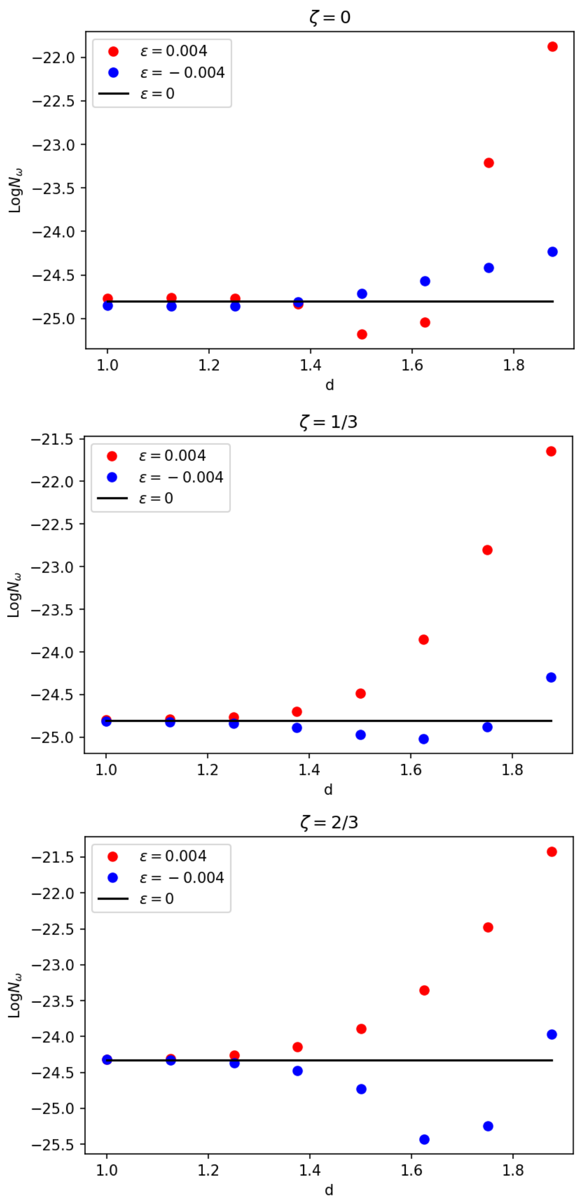

Figure 3.3: Number of massless scalar particles N_ω with frequency $\omega = 0.1$ produced during a cosmological expansion described by the scale factor (3.88) (with $a_{\rm in} = 0.5$ and $r = 0.01$) as a function of the parameter d in the modified gravity theory $f(Q)$ from Eq. (3.86), with $A \simeq 1.418 \times 10^{-4}$. The particle production N_ω is shown for various values of the coupling ζ between the scalar field and the non-metricity scalar $Q = 6H^2$, and for different choices of ϵ, an additional parameter of the $f(Q)$ modification in Eq. (3.86).

ζ	ϵ	$d_{\min}$	ΔQ
0	0.004	1.59	4.23%
1/3	−0.004	1.61	0.89%
2/3	−0.004	1.69	7.76%

Table 3.2: This table lists, for each value of the coupling ζ, the maximum quantum capacity gain ΔQ (Eq. (3.89)) attainable within the modified gravity model (3.86) when restricting to $|\epsilon| = 0.004$. The second and third columns give, respectively, the values of the parameters ϵ and d of the power-law modification required to achieve the gain ΔQ.

3.3.2 Entanglement creation and preservation

From the literature (E.g. Refs. [200, 201, 202]), it is well known that the particles created from vacuum, with momentum $\mathbf{k}$ by a cosmological expansion are maximally entangled with the particle created from vacuum with momentum $-\mathbf{k}$. In this way, the entanglement entropy between two particles with momenta $\mathbf{k}$ and $-\mathbf{k}$ is zero before the cosmological expansion and becomes then $h(1/2 + N_{\mathbf{k}})$ after it.

The formalism introduced in Sec. 3.2 is now used to generalize this result to a whatever initial maximally entangled state in place of the vacuum. In other words, the focus is on the preservation of entanglement up to a cosmological expansion. A two-modes Gaussian state is considered for this purpose. Its covariance matrix is expressed by Eq. (3.40), where the two modes $\mathbf{k}$ and $-\mathbf{k}$ have opposite direction.

With these requirements, Eqs. (3.49), (3.50), (3.51) and (3.52), from Eq. (2.36) simplify to

$$\tilde{n}_{\mathbf{k}} = |\alpha_k|^2 n_{\mathbf{k}} + |\beta_k|^2(1 + n_{-\mathbf{k}}) - 2\Re\left(\alpha_k^* \beta_k \chi_{\mathbf{k},-\mathbf{k}}\right); \tag{3.90}$$

$$\tilde{m}_{\mathbf{k}} = \alpha_k^{*2} m_{\mathbf{k}} + \beta_k^{*2} m_{-\mathbf{k}} - 2\alpha_k \beta_k^* \gamma_{\mathbf{k},-\mathbf{k}}^* . \tag{3.91}$$

$$\tilde{\gamma}_{\mathbf{k},-\mathbf{k}} = -\alpha_k \beta_k^* m_{\mathbf{k}}^* - \alpha_k^* \beta_k m_{-\mathbf{k}} + (|\alpha_k|^2 + |\beta_k|^2)\gamma_{\mathbf{k},-\mathbf{k}}; \tag{3.92}$$

$$\tilde{\chi}_{\mathbf{k},-\mathbf{k}} = -\alpha_k^* \beta_k^* (1 + n_{\mathbf{k}}) - \beta_k^* \alpha_k^* n_{-\mathbf{k}} + (\alpha_k^{*2} + \beta_k^{*2})\chi_{\mathbf{k},-\mathbf{k}} . \tag{3.93}$$

As input, a maximally entangled state, represented with the matrix (3.44), is taken. In this case, Eqs. (3.90), (3.91), (3.92) and (3.93) become respectively

$$\tilde{n}_{\pm\mathbf{k}} = (1 + 2N_k) n_{\mathbf{k}} + N_k - 2\sqrt{N_k(N_k+1)}\cos(\theta - \varphi_\alpha + \varphi_\beta), \tag{3.94}$$

$$\tilde{m}_{\mathbf{k}} = 0; \tag{3.95}$$

$$\tilde{\gamma}_{\pm\mathbf{k},\mp\mathbf{k}} = 0; \tag{3.96}$$

$$\begin{aligned}\tilde{\chi}_{\mathbf{k},-\mathbf{k}} = &-\sqrt{N_k(1+N_k)}e^{-i\varphi_\alpha - i\varphi_\beta} + (1+N_k)e^{-2i\varphi_\alpha + i\theta}\sqrt{n_{\mathbf{k}}(1+n_{\mathbf{k}})} \\ &+ N_k e^{-2i\varphi_\beta - i\theta}\sqrt{n_{\mathbf{k}}(1+n_{\mathbf{k}})},\end{aligned} \tag{3.97}$$

where φ_α and φ_β are the phases of α_k and β_k, respectively.

From Eq. (3.41) and by using the parameters (3.94), (3.95), (3.96) and (3.97) the two symplectic eigenvalues are both equal to 1/2. Therefore, the opposite modes maximally entangled state is still

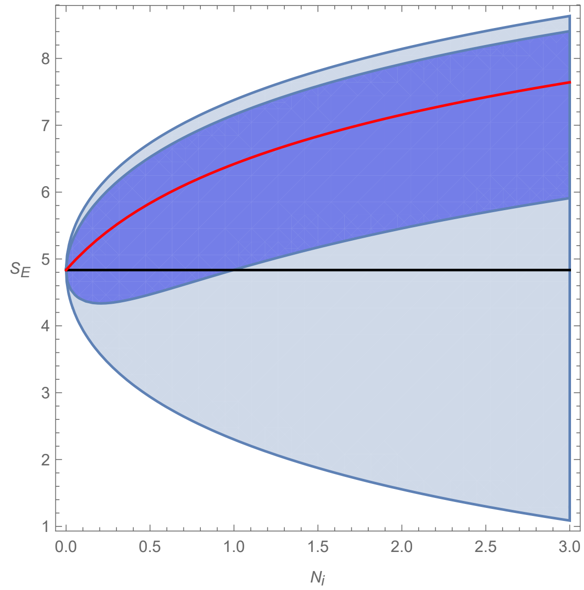

Figure 3.4: The entanglement entropy $\mathcal{S}_E$ - by Eq. (3.99) - of a state made initially by 10 particles with momentum i maximally entangled with other 10 particles with opposite momentum - labelled with $-$i after a cosmological expansion, creating $N_{\rm i}$ particle in both the modes considered. The initial entanglement entropy is represented by the black line, while the light blue region represents the possible values of the final entanglement entropy (from Eq. (3.99)) by spanning c from -1 to $+1$. The red line represents the average entanglement entropy and the dark blue region encloses the values around the average within a standard deviation (i.e. spanning c from $-\frac{1}{\sqrt{2}}$ to $+\frac{1}{\sqrt{2}}$).

maximally entangled after the cosmological expansion. However, its entanglement entropy changes, becoming

$$\begin{aligned} \mathsf{S}_{\rm E}(\tilde{\sigma}) = h\left(\frac{1}{2}+\tilde{n}_{\mathbf{k}}\right) = h\bigg(&\frac{1}{2}+n_{\mathbf{k}}+N_k(1+2n_{\mathbf{k}}) \\ &-2\sqrt{n_{\mathbf{k}}(n_{\mathbf{k}}+1)}\sqrt{N_k(N_k+1)}\cos(\theta-\varphi_\alpha+\varphi_\beta)\bigg)\,, \end{aligned} \tag{3.98}$$

The result in Eq. (3.98) agrees with the one provided in the literature [200, 201, 202] when starting with the vacuum, i.e. $n_{\mathbf{k}} \to 0$, providing a generalization of the last scenario.

The final entanglement entropy would be dependent by the parameter θ, arising from a unitary evolution of the initial state. Since the time where the state is initially created is assumed to be indefinite in the remote past, the value of θ would be not determined as well. Therefore, θ can be considered as a random variable going from $-\pi$ to $+\pi$. In this way, the variable $c \coloneqq \cos(\theta-\varphi_\alpha+\varphi_\beta)$ becomes a random variable ranging from -1 to $+1$ with a probability distribution with average 0 and standard deviation $\frac{1}{\sqrt{2}}$. The output entanglement entropy can be rewritten in terms of c, for simplicity, as

$$\mathsf{S}_{\rm E}(\tilde{\sigma}) = h\left(\frac{1}{2}+n_{\mathbf{k}}+N_k(1+2n_{\mathbf{k}})-2\sqrt{n_{\mathbf{k}}(n_{\mathbf{k}}+1)}\sqrt{N_k(N_k+1)}c\right)\,, \tag{3.99}$$

In Figs. 3.4 and 3.5 the entanglement entropy (3.99) is shown before and after the cosmological expansion. In the aforementioned figures, for $\mathcal{S}_E(\tilde{\sigma})$, it is shown the average (red line), the region

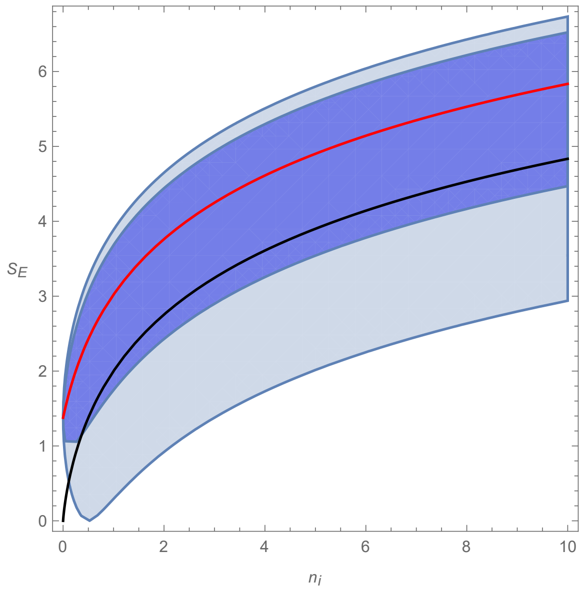

Figure 3.5: The entanglement entropy S_{E} - by Eq. (3.99) - of a state made initially by n_{i} entangled particles between the mode i and its opposite $-$i, after a cosmological expansion creating $N_{\mathrm{i}} = 0.5$ particles in the mode i momentum i maximally entangled with other 10 particles with opposite momentum. The meanings of the black line, red line, dark blue region and light blue region are analog to the ones assigned in Fig. 3.4.

of values between the standard deviation of $\cos(\varphi + \theta)$ (dark blue region) and the region of all the possible values (light blue region).

From Fig. 3.4, the more is the particle production, the more is the average entanglement entropy gained from the cosmological expansion. It is interesting how there is a non-null probability of *entanglement degradation*, i.e. of a decreasing of the entanglement entropy after the cosmological expansion. The probability of degradation can be computed to be

$$p_{\mathrm{degr}} = \frac{1}{\pi} \arccos\left(\frac{1 + 2n_{\mathrm{i}}}{2\sqrt{n_{\mathrm{i}}(n_{\mathrm{i}}+1)}} \sqrt{\frac{N_{\mathrm{i}}}{N_{\mathrm{i}}+1}} \right) . \tag{3.100}$$

From Fig. 3.5, the enhancement of entanglement is guaranteed is n_{i} is particularly low. From Eq. (3.100), this happens when the argument of the function arccos is greater than one i.e. when the the following is satisfied

$$N_{\mathrm{i}} > 4n_{\mathrm{i}} + 4n_{\mathrm{i}}^2 . \tag{3.101}$$

Resuming, a scenario with the greatest particle production is the one maximizing the final entanglement entropy between particles with opposite modes. This is quite obvious having the vacuum as initial state. However, the situation is more tricky when considering the presence of n_{i} entangled particles before the cosmological expansion. Indeed, in this case, the initial entanglement have a probability, one has a degradation probability given by Eq. (3.100). The more is the particle production, the less is this probability, until entanglement enhancement is guaranteed when condition (3.101) is reached.

3.4 Information transmission through a semitransparent moving mirror

In Sec. 3.3, the particle production by a cosmological expansion was proved to decrease the transmission capabilities of a channel from remote past to far future. This result was expected, since the channel is noiseless in case of no cosmological expansion, which in turns constitutes a source of communication noise. However, one may wonder how particle production affects quantum channels which are already noisy. In particular, it is worth exploring if the effects predicted by quantum field theory in curved spacetime may help the communication of a channel or if it provides a further obstacle to it.

A semitransparent mirror, with transmission coefficient $\tau_c < 1$, provides a straightforward example of a lossy quantum channel, whose loss is given by the reflected fraction of incident light. For this reason, to solve the aforementioned puzzle, the transmission of scalar particle through a $(1+1)$D semitransparent mirror was considered. From an optical perspective, a $(1+1)$D mirror can be emulated by a realistic $(3+1)$D in an environment where particle are guided towards one particular direction [203]. Therefore, to provide more realistic model for the dynamical Casimir effect, it is worth to extend it when mirrors are not completely reflecting - since any material is no more reflecting for frequencies high enough.

Moreover, as specified in Sec. 2.3.2, a perfectly reflecting mirror emulates the radiation emitted by a collapsing shell of matter. To this scenario, a particle reflected by the mirror would return to the source, meaning that the it is re-expelled from the collapsing matter to a distant observer. On the contrary, a wave transmitted from a moving mirror would enclose the possibility that incoming radiation is swallowed by the collapsing matter shell when crossing it. Therefore, in the black hole-mirror analogy, the mirror semitransparency constitutes a nice extension - including the possibility of absorption of radiation from the collapsing matter.

The system considered is made by a massless scalar field $\hat{\Phi}$ and a semitransparent mirror in a $(1+1)$D spacetime. The static coordinates are defined as (x,t). The mirror is expressed by a delta-like classical potential, leading to the Lagrangian density

$$\mathcal{L} = \partial_\mu \hat{\Phi} \partial^\mu \hat{\Phi} + \eta \hat{\Phi} \delta(x - x_{\mathrm{m}}) \,, \tag{3.102}$$

where x_m indicates the mirror position. From Eq. (3.102), the reflection and transmission amplitudes are dispersive - i.e. dependent on the frequency of the incident wave ω - and they are respectively [204]

$$r(\omega) = \frac{-i\eta}{\omega + i\eta} \,; \quad s(\omega) = \frac{\omega}{\omega + i\eta} \,. \tag{3.103}$$

In this way, the transmission coefficient of the mirror corresponds to $|s(\omega)|^2$.

The field $\hat{\Phi}$ can be expanded as

$$\Phi = \sum_{\mathrm{J=L,R}} \int_0^\infty d\omega \left(\phi_\omega^{\mathrm{J}} \hat{a}_\omega^{\mathrm{J}} + \phi_\omega^{\mathrm{J}*} \hat{a}_\omega^{\mathrm{J}\dagger} \right) \,, \tag{3.104}$$

where, by following the notation from Sec. 2.3.2, ϕ_ω^{R} and ϕ_ω^{L} are respectively the right-travelling and left travelling modes. By using the null coordinates $u = t - x$ and $v = t + x$, they read

$$\phi^{\mathrm{L}}_\omega(u,v) = \frac{1}{\sqrt{4\pi|\omega|}}\left(s(\omega)e^{-i\omega v}\theta(u - v + 2x_{\mathrm{m}}) + \left(e^{-i\omega v} + r(\omega)e^{-i\omega u}\right)\theta(v - u - 2x_{\mathrm{m}})\right)\,, \tag{3.105}$$

$$\phi^{\mathrm{R}}_\omega(u,v) = \frac{1}{\sqrt{4\pi|\omega|}}\left(s(\omega)e^{-i\omega u}\theta(v - u - 2x_{\mathrm{m}}) + \left(e^{-i\omega u} + r(\omega)e^{-i\omega v}\right)\theta(u - v + 2x_{\mathrm{m}})\right). \tag{3.106}$$

If the mirror is moving, the reflection and transmission coefficients $r(\omega)$ and $s(\omega)$ would change accordingly and the situation become way more complex [205]. To avoid this problem, the approach used in Ref. [206] is used. To this purpose, one can use the mirror null comoving coordinates $(\overline{u}, \overline{v})$, to build a complete and orthonormal set of normal modes $g^{\mathrm{J=R,L}}_\omega(\overline{u}, \overline{v})$, analog to the ones in Eq. (3.105) and (3.106), i.e.

$$g^{\mathrm{L}}_\omega(\overline{u},\overline{v}) = \frac{1}{\sqrt{4\pi|\omega|}}\left(s(\omega)e^{-i\omega\overline{v}}\theta(\overline{u} - \overline{v}) + \left(e^{-i\omega\overline{v}} + r(\omega)e^{-i\omega\overline{u}}\right)\theta(\overline{v} - \overline{u})\right)\,, \tag{3.107}$$

$$g^{\mathrm{R}}_\omega(\overline{u},\overline{v}) = \frac{1}{\sqrt{4\pi|\omega|}}\left(s(\omega)e^{-i\omega\overline{u}}\theta(\overline{v} - \overline{u}) + \left(e^{-i\omega\overline{u}} + r(\omega)e^{-i\omega\overline{v}}\right)\theta(\overline{u} - \overline{v})\right)\,. \tag{3.108}$$

The relation between the coordinates (u, v) and $(\overline{u}, \overline{v})$ is [116, 121]

$$\frac{d\overline{u}(u)}{du} = \sqrt{\partial_u p(u)}\,, \qquad \frac{d\overline{v}(v)}{dv} = \sqrt{\partial_v f(v)}\,, \tag{3.109}$$

which is obviously dependent on the mirror trajectory $u_{\mathrm{m}} = f(v)$ (or, $v_{\mathrm{m}} = p(u)$). Since both $\{\phi^{\mathrm{J}}_\omega\}_{\omega,\mathrm{J=R,L}}$ and $\{g^{\mathrm{J}}_\omega\}_{\omega,\mathrm{J=R,L}}$ form a complete and orthonormal set of modes, the input modes can be written through a completeness relation as

$$\phi^{\mathrm{J}}_\omega = \sum_{\mathrm{J'=L,R}}\int_{-\infty}^{+\infty} d\omega'\chi(\omega')\left(\phi^{\mathrm{J}}_\omega, g^{\mathrm{J'}}_{\omega'}\right)_{\mathrm{KG}} g^{\mathrm{J'}}_{\omega'}\,, \tag{3.110}$$

where χ is the sign function. The output signal is considered at the right of the mirror. In this way, the outgoing left-travelling waves can be neglected from now on.

At infinite past and at the right side of the mirror, one has $\phi^{\mathrm{R}}_\omega = g^{\mathrm{R}}_{\omega'} = 0$, $\phi^{\mathrm{L}}_\omega = \frac{e^{-i\omega v}}{\sqrt{4\pi|\omega|}}$ and $g^{\mathrm{L}}_\omega = \frac{e^{-i\omega\overline{v}}}{\sqrt{4\pi|\omega|}}$, assuming the mirror to have a time-like trajectory. In this way, the Klein-Gordon scalar product in Eq. (3.110) for the left-travelling modes can be easily computed by considering the Cauchy surface at the right-infinite past. Then, from Eq. (3.110), one has

$$\begin{aligned}\phi^{\mathrm{L}}_\omega =& \frac{1}{\sqrt{4\pi\omega}}e^{-i\omega v}\\ &+\sqrt{\frac{\omega}{4\pi}}i\int_{-\infty}^{+\infty} dv'\left(\frac{1}{2}\chi(\overline{u}(u) - \overline{v}(v')) - \theta(\overline{u}(u) - \overline{v}(v'))e^{-\eta(\overline{u}(u)-\overline{v}(v'))}\right)e^{-i\omega v'}\,.\end{aligned} \tag{3.111}$$

Analogously, the right-travelling modes are computed as

$$\phi^{\mathrm{R}}_\omega = -i\sqrt{\frac{\omega}{4\pi}}\int_{-\infty}^{u} du' e^{-\eta\left(\overline{u}(u)-\overline{u}(u')\right)}e^{-i\omega u'}\,. \tag{3.112}$$

The output modes, in the far future and right side of the mirror, read $\phi^{\mathrm{out}}_\omega \sim \frac{e^{-i\omega u}}{4\pi|\omega|}$. Therefore, by choosing this Cauchy surface, the Bogoliubov coefficients through the Klein-Gordon scalar product

(2.17) between $\phi^{\rm out}_\omega$ and $\phi^{\rm J}_\omega$. In particular, by defining $\alpha^{\rm J}_{\omega\omega'} := \left(\phi^{\rm out}_\omega, \phi^{\rm J}_{\omega'}\right)$ and $\beta^{\rm J}_{\omega\omega'} := \left(\phi^{\rm out*}_\omega, \phi^{\rm J}_{\omega'}\right)^*$, one has

$$\alpha^{\rm L}_{\omega\omega'} = -\frac{\eta}{2\pi}\sqrt{\frac{\omega'}{\omega}}\int_{-\infty}^{+\infty} dv' \int_{-\infty}^{+\infty} d\overline{u}\theta(\overline{u}-\overline{v}(v'))e^{\eta\overline{v}(v')+i\omega' v'}e^{-\eta\overline{u}-i\omega u(\overline{u})}\,, \tag{3.113}$$

$$\alpha^{\rm R}_{\omega\omega'} = \delta(\omega-\omega') -\frac{\eta}{2\pi}\sqrt{\frac{\omega'}{\omega}}\int_{-\infty}^{+\infty} du' \int_{-\infty}^{+\infty} d\overline{u}\theta(\overline{u}-\overline{u}(u'))e^{\eta\overline{u}(u')+i\omega' u'}e^{-\eta\overline{u}-i\omega u(\overline{u})}\,, \tag{3.114}$$

$$\beta^{\rm L}_{\omega\omega'} = -\frac{\eta}{2\pi}\sqrt{\frac{\omega'}{\omega}}\int_{-\infty}^{+\infty} dv' \int_{-\infty}^{+\infty} d\overline{u}\theta(\overline{u}-\overline{v}(v'))e^{\eta\overline{v}(v')-i\omega' v'}e^{-\eta\overline{u}-i\omega u(\overline{u})}dv'd\overline{u}, \tag{3.115}$$

$$\beta^{\rm R}_{\omega\omega'} = -\frac{\eta}{2\pi}\sqrt{\frac{\omega'}{\omega}}\int_{-\infty}^{+\infty} du' \int_{-\infty}^{+\infty} d\overline{u}\theta(\overline{u}-\overline{u}(u'))e^{\eta\overline{u}(u')-i\omega' u'}e^{-\eta\overline{u}-i\omega u(\overline{u})}\,. \tag{3.116}$$

3.4.1 Mirrors with a finite acceleration period

To find analytical solutions for the Bogoliubov coefficients (3.113), (3.114), (3.115) and (3.116) a particular prescription for the mirror trajectory is considered. In particular, the mirror is considered to be static at $x = 0$ before a time $t = 0$. Afterwards, the mirror starts to accelerate with a certain trajectory $z(t)$, reaching a velocity V at the time t_0. After t_0, the mirror stops to accelerate and continues to travel inertially at the velocity V - positive if the mirror is right-travelling and negative otherwise. For a notation convenience, the velocity V is expressed by the parameter $\nu := \frac{1-V}{1+V}$, so that $\nu > 1$ if the mirror is travelling towards the left and $\nu < 1$ otherwise.

From Eq. (3.109), the trajectory of the mirror can be expressed through $\overline{u}(u)$ or $\overline{v}(v)$, reading

$$\overline{u}_{tot}(u) = \begin{cases} u, & \text{if } u \leq 0,\\ \overline{u}(u), & \text{if } 0 < u \leq u_0,\\ \overline{u}(u_0) + \nu^{-1/2}(u-u_0), & \text{if } u > u_0, \end{cases} \tag{3.117}$$

$$\overline{v}_{tot}(v) = \begin{cases} v, & \text{if } v \leq 0,\\ \overline{v}(v), & \text{if } 0 < v \leq v_0,\\ \overline{v}(v_0) + \sqrt{\nu}(v-v_0), & \text{if } v > v_0. \end{cases} \tag{3.118}$$

By putting the trajectories (3.117) and (3.118) into Eqs. (3.113), (3.114), (3.115) and (3.116), one obtains the Bogoliubov coefficients

$$\begin{aligned}\alpha^{\rm L}_{\omega\omega'} =& \mathcal{O}(u_0)\\ &-\frac{\eta}{2\pi}\sqrt{\frac{\omega'}{\omega}}\left[\frac{1}{(\omega\sqrt{\nu}-i\eta)\,(-\omega'+i\eta)} - \frac{1}{(-\omega'+i\eta)(\omega-\omega'+i\epsilon)} - \frac{1}{(\omega\nu-\omega'-i\nu\epsilon)\,(\omega\sqrt{\nu}-i\eta)}\right].\end{aligned} \tag{3.119}$$

$$\begin{aligned}\alpha^{\rm R}_{\omega\omega'} =& \delta(\omega-\omega') + \mathcal{O}(u_0)\\ &-\frac{\eta}{2\pi}\sqrt{\frac{\omega'}{\omega}}\left[\frac{1}{(\omega\sqrt{\nu}-i\eta)\,(-\omega'+i\eta)} - \frac{1}{(-\omega'+i\eta)(\omega-\omega'+i\epsilon)} - \frac{1}{(\omega-\omega'-i\epsilon)\,(\omega\sqrt{\nu}-i\eta)}\right].\end{aligned} \tag{3.120}$$

$$\beta^{\rm L}_{\omega\omega'} = -\frac{\eta}{2\pi}\sqrt{\frac{\omega'}{\omega}}\left[\frac{1}{(\omega\sqrt{\nu}-i\eta)\,(\omega'+i\eta)} - \frac{1}{(\omega'+i\eta)(\omega+\omega')} - \frac{1}{(\omega\nu+\omega')\,(\omega\sqrt{\nu}-i\eta)}\right] + \mathcal{O}(u_0)\,. \tag{3.121}$$

$$\beta^{\rm R}_{\omega\omega'} = -\frac{\eta}{2\pi}\sqrt{\frac{\omega'}{\omega}}\left[\frac{1}{(\omega\sqrt{\nu}-i\eta)\,(\omega'+i\eta)} - \frac{1}{(\omega'+i\eta)(\omega+\omega')} - \frac{1}{(\omega+\omega')\,(\omega\sqrt{\nu}-i\eta)}\right] + \mathcal{O}(u_0)\,, \tag{3.122}$$

where ϵ is the regularization parameter introduced below Eq. (2.66b). From its definition, the Dirac delta in Eq. (3.120) comes out from ϵ through the limit

$$\delta(\omega-\omega') = \lim_{\epsilon\to 0}\frac{1}{\pi}\frac{\epsilon}{\epsilon^2+(\omega-\omega')^2} \tag{3.123}$$

In Eqs. (3.119), (3.120), (3.121) and (3.122), $\mathcal{O}(u_0)$ refers to a term depending on the acceleration period, from $t=0$ to $t=t_0$. One can prove that those terms are proportional to u_0 and finite for $\epsilon\to 0$. Therefore, if the acceleration period is very short - i.e. $u_0\omega \ll 1$, then the terms $\mathcal{O}(u_0)$ can be neglected. This case is considered, both for the reason above and because - as later shown - those term do not affect the quantum communication capabilities of the channel transmission.

The particle production reads

$$N_\omega = \int_0^\infty d\omega(|\beta^{\mathrm{L}}_{\omega\omega}|^2 + |\beta^{\mathrm{R}}_{\omega\omega'}|^2)\,. \tag{3.124}$$

By putting Eqs. (3.121) and (3.122) in Eq. (3.124), in case of a very short acceleration period, the particle production can be numerically computed, with the results shown in Fig. 3.6. From it, the particle production is proportional with the reflectivity of the mirror η. This is expected since a reflective mirror provides a stronger boundary on the field modes - while full transparency means no boundary at all. The last two plots in Fig. 3.6 show the particle production for different values of the mirror final speed V - the second (resp. third) showing the case where the mirror travels towards its right (resp. left). By comparing those, even if $|V|$ is the same, the particle production is way higher if the mirrors goes towards the detector.

3.4.2 Quantum channel from the mirror transmission

The communication protocol considered involves a one-mode Gaussian state sent through the mirror from its left to its right. The transmissivity τ and the parameter in the additive noise (3.23) are given by Eqs. (3.65) and (3.66) with $n=1$.

From Eq. (3.120), by considering $\delta(0)=\lim_{\epsilon\to 0}\frac{1}{\pi\epsilon}$, one obtains

$$\alpha^{\mathrm{R}}_{\omega\omega} = \delta(0)\left(1-\frac{\eta}{2}\left(\frac{1}{\omega'-i\eta}-\frac{1}{\omega\sqrt{\nu}-i\eta}\right)\right)\,. \tag{3.125}$$

The beta Bogoliubov coefficients (3.115) and (3.116) have no divergent behaviour when $\omega=\omega'$. For this reason, from Eq. (3.66) one has $B=C=0$, hence, from Eqs. (3.65) and (3.23)

$$\tau = \frac{4\Omega^4\nu+\Omega^2\left(1+\sqrt{\nu}\right)^2}{4\left(\Omega^2\nu+1\right)\left(\Omega^2+1\right)}\,;\quad \overline{n}=0\,. \tag{3.126}$$

where $\Omega \coloneqq \omega/\eta$. From Eq. (3.126), the channel turns out to be lossy since $\tau<1$. Therefore, the parameter τ can be seen as the mirror average transmission coefficient, modified by the mirror motion and acceleration. When $\nu=1$, the mirror is static and $\tau=\frac{\omega^2}{\omega^2+\eta^2}$ which is the expected transmission coefficient $|s(\omega)|^2$ in Eq. (3.103).

Interestingly, the transmissivity of the channel (3.126) is independent from the mirror acceleration period. In fact, this period gives the terms indicated by $\mathcal{O}(u_0)$ in the Bogoliubov coefficients in Eqs. (3.119), (3.120), (3.121) and (3.122), which are convergent for $\omega=\omega'$ and $\epsilon\to 0$ and therefore they neglect when put in Eq. (3.65). This means that, the average transmission coefficient of a moving

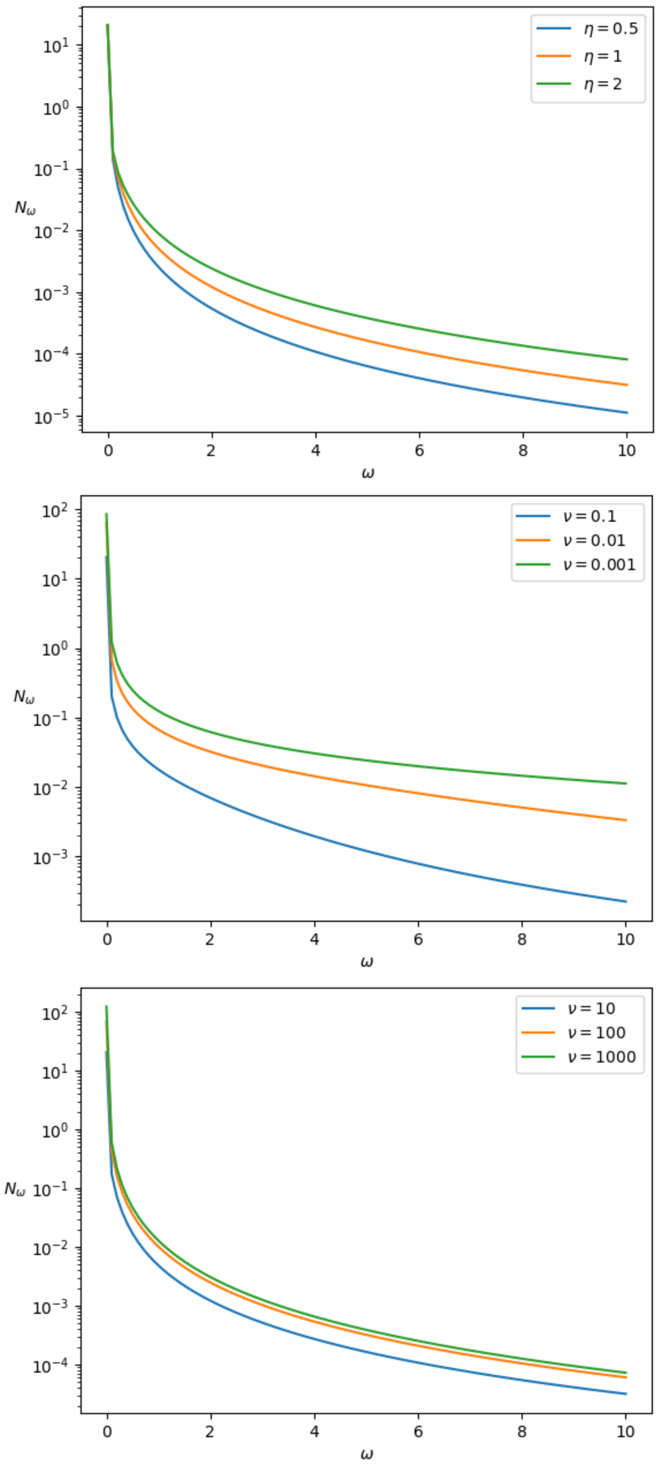

Figure 3.6: Particles produced by $(1+1)$D semitransparent mirrors with reflectivity η, accelerating very fast from being static to reach a final speed V - parametrized by $\nu = \frac{1-V}{1+V}$.

mirror depends solely on its initial and final velocity, regardless the way it accelerates to it. This is explained by the fact the transmission coefficient is averaged from infinite past to infinite future, so that any finite acceleration period turns out to be negligible[6].

If the mirror goes towards its right, i.e. towards the receiver, then τ from Eq. (3.126) decreases to reach the value $\frac{1}{4}|s(\omega)|^2$, i.e. 1/4 w.r.t. its static value. If the mirror goes towards its left, i.e. towards the sender, the transmissivity τ increases as long as $\nu < \nu_{\text{crit}}$, where

$$\nu_{\text{crit}}(\Omega) = \frac{9}{2} + \frac{4}{\Omega^2} + \frac{1 + (3\Omega^2+1)\sqrt{(9\Omega^2+1)(\Omega^2+1)}}{2\Omega^4}\,. \tag{3.127}$$

When $\nu > \nu_{\text{crit}}$, the transmissivity τ decreases again to reach $\tau = \frac{\Omega^2+\frac{1}{4}}{\Omega^2+1}$ as $\nu \to \infty$.

The existence of a speed ν_{crit} - over which the transmissivity decreases - is a feature arising purely from quantum field theory in curved spacetime, without occurring in the classical case. In fact, classically, the transmission coefficient is obtained by averaging the one when the mirror is static $|s(\omega)|^2$ and the one when the mirror is traveling at a speed V, i.e. $|s(\sqrt{\nu}\omega)|^2$ - since the frequency ω of an incoming wave is shifted in the mirror frame through its motion. In this way, classically, an average transmission coefficient is provided by

$$\tau_{\text{c}} = \frac{1}{2}(|s(\omega)|^2 + |s(\sqrt{\nu}\omega)|^2) = \frac{2\nu\Omega^4 + (1+\nu)\Omega^2}{2(\Omega^2+1)(\nu\Omega^2+1)}\,. \tag{3.128}$$

From Eq. (3.128), τ_{c} increases always as ν increases, as expected from the mirror Doppler blueshift. In this way, the fact that τ decreases when ν_{crit} clearly indicates an interference with the particles produced during the short acceleration period.

Interestingly, ν_{crit} decreases with Ω. Moreover, for $\Omega \to \infty$, $\nu_{\text{crit}} \to 9$, corresponding to a velocity $V_{\text{crit}} = -0.8$. Therefore, to see the effects of the particle production in the mirror transmission coefficient, the mirror needs to accelerate towards the sender and reaching a speed $|V| > 0.8$.

A plot for τ is portrayed in Fig. 3.7, where the static case $\nu = 1$, the case $\nu = 10$ - where V is close to -0.8 - and $\nu = 1000$ - i.e. very close to the speed of light - are compared. Moreover, by comparing τ and τ_{c} from Eqs. (3.126) and (3.128), one has $\tau_c > \tau$. In particular, one can compute

$$\Delta\tau = \frac{\tau_c - \tau}{\tau_c} = \frac{(1-\sqrt{\nu})^2}{2(2\nu\Omega^2 + 1 + \nu)}\,, \tag{3.129}$$

which is plotted in Fig. 3.8. Since $\Delta\tau > 0$, the question asked at the beginning of the section can be answered, as that the effects from quantum field theory in curved spacetime create a noisy effects even to "already noisy" quantum channels. By putting Eq. (3.126) into Eqs. (3.36) and (3.39), the classical and quantum capacity can easily be obtained. They are shown respectively in Figs. 3.9 and 3.10. By looking at Fig. 3.9, to transmit as much classical information as possible, the mirror should accelerate towards the sender at a speed as close as possible to the speed of light. On the contrary, from Fig, 3.10, to optimize the transmission of quantum information, the mirror should accelerate to a speed not greater than ν_{crit}. This reflects the fact that the decreasing of τ for $\nu > \nu_{\text{crit}}$ affects the transmission of quantum information, while to transmit classical information the scenario is analog to the classical one.

[6]The situation can be reproduced in laboratory as long as the acceleration period is way shorter than the measurement period.

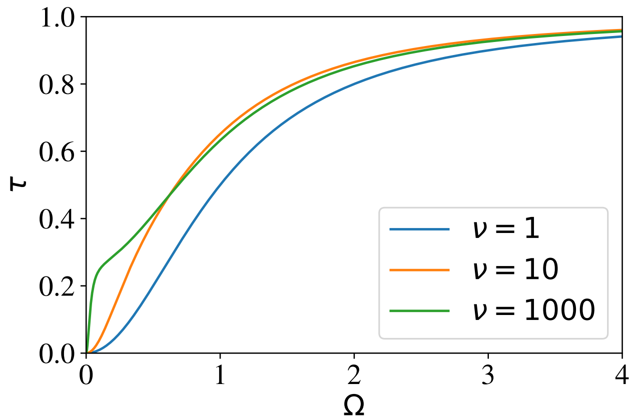

Figure 3.7: Average transmission coefficient τ, from Eq. (3.126), of a mirror accelerating towards the radiation source, from being static, to a velocity $V = \frac{\nu-1}{\nu+1}$.

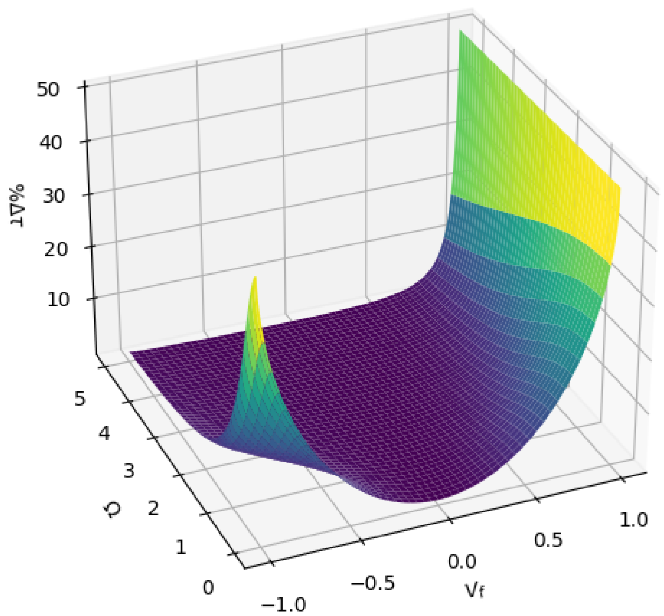

Figure 3.8: Decreasing $\Delta\tau$ (in percentage) of the transmission coefficient, obtained from Eq. (3.129), when considering quantum field theory in curved spacetime instead of a classical theory.

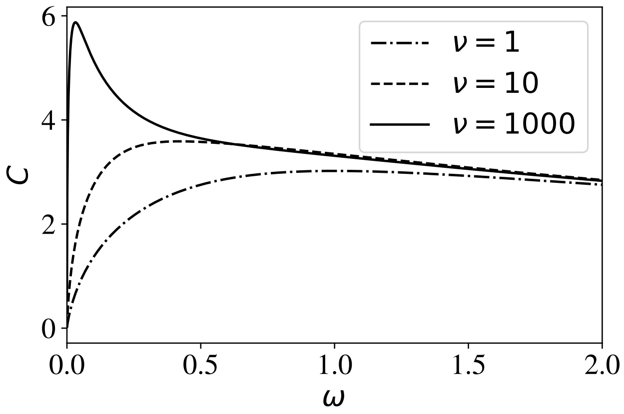

Figure 3.9: Energy bounded classical capacity - with $E = 5$ - of the channel arising from the transmission of a signal through a mirror whose trajectory is described in Fig. 3.7.

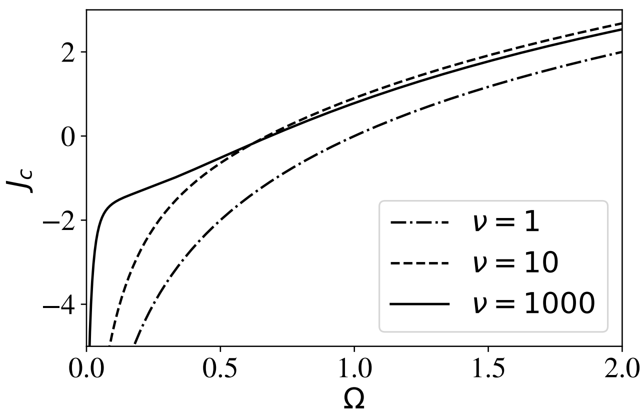

Figure 3.10: Quantum capacity of the channel arising from the transmission of a signal through a mirror whose trajectory is described in Fig. 3.7.

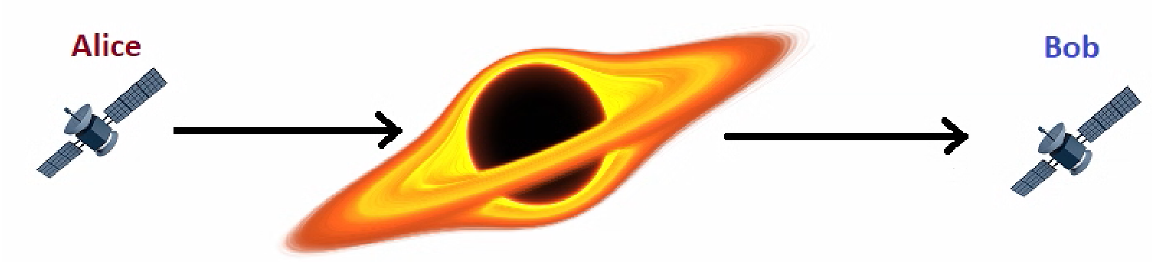

Figure 3.11: The communication protocol whose properties are given by the Bogoliubov coefficients (2.46a) and (2.46b). The two communicating parts are separated through a black hole and want to communicate through it.

3.5 Can information be recovered from evaporating black holes?

This question lies at the heart of one of the most profound problems in theoretical physics: the black hole information paradox. According to Hawking's semiclassical analysis, black holes radiate thermally and eventually evaporate completely, apparently erasing the information about the initial state of the matter that formed them. However, the problem is here addressed by using a mathematical tool allowing for simplified calculations regarding black hole radiation, i.e. $(1+1)$D moving mirrors (see Sec. 2.3.2).

As shown in Sec. 2.3.2, a Carlitz-Willey accelerated mirror (2.69) would lead to the same radiation occurring for an eternal black hole, i.e. (2.47), given by the Bogoliubov coefficients (2.46a) and (2.46b) with $l = l'$ and $m = m'$. From the same Bogoliubov coefficients, the relative bosonic communication channel can be studied as in Sec. 3.2. The resulting communication protocol involves Alice sending a one-mode Gaussian state, with frequency ω into an eternal Schwarzschild black hole with mass M while the receiver Bob is on the opposite side of it, attempting to retrieve Alice's signal. This scenario is shown in Fig. 3.11. By putting the coefficients (2.46a) and (2.46b) into Eqs. (3.65) and (3.66) the following channel parameters are obtained

$$\tau = 0\,; \quad \overline{n} = \frac{1}{e^{8\pi M\omega} - 1}\,. \tag{3.130}$$

This means that Alice's signal is completely erased by the black hole and that the only thing Bob achieves is $\overline{n}$, which is Hawking radiation itself, as additive noise. This is exactly what is expected for an eternal black hole, emitting radiation and swallowing each ingoing signal.

It is now insteresting to see what happens if the black hole evaporates. To answer this question a mirror analog to an evaporating black hole must be defined. This was done in Ref. [207], where the trajectory of the mirror emulating an evaporating black hole is schematized in Fig. 3.12. This trajectory is analog to the one in Eq. (2.73) but κ is time-dependent - namely $\kappa = \frac{1}{4M(t)}$ - and $M(t)$ follows the evaporation curve (2.63). When the black hole completely evaporates, the mirror should be static again, because each input signal would be perfectly reflecting at that point. However, the transition from the Schwarzschild spacetime to a Minkowski spacetime occurs smoothly in the trajectory in Fig. 3.12. This smoothness was imposed in Ref. [207] since a sharp trajectory transition - as studied in Sec. 3.4 - would create a huge number of particles. However, the energetic content of a black hole - i.e. its mass - should be very low at the end of the evaporation stage. In this way, a sharp trajectory transition would create a huge amount of particles violating energy conservation.

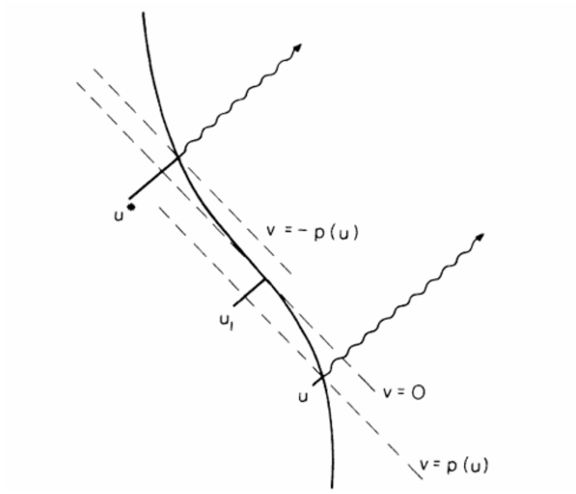

Figure 3.12: Trajectory of mirror emulating an evaporating black hole from the study in Ref. [207].

Even if the model in Ref. [207] is reasonable, there is actually no hint of a process involving a smooth transition during the black hole complete evaporation. Moreover, the mass evolution in Eq. (2.63) was obtained by considering an adiabatic evaporation [30]. In particular, it was obtained by considering Eq. (2.72) for the flux of energy emitted. However, this flux slightly deviates from Eq. (2.72) when the black hole mass is changing. In other words, to obtain Eq. (2.63), the black hole evaporation considered to be so slow that any *backreaction effects* that the effects given by the horizon shrinking are negligible. While this is obviously true on the early evaporation stage, the mass can evolve in a considerable way at late evaporation stages, requiring a generalization of the flux (2.72).

Therefore, the evaporating black hole analog mirror model of Ref. [207] is now revisited by considering a different flux of energy emitted. Moreover, a sharp transition when the black hole completely evaporates is now allowed without violating energy conservation. As mirror trajectory, Eq. (2.73) is considered, to let Hawking radiation switching on at $t \sim 0$. However, the parameter $\kappa = \frac{1}{4M}$ in Eq. (2.73) is now time-dependent as the black hole mass changes. To study the black hole mass evolution, the energy conservation is employed, i.e. $\frac{dE}{dt} = -\frac{dM}{dt}$. From the mirror analogy, $\frac{dE}{dt}$ is given by the flux F of energy radiated at the right of the mirror given by Eq. (2.68). If κ is not time-dependent, one obtains Eq. (2.71) and the energy conservation $F = -\frac{dM}{dt}$ gives exactly the black hole mass evolution (2.63).

In case κ evolves in time, by putting Eq. (2.73) into Eq. (2.68), one has a third order differential equation as

$$\dot{M} = -F(t, M, \dot{M}, \ddot{M}, \dddot{M}), \tag{3.131}$$

with initial conditions $M(0) = M_0$, $\dot{M}(0) = \frac{1}{768\pi M_0^2}$, $\ddot{M}(0) = \frac{1}{384\pi M_0^3}$, as they are the derivatives occurring in the adiabatic case. Eq. (3.131) can be simplified by considering two range of times:

- $0 \leq t \leq t_0$, the deviations from the Hawking flux (2.71) are negligible - i.e. the process can be considered as adiabatic.

- $t_0 < t < t_{\text{ev}}$, where the aforementioned deviations become non-negligible.

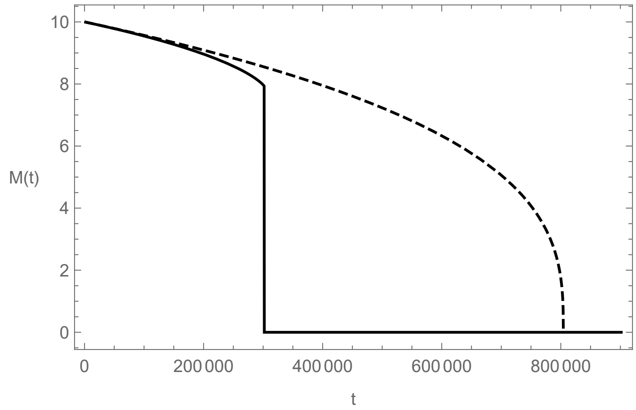

Figure 3.13: Mass evolution curve $M(t)$ of a black hole with initial mass $M_0 = 10$ obtained from Eq. (3.132) (continuous line) and from Eq. (2.63) (dashed line).

For t_0, the condition is that $\frac{\dot{M}}{M} t_0 \ll 1$, which is verified if $t_0 \gg 2M_0$. Since the evaporation time t_{ev} is expected to be of the order M_0^3, then the existence of a time t_0 such that the mass transformation is adiabatic before it implies $M_0^3 \gg M_0$, i.e. $M_0 \gg 1$.

In the range $0 < t < t_0$, the flux of energy radiation can be approximated to the adiabatic one in Eq. (2.71), while in the range $t_0 < t < t_{\text{ev}}$ one can approximate $W(\exp(-t/2M(t))) \sim \exp(-t/2M(t))$ in Eq. (2.73). In this way, Eq. (3.131) becomes

$$\begin{cases} \dot{M} = \frac{1}{768\pi M^2} & \text{for } 0 < t < t_0\,. \\ \dot{M} = -\dfrac{3\frac{\ddot{M}^2}{M^2}t^2 + \frac{1}{4M^2}\left(1-\frac{\dot{M}}{M}t\right)^4 + 2\frac{\dddot{M}}{M}t\left(1-\frac{\dot{M}}{M}t\right) - 12\frac{\ddot{M}\dot{M}}{M^2}t}{192\pi\left(1-\frac{\dot{M}}{M}t\right)^2} & \text{for } t > t_0\,. \\ M(t=0) = M_0\,. \end{cases} \tag{3.132}$$

The numerical solution of Eq. (3.132) for the mass evaporation curve is plotted in Fig. 3.13 and compared with the Hawking one (2.63). The parameter t_0 was fixed at $200M_0$ and by doing this, the evaporation time t_{ev} results to be $\sim 10^3$ times greater than t_0, validating our approximation.

From Fig. 3.13, the event horizon shrinking inreases the mass evaporation rate. This result is in line to the one predicted by models involving Hawking radiation via a tunneling effect [94, 208]. Moreover, a very noticeable thing one sees from Fig. 3.13 is the sudden mass drop occurring on a critical time called t_c.

Remarkably, this stiffness is not given by any singularity, but it is actually smooth and it can be analytically predicted. In fact, for $t < t_c$ the mass derivatives are not expected to depart too much from their value in the adiabatic case. In this way, the orders of $\dot{M}$, $\ddot{M}$ and $\dddot{M}$ are expected respectively to be

$$\begin{cases} \dot{M} \sim 10^{-3}/M_0^2\,; \\ \ddot{M} \sim 10^{-6}/M_0^5\,; \\ \dddot{M} \sim 10^{-9}/M_0^8\,. \end{cases} \tag{3.133}$$

Bearing this in mind, in Eq. (3.131) for $t_0 < t < t_c$ the second term on the numerator in the r.h.s.

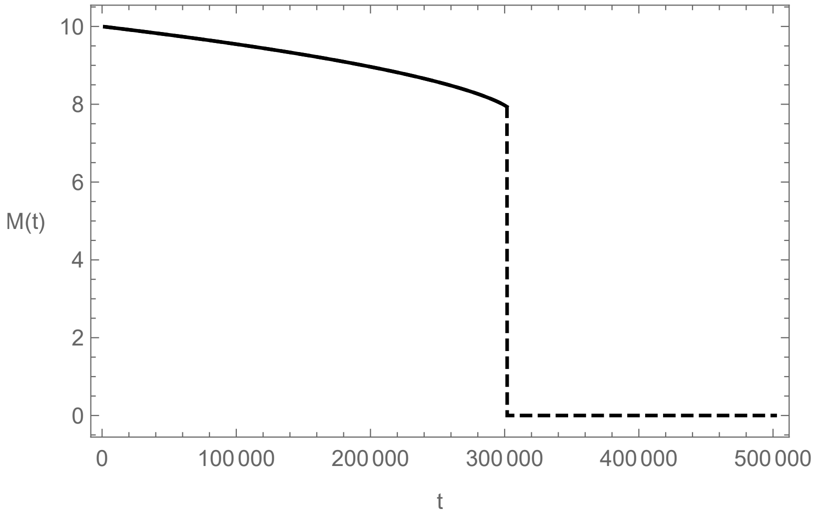

Figure 3.14: Numerical solutions for the mass evolution from Eq. (3.134) (thick line) and the one from Eq. (3.132) (dashed line).

is dominant w.r.t. the other numerator terms so that one may write

$$\dot{M} \sim -\frac{1}{768\pi M^2}\left(1-\frac{\dot{M}}{M}t\right)^2 . \tag{3.134}$$

From Fig. 3.14, the solutions of Eqs. (3.134) and (3.132) basically coincide when $t < t_c$. By manipulating Eq. (3.135), one has

$$\dot{M} = -\frac{384\pi M^4}{t^2} + \frac{M}{t} + \frac{384\pi M^4}{t^2}\sqrt{1-\frac{t}{192\pi M^3}}\,, \tag{3.135}$$

whose solution exists only if $t \leq 192\pi M^3(t)$. Therefore, as t increases to $192\pi M^3$, $\ddot{M}(t)$ diverges as $\sim \left(1-\frac{t}{192\pi M^3}\right)^{-1/2}$. As a consequence, the terms in Eq. (3.132) in the numerator which were neglected to achieve Eq. (3.134) suddenly increase, in a neighborhood of $t = 192\pi M^3(t)$, becoming dominant and making $M(t)$ to drop sharply as Fig. (3.13) shows.

At this point, t_c can be associated to the time at which the square root of Eq. (3.135) nullifies, i.e. $t_c = 192\pi M_c^3$, where M_c is a critical mass, studied numerically to be $M_c \sim 0.7937 M_0 \simeq 2^{-1/3} M_0$ - tested for masses from $M_0 = 5$ to $M_0 = 50$. Therefore, one has have

$$M_c \simeq \frac{M_0}{\sqrt[3]{2}} \Longrightarrow t_c \simeq 96\pi M_0^3 = \frac{3}{8} t_{ev}^H, \tag{3.136}$$

where $t_{\text{ev}}^H := 256\pi M_0^3$ is the evaporation time predicted in the adiabatic process.

When $t > t_c$, the mass drops to zero in a finite but very short time. Effectively, one has $t_{\text{ev}} \sim t_c = \frac{3}{8} t_{\text{ev}}^H$. To conclude, the BH evaporates faster by taking into account mass evaporation effects on the radiation, reducing the evaporation time by a factor $\sim 3/8$.

Physically speaking, the sharp drop of the mass is consistent with the sharp transition from a Schwarzschild to a Minkowski spacetime - or, in the analog mirror framework, from the sharp deceleration that the mirror should have at t_{ev} to return static. Both the processes, in fact, are expected to create a huge amount of particles, carrying energy that should be drained from the black hole mass. This explains why the complete evaporation occurs when the black hole mass reaches M_c. In fact, the critical mass would correspond to the energy needed for the evaporation to occur, i.e. to the energy needed to create the particles occurring from the Schwarzschild-Minkowski transition.

Another possible interpretation relies on the failure of quantum field theory in curved spacetime on late stages of black hole evaporation. Indeed, quantum gravity effects are expected to occur as $\dot{M} \sim M$. In the just studied scenario, this happens way before than in the adiabatic evaporation process. Therefore, the stiffness at t_c may simply tell us that quantum gravity is needed not only when $M \ll 1$ but even before, i.e. when $M - M_c \ll 1$.

In a quantum communication perspective, by using a mirror analogy, an evaporating black hole consists in a Carlitz-Willey accelerated mirror which sharply returns static after its evaporation at $t_c = 192\pi M_0^3$. Then, both the sender and the receiver are considered at the right of this mirror. Clearly, since the mirror is asymptotically static both at infinite past and infinite future, for the transmissivity one has $\tau = 1$.

To compute the additive noise, the parameters B and C must be explicitly computed. The main source of noise is expected to occur at the time t_c, where the mirror supposedly goes from a speed $V = \dot{z}(t_c)$ very close to the speed of light to be static at $V = 0$. The situation is very similar to the one in Sec. 3.4.1 for impulsive accelerated mirrors going from $V = 0$ to a speed parametrized by ν. One can easily study the inverse situation, i.e. the one when the mirror goes from a speed parametrized by ν to be static, obtaining, in the perfectly reflecting limit $\eta \to \infty$, the following Bogoliubov coefficients

$$\alpha^{\mathrm{R}}_{\omega\omega'} = -\frac{i}{2\pi}\sqrt{\frac{\omega'}{\omega}}\left(\frac{1}{\omega - \omega' + i\epsilon} - \frac{1}{\omega - \omega'\nu - i\nu\epsilon}\right)\,; \tag{3.137}$$

$$\alpha^{\mathrm{L}}_{\omega\omega'} = 0\,; \tag{3.138}$$

$$\beta^{\mathrm{R}}_{\omega\omega'} = -\frac{i}{2\pi}\sqrt{\frac{\omega'}{\omega}}\left(\frac{1}{\omega + \omega'} - \frac{1}{\omega + \omega'\nu}\right)\,; \tag{3.139}$$

$$\beta^{\mathrm{L}}_{\omega\omega'} = 0\,. \tag{3.140}$$

Since $\nu \gg 1$, the two non-null coefficients (3.137) and (3.139) can be approximated to

$$\alpha^{\mathrm{R}}_{\omega\omega'} = -\frac{i}{2\pi}\sqrt{\frac{\omega'}{\omega}}\frac{1}{\omega - \omega' + i\epsilon}\,; \tag{3.141}$$

$$\beta^{\mathrm{R}}_{\omega\omega'} = -\frac{i}{2\pi}\sqrt{\frac{\omega'}{\omega}}\frac{1}{\omega + \omega'}\,. \tag{3.142}$$

By putting Eqs. (3.141) and (3.142) into Eqs. (3.66) one can easily obtain

$$B = N_\omega = \frac{1}{\delta(0)}\frac{\ln\frac{\omega_c}{\omega}}{4\pi^2\omega} - 1\,; \quad C = \frac{1}{\delta(0)}\frac{\ln\frac{\omega_c}{\omega}}{4\pi^2\omega}\,, \tag{3.143}$$

where ω_c is an ultraviolet cutoff. Despite the divergence on the numerator and denominator, there is no way to relate ω_c to the Dirac delta $\frac{1}{\pi\epsilon}$ as done for eternal black holes in Sec. 2.3. In fact, in the aforementioned section, the divergence in Eq. (2.47) was related to $\delta^3(0)$ by using Eq. (2.21a). However, this method does not work for the coefficients (3.141) and (3.142) since $|\alpha^{\mathrm{R}}_{\omega\omega'}|^2 =$

$|\beta^{\mathrm{R}}_{\omega\omega'}|^2 + \delta(0)$. Therefore, the cutoff ω_c appears to be unrelated with $\delta(0)$, and therefore to the infinitesimal ϵ in Eq. (3.141). Nevertheless, energy conservation implies

$$\int_0^{\omega_c} \omega N_\omega = M_c \,. \tag{3.144}$$

In this way, ω_c is related to the critical mass M_c as

$$M_c = \frac{\omega_c}{4\pi^2} \,. \tag{3.145}$$

From Eq. (3.145), ω_c turns out to be a finite-valued parameter. As a consequence, the parameters B and C from Eq. (3.143) become negligible. This is of course a consequence of a finite particle production averaged on an infinite range of time. By using the wave packets introduced in Sec. 2.3, a finite additive noise is expected. This noise would fade as the communication scheme occurs in delay w.r.t. the evaporation time.

To conclude, by using the mirror-analog model, if a message is sent into an already formed evaporating black hole, it should come out unaltered after the black hole complete evaporation. The outgoing message would be accompanied by an additive noise which is $\sim M_c$ if the message is sent just after the black hole formation, fading if sent afterwards.

This result appears to be out of the box w.r.t. the standard picture emerging from many approaches to black-hole evaporation, predicting a scrambling of the information fallen into a black hole. The different prediction originates from the specific assumptions of the mirror-analog model. In most treatments, the dynamics across the horizon is analyzed using semiclassical QFT on a fixed background, where the event horizon is assumed to persist long enough for the infalling degrees of freedom to be effectively absorbed. In contrast, the mirror model does not incorporate a true geometric horizon, but rather an effective, time-dependent boundary condition encoding the causal structure seen by the external observer. Because the mirror trajectory is constructed to reproduce the Hawking flux without appealing to trans-horizon propagation, information is never truly lost behind a one-way surface: it is instead temporally delayed and re-emitted.

This simplifying feature makes the mirror model extremely transparent but also non-geometric. The absence of a strict event horizon implies that any ingoing signal is always, in principle, reflected back - though possibly after an exponentially long time. For this reason, the model naturally predicts that information injected after the formation stage will eventually reappear in the outgoing radiation, up to a calculable amount of additive noise. Clearly, this is a more *unitary-by-construction* scenario than the standard semiclassical picture, and future refinements should compare the mirror-induced re-emission with more realistic dynamical geometries.

Interestingly, this result is in line with the fact that an external observer would never see an object free falling to a black hole crossing its horizon. In this way, if the horizon shrinks with the evaporation, the object would shrink with him until the complete evaporation would let the object free traveling again on the other side, effectively crossing the evaporated black hole. A recent paper [209] proved that a free falling observer would never cross the black hole horizon even in its proper frame, effectively freezing in its proximity. In this way, the information of an object falling into the horizon is recovered after the evaporation it each frame - as predicted by the analog mirror model.

The mirror as a black hole analog model, therefore, appears to be consistent more with the *atemporal black hole* addressed in Ref. [209] that with the usual black hole studied in the literature. Further works, exploring the evaporation properties of such black hole models, are currently ongoing.

3.6 Effects of an additive noise to quantum channels

To conclude the Chapter, the effects of a noisy background into a perfect quantum channel is explored. In fact, any detector placed in the outer space, including the ones designed for high-precision cosmological measurements, is unavoidably immersed in a particle bath, providing noise. The major source of thermal noise, permeating all the Universe, is the *cosmic microwave background* (or CMB, for brevity) [163] constituting the primary relic radiation from the Big Bang.

As occurred for a cosmological particle production (see Fig. 3.2), also a small amount of particle in the background noisy could affect the qubits communication by a considerable amount.

This possibility is now explored with a quantum communication protocol. In particular, Alice sends a one-mode bosonic message, with frequency ω, to Bob, achieving the message together with an additive noise $\overline{n}$. The transmissivity of the channel is $\tau = 1$, since the Bogoliubov coefficients are the trivial ones, i.e. $\alpha_{\mathbf{kk'}} = \delta^3(\mathbf{k} - \mathbf{k'})$ and $\beta_{\mathbf{kk'}} = 0$. The particle-bounded classical capacity and the quantum capacity, from Eqs. (3.36) and (3.38) are respectively

$$C_N^{(1)} = h\left(\frac{1}{2} + N + \overline{n}\right) - h\left(\frac{1}{2} + \overline{n}\right) ; \tag{3.146}$$

$$Q^{(1)} = -1 - \log \overline{n} \, . \tag{3.147}$$

From Eq. (3.146), classical communication is affected by a small additive noise $\overline{n} \ll N$ by a negligible amount, namely $\overline{n} \log \overline{n}$. On the contrary, from Eq. (3.147) a very small noise on the background would limit the rate of qubits one can reliably communicate. Fig. 3.15 shows the quantum capacity of the channel in terms of the additive noise. The situation is very similar to the one presented in Sec. 3.3[7]. Again, even if the background noise is very small ($\overline{n} \sim 10^{-30}$) then there is a finite and relatively low number of qubits (~ 100) one can possibly communicate reliably, confirming the initial prediction.

3.6.1 Quantum capacity in presence of an Anton-Schmidt black hole

The results found so far for additive noise channels give hope to detect even a very small radiation by simply check the preserved quantum information on quantum states. For this reason, the effects of the radiation emitted by black holes on communication protocols is now investigated. Currently, Hawking radiation is impossible to detect due to its energy magnitude, several orders weaker than the CMB - despite progresses on its possible detection by primordial black hole observation [210, 211]. However, a reliable communication protocol with hundreds of qubits, as proved in the previous subsection, may lose quantum information, making possible to achieve low energy radiation by quantify the information loss.

The number of particles on the background, in presence of a black hole, was obtained in Sec. 2.3 and follow the spectrum

$$\overline{n} = \frac{1}{e^{\omega/T} - 1} \, . \tag{3.148}$$

The black hole temperature T is $(8\pi M)^{-1}$ in the Schwarzschild scenario, but it can be generalized as in Eq. (2.60) for black holes in a cosmological fluid of density ϱ and pressure P. By putting Eq.

[7] by comparing Figs. 3.2 and 3.15, the last one shows a slightly less quantum capacity for the same additive number of particles.

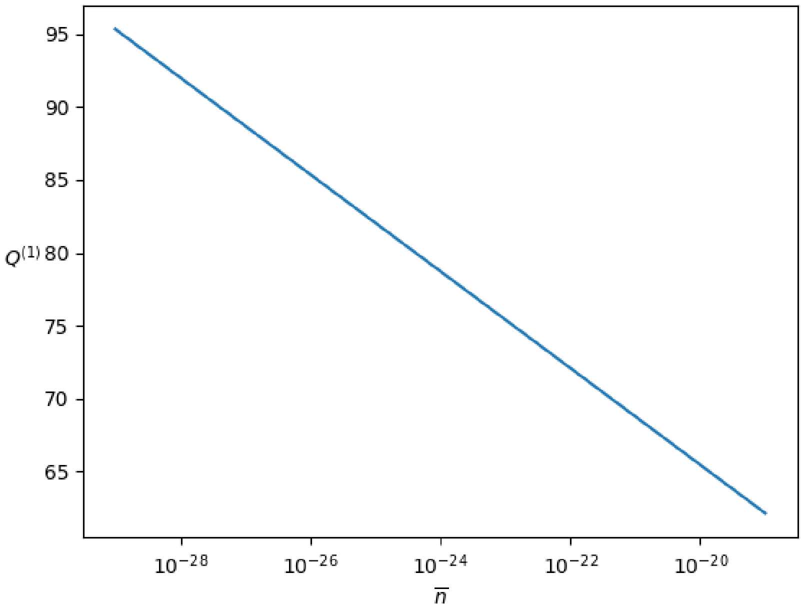

Figure 3.15: Plot of the one-shot quantum capacity $Q^{(1)}$ (Eq. (3.38)) of an additive noise channel ($\tau = 1$), in terms of the additive noise itself, made by $\overline{n}$ particles.

(3.148) into Eq. (3.147) one obtains the quantum capacity of a channel in presence of a black hole which, in turn, depends on the black hole temperature.

The fact that the background fluid modifies the black hole temperature open the possibility to test the cosmological fluid once Hawking radiation has been achieved - and therefore, once the quantum information loss of the protocol just studied has been quantified. For this reason, the loss of quantum capacity is investigated for different parameters of the cosmological fluid. Among them, *Anton-Schmidt fluids* are chosen. Their equation of state reads

$$P(\varrho) = A\left(\frac{\varrho}{\varrho_*}\right)^{-n} \ln\left(\frac{\varrho}{\varrho_*}\right) . \tag{3.149}$$

In solid-state physics, Anton-Schmidt fluids describe the isotropic deformation of crystalline solids under pressure [212]. In this context, A is a constant depending on the material, ρ_* is a reference density and n is related to the bulk modulus of the solid.

In cosmology, Anton-Schmidt fluids - generalizing the logotropic fluid, obtained for $n = 0$ in Eq. (3.149) - found a lot of applications as a single fluid behaving like dark matter in the early Universe and dark energy in the late Universe [17, 62, 18, 19, 213]. In fact, for high densities, i.e. early Universe, the pressure drops to zero and the fluid mimics pressureless matter, allowing structure formation as cold dark matter does. For low densities, i.e. late Universe, pressure becomes negative and the fluid allows an accelerated expansion.

The Anton-Schmidt fluid has also been investigated within the Tolman-Oppenheimer-Volkov formalism [214, 215] to derive analytical solutions for static and spherically symmetric black holes [216]. In particular, by relating the parameters A, ϱ_* and n and to the black hole mass, one obtains spacetime solutions corresponding to Schwarzschild-de Sitter geometries as well as naked singularities.

For this reason, the thermodynamics of a black hole is now studied under the pressure of an Anton-Schmidt fluid. The metric line element is given by Eq. (2.56) where $f(r,\varrho)$ is given by Eq. (2.57). Therefore, the aim is now to find the parameter $h(r,\varrho)$ in Eq. (2.57). To do that, the first thermodynamic law $dE = dM = TdS - PdV$ is employed. This law, under the integrability condition [217, 218] $\frac{\partial^2 S}{\partial V \partial T} = \frac{\partial^2 S}{\partial T \partial V}$, becomes

$$TS = (\rho + P)V\,. \tag{3.150}$$

By putting Eqs. (2.53), (2.59), (2.60) and (3.149) into Eq. (3.150), one has

$$8\pi r^2(P - 2\varrho)P_\varrho + 6(\varrho + P)h_\varrho - 3(rh)'P_\varrho = 0\,, \tag{3.151}$$

where the subscript ϱ and the prime denote the partial derivatives with respect to the density and radial coordinate, respectively.

The computation of Eq. (3.151) was performed in the Appendix A. In particular, a general solution of Eq. (3.151) for $h(r,\varrho)$ was first found. Then, the possible solutions are restricted to the ones giving a valid event horizon and where the null-energy, weak-energy, and dominant energy conditions, explained in Sec. 2.2 are respected. The final solution is

$$h(r,\varrho) = \frac{8}{3}\pi r^2 P(\rho) - r^{\frac{2}{\beta}-1}(a(\rho))^{1/\beta}\,, \tag{3.152}$$

where

$$a(\varrho) \equiv \exp\left(\int \frac{P_\varrho}{P+\varrho}\,d\varrho\right), \tag{3.153}$$

with integration condition $a(\varrho_* e^{1/n}) = 1$ and β is a parameter, namely

- $\beta = 2/3$, giving the usual asymptotic anti-de Sitter metric solution

$$f(r,\varrho) = -\frac{2M}{r} + \frac{8}{3}\pi r^2 P(\varrho)\,. \tag{3.154}$$

- $\beta = 2$, giving a black hole solution from Eq. (2.56) with

$$f(r,\varrho) = \sqrt{a(\varrho)} - \frac{2M}{r}\,. \tag{3.155}$$

  This solution respects the energy conditions only if the Anton-Schmidt parameter n is positive.

The metric solution (3.154) is considered to be trivial, since it simply means that the Anton-Schmidt fluid gives a further pressure to the black hole. Instead, the solution (3.155) is a non-trivial solution representing a Schwarzschild black hole with altered refractive index. The properties of such a black hole are studied extensively in Ref. [P2]. One can easily prove that the metric (2.56) with $f(r,\rho)$ from Eq. (3.155), where put on the Einstein equations (2.12) gives the stress-energy tensor $\frac{|\Lambda|}{8\pi}g_{\mu\nu}$, canceling with the cosmological constant term. The horizon is shifted to $r_{\rm h} = 2M\sqrt{a(\varrho)}$.

By putting Eq. (3.155) into Eq. (2.60), one obtains

$$T = \frac{a(\varrho)}{8\pi M}\,. \tag{3.156}$$

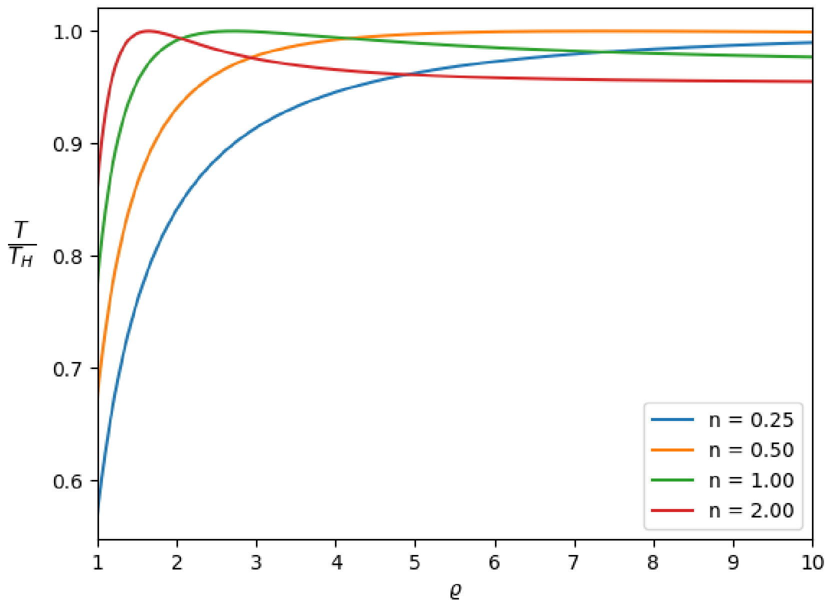

Figure 3.16: Temperature of an asymptotic anti-de Sitter black hole in an Anton-Schmidt cosmological fluid (3.156), in terms of the density of the fluid ϱ, w.r.t. the Hawking temperature $T_{\mathrm{H}} = \frac{1}{8\pi M}$. The Anton-Schmidt parameters in Eq. (3.149) are $A = 1$ and $\rho_* = 1$

From Eq. (3.156), the function $a(\varrho)$ corresponds to the ratio between the Anton-Schmidt black hole temperature and the Hawking temperature $T_{\mathrm{H}} = (8\pi M)^{-1}$. From (3.153), $a(\varrho) = T/T_{\mathrm{H}}$ can be numerically computed, with the result shown in Fig. 3.16. From this figure, both for high and low densities, the black hole temperature decreases. Therefore, if black holes are immersed into an Anton-Schmidt black hole (thought as a cosmological fluid model), then its particle production can drastically decrease and with it, also the noise given to communication protocols. Moreover, in the logotropic limit $n \ll 1$, the black hole temperature is basically unaltered for high densities - i.e. early Universe - while it drops to zero for low densities regimes - i.e. late Universe. This feature can compromise even more the possibility to observe black hole radiation. On the other face of the medal, by performing the communication protocol in presence of a black hole, if the communication noise is less than expected, then the nature of a cosmological fluid can be tested. This provides another example on how quantum communication protocols can be used as a mean to test gravity theories as well as eventual presence and properties of cosmological fluids.

Chapter 4

Quantum communication via localized quantum systems

Contents

The preservation of the information content of particle with a well-defined momentum and frequency, up to Bogoliubov transformations or background noisy, was analyzed in Chapter 3. The use of such states relies on their simplicity and the conceptual clarity.

However, because of the uncertainty principle, such states are not well localized in space and time. In fact, a one-mode bosonic state with momentum $\mathbf{k}$ would have an infinite space and time extension. In Chapter 3 this problem was faced by considering the sender and the receiver at an infinite time distance w.r.t. each other - i.e. the sender at "remote past" and the receiver at "far future". This allowed a causal loss of information also for infinitely spatially extended wave packet modes. This approach is clearly failing whenever the communication occurs in finite times.

To provide more realistic communication protocols, spatially localized wave-packets are now employed. The goal is to know how this packets may encode information and how this information would be communicated and preserved up to gravitational effects, analogously to the analysis performed in Chapter 3. The transfer of information is studied between a pair of distant Unruh-deWitt detectors, interacting with a background scalar field. To allow bosonic quantum communication, harmonic oscillator detectors are used instead of the two-levels detectors, modeled in Sec. 2.4.1. In this context, a non-perturbative approach for the communication is shown and extended in non-inertial frameworks and dynamical spacetimes.

Regarding the preservation of information, a single wave packet field mode, interacting with another background field, is considered to investigate how much information is exchanged with the background by time-evolving the system. In particular, by using the linearized quantum gravity theory the quantum gravitational field is employed as background, with the goal of discerning classical and quantum behaviour of gravity in quantum information theory, as well as to predict some quantum decoherence effects as predicted by many semiclassical and quantum theories of gravity [219, 220, 48, 221].

The structure of the chapter is the following. In Sec. 4.1 the communication protocol between a pair of harmonic oscillator detector is introduced. The scheme is generalized for each detector trajectory and background spacetime. The communication channel turns out to be a bosonic Gaussian channel whose general properties are investigated. In Sec. 4.2, the communication capacities are investigated in a Minkowski background by considering two specific examples for the field-detector interaction switching-in. Causality in the communication scheme is proved. Moreover, different trajectories for the detectors are explored, to see if non-inertiality could allow a reliable communication of quantum messages. In Sec. 4.3, the effects of a cosmological expansion in the protocol just described is addressed. Finally, in Sec. 4.4, the information loss in a localized wavepacket, due to the interaction with a quantum gravitational field, is investigated. By considering a particle in a superposition of two different localizations, an intrinsic decoherence due to delf-gravity is addressed as well with quantum communication means.

This chapter is based on Refs. ([P4, P5, P7, P8, P9]).

4.1 Communication between Unruh-deWitt detectors

A pair of distant Unruh-deWitt detectors, interacting with a background field, models Wi-Fi communication between quantum systems. An Unruh-deWitt detector, can be though as a quantum antenna [222], spreading the information of its initial state to the background field . The information is then retrieved from the field by a receiver through another particle detector.

A communication protocol like this was studied in the literature by considering two-levels systems [43, 45] as detectors, allowing qubit communication. Remarkably, these quantum systems - as the one originally used by Unruh in Ref. [35] - provide simple solutions for their communication properties. However, most of the solutions provided for communication properties involves a perturbative field-detector coupling, leading to perturbatively small communication capacities. Some exceptions involve the use of gapless detectors [223, 224] or a rapid detector-field interaction [225].

Instead, to communicate bosons - with all the advantages explained in Sec. 3.1, one needs to use infinite-levels quantum systems, i.e. harmonic oscillators, as Unruh-deWitt detectors [226]. Beside the communication advantage, those systems are also promising to describe the interaction with the field beyond perturbation theory [227].

For this reason, the main focus of this chapter is on harmonic oscillator detectors, communicating via a background massless scalar field in a generic background spacetime with metric $g_{\mu\nu}$ - emulating photons when discarding polarization effects [228]. The two non-relativistic harmonic oscillators are called A and B. If the two detectors are static and in a flat background, the interaction between each detector and the field is univocally given by the Hamiltonian (2.80), where $\hat{O} = \hat{q}_\mathrm{i} = \frac{\hat{a}_\mathrm{i}+\hat{a}_\mathrm{i}^\dagger}{\sqrt{2m_\mathrm{i}\omega_\mathrm{i}}}$ with $\hat{a}_{\mathrm{i}=\mathrm{A,B}}$ and its conjugate are the ladder operators of the oscillator i. The Hamiltonian relative to the detector i is then

$$\hat{H}_\mathrm{i} = \omega_\mathrm{i}\left(a_\mathrm{i}^\dagger a_\mathrm{i} + \frac{1}{2}\right), \tag{4.1}$$

where ω_i is the energy gap of the oscillator i (i.e. its frequency).

If the two detectors are in a curved spacetime, or in motion with respect to each other, then one has to take into account the frame-dependence of the Hamiltonians (2.80) and (4.1). As discussed in Sec. 2.4.1, each detector $\mathrm{i} = \mathrm{A,B}$ has a set of locally non-relativistic coordinates - called Fermi-normal coordinates, which can be used as detector proper coordinates, i.e. $(t_\mathrm{i}, \mathbf{x}_\mathrm{i})$. Therefore, the interaction between the detector $\mathrm{i} = \mathrm{A,B}$ and the field, in the detector $\mathrm{j} = \mathrm{A,B}$ frame, reads

$$\hat{H}^\mathrm{j}_{\Phi-\mathrm{i}}(t_\mathrm{j}) = \int_{\Sigma_{t_\mathrm{j}}} \mathrm{d}\mathbf{x}_\mathrm{j}\sqrt{-g_\mathrm{j}(\mathbf{x}_\mathrm{j}, t_\mathrm{j})}F_\mathrm{i}(\mathbf{x}_\mathrm{j}, t_\mathrm{j})\hat{q}_\mathrm{i}(t_\mathrm{j}) \otimes \hat{\Phi}(\mathbf{x}_\mathrm{j}, t_\mathrm{j}), \tag{4.2}$$

where $g_\mathrm{i} := \det g^\mathrm{i}_{\mu\nu}$ and $g^\mathrm{i}_{\mu\nu}$ is the metric tensor of the spacetime the detector i lies on (if the detectors have a relative motion w.r.t. each other, then $g^\mathrm{A}_{\mu\nu} \neq g^\mathrm{B}_{\mu\nu}$). From Eq. (4.2), one has $\hat{H}^\mathrm{i}_{\Phi-\mathrm{i}} \neq \hat{H}^{\mathrm{j}\neq\mathrm{i}}_{\Phi-\mathrm{i}}$, meaning that the field-detector interaction itself is frame-dependent. According to Eq. (4.2), the Hamiltonian describing the interaction of the field with both the detectors, seen by the observer i, can be written as

$$\hat{H}^\mathrm{i}_\mathrm{I}(t_\mathrm{i}) = \hat{q}_\mathrm{A}(t_\mathrm{i}) \otimes \hat{\varphi}^\mathrm{i}_\mathrm{A}(t_\mathrm{i}) + \hat{q}_\mathrm{B}(t_\mathrm{i}) \otimes \hat{\varphi}^\mathrm{i}_\mathrm{B}(t_\mathrm{i}), \tag{4.3}$$

where, for the sake of simplicity, the following was introduced

$$\hat{\varphi}^\mathrm{j}_\mathrm{i}(t_\mathrm{j}) = \int_{\Sigma_{t_\mathrm{j}}} \mathrm{d}\mathbf{x}_\mathrm{j} F_\mathrm{i}(\mathbf{x}_\mathrm{j}, t_\mathrm{j})\hat{\Phi}(\mathbf{x}_\mathrm{j}, t_\mathrm{j})\sqrt{-g_\mathrm{j}(\mathbf{x}_\mathrm{j}, t_\mathrm{j})}\,. \tag{4.4}$$

4.1.1 Time evolution of the system with the quantum Langevin equation

The Heisenberg evolution of the operators $\hat{q}_\mathrm{A}$ and $\hat{q}_\mathrm{B}$ is now analyzed. In the frame of the detector $\mathrm{i} = \mathrm{A,B}$, the evolution of $\hat{q}_\mathrm{i}$ is given by the sum between the Hamiltonian of the harmonic oscillator i, given by Eq. (4.1) and the interaction Hamiltonian given by Eq. (4.3). This last is the one occurring in a special case of the Caldeira-Legett model for the quantum Brownian motion, where the field plays the role of an Ohmic environment [229, 230, 231]. Therefore, by analogy, the Heisenberg evolution of the moment operator $\hat{q}_{\mathrm{i}=\mathrm{A,B}}$ is then given by the following quantum Langevin equation

$$m_\mathrm{i}\frac{d^2}{dt_\mathrm{i}^2}\hat{q}_\mathrm{i}(t_\mathrm{i}) + m_\mathrm{i}\omega_\mathrm{i}^2\hat{q}_\mathrm{i}(t_\mathrm{i}) - \sum_{\mathrm{j}=\mathrm{A,B}}\int_{-\infty}^{t_\mathrm{i}} \mathrm{d}s_\mathrm{i}\chi^\mathrm{i}_\mathrm{ij}(t_\mathrm{i}, s_\mathrm{i})\hat{q}_\mathrm{j}(s_\mathrm{i}) = \hat{\varphi}^\mathrm{i}_\mathrm{i}(t_\mathrm{i}), \tag{4.5}$$

where the *dissipation kernel* was defined as

$$\chi^\mathrm{i}_\mathrm{ij}(t_\mathrm{i}, s_\mathrm{i}) := i\theta(t_\mathrm{i} - s_\mathrm{i})\langle\phi|\left[\hat{\phi}^\mathrm{i}_\mathrm{i}(t_\mathrm{i}), \hat{\phi}^\mathrm{i}_\mathrm{j}(s_\mathrm{i})\right]|\phi\rangle, \tag{4.6}$$

and $|\phi\rangle$ is the initial state of the scalar field.

At this point, the Heisenberg evolution of the system is implicitly given by coupling the two quantum Langevin equations obtained from Eq. (4.5) for $\mathrm{i} = \mathrm{A}$ and $\mathrm{i} = \mathrm{B}$. However, these equation work with a different proper time. Since, the protocol consists in Alice - having the detector A - sending her state to Bob - holding the detector B - the channel properties are computed from Bob's observations. Therefore, it makes sense to compute the evolution of $\hat{q}_{\mathrm{i=A,B}}$ is computed in Bob's proper time. Eq. (4.5) with $\mathrm{i} = \mathrm{A}$, in terms of t_{B}, becomes

$$m_{\mathrm{A}}\frac{1}{\dot{t}_{\mathrm{A}}^2}\ddot{\hat{q}}_{\mathrm{A}} - m_{\mathrm{A}}\frac{\ddot{t}_{\mathrm{A}}}{\dot{t}_{\mathrm{A}}^3}\dot{\hat{q}}_{\mathrm{A}} + m_{\mathrm{A}}\omega_{\mathrm{A}}^2\hat{q}_{\mathrm{A}} - \sum_{\mathrm{j=A,B}} \mathrm{d}s_{\mathrm{B}} \int_{-\infty}^{t_{\mathrm{B}}} \chi_{\mathrm{Aj}}^{\mathrm{A}}(t_{\mathrm{B}}, s_{\mathrm{B}})\hat{q}_{\mathrm{j}}(s_{\mathrm{B}})\dot{t}_{\mathrm{A}}(s_{\mathrm{B}}) = \hat{\varphi}_{\mathrm{A}}^{\mathrm{A}}(t_{\mathrm{B}}) , \tag{4.7}$$

where the upper dot indicates the derivative w.r.t. t_{B}.

From now on, Bob's proper time t_{B} is indicated simply by t. The two Langevin equations, i.e. Eq. (4.5) with $\mathrm{i} = \mathrm{B}$ and Eq. (4.7) can be compactly written as

$$\ddot{\mathbf{q}}(t) - \frac{\dot{\mathbb{F}}(t)}{\mathbb{F}(t)}\dot{\mathbf{q}}(t) + (\mathbb{F}(t)\Omega)^2\mathbf{q}(t) - \mathbb{F}^2(t)\mathbb{M}^{-1}\int_{-\infty}^{t} \mathrm{d}r\mathbb{F}(r)\chi(t,r)\mathbf{q}(r) = \mathbb{F}^2(t)\mathbb{M}^{-1}\boldsymbol{\varphi}(t) , \tag{4.8}$$

where

$$\begin{gathered}\hat{\mathbf{q}} \coloneqq \begin{pmatrix}\hat{q}_{\mathrm{A}}\\ \hat{q}_{\mathrm{B}}\end{pmatrix}; \quad \mathbb{M} \coloneqq \mathrm{diag}(m_{\mathrm{A}}, m_{\mathrm{B}}); \quad \Omega \coloneqq \mathrm{diag}(\omega_{\mathrm{A}}, \omega_{\mathrm{B}}); \quad \mathbb{F}(t) \coloneqq \mathrm{diag}(\dot{t}_{\mathrm{A}}(t), 1);\\ \hat{\boldsymbol{\varphi}} \coloneqq \begin{pmatrix}\hat{\varphi}_{\mathrm{A}}^{\mathrm{A}}\\ \hat{\varphi}_{\mathrm{B}}^{\mathrm{B}}\end{pmatrix}; \quad \chi(t,s) \coloneqq \begin{pmatrix}\chi_{\mathrm{AA}}^{\mathrm{A}} & \chi_{\mathrm{AB}}^{\mathrm{A}}\\ \chi_{\mathrm{BA}}^{B} & \chi_{\mathrm{BB}}^{\mathrm{B}}\end{pmatrix} .\end{gathered} \tag{4.9}$$

Instead of the evolution of $\hat{q}_{\mathrm{i}}$, the one of $\hat{Q}_{\mathrm{i}} = \frac{\hat{a}_{\mathrm{i}}+\hat{a}_{\mathrm{i}}^\dagger}{\sqrt{2}} = \sqrt{m_{\mathrm{i}}\omega_{\mathrm{i}}}\hat{q}_{\mathrm{i}}$ is more convenient to study, since its expectation value is adimensional. In so doing, Eq. (4.8) can be rewritten as

$$\ddot{\mathbf{Q}}(t) - \frac{\dot{\mathbb{F}}(t)}{\mathbb{F}(t)}\dot{\mathbf{Q}}(t) + (\mathbb{F}(t)\Omega)^2\mathbf{Q}(t) - \mathbb{F}^2(t)\sqrt{\frac{\Omega}{\mathbb{M}}}\int_{-\infty}^{t} \mathbb{F}(r)\chi(t,r)(\sqrt{\mathbb{M}\Omega})^{-1}\mathbf{Q}(r)dr = \mathbb{F}^2(t)\sqrt{\frac{\Omega}{\mathbb{M}}}\boldsymbol{\varphi}(t) , \tag{4.10}$$

where $\mathbf{Q} = \sqrt{\mathbb{M}\Omega}\mathbf{q}$.

The solution of Eq. (4.10) can be found in terms of Green functions. In particular, the Green function matrix $\mathbb{G} = \begin{pmatrix}G_{\mathrm{AA}}(t,s) & G_{\mathrm{AB}}(t,s)\\ G_{\mathrm{BA}}(t,s) & G_{\mathrm{BB}}(t,s)\end{pmatrix}$ is defined such that it satisfies the homogeneous form of the Langevin equation (4.10), i.e.

$$\ddot{\mathbb{G}}(t,s) - \frac{\dot{\mathbb{F}}(t)}{\mathbb{F}(t)}\dot{\mathbb{G}}(t,s) + (\mathbb{F}(t)\Omega)^2\mathbb{G}(t,s) - \mathbb{F}^2(t)\sqrt{\frac{\Omega}{\mathbb{M}}}\int_{-\infty}^{t} \mathbb{F}(r)\chi(t,r)(\sqrt{\mathbb{M}\Omega})^{-1}\mathbb{G}(r,s)dr = \delta(t-s)\mathbb{I} . \tag{4.11}$$

By imposing the causality condition $\mathbb{G}(t \leq s) = 0$, the Green function matrix follows the boundary conditions $\mathbb{G}(t = s, s) = 0$ and $\dot{\mathbb{G}}(t \to s, s) = \mathbb{I}$. In this way, the operators $\mathbf{Q} = (\hat{Q}_{\mathrm{A}}, \hat{Q}_{\mathrm{B}})$ can be defined at a time t by knowing them at a time s by using the Green function matrix, namely

$$\mathbf{Q}(t) = \dot{\mathbb{G}}(t,s)\mathbf{Q}(s) + \mathbb{G}(t,s)\dot{\mathbf{Q}}(s) + \int_{s}^{t} \mathrm{d}r\mathbb{G}(t,r)\sqrt{\frac{\Omega}{\mathbb{M}}}\mathbb{F}^2(r)\boldsymbol{\varphi}(r) . \tag{4.12}$$

4.1.2 Quantum channel between detectors

A pair of harmonic oscillator detectors can be considered as a two-modes bosonic Gaussian system (studied in Sec. 3.1.4) where each harmonic oscillator represents a mode. From Eq. (3.5), its covariance matrix is

$$\sigma = \left(\begin{array}{c|c}\sigma_{\mathrm{AA}} & \sigma_{\mathrm{AB}}\\ \hline \sigma_{\mathrm{AB}} & \sigma_{\mathrm{BB}}\end{array}\right) . \tag{4.13}$$

The submatrices $\sigma_{\rm ii}$ with $\rm i = A, B$ is the covariance matrix of the substate made by the single harmonic oscillator i. Instead, $\sigma_{\rm AB}$ represents the correlations between the two detectors - imposed to be null at the time s, i.e. the beginning of the protocol.

By looking at the explicit form of the submatrices, in Eq. (3.11), the covariance matrix (4.13) is characterized by the quadrature operators $\hat{Q}_{\rm A}$, $\hat{Q}_{\rm B}$, $\hat{P}_{\rm A}$ and $\hat{P}_{\rm B}$. The evolution of $\hat{Q}_{\rm i=A,B}$ is given by Eq. (4.12). Instead, the evolution of $\hat{P}_{\rm i}$ can be derived from its Heisenberg equation, giving the equivalence $\frac{d}{dt_{\rm i}}\hat{Q}_{\rm i} = \omega_{\rm i}\hat{P}_{\rm i}$ - or $\dot{\mathbf{Q}}(t) = \mathbb{F}(t)\Omega\mathbf{P}(t)$ by using the notation (4.9) - obtaining

$$\mathbf{P}(t) = (\mathbb{F}(t)\Omega)^{-1}\,\ddot{\mathbb{G}}(t,s)\mathbf{Q}(s) + (\mathbb{F}(t)\Omega)^{-1}\,\dot{\mathbb{G}}(t,s)\mathbb{F}(s)\Omega\mathbf{P}(s) \tag{4.14}$$

$$+ (\mathbb{F}(t)\Omega)^{-1}\int_s^t \mathrm{d}r\dot{\mathbb{G}}(t,r)\sqrt{\frac{\Omega}{\mathbb{M}}}\mathbb{F}^2(r)\boldsymbol{\varphi}(r)\,. \tag{4.15}$$

Moreover, in Eq. (4.12), $\dot{\mathbf{Q}}$ can be written in terms of $\mathbf{P}$ as

$$\mathbf{Q}(t) = \dot{\mathbb{G}}(t,s)\mathbf{Q}(s) + \mathbb{G}(t,s)\mathbb{F}(s)\Omega\mathbf{P}(s) + \int_s^t \mathrm{d}r\mathbb{G}(t,r)\sqrt{\frac{\Omega}{\mathbb{M}}}\mathbb{F}^2(r)\boldsymbol{\varphi}(r)\,. \tag{4.16}$$

The covariance matrix (4.13) is now rewritten in a different basis for computational purposes. Namely, one defines $\sigma_c := P\sigma P$, where P is the permutation matrix

$$P = \begin{pmatrix} 1 & 0 & 0 & 0 \\ 0 & 0 & 1 & 0 \\ 0 & 1 & 0 & 0 \\ 0 & 0 & 0 & 1 \end{pmatrix}\,. \tag{4.17}$$

In so doing, σ_c reads

$$\sigma_c = \left(\begin{array}{c|c} \sigma_{QQ} & \sigma_{QP} \\ \hline \sigma_{PQ} & \sigma_{PP} \end{array}\right)\,, \tag{4.18}$$

where, for $\hat{\alpha}, \hat{\beta} = \hat{Q}, \hat{P}$, the submatrices are defined as

$$\sigma_{\alpha,\beta} = \frac{1}{2}\begin{pmatrix} \langle\left\{\hat{\alpha}_{\rm A}, \hat{\beta}_{\rm A}\right\}\rangle & \langle\left\{\hat{\alpha}_{\rm A}, \hat{\beta}_{\rm B}\right\}\rangle \\ \langle\left\{\hat{\alpha}_{\rm B}, \hat{\beta}_{\rm A}\right\}\rangle & \langle\left\{\hat{\alpha}_{\rm B}, \hat{\beta}_{\rm B}\right\}\rangle \end{pmatrix}\,. \tag{4.19}$$

In this way, for the submatrices of the matrix (4.18), by using Eqs. (4.14) and (4.16), one has

$$\begin{aligned}\sigma_{QQ}(t) =& \dot{\mathbb{G}}(t,s)\sigma_{QQ}(s)\dot{\mathbb{G}}^T(t,s) + \dot{\mathbb{G}}(t,s)\sigma_{QP}(s)\mathbb{F}(s)\Omega\mathbb{G}^T(t,s) + \mathbb{G}(t,s)\Omega\mathbb{F}(s)\sigma_{PQ}(s)\dot{\mathbb{G}}^T(t,s) \\ &+ \mathbb{G}(t,s)\mathbb{M}^{-1}\mathbb{F}(s)\sigma_{PP}(s)\mathbb{F}(s)\Omega\mathbb{G}^T(t,s) \\ &+ \int_s^t\int_s^t \mathbb{G}(t,r)\sqrt{\frac{\Omega}{\mathbb{M}}}\mathbb{F}^2(r)\nu(r,r')\mathbb{F}^2(r')\sqrt{\frac{\Omega}{\mathbb{M}}}\mathbb{G}^T(t,r')drdr'\,;\end{aligned} \tag{4.20}$$

$$\begin{aligned}\sigma_{QP}(t) =& \dot{\mathbb{G}}(t,s)\sigma_{QQ}(s)\ddot{\mathbb{G}}^T(t,s)\left(\mathbb{F}(t)\Omega\right)^{-1} + \dot{\mathbb{G}}(t,s)\sigma_{QP}(s)\Omega\mathbb{F}(s)\dot{\mathbb{G}}^T(t,s)\left(\mathbb{F}(t)\Omega\right)^{-1} \\ &+ \mathbb{G}(t,s)\Omega\mathbb{F}(s)\sigma_{PQ}(s)\ddot{\mathbb{G}}^T(t,s)\left(\mathbb{F}(t)\Omega\right)^{-1} + \mathbb{G}(t,s)\Omega\mathbb{F}(s)\sigma_{PP}(s)\mathbb{F}(s)\Omega\dot{\mathbb{G}}^T(t,s)\left(\mathbb{F}(t)\Omega\right)^{-1} \\ &+ \int_s^t\int_s^t \mathbb{G}(t,r)\sqrt{\frac{\Omega}{\mathbb{M}}}\mathbb{F}^2(r)\nu(r,r')\mathbb{F}^2(r')\sqrt{\frac{\Omega}{\mathbb{M}}}\dot{\mathbb{G}}^T(t,r')\left(\mathbb{F}(t)\Omega\right)^{-1}(t)drdr'\,;\end{aligned} \tag{4.21}$$

$$\sigma_{PQ}(t) = \sigma_{QP}^T(t)\,; \tag{4.22}$$

$$\sigma_{PP}(t) = (\mathbb{F}(t)\Omega)^{-1}\,\ddot{\mathbb{G}}(t,s)\sigma_{QQ}(s)\ddot{\mathbb{G}}^T(t,s)\,(\mathbb{F}(t)\Omega)^{-1} + (\mathbb{F}(t)\Omega)^{-1}\,\ddot{\mathbb{G}}(t,s)\sigma_{QP}(s)\mathbb{F}(s)\Omega\dot{\mathbb{G}}^T(t,0)\,(\mathbb{F}(t)\Omega)^{-1}$$
$$+ (\mathbb{F}(t)\Omega)^{-1}\,\dot{\mathbb{G}}(t,s)\Omega\mathbb{F}(s)\sigma_{PQ}(s)\ddot{\mathbb{G}}^T(t,s)\,(\mathbb{F}(t)\Omega)^{-1} + (\mathbb{F}(t)\Omega)^{-1}\,\dot{\mathbb{G}}(t,s)\Omega\mathbb{F}(s)\sigma_{PP}(s)\mathbb{F}(s)\Omega\dot{\mathbb{G}}^T(t,s)\,(\mathbb{F}(t)\Omega)^{-1}$$
$$+ \int_s^t\int_s^t (\mathbb{F}(t)\Omega)^{-1}\,\dot{\mathbb{G}}(t,r)\sqrt{\frac{\Omega}{\mathbb{M}}}\mathbb{F}^2(r)\nu(r,r')\mathbb{F}^2(r')\sqrt{\frac{\Omega}{\mathbb{M}}}\dot{\mathbb{G}}^T(t,r')\,(\mathbb{F}(t)\Omega)^{-1}\,(t)drdr'\,, \tag{4.23}$$

where the noise kernel was defined as

$$\nu(t,t') = \frac{1}{2}\begin{pmatrix} \langle\{\hat{\varphi}_{\rm A}^{\rm A}(t),\hat{\varphi}_{\rm A}^{\rm A}(t')\}\rangle & \langle\{\hat{\varphi}_{\rm B}^{\rm B}(t),\hat{\varphi}_{\rm A}^{\rm A}(t')\}\rangle \\ \langle\{\hat{\varphi}_{\rm A}^{\rm A}(t),\hat{\varphi}_{\rm B}^{\rm B}(t')\}\rangle & \langle\{\hat{\varphi}_{\rm B}^{\rm B}(t),\hat{\varphi}_{\rm B}^{\rm B}(t')\}\rangle \end{pmatrix}. \tag{4.24}$$

Compactly, one can rewrite Eqs. (4.20), (4.21), (4.22) and (4.23) as

$$\sigma_c(t) = \mathbf{T}\sigma_c(s)\mathbf{T}^T + \mathbf{N}\,, \tag{4.25}$$

where

$$\mathbf{T} = \left(\begin{array}{c|c} \dot{\mathbb{G}}(t,s) & \mathbb{G}(t,s)\Omega\mathbb{F}(s) \\ \hline \mathbb{F}^{-1}(t)\Omega^{-1}\ddot{\mathbb{G}}(t,s) & \mathbb{F}^{-1}(t)\Omega^{-1}\dot{\mathbb{G}}(t,s)\Omega\mathbb{F}(s) \end{array}\right); \tag{4.26}$$

$$\mathbf{N} = \left(\begin{array}{c|c} \mathbf{N}_{QQ} & \mathbf{N}_{QP} \\ \hline \mathbf{N}_{QP}^T & \mathbf{N}_{PP} \end{array}\right), \tag{4.27}$$

with

$$\mathbf{N}_{QQ} = \int_s^t\int_s^t \mathbb{G}(t,r)\sqrt{\frac{\Omega}{\mathbb{M}}}\mathbb{F}^2(r)\nu(r,r')\mathbb{F}^2(r')\sqrt{\frac{\Omega}{\mathbb{M}}}\mathbb{G}^T(t,r')drdr'\,; \tag{4.28}$$

$$\mathbf{N}_{QP} = \int_s^t\int_s^t \mathbb{G}(t,r)\sqrt{\frac{\Omega}{\mathbb{M}}}\mathbb{F}^2(r)\nu(r,r')\mathbb{F}^2(r')\sqrt{\frac{\Omega}{\mathbb{M}}}\dot{\mathbb{G}}^T(t,r')\Omega^{-1}\mathbb{F}^{-1}(t)drdr'\,; \tag{4.29}$$

$$\mathbf{N}_{PP} = \int_s^t\int_s^t \mathbb{F}^{-1}(t)\Omega^{-1}\dot{\mathbb{G}}(t,r)\sqrt{\frac{\Omega}{\mathbb{M}}}\mathbb{F}^2(r)\nu(r,r')\mathbb{F}^2(r')\sqrt{\frac{\Omega}{\mathbb{M}}}\dot{\mathbb{G}}^T(t,r')\Omega^{-1}\mathbb{F}^{-1}(t)drdr'\,. \tag{4.30}$$

By switching back to the initial basis for the covariance matrix, since $PP = \mathbb{I}$, the two-mode transformation (4.25) still holds by applying the same transformation P to the matrices $\mathbb{T}$ and $\mathbb{N}$.

The communication channel considered has Alice's detector A state as input, represented by $\sigma_{\rm AA}(s) =: \sigma_{\rm in}$. The output state is instead the state of the detector B at a time t, namely $\sigma_{\rm out} := \sigma_{\rm BB}(t)$. The matrices $\sigma_{\rm in}$ and $\sigma_{\rm out}$ can be related through Eq. (3.14), where the matrices $\mathbb{T}$ and $\mathbb{N}$ read

$$\mathbb{T} = \begin{pmatrix} \dot{G}_{\rm BA}(t,s) & G_{\rm BA}(t,s)\dot{t}_{\rm A}(s)\omega_{\rm A} \\ \frac{\ddot{G}_{\rm BA}(t,s)}{\omega_{\rm B}} & \dot{G}_{\rm BA}(t,s)\dot{t}_{\rm A}(s)\frac{\omega_{\rm A}}{\omega_{\rm B}} \end{pmatrix}; \tag{4.31}$$

$$\mathbb{N} = \begin{pmatrix} \dot{G}_{\rm BB} & G_{\rm BB}\omega_{\rm B} \\ \ddot{G}_{\rm BB}\omega_{\rm B}^{-1} & \dot{G}_{\rm BB} \end{pmatrix}\sigma_{\rm BB}(s)\begin{pmatrix} \dot{G}_{\rm BB} & \ddot{G}_{\rm BB}\omega_{\rm B}^{-1} \\ G_{\rm BB}\omega_{\rm B} & \dot{G}_{\rm BB} \end{pmatrix} + \mathbb{N}'_{\rm B}\,, \tag{4.32}$$

where $\mathbb{N}'_{\rm B} = \begin{pmatrix} N'_{11} & N'_{12} \\ N'_{12} & N'_{22} \end{pmatrix}$ with

$$N_{11} = \frac{\omega_{\rm A}}{m_{\rm A}}\int_s^t {\rm d}r\int_s^t {\rm d}r'\dot{t}_{\rm A}^2(r)\dot{t}_{\rm A}^2(r')G_{\rm BA}(t,r)\nu_{\rm AA}(r,r')G_{\rm BA}(t,r')$$
$$+\sqrt{\frac{\omega_{\rm A}\omega_{\rm B}}{m_{\rm A}m_{\rm B}}}\int_s^t {\rm d}r\int_s^t {\rm d}r'\dot{t}_{\rm A}^2(r')G_{\rm BB}(t,r)\nu_{\rm BA}(r,r')G_{\rm BA}(t,r')$$
$$+\sqrt{\frac{\omega_{\rm A}\omega_{\rm B}}{m_{\rm A}m_{\rm B}}}\int_s^t {\rm d}r\int_s^t {\rm d}r'\dot{t}_{\rm A}^2(r)G_{\rm BA}(t,r)\nu_{\rm AB}(r,r')G_{\rm BB}(t,r') + \frac{\omega_{\rm B}}{m_{\rm B}}\int_s^t {\rm d}r\int_s^t {\rm d}r' G_{\rm BB}(t,r)\nu_{\rm BB}(r,r')G_{\rm BB}(t,r')\,; \tag{4.33}$$

$$
\begin{aligned}
N_{12} = &\frac{\omega_{\mathrm{A}}}{m_{\mathrm{A}}\omega_{\mathrm{B}}}\int_s^t \mathrm{d}r\int_s^t \mathrm{d}r'\dot{t}_{\mathrm{A}}^2(r)\dot{t}_{\mathrm{A}}^2(r')G_{\mathrm{BA}}(t,r)\nu_{\mathrm{AA}}(r,r')\dot{G}_{\mathrm{BA}}(t,r')\\
&+\sqrt{\frac{\omega_{\mathrm{A}}}{m_{\mathrm{A}}m_{\mathrm{B}}\omega_{\mathrm{B}}}}\int_s^t \mathrm{d}r\int_s^t \mathrm{d}r'\dot{t}_{\mathrm{A}}^2(r')G_{\mathrm{BB}}(t,r)\nu_{\mathrm{BA}}(r,r')\dot{G}_{\mathrm{BA}}(t,r')\\
&+\sqrt{\frac{\omega_{\mathrm{A}}}{m_{\mathrm{A}}m_{\mathrm{B}}\omega_{\mathrm{B}}}}\int_s^t \mathrm{d}r\int_s^t \mathrm{d}r'\dot{t}_{\mathrm{A}}^2(r)G_{\mathrm{BA}}(t,r)\nu_{\mathrm{AB}}(r,r')\dot{G}_{\mathrm{BB}}(t,r') + m_{\mathrm{B}}^{-1}\int_s^t \mathrm{d}r\int_s^t \mathrm{d}r' G_{\mathrm{BB}}(t,r)\nu_{\mathrm{BB}}(r,r')\dot{G}_{\mathrm{BB}}(t,r')\,;
\end{aligned}
\tag{4.34}
$$

$$
\begin{aligned}
N_{22} = &\frac{\omega_{\mathrm{A}}}{m_{\mathrm{A}}\omega_{\mathrm{B}}}\int_s^t \mathrm{d}r\int_s^t \mathrm{d}r'\dot{t}_{\mathrm{A}}^2(r)\dot{t}_{\mathrm{A}}^2(r')\dot{G}_{\mathrm{BA}}(t,r)\nu_{\mathrm{AA}}(r,r')\dot{G}_{\mathrm{BA}}(t,r')\\
&+\sqrt{\frac{\omega_{\mathrm{A}}}{m_{\mathrm{A}}m_{\mathrm{B}}\omega_{\mathrm{B}}^3}}\int_s^t \mathrm{d}r\int_s^t \mathrm{d}r'\dot{t}_{\mathrm{A}}^2(r')\dot{G}_{\mathrm{BB}}(t,r)\nu_{\mathrm{BA}}(r,r')\dot{G}_{\mathrm{BA}}(t,r')\\
&+\sqrt{\frac{\omega_{\mathrm{A}}}{m_{\mathrm{A}}m_{\mathrm{B}}\omega_{\mathrm{B}}^3}}\int_s^t \mathrm{d}r\int_s^t \mathrm{d}r'\dot{t}_{\mathrm{A}}^2(r)\dot{G}_{\mathrm{BA}}(t,r)\nu_{\mathrm{AB}}(r,r')G_{\mathrm{BB}}(t,r') + \frac{1}{m_{\mathrm{B}}\omega_{\mathrm{B}}}\int_s^t \mathrm{d}r\int_s^t \mathrm{d}r'\dot{G}_{\mathrm{BB}}(t,r)\nu_{\mathrm{BB}}(r,r')\dot{G}_{\mathrm{BB}}(t,r')\,.
\end{aligned}
\tag{4.35}
$$

At this point, if the matrices $\mathbb{T}$ and $\mathbb{N}$ satisfy Eq. (3.15), then the channel from σ_{in} to σ_{out} is a one-mode Gaussian channel, with transmissivity

$$
\tau := \det\mathbb{T} = \dot{t}_{\mathrm{A}}(s)\frac{\omega_{\mathrm{A}}}{\omega_{\mathrm{B}}}\left(\dot{G}_{\mathrm{BA}}^2(t,s) - G_{\mathrm{BA}}(t,s)\ddot{G}_{\mathrm{BA}}(t,s)\right)\,. \tag{4.36}
$$

and noise given by $W := \det\mathbb{N}$ from Eq. (4.32) - not explicitly reported due to its long expression.

4.2 Communication capacities in a Minkowski background

To prove the effectiveness and the causality of the communication protocol two examples are provided. In those, the detectors lie in a Minkowski background. When possible, the effects of their non-inertial trajectory are addressed. The main difference between the two examples is on their switching-in function with the field. In particular, two opposite situations are considered i.e. *i)* the detectors continuing to interact forever with the background after their switching-in and *ii)* the detector interacting with the field in a very short time (also called *rapid interaction*) in the literature [225].

4.2.1 Long term steady interaction

The first scenario considered involves two static detectors lying in a Minkowski spacetime. This prescription is very pedagogical to understand how this communication scheme generally works.

In a Minkowski spacetime, one has trivially $t_{\mathrm{A}}(t) = t$ and the position of the detector i is given by $\mathbf{x}_{\mathrm{i}}$, by using the Minkowski coordinates $(\mathbf{x}, t)$. For both the detectors, the interaction with the field switches in sharply at the time $t = 0$ remains steady afterwards, namely

$$
\lambda_{\mathrm{i=A,B}}(t) = \lambda_{\mathrm{i}}\theta(t)\,. \tag{4.37}
$$

The parameter λ_{i} represents a coupling strength and it has the dimension of an energy.

Moreover, the detectors have the following Gaussian smearing function

$$
f_{\mathrm{i=A,B}}(\mathbf{x}) = \frac{e^{-|\mathbf{x}-\mathbf{x}_{\mathrm{i}}|^2/\sigma^2}}{(\sqrt{\pi}\sigma)^3}\,, \tag{4.38}
$$

where σ plays the role of the detectors' effective size. The background field is considered to be in the vacuum state before the interaction and, finally, the initial state of the detector B, influencing the noise parameter $W := \det \mathbb{N}$, is supposed to be the ground state $\sigma = \frac{1}{2}\mathbb{I}$.

By using this prescription, the elements of the dissipation kernel (4.6) can be computed to be

$$\chi_{\mathrm{i=j}}(t) = \frac{\lambda_{\mathrm{i}}^2 t}{2\pi^2\sigma^3}\theta(t)\sqrt{\frac{\pi}{2}}e^{-\frac{t^2}{2\sigma^2}}\,, \tag{4.39}$$

$$\chi_{\mathrm{AB}}(t) = \chi_{\mathrm{BA}}(t) = \frac{\lambda_{\mathrm{A}}\lambda_{\mathrm{B}}}{4\pi^2\sigma d}\theta(t)\sqrt{\frac{\pi}{2}}\left(e^{-\frac{(t-d)^2}{2\sigma^2}} - e^{-\frac{(t+d)^2}{2\sigma^2}}\right)\,, \tag{4.40}$$

with $d = |\mathbf{x}_{\mathrm{A}} - \mathbf{x}_{\mathrm{B}}|$ indicating the detectors' spatial distance.

For the noise kernel (4.24), instead, one has

$$\nu_{\mathrm{i=j}}(t) = \frac{\lambda_{\mathrm{i}}^2}{8\pi^2\sigma^2}\left(1 - \frac{\sqrt{2}t}{\sigma}D_+\left(\frac{t}{\sqrt{2}\sigma}\right)\right) \tag{4.41}$$

$$\nu_{\mathrm{AB}}(t) = \nu_{\mathrm{BA}}(t) = \frac{\sqrt{2}\lambda_{\mathrm{A}}\lambda_{\mathrm{B}}}{8\pi^2\sigma d}\left(D_+\left(\frac{t+d}{\sqrt{2}\sigma}\right) - D_+\left(\frac{t-d}{\sqrt{2}\sigma}\right)\right)\,, \tag{4.42}$$

where $D_+(x) = e^{-x^2}\int_0^x dy e^{y^2}$ is the Dawson function.

At this point, the homogeneous quantum Langevin equation (4.11) must be computed to obtain the Green function matrix $\mathbb{G}$. Since the background spacetime has a time-translational symmetry, then $\mathbb{G}(t,s) = \mathbb{G}(t-s)$. Moreover, since the protocol starts at a time 0, then $s = 0$ is considered[1].

The size of the detectors σ is supposed to be much smaller then their distance d, to emphasize the fact of a communication at distance. In this limit, by using the elements of the dissipation kernel (4.39) and (4.40), Eq. (4.11) simplifies to the following system

$$\begin{aligned}
\ddot{G}_{\mathrm{AA}}(t) - \Sigma_{\mathrm{A}}^2 G_{\mathrm{AA}}(t) + 2\gamma_{\mathrm{A}}\dot{G}_{\mathrm{AA}}(t) =& 2\frac{\sqrt{\gamma_{\mathrm{A}}\gamma_{\mathrm{B}}}}{d}G_{\mathrm{BA}}(t-d)\theta(t-d)\,;\\
\ddot{G}_{\mathrm{AB}}(t) - \Sigma_{\mathrm{A}}^2 G_{\mathrm{AB}}(t) + 2\gamma_{\mathrm{A}}\dot{G}_{\mathrm{AB}}(t) =& 2\frac{\sqrt{\gamma_{\mathrm{A}}\gamma_{\mathrm{B}}}}{d}G_{\mathrm{BB}}(t-d)\theta(t-d)\,;\\
\ddot{G}_{\mathrm{BA}}(t) - \Sigma_{\mathrm{B}}^2 G_{\mathrm{BA}}(t) + 2\gamma_{\mathrm{B}}\dot{G}_{\mathrm{BA}}(t) =& 2\frac{\sqrt{\gamma_{\mathrm{A}}\gamma_{\mathrm{B}}}}{d}G_{\mathrm{AA}}(t-d)\theta(t-d)\,;\\
\ddot{G}_{\mathrm{BB}}(t) - \Sigma_{\mathrm{B}}^2 G_{\mathrm{BB}}(t) + 2\gamma_{\mathrm{B}}\dot{G}_{\mathrm{BB}}(t) =& 2\frac{\sqrt{\gamma_{\mathrm{A}}\gamma_{\mathrm{B}}}}{d}G_{\mathrm{AB}}(t-d)\theta(t-d)\,,
\end{aligned} \tag{4.43}$$

with initial conditions $G_{\mathrm{AA}}(0) = G_{\mathrm{BB}}(0) = 1$ and $G_{\mathrm{AB}}(0) = G_{\mathrm{BA}}(0) = 0$. Moreover, in Eq. (4.43), $\gamma_{\mathrm{i=A,B}} := \frac{\lambda_{\mathrm{i}}^2}{8\pi m_{\mathrm{i}}}$ and $\Sigma_{\mathrm{i=A,B}}^2 := \sqrt{\frac{8}{\pi}\frac{\gamma_{\mathrm{i}}}{\sigma} - \omega_{\mathrm{i}}^2}$ were defined for the sake of simplicity.

Eq. (4.43) can be solved analytically by induction. In particular, at first, one must compute Eq. (4.43) in the range of times $0 < t < d$. Then, by knowing the solution in the range $(n-1)d < t < nd$, one is able to analytically solve it in the range $nd < t < (n+1)d$.

In the first range of times $0 < t < d$, all the elements of the Green function matrix behave as a free damped harmonic oscillator. For the diagonal elements of the Green function matrix G_{ii}, using the boundary conditions $\dot{G}_{\mathrm{ii}}(0) = 1$ and $G_{\mathrm{ii}}(0) = 0$, one gets

$$G_{\mathrm{ii}}(t) = \theta(t)\frac{e^{-\gamma_{\mathrm{i}}t}\sinh(\sqrt{\gamma_{\mathrm{i}}^2 + \Sigma_{\mathrm{i}}^2})t}{\sqrt{\gamma_{\mathrm{i}}^2 + \Sigma_{\mathrm{i}}^2}}\,. \tag{4.44}$$

[1]As reported in Sec. 4.2.2, this choice is not trivial. In fact, a time s prior to the interaction between Alice and the field could change the channel properties.

For the Green function matrix elements G_{AB} and G_{BA}, from Eq. (4.43) and with boundary conditions $G_{\mathrm{AB}}(t=0)=0$ and $\dot{G}_{\mathrm{AB}}(t=0)=0$ one has trivially $G_{\mathrm{BA}}=G_{\mathrm{AB}}=0$.

At this point, Eq. (4.43) can be computed in the range of times $d<t<2d$. For the diagonal elements $G_{\mathrm{ii}}(t)$, from the first of fourth equation of the system (4.43), one has again the solution (4.44), since the r.h.s. of those equations are null in this range.

The second and third differential equation of the system (4.43), for G_{AB} and G_{BA} become non-homogeneous at $t>d$. By imposing the continuity of G_{AB} and $\dot{G}_{\mathrm{AB}}$ at $t=d$ the off-diagonal Green's function G_{AB}, in the range $d<t<3d$, reads

$$\begin{aligned}
G_{\mathrm{AB}}(t) = {} & \frac{2}{d}\frac{\sqrt{\gamma_{\mathrm{A}}\gamma_{\mathrm{B}}}\theta(t-d)}{\left(4\gamma_{\mathrm{A}}\gamma_{\mathrm{B}}(\Sigma_{\mathrm{A}}^2+\Sigma_{\mathrm{B}}^2)-4\Sigma_{\mathrm{B}}^2\gamma_{\mathrm{A}}^2-4\Sigma_{\mathrm{A}}^2\gamma_{\mathrm{B}}^2+(\Sigma_{\mathrm{A}}^2-\Sigma_{\mathrm{B}}^2)^2\right)} \\
\times & \left(\frac{\left(2\gamma_{\mathrm{A}}^2+(\Sigma_{\mathrm{A}}^2-\Sigma_{\mathrm{B}}^2)-2\gamma_{\mathrm{A}}\gamma_{\mathrm{B}}\right)\sinh\left((t-d)\sqrt{\gamma_{\mathrm{A}}^2+\Sigma_{\mathrm{A}}^2}\right)}{\sqrt{\gamma_{\mathrm{A}}^2+\Sigma_{\mathrm{A}}^2}}e^{-\gamma_{\mathrm{A}}(t-d)}\right. \\
+ & \frac{\left(2\gamma_{\mathrm{B}}^2+(\Sigma_{\mathrm{B}}^2-\Sigma_{\mathrm{A}}^2)-2\gamma_{\mathrm{B}}\gamma_{\mathrm{A}}\right)\sinh\left((t-d)\sqrt{\gamma_{\mathrm{B}}^2+\Sigma_{\mathrm{B}}^2}\right)}{\sqrt{\gamma_{\mathrm{B}}^2+\Sigma_{\mathrm{B}}^2}}e^{-\gamma_{\mathrm{B}}(t-d)} \\
& \left.+2(\gamma_{\mathrm{A}}-\gamma_{\mathrm{B}})\left(\cosh\left((t-d)\sqrt{\gamma_{\mathrm{A}}^2+\Sigma_{\mathrm{A}}^2}\right)e^{-\gamma_{\mathrm{A}}(t-d)}-\cosh\left((t-d)\sqrt{\gamma_{\mathrm{B}}^2+\Sigma_{\mathrm{B}}^2}\right)e^{-\gamma_{\mathrm{B}}(t-d)}\right)\right).
\end{aligned} \tag{4.45}$$

For $G_{\mathrm{BA}}(t)$, one can prove that $G_{\mathrm{BA}}(t)=G_{\mathrm{AB}}(t)$.

By considering a particular range for the parameters ω_{i}, γ_{i}, d and σ, the solutions in Eqs. (4.44) and (4.45), valid at times $0\le t<2d$, are approximatively valid also for $t\ge 2d$. To show is, a Fourier transform is applied on both sides of the Homogeneous Langevin equation (4.11), obtaining, respectively for the diagonal and off-diagonal Green function matrix elements

$$\widetilde{G}_{\mathrm{ii}}(z)=\frac{-\Sigma_{\mathrm{i}}^2-z^2-2iz\gamma_{\mathrm{i}}}{\det\widetilde{\mathbb{G}}(z)^{-1}}\,, \tag{4.46}$$

and

$$\widetilde{G}_{\mathrm{i}\neq\mathrm{j}}(z)=\frac{\frac{2\sqrt{\gamma_{\mathrm{i}}\gamma_{\mathrm{j}}}}{d}e^{izd}}{\det\widetilde{\mathbb{G}}(z)^{-1}}\,. \tag{4.47}$$

The determinant of $\widetilde{\mathbb{G}}$ reads explicitly

$$\det\widetilde{\mathbb{G}}(z)^{-1}=\left(\Sigma_{\mathrm{A}}^2+z^2+2iz\gamma_{\mathrm{A}}\right)\left(\Sigma_{\mathrm{B}}^2+z^2+2iz\gamma_{\mathrm{B}}\right)-\frac{4\gamma_{\mathrm{A}}\gamma_{\mathrm{B}}}{d^2}e^{2idz}\,. \tag{4.48}$$

From Eq. (4.48), if $4\gamma_{\mathrm{A}}\gamma_{\mathrm{B}}\ll d^2|\Sigma_{\mathrm{A}}^2\Sigma_{\mathrm{B}}^2|$, then the last term in $\det\widetilde{\mathbb{G}}$ can be neglected and the Fourier-transformed Green functions (4.46) and (4.47) respectively reduce to

$$\widetilde{G}_{\mathrm{ii}}(z)=-\frac{1}{\Sigma_{\mathrm{i}}^2+z^2+2iz\gamma_{\mathrm{i}}}, \tag{4.49}$$

and

$$\widetilde{G}_{\mathrm{i}\neq\mathrm{j}}(z)=-\frac{2\sqrt{\gamma_{\mathrm{i}}\gamma_{\mathrm{j}}}e^{idz}}{d\left(\Sigma_{\mathrm{A}}^2+z^2+2iz\gamma_{\mathrm{A}}\right)\left(\Sigma_{\mathrm{B}}^2+z^2+2iz\gamma_{\mathrm{B}}\right)}, \tag{4.50}$$

The inverse Fourier transform of Eqs. (4.49) and (4.50) can now be computed. By imposing the causality condition, the solutions (4.44) and (4.45), are respectively recovered.

Therefore, if $4\gamma_{\rm A}\gamma_{\rm B} \ll d^2|\Sigma_{\rm A}^2\Sigma_{\rm B}^2|$, then the solutions of Eq. (4.43) at times $t \geq 2d$ can be approximated to the ones at times $0 \leq t < 2d$, given by Eqs. (4.44) and (4.45).

The case where the two detectors are identical - i.e. they have the same frequency, mass and interaction strength - is addressed, implying $\Sigma \coloneqq \Sigma_{\rm A} = \Sigma_{\rm B}$ and $\gamma \coloneqq \gamma_{\rm A} = \gamma_{\rm B}$. Eq. (4.45) in this case reduces to

$$G_{\rm AB}(t) = \gamma\frac{(t-d)\theta(t-d)e^{-\gamma(t-d)}}{d\gamma_\Sigma^2}\cosh(\gamma_\Sigma(t-d))\left(1-\frac{\tanh(\gamma_\Sigma(t-d))}{\gamma_\Sigma(t-d)}\right), \tag{4.51}$$

where the parameter $\gamma_\Sigma \coloneqq \sqrt{\gamma^2+\Sigma^2}$ is introduced for convenience.

The approximation to consider Eqs. (4.44) and (4.51) valid also at times $t \geq 2d$ can be performed by holding the condition

$$4\gamma^2 \ll d^2\Sigma^4\,. \tag{4.52}$$

In this case, the transmissivity τ can be computed by using Eqs. (4.36) and (4.51), giving

$$\tau = \frac{\gamma^2}{d^2}\frac{(t-d)^2e^{-2\gamma(t-d)}}{\gamma_\Sigma^2}\left(\frac{\sinh^2\left(\gamma_\Sigma(t-d)\right)}{\gamma_\Sigma^2(t-d)^2}-1\right). \tag{4.53}$$

After a long calculation, and performing approximations involving $\sigma \ll d$, the noise parameter $W \coloneqq \det\mathbb{N}$ can be analogously computed from Eqs. (4.33), (4.34), (4.35) and using the Green functions (4.44) and (4.51)

$$\begin{aligned}
W = \frac{m^4}{2048\pi\, d^4\gamma^2\gamma_\Sigma^{12}\Sigma^8\sigma^2}\Bigg\{&-4\Sigma^8\Big(e^{-2(t-d)\gamma}\gamma^3\theta(t-d)\big[(1+(t-d)^2\gamma_\Sigma^2)\cosh(2(t-d)\gamma_\Sigma)\\
&-2(t-d)\gamma_\Sigma\sinh(2(t-d)\gamma_\Sigma)\big]+2d^2e^{-2t\gamma}\gamma\gamma_\Sigma^4\sinh^2(t\gamma_\Sigma)\Big)^2\\
&+\Big(\theta(t-d)\{-e^{-2(t-d)\gamma}\gamma^3\big(4\gamma^5-4(t-d)\gamma^4\Sigma^2-10(t-d)\gamma^2\Sigma^4\\
&-6(t-d)\Sigma^6+\gamma\Sigma^4(9+2(t-d)^2\Sigma^2)-\gamma^3\Sigma^2(-11-2(t-d)^2\Sigma^2)\big)\cosh(2(t-d)\gamma_\Sigma)\\
&+e^{-2(t-d)\gamma}\gamma^3\gamma_\Sigma\big(4\gamma^4-4(t-d)\gamma^3\Sigma^2-8(t-d)\gamma\Sigma^4+\Sigma^4(5+2(t-d)^2\Sigma^2)\\
&+\gamma^2\Sigma^2(9+2(t-d)^2\Sigma^2)\big)(-\sinh(2(t-d)\gamma_\Sigma))\}-2d^2e^{-2t\gamma}\gamma\gamma_\Sigma^4\Sigma^4(\gamma\cosh(2t\gamma_\Sigma)+\gamma_\Sigma\sinh(2t\gamma_\Sigma))\Big)\\
&\times\Big(\theta(t-d)\{-e^{-2(t-d)\gamma}\gamma^3\big(2(t-d)\gamma^2\Sigma^2-2(t-d)\Sigma^4\\
&-\gamma\Sigma^2(1+2(t-d)^2\Sigma^2)+\gamma^3(1-2(t-d)^2\Sigma^2)\big)\cosh(2(t-d)\gamma_\Sigma)\\
&+e^{-2(t-d)\gamma}\gamma^3\gamma_\Sigma\big(4(t-d)\gamma\Sigma^2-\Sigma^2(1+2(t-d)^2\Sigma^2)+\gamma^2(-1-2(t-d)^2\Sigma^2)\big)\sinh(2(t-d)\gamma_\Sigma)\\
&+2d^2e^{-2t\gamma}\gamma\gamma_\Sigma^4\Sigma^2(\gamma\cosh(2t\gamma_\Sigma)-\gamma_\Sigma\sinh(2t\gamma_\Sigma))\}\Big)\Bigg\}.
\end{aligned} \tag{4.54}$$

From the definition of $\Sigma \coloneqq \Sigma_{\rm i=A,B}$ under Eq. (4.43), the condition (4.52) is satisfied in two cases, i.e. $\gamma \ll \sqrt{\frac{\pi}{8}}\sigma\omega^2$ and $\gamma \gg \sqrt{\frac{\pi}{8}}\sigma\omega^2$, where $\omega \coloneqq \omega_{\rm i=A,B}$, while it is not satisfied when γ is of the same order of $\sqrt{\frac{\pi}{8}}\sigma\omega^2$. The first two scenarios - called respectively *underdamped* and *overdamped* cases - can be studied analytically through Eqs. (4.53) and (4.54), while the last one - called *resonant* case is then studied numerically.

4.2.1.1 Underdamped case

In this scenario, the coupling $\lambda \coloneqq \lambda_{\rm i=A,B}$ is much smaller than $\sqrt{\frac{\pi}{8}}m\sigma\omega^2$. This case is then reducible to the perturbative scenario, studied extensively in Ref. [227] for two-level detectors.

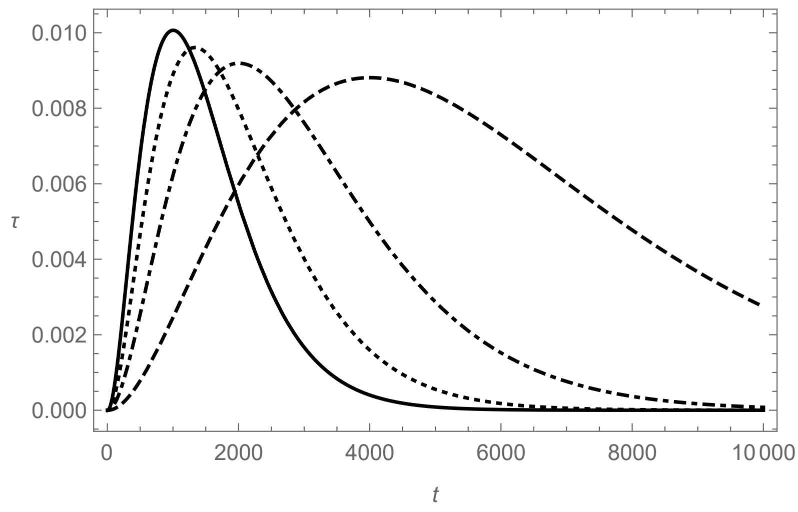

Figure 4.1: The transmissivity τ in time, from Eq. (4.53), of the channel between two harmonic oscillator detectors interacting with a scalar field through a sharp switching in (4.37) in the underdamped scenario $\Sigma^2 < 0$. The values considered for the parameter $\gamma = \frac{\lambda^2}{8\pi m}$ are $\gamma = 10^{-3}$ (thick line), $\gamma = 0.75 \cdot 10^{-3}$ (dotted line), $\gamma = 0.5 \cdot 10^{-3}$ (dot-dashed line), $\gamma = 0.25 \cdot 10^{-3}$ (dashed line). The other parameters were chosen to be $\sigma = 0.01$, $\omega = 1$, $d = 4$.

The underdamped scenario is characterized by the parameter Σ^2 assuming negative values. By looking at the transmissivity in Eq. (4.53), τ grows very slowly once $t \geq d$. By performing a Taylor expansion of the right hand side of Eq. (4.53) with respect to small $t-d$, the lowest order term would be proportional to $(t-d)^4$. Therefore, τ grows very slowly to reach a peak before exponentially decaying as $e^{-\gamma(t-d)}$. The behaviour of τ in time is shown in Fig. 4.1. If $|\Sigma^2| \gg \gamma^2$ (γ_Σ^2 is negative in this case), then the peak on τ is reached at a time $t_{\max} \sim \gamma^{-1}$ and this maximum value reads

$$\tau(t_{\max}) \sim \frac{e^{-2}}{d^2\left(\omega^2 - \sqrt{\frac{\pi}{8}\frac{\gamma}{\sigma}} - \gamma^2\right)} \,. \tag{4.55}$$

From Eq. (4.55) the peak of the transmissivity in time $\tau(t_{\max})$ increases by increasing γ or by decreasing ω keeping γ.

The noise W from Eq. (4.54), as a function of time t, is shown in Fig. 4.2. This figure shows how, after a certain time, W becomes asymptotically constant. Its asymptotic value can be analytically found from Eq. (4.54) as

$$\lim_{t\to\infty} W = \frac{(4\gamma^2 + |\Sigma^2| + 2d^2\Sigma^4)(1 + 2d^2|\Sigma^2|)}{32 \cdot 64\pi\sigma^2 d^4\gamma^2\Sigma^8} \,. \tag{4.56}$$

The energy-bounded classical capacity C can now be evaluated through Eq. (3.36). The encoding energy E was chosen to be of the order of $1/\sigma$ to compensate the smallness of the detectors. The result is plotted in Fig. 4.3 From it, the behaviour of C in time turns out to be very similar to the one of τ shown in Fig. 4.1. Notice that a smaller ω involves a greater energy-bounded classical capacity, since by decreasing ω there would be more bits that can be encoded to the oscillator can be increased with the same energy bound E.

Summarizing, in the underdamped case $-\Sigma^2 \gg 2\gamma/d$, increasing the frequency of the detectors is never convenient to the purpose of the optimization of the communication capabilities of this

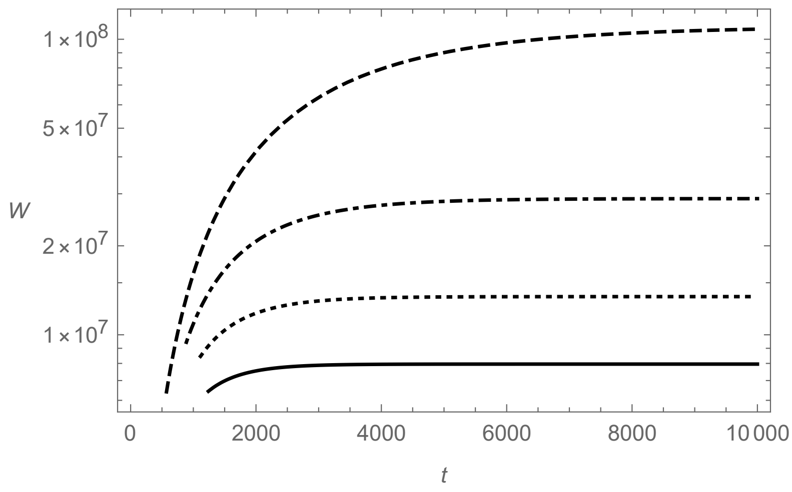

Figure 4.2: The noise parameter $W := \det \mathbb{N}$ in time, from Eq. (4.54), corresponding to the same channel, with the same parameters, of Fig. 4.1, together with a mass $m = 1$.

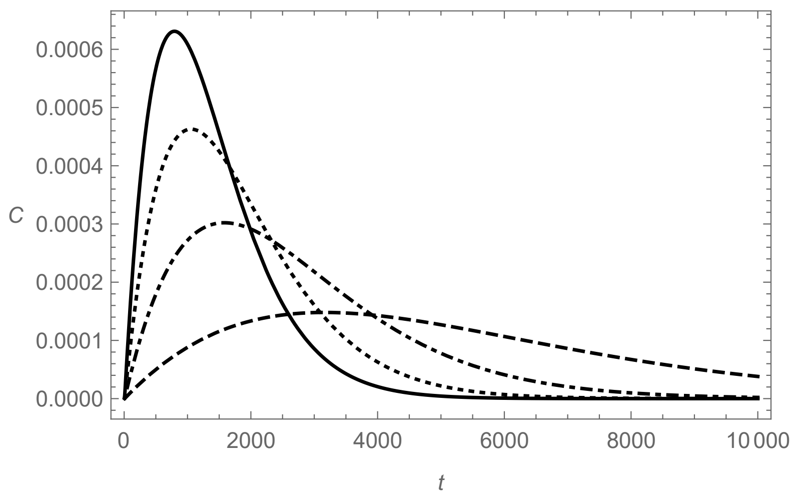

Figure 4.3: Classical capacity C with the energy bound $E = 100$ of the channel described in Fig. 4.2.

protocol. Instead, to this purpose, one can increase the parameter γ and therefore increase the coupling or decrease the oscillator mass. Moreover, from Eq. (4.54), the decreasing of the mass would also lower the noise W, effectively increasing the capacity by keeping γ fixed. However, γ cannot increase arbitrarily, since the condition (4.52) must be satisfied. In the same way, m cannot arbitrarily decrease.

Finally, since, as mentioned in Sec. 3.1.3.2, a necessary condition for the quantum capacity to be non-zero is $\tau > 1/2$, one always have $Q = 0$ in this case.

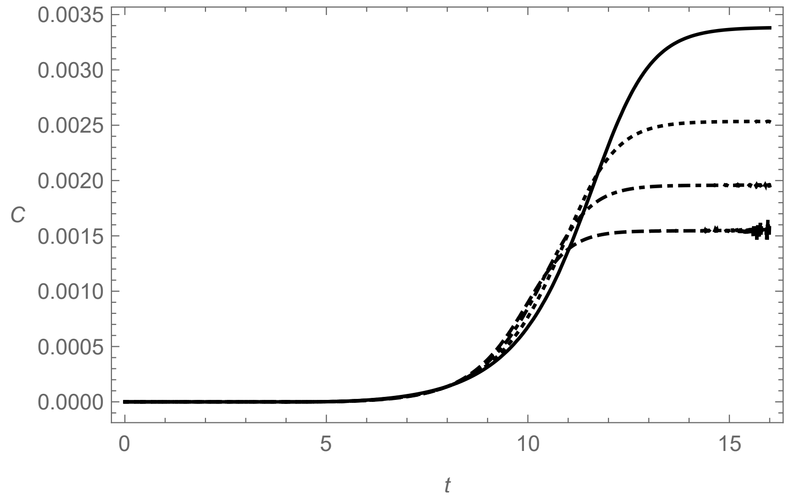

Figure 4.4: Classical capacity C with the energy bound $E = 100$ of the channel between two harmonic oscillator detectors interacting with a scalar field through a sharp switching in (4.37) in the overdamped scenario $\Sigma^2 > 0$. The values considered for the parameter $\gamma = \frac{\lambda^2}{8\pi m}$ are $\gamma = 0.01$ (thick line), $\gamma = 0.011$ (dotted line), $\gamma = 0.012$ (dot-dashed line) and $\gamma = 0.013$ (dashed line). The other parameters were chosen to be $\sigma = 0.01$, $\omega = 1$, $d = 4$ and $m = 1$.

4.2.1.2 Overdamped case

The regime $\lambda^2 \gg \sqrt{\frac{\pi}{8}} m\sigma\omega^2$ is now considered. Notice that this range includes arbitrarily high values of λ^2, so that it goes beyond perturbation theory. Analytical solutions are provided in Eqs. (4.53) and (4.54). The overdamped case is characterized by a positive Σ^2, meaning that both τ and W increase exponentially in time. In particular, from Eqs. (4.53) and (4.54), one gets respectively

$$\tau \sim \frac{\gamma^2}{4d^2\gamma_\Sigma^4} e^{2(t-d)(\gamma_\Sigma - \gamma)} \, ; \tag{4.57}$$

$$\begin{aligned} W \sim \frac{\gamma^4 e^{4(\gamma_\Sigma - \gamma)(t-d)}}{256 d^4 \Sigma^8 \gamma_\Sigma^9} \Big(& \Sigma^4 \gamma_\Sigma + 8\gamma^4\gamma_\Sigma + 12\gamma^3\Sigma^2 + 8\gamma^2\Sigma^2\gamma_\Sigma + 8\gamma^5 \\ & + 4\gamma\Sigma^4 + \frac{4d^2\Sigma^4\gamma_\Sigma^3 \left(\gamma + \gamma_\Sigma\right)^2 e^{2d(\gamma_\Sigma - \gamma)}}{\gamma^2} \Big) \, . \end{aligned} \tag{4.58}$$

The classical capacity (3.36) can be simplified by using the fact that $h(x \to \infty) \sim 1 + \log(x \to \infty)$, leading to

$$C(t \to \infty) \sim \log\left(1 + \frac{\tau}{\sqrt{W}} \frac{E}{\omega}\right) - \log\left(1 + \frac{\tau}{\sqrt{W}}\right) \, . \tag{4.59}$$

The ratio $\tau/\sqrt{W}$, for $t \to \infty$, assumes a finite value, since τ and $\sqrt{W}$ exponentially increase with the same rate. This leads, as shown in Fig. 4.4, to a finite valued classical capacity C at $t \to \infty$. Since E/ω is strictly positive, the capacity C is a monotonic function of the ratio $\tau/\sqrt{W}$. By studying this ratio, the asymptotic value of the classical capacity decreases by increasing γ. Since this parameter is proportional to the coupling strength λ, the result means that a greater coupling with the field does not necessarily involve a greater communication capacity. In fact, beside increasing the transmissivity, a greater the coupling λ also increases the noise. However, again, γ cannot be arbitrarily manipulated to be low, since the condition (4.52) must be satisfied.

Finally, by estimating the maximized coherent information via Eq. (3.39) one has trivially $Q^{(1)} = 0$, since an exponential increasing of τ drops I_c exponentially.

4.2.1.3 Resonant case

Both the scenarios studied in Secs. (4.2.1.1) and (4.2.1.2) suggests a higher quality of the detector channel the smaller $|\Sigma^2|$ is. Therefore, the case $|\Sigma^2| = 0$ is firstly employed, namely $\lambda^2 = \frac{\pi}{8} m\sigma\omega^2$.

The transmissivity τ and the noise W are computed by taking the numercial solution of Eq. (4.43) in Eqs. (4.36), (4.33), (4.34) and (4.35). From them, the classical capacity is obtained and depicted in time in Fig. 4.5 in the specific case $\Sigma^2 \equiv 0$. The bumps in the classical capacity (4.5) is

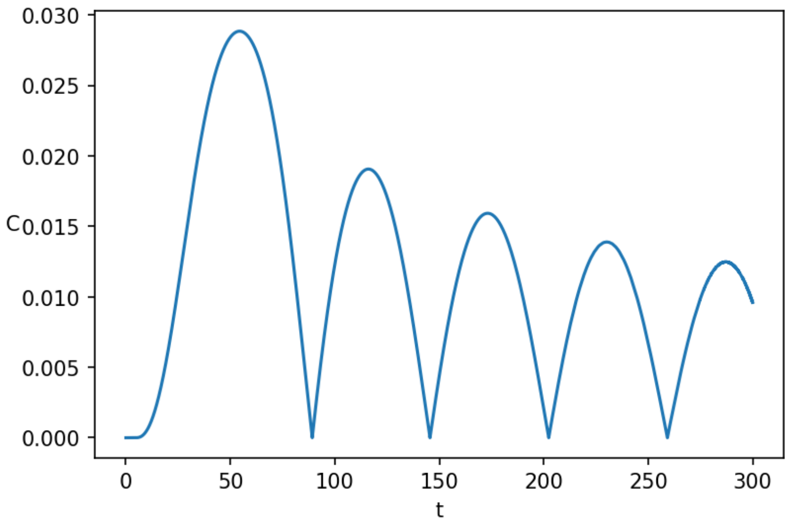

Figure 4.5: Classical capacity C with the energy bound $E = 100$ of the channel between two harmonic oscillator detectors interacting with a scalar field through a sharp switching in (4.37) when $\Sigma^2 = 0$. The parameters used are $\sigma = 0.01$, $\omega = 1$, $d = 4$, $m = 1$ and $\gamma = \frac{\pi}{8}\sigma\omega^2$.

given from the oscillation between positive and negative values of the transmissivity τ (since, from Eq. (3.36), the classical capacity depends on $|\tau|$). Both the amplitude of the oscillations of $|\tau|$ and the noise W increase exponentially as in the overdamped scenario 4.2.1.2. Therefore, the amplitude of the peaks of the capcity in Fig. (4.5) decrease in time so that, for $t \to \infty$, then $C \to 0$.

To quantify the departure of Σ^2 from zero, the parameter ε is introduced, following the equation

$$\gamma = \sqrt{\frac{\pi}{8}}\sigma\omega^2 + \varepsilon\,. \tag{4.60}$$

From Fig. 4.6, one observes that, by decreasing Σ^2 slightly (to become negative but in the range $|\Sigma|^2 \ll 1$), i.e. by chooseing small negative values of ε, then the strong oscillatory behaviour in Fig. 4.5 disappears smoothly[2] to reach the underdamped behaviour shown in Fig. 4.3. In the same way,

[2]From Fig. 4.6 one evinces that the capacity oscillates as two interfering oscillations. By increasing $|\varepsilon|$ with $\varepsilon < 0$, one oscillation increases its wave-length and the other decreases it. Therefore, for $|\varepsilon|$ high enough, one ends up with one single long oscillation (achieving the underdamped behaviour in Sec. 4.2.1.1) and the other one negligible

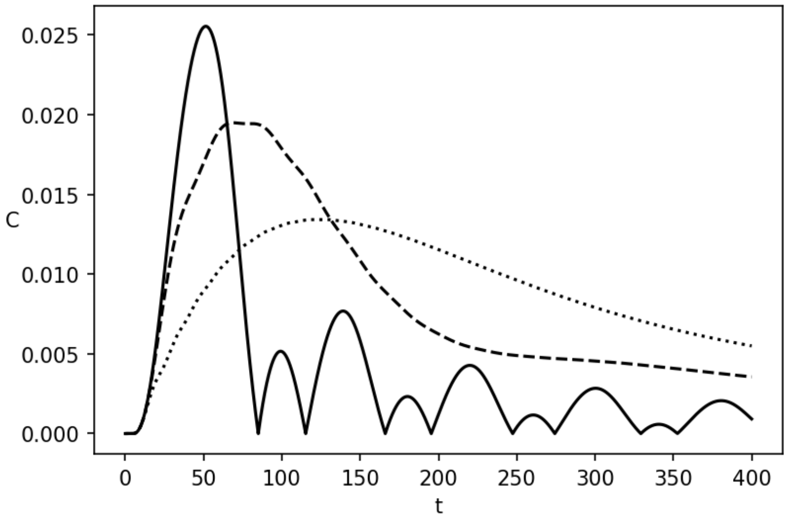

Figure 4.6: Classical capacity C with the energy bound $E = 100$ of the channel between two harmonic oscillator detectors interacting with a scalar field through a sharp switching in (4.37). The parameter γ follows Eq. (4.60) with $\varepsilon = -10^{-3.5}$ (dotted line), $\varepsilon = -10^{-4.1}$ (dashed line) and $\varepsilon = -10^{-4.7}$ (solid line). The other parameters were chosen to be $\sigma = 0.01$, $\omega = 1$, $d = 4$ and $m = 1$.

from Fig. 4.7, for small positive values of Σ^2, i.e. small positive ϵ, the oscillatory behaviour shown in Fig. 4.5 smoothly disappears to follow the overdamped behaviour shown in Fig. 4.4. The best late time classical capacity occurs, from the numerical calculations performed, at a value

$$\gamma = \gamma_{\max}(\omega) := \frac{d}{4} \frac{\omega^2}{\left(\sqrt{\frac{8}{\pi} \frac{d}{4\sigma}} - 1\right)} . \tag{4.61}$$

A parameter γ following Eq. (4.61) is given, more or less, by the dotted line in Fig. 4.7.

Finally, the optimizing frequency ω, to have the best value of C_∞, is studied as well. A finite value for $\omega_{\max}$ is expected since, from Eqs. (4.57) and (4.58), the ratio $\tau/\sqrt{W}$ increases with ω. However, from Eq. (4.59), the more is ω, the less are the number of qubits one can encode with the same energy budget. By plotting in Fig. 4.8 the numerical results for the capacity for different ω, and $\gamma = \gamma_{\max}(\omega)$ this expectation is confirmed, having a maximizing frequency called $\omega_{\max}$. Its value is $\omega_{\max} \sim 3.4$ with the parameters chosen in Fig. 4.8. However, this parameter was numerically found for other configurations of σ and d as well in Fig. 4.9. Hence, for the set of values of σ and d chosen in Fig. 4.9, the best detectors' parameters ω and γ to improve the quality of classical communication are found.

The maximized coherent information (3.39) is always negative, meaning that a reliable communication of quantum messages is not possible with this setup.

To conclude, the protocol studied in this section shows that:

1. harmonic oscillators behave as quantum antennas and they communicate in a causal way;

2. the classical capacity turns on smoothly in the overdamped case with a short delay after the causal connection (see Fig. (4.4));

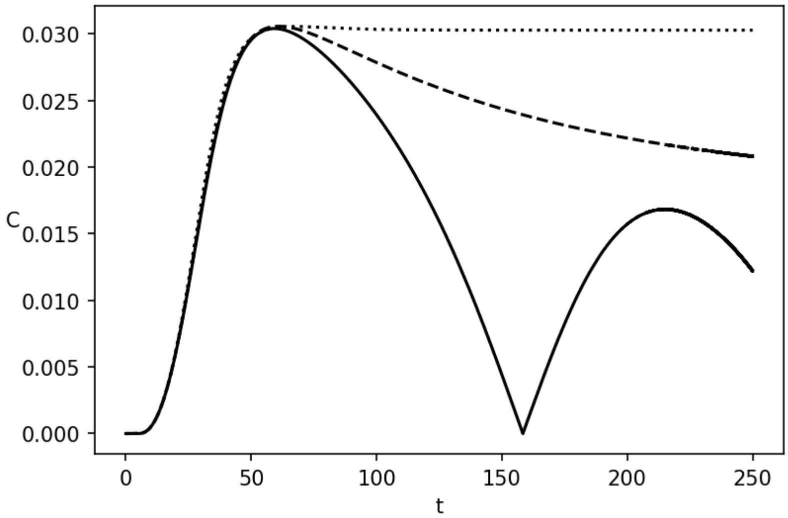

Figure 4.7: Classical capacity C with the energy bound $E = 100$ of the channel between two harmonic oscillator detectors interacting with a scalar field through a sharp switching in (4.37). The parameter γ follows Eq. (4.60) with $\varepsilon = 10^{-4.5}$ (dotted line), $\varepsilon = 10^{-4.7}$ (dashed line) and $\varepsilon = 10^{-4.8}$ (solid line). The other parameters were chosen to be $\sigma = 0.01$, $\omega = 1$, $d = 4$ and $m = 1$.

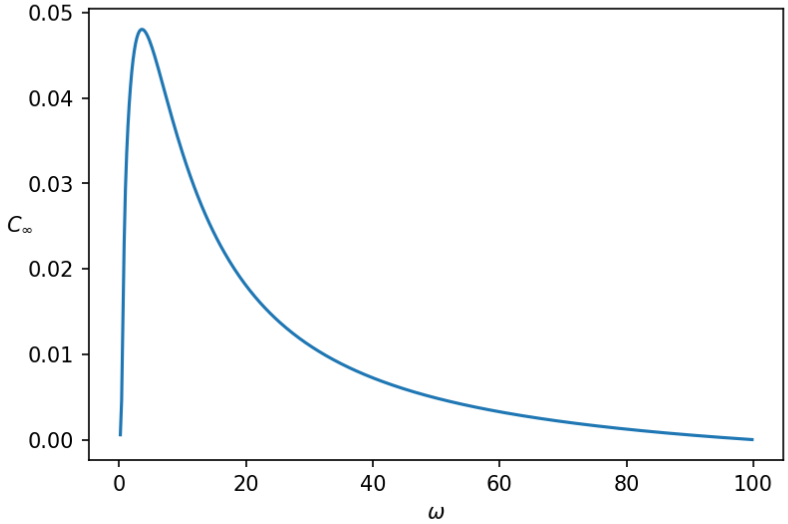

Figure 4.8: Late time value of the energy bounded classical capacity C_∞, with bound $E = 100$, of the channel between two harmonic oscillator detectors interacting with a scalar field through a sharp switching in (4.37), in term of ω. For the parameter γ, the optimizing value $\gamma = \gamma_{\max}(\omega)$ from Eq. (4.61) was chosen. The other parameters chosen are $d = 4$, $\sigma = 0.01$ and $m = 1$.

3. analytic solutions for the communication capacities can be found beyond perturbation theory. However, increasing the coupling with the field also increases the communication noise, so that an indefinite increasing of the interaction strength λ is not convenient. On the contrary, finite

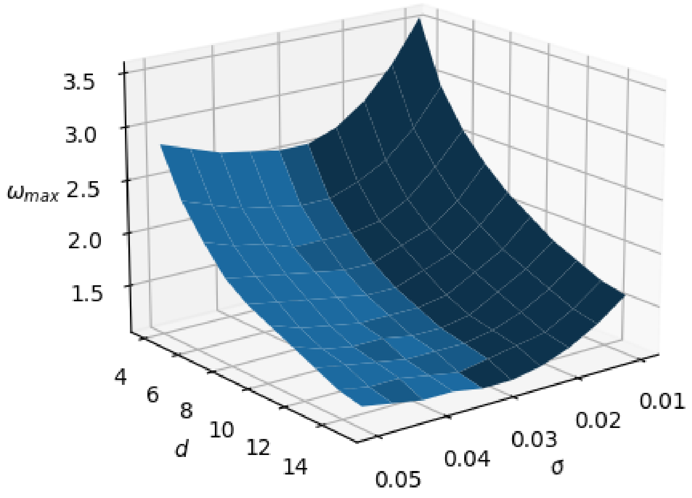

Figure 4.9: Plot of the frequency $\omega_{\max}$ maximizing the late time classical capacity of the channel described in Fig. 4.8, together with a parameter $\gamma = \gamma_{\max}(\omega)$ following Eq. (4.61), for different values of the detectors' effective size σ and distance d.

values for $\gamma = \frac{\lambda^2}{m}$ and ω are found in Eq. (4.61) and Fig. 4.9 to optimize the communication capabilities of the protocol.

Therefore, harmonic oscillator detectors behave as localized quantum systems able to communicate through a background field while respecting the causality conditions imposed by relativity.

4.2.2 Rapid interaction

To simplify the expressions provided in Sec. 4.2, eventually providing examples with different trajectories and/or background spacetime, a particular prescription for the timing of the interaction is now employed. In particular, a rapid interaction between field and detector [225] allows for very simple calculations, despite the limitations given by the uncertainty principle - which, since violated, have to imposed.

The communication protocol between harmonic oscillator detectors is now studied in the case where the field-detector interaction occurs only at a particular time. Alice, with the detector A, interacts with the field at a time $t_{\mathrm{A}} = t_{\mathrm{I}}^{\mathrm{A}}$. To achieve Alice's message, the detector B, held by Bob, has to interact with the field at a time $t = t_{\mathrm{I}}^{\mathrm{B}}$ depending on $t_{\mathrm{I}}^{\mathrm{A}}$ and on the distance $d(t)$ between the two detectors - in Bob's frame. In particular, one has

$$t_{\mathrm{I}}^{\mathrm{B}} = (t_{\mathrm{I}}^{\mathrm{A}})_{\mathrm{B}} + d((t_{\mathrm{I}}^{\mathrm{A}})_{\mathrm{B}})\,, \tag{4.62}$$

where $(t_{\mathrm{I}}^{\mathrm{A}})_{\mathrm{B}} \coloneqq t_{\mathrm{A}}^{-1}(t_{\mathrm{I}}^{\mathrm{A}})$ is Alice's interaction time $t_{\mathrm{I}}^{\mathrm{A}}$ in Bob's frame.

In this situation, for the interaction distribution in space and time, the separable form $F_{\mathrm{i=A,B}}(\mathbf{x}_{\mathrm{i}}, t_{\mathrm{i}}) = f_{\mathrm{i}}(\mathbf{x}_{\mathrm{i}})\lambda_{\mathrm{i}}(t_{\mathrm{i}})$ is again employed. The switching-in function $\lambda_{\mathrm{i}}(t_{\mathrm{i}})$, for both the detectors $\mathrm{i} = \mathrm{A}, \mathrm{B}$, in case of rapid interaction reads

$$\lambda_{\mathrm{i}}(t_{\mathrm{i}}) = \lambda_{\mathrm{i}}\delta(t_{\mathrm{i}} - t_{\mathrm{I}}^{\mathrm{i}})\,. \tag{4.63}$$

By using the switching-in function in Eq. (4.63) the dissipation kernel (4.6) can be simplified as $\chi_{\rm AA} = \chi_{\rm BB} = 0$. Therefore, the homogeneous quantum Langevin equation (4.11) can be rewritten as

$$\begin{cases} \ddot{G}_{\rm AA}(t,s) - \frac{\ddot{t}_{\rm A}(t)}{\dot{t}_{\rm A}(t)}\dot{G}_{\rm AA}(t,s) + \dot{t}_{\rm A}^2(t)\omega_{\rm A}^2 G_{\rm AA}(t,s) - \dot{t}_{\rm A}^2(t)\sqrt{\frac{\omega_{\rm A}}{\omega_{\rm B} m_{\rm A} m_{\rm B}}}\int_{-\infty}^t \dot{t}_{\rm A}(r)\chi_{\rm AB}^{\rm A}(t,r)G_{\rm BA}(r,s)dr = 0\,; \\ \ddot{G}_{\rm AB}(t,s) - \frac{\ddot{t}_{\rm A}(t)}{\dot{t}_{\rm A}(t)}\dot{G}_{\rm AB}(t,s) + \dot{t}_{\rm A}^2(t)\omega_{\rm A}^2 G_{\rm AB}(t,s) - \dot{t}_{\rm A}^2(t)\sqrt{\frac{\omega_{\rm A}}{\omega_{\rm B} m_{\rm A} m_{\rm B}}}\int_{-\infty}^t \dot{t}_{\rm A}(r)\chi_{\rm AB}^{\rm A}(t,r)G_{\rm BB}(r,s)dr = 0\,; \\ \ddot{G}_{\rm BA}(t,s) + \omega_{\rm B}^2 G_{\rm BA}(t,s) - \sqrt{\frac{\omega_{\rm B}}{\omega_{\rm A} m_{\rm A} m_{\rm B}}}\int_{-\infty}^t \chi_{\rm BA}^{\rm B}(t,r)G_{\rm AA}(r,s)dr = 0\,; \\ \ddot{G}_{\rm BB}(t,s) + \omega_{\rm B}^2 G_{\rm BB}(t,s) - \sqrt{\frac{\omega_{\rm B}}{\omega_{\rm A} m_{\rm A} m_{\rm B}}}\int_{-\infty}^t \chi_{\rm BA}^{\rm B}(t,r)G_{\rm AB}(r,s)dr = 0\,. \end{cases} \tag{4.64}$$

To compute the off-diagonal elements of the dissipation kernel (4.6), the operators $\hat{\varphi}_{\rm i}^{\rm j}$ from Eq. (4.4), are firstly examined. With the delta-like switching in (4.63), it becomes

$$\hat{\varphi}_{\rm i}^{\rm i}(t_{\rm i}) = \lambda_{\rm i}\delta(t_{\rm i} - t_{\rm I}^{\rm i})\int f_{\rm i}(\mathbf{x}_{\rm i})\hat{\Phi}(\mathbf{x}_{\rm i}, t_{\rm I}^{\rm i})\sqrt{-g_{\rm i}(\mathbf{x}_{\rm i}, t_{\rm I}^{\rm i})}d\mathbf{x}_{\rm i}\,, \tag{4.65}$$

if seen by the proper observer, and

$$\hat{\varphi}_{\rm i}^{\rm j}(t_{\rm j}) = \lambda_{\rm i}\int \delta(t_{\rm i}(\mathbf{x}_{\rm j}, t_{\rm j}) - t_{\rm I}^{\rm i})f_{\rm i}(\mathbf{x}_{\rm j}, t_{\rm j})\hat{\Phi}(\mathbf{x}_{\rm j}, t_{\rm j})\sqrt{-g_{\rm j}(\mathbf{x}_{\rm j}, t_{\rm j})}d\mathbf{x}_{\rm j}\,, \tag{4.66}$$

if seen by an external observer j. For the Dirac delta in Eq. (4.66) one has

$$\delta(t_{\rm i}(\mathbf{x}_{\rm j}, t_{\rm j}) - t_{\rm I}^{\rm i}) = \left|\frac{\partial t_{\rm i}(t_{\rm j}, \mathbf{x}_{\rm j})}{\partial t_{\rm j}}\right|^{-1}\delta(t_{\rm j} - t_{\rm i}^{-1}(t_{\rm I}^{\rm i}, \mathbf{x}_{\rm j}))\,. \tag{4.67}$$

Eq. (4.66) can be simplified when $t_{\rm i}(\mathbf{x}_{\rm j}, t_{\rm j}) \sim t_{\rm i}(t_{\rm j})$. This happens when the relation between the times $t_{\rm i}$ and $t_{\rm j}$ could be considered to be approximately the same along the spatial extension of the detector. To test the validity of this approximation, the following condition must be verified, namely

$$\int \frac{|t_{\rm i}(\mathbf{x}_{\rm j}, t_{\rm j}) - t_{\rm i}(\boldsymbol{\xi}_{\rm i}^{\rm j}, t_{\rm j})|}{t_{\rm i}(\boldsymbol{\xi}_{\rm i}^{\rm j}, t_{\rm j})} f_{\rm i}(\mathbf{x}_{\rm j}, t_{\rm j})\sqrt{-g_{\rm j}(\mathbf{x}_{\rm j}, t_{\rm j})}d\mathbf{x}_{\rm j} \ll 1\,, \tag{4.68}$$

where $\boldsymbol{\xi}_{\rm i}^{\rm j}$ indicates the position of the detector i seen by j.

If the condition (4.68) is valid, then Eq. (4.66) becomes

$$\hat{\varphi}_{\rm i}^{\rm j}(t_{\rm j}) \sim \lambda_{\rm i}\left(\frac{\partial t_{\rm i}(t_{\rm j})}{\partial t_{\rm j}}\right)^{-1}\delta(t_{\rm j} - t_{\rm i}^{-1}(t_{\rm I}^{\rm i}))\int f_{\rm i}(\mathbf{x}_{\rm j}, t_{\rm i}^{-1}(t_{\rm I}^{\rm i}))\hat{\Phi}(\mathbf{x}_{\rm j}, t_{\rm i}^{-1}(t_{\rm I}^{\rm i}))\sqrt{-g_{\rm j}(\mathbf{x}_{\rm j}, t_{\rm i}^{-1}(t_{\rm I}^{\rm i}))}d\mathbf{x}_{\rm j}\,. \tag{4.69}$$

Since $t_{\rm I}^{\rm B} > (t_{\rm I}^{\rm A})_{\rm B}$, from Eqs. (4.6) and (4.69) one trivially has $\chi_{\rm AB}^{\rm A}(t,s) \sim 0$. The element $\chi_{\rm BA}^{\rm B}$ instead reads

$$\chi_{\rm BA}^{\rm B}(t,s) = \frac{\lambda_{\rm A}\lambda_{\rm B}}{\frac{\partial t_{\rm A}((t_{\rm I}^{\rm A})_{\rm B})}{\partial t_{\rm B}}}\delta(t - t_{\rm I}^{\rm B})\delta(s - (t_{\rm I}^{\rm A})_{\rm B})I((t_{\rm I}^{\rm A})_{\rm B}, t_{\rm I}^{\rm B})\,, \tag{4.70}$$

where for simplicity, the function $I(t,s)$ was defined as

$$I(t,s) := i\int d\mathbf{x}\int d\mathbf{x}' f_{\rm A}(\mathbf{x}', t)f_{\rm B}(\mathbf{x}, s)\sqrt{g_{\rm B}(\mathbf{x}', t)g_{\rm B}(\mathbf{x}, s)}\,\langle\phi|\left[\hat{\Phi}(\mathbf{x}', t), \hat{\Phi}(\mathbf{x}, s)\right]|\phi\rangle\,. \tag{4.71}$$

The homogeneous QLE (4.64) can be rewritten as

$$\begin{cases} \ddot{G}_{\mathrm{AA}}(t,s) - \frac{\ddot{t}_{\mathrm{A}}(t)}{\dot{t}_{\mathrm{A}}(t)}\dot{G}_{\mathrm{AA}}(t,s) + \dot{t}_{\mathrm{A}}^2(t)\omega_{\mathrm{A}}^2 G_{\mathrm{AA}}(t,s) = 0\,; \\ \ddot{G}_{\mathrm{AB}}(t,s) - \frac{\ddot{t}_{\mathrm{A}}(t)}{\dot{t}_{\mathrm{A}}(t)}\dot{G}_{\mathrm{AB}}(t,s) + \dot{t}_{\mathrm{A}}^2(t)\omega_{\mathrm{A}}^2 G_{\mathrm{AB}}(t,s) = 0\,; \\ \ddot{G}_{\mathrm{BA}}(t,s) + \omega_{\mathrm{B}}^2 G_{\mathrm{BA}}(t,s) = \sqrt{\frac{\omega_{\mathrm{B}}}{\omega_{\mathrm{A}} m_{\mathrm{A}} m_{\mathrm{B}}}}\lambda_{\mathrm{A}}\lambda_{\mathrm{B}}\frac{1}{\dot{t}_{\mathrm{A}}((t_{\mathrm{I}}^{\mathrm{A}})_{\mathrm{B}})} I(t_{\mathrm{I}}^{\mathrm{B}},(t_{\mathrm{I}}^{\mathrm{A}})_{\mathrm{B}}) G_{\mathrm{AA}}((t_{\mathrm{I}}^{\mathrm{A}})_{\mathrm{B}},s)\delta(t-t_{\mathrm{I}}^{\mathrm{B}})\,; \\ \ddot{G}_{\mathrm{BB}}(t,s) + \omega_{\mathrm{B}}^2 G_{\mathrm{BB}}(t,s) = 0\,, \end{cases} \tag{4.72}$$

with boundary conditions $G_{\mathrm{ij}}(t \to s^+, s) = 0$ and $\dot{G}_{\mathrm{ij}}(t \to s^+, s) = \delta_{\mathrm{ij}}$. The solutions for G_{AA}, G_{AB} and G_{BB} are

$$G_{\mathrm{AA}}(t,s) = \frac{\sin(\omega_{\mathrm{A}}(t_{\mathrm{A}}(t) - t_{\mathrm{A}}(s)))}{\omega_{\mathrm{A}}\dot{t}_{\mathrm{A}}(s)}\,; \tag{4.73}$$

$$G_{\mathrm{AB}}(t,s) = 0\,; \tag{4.74}$$

$$G_{\mathrm{BB}}(t,s) = \frac{\sin(\omega_{\mathrm{B}}(t-s))}{\omega_{\mathrm{B}}}\,. \tag{4.75}$$

For $G_{\mathrm{BA}}(t,s)$, using Eq. (4.73), one has

$$G_{\mathrm{BA}}(t,s) = \theta(t-t_{\mathrm{I}}^{\mathrm{B}})\sqrt{\frac{\omega_{\mathrm{B}}}{\omega_{\mathrm{A}} m_{\mathrm{A}} m_{\mathrm{B}}}}\frac{\lambda_{\mathrm{A}}\lambda_{\mathrm{B}} I(t_{\mathrm{I}}^{\mathrm{B}},(t_{\mathrm{I}}^{\mathrm{A}})_{\mathrm{B}})}{\omega_{\mathrm{A}}\omega_{\mathrm{B}}\dot{t}_{\mathrm{A}}((t_{\mathrm{I}}^{\mathrm{A}})_{\mathrm{B}})\dot{t}_{\mathrm{A}}(s)}\sin(\omega_{\mathrm{B}}(t-t_{\mathrm{I}}^{\mathrm{B}}))\sin(\omega_{\mathrm{A}}(t_{\mathrm{A}}(t_{\mathrm{I}}^{\mathrm{A}})_{\mathrm{B}} - t_{\mathrm{A}}(s)))\,. \tag{4.76}$$

The transmissivity of the channel, from Eq. (4.36), is then

$$\tau(t,s) = \frac{\lambda_{\mathrm{A}}^2\lambda_{\mathrm{B}}^2}{m_{\mathrm{A}} m_{\mathrm{B}}\omega_{\mathrm{A}}^2\dot{t}_{\mathrm{A}}^2((t_{\mathrm{I}}^{\mathrm{A}})_{\mathrm{B}})\dot{t}_{\mathrm{A}}(s)} I^2(t_{\mathrm{I}}^{\mathrm{B}},(t_{\mathrm{I}}^{\mathrm{A}})_{\mathrm{B}})\sin^2(\omega_{\mathrm{A}}(t_I^{\mathrm{A}} - t_{\mathrm{A}}(s)))\,. \tag{4.77}$$

To calculate the noise from Eq. (4.32), the elements of the noise kernel (4.24) are firstly examined. From Eq. (4.63), one has

$$\nu_{\mathrm{ij}}(t_{\mathrm{i}},s_{\mathrm{j}}) = \frac{\lambda_{\mathrm{i}}\lambda_{\mathrm{j}}}{2}\delta(t_{\mathrm{i}}-t_{\mathrm{I}}^{\mathrm{i}})\delta(s_{\mathrm{j}}-t_{\mathrm{I}}^{\mathrm{j}})\int d\mathbf{x}_{\mathrm{i}}\int d\mathbf{x}_{\mathrm{j}} f_{\mathrm{i}}(\mathbf{x}_{\mathrm{i}})\tilde{f}_j(\mathbf{x}_{\mathrm{j}})\sqrt{g_{\mathrm{i}}(\mathbf{x}_{\mathrm{i}},t_{\mathrm{I}}^{\mathrm{i}})g_{\mathrm{j}}(\mathbf{x}_{\mathrm{j}},t_{\mathrm{I}}^{\mathrm{j}})} \times \langle\phi|\left\{\hat{\Phi}(\mathbf{x}_{\mathrm{i}},t_{\mathrm{I}}^{\mathrm{i}}),\hat{\Phi}(\mathbf{x}_{\mathrm{j}},t_{\mathrm{I}}^{\mathrm{j}})\right\}|\phi\rangle\,. \tag{4.78}$$

Using Eq. (4.78) and the Green function matrix elements (4.73), (4.75) and (4.76), Eqs. (4.33), (4.34) and (4.35) drastically simplify to become respectively

$$N_{11} = \frac{\lambda_{\mathrm{B}}^2}{m_{\mathrm{B}}\omega_{\mathrm{B}}}\sin^2(\omega_{\mathrm{B}}(t-t_{\mathrm{I}}^{\mathrm{B}}))J_{\mathrm{B}}(t_{\mathrm{I}}^{\mathrm{B}})\,; \tag{4.79}$$

$$N_{21} = N_{12} = \frac{\lambda_{\mathrm{B}}^2}{m_{\mathrm{B}}\omega_{\mathrm{B}}}\sin(\omega_{\mathrm{B}}(t-t_{\mathrm{I}}^{\mathrm{B}}))\cos(\omega_{\mathrm{B}}(t-t_{\mathrm{I}}^{\mathrm{B}}))J_{\mathrm{B}}(t_{\mathrm{I}}^{\mathrm{B}})\,; \tag{4.80}$$

$$N_{22} = \frac{\lambda_{\mathrm{B}}^2}{m_{\mathrm{B}}\omega_{\mathrm{B}}}\cos^2(\omega_{\mathrm{B}}(t-t_{\mathrm{I}}^{\mathrm{B}}))J_{\mathrm{B}}(t_{\mathrm{I}}^{\mathrm{B}})\,, \tag{4.81}$$

where, for the sake of simplicity, the following is defined

$$J_{\mathrm{B}}(t) := \frac{1}{2}\int d\mathbf{x}_{\mathrm{B}}\int d\mathbf{x}'_{\mathrm{B}} f_{\mathrm{B}}(\mathbf{x}_{\mathrm{B}},t)f_{\mathrm{B}}(\mathbf{x}'_{\mathrm{B}},t)\sqrt{g_{\mathrm{B}}(\mathbf{x}_{\mathrm{B}},t)g_{\mathrm{B}}(\mathbf{x}'_{\mathrm{B}},t)}\,\langle\phi|\left\{\hat{\Phi}(\mathbf{x}_{\mathrm{B}},t),\hat{\Phi}(\mathbf{x}'_{\mathrm{B}},t)\right\}|\phi\rangle\,. \tag{4.82}$$

To represent the initial state of Bob's detector B the one-mode covariance matrix (3.12) with $\mathrm{i} = \mathrm{B}$ is employed and rewritten as

$$\sigma_{\mathrm{ii}}(s) = \begin{pmatrix} \left(\frac{1}{2}+\mathfrak{n}_{\mathrm{i}}\right)e^{l_{\mathrm{i}}} & 0 \\ 0 & \left(\frac{1}{2}+\mathfrak{n}_i\right)e^{-l_{\mathrm{i}}} \end{pmatrix}\,, \tag{4.83}$$

where $\mathfrak{n}_{\rm i}$ represents the number of entropic particles in the mode i and $l_{\rm i}$ is a squeezing parameter[3].

At this point, the determinant of the matrix (4.32), giving the parameter W, reads

$$W = \left(\frac{1}{2} + \mathfrak{n}_{\rm B}\right)^2 + \frac{\lambda_{\rm B}^2}{m_{\rm B}\omega_{\rm B}} J(t_{\rm I}^{\rm B}) \left(\frac{1}{2} + \mathfrak{n}_{\rm B}\right) \left(e^{l_{\rm B}} \cos^2(\omega_{\rm B}(t_{\rm I}^{\rm B} - s)) + e^{-l_{\rm B}} \sin^2(\omega_{\rm B}(t_{\rm I}^{\rm B} - s))\right) . \quad (4.84)$$

4.2.2.1 Energy conditions

The capacities of the channel can be computed by inserting the transmissivity (4.77) and the noise parameter (4.84) into Eq. (3.36) for the constrained classical capacity and into Eq. (3.39) for the quantum capacity. From Eqs. (4.77) and (4.84) one may adjust the parameters $\lambda_{\rm i=A,B}$, $m_{\rm i=A,B}$ and $\omega_{\rm i=A,B}$ to obtain arbitrarily high capacities. This is due to the fact that a rapid interaction, modeled by the delta-like switching-in (4.63) bypasses the limitations given by the uncertainty principle - since an infinitesimal interaction time implies an infinite uncertainty on the energy. This means that, to provide a realistic protocol, such energetic conditions must be imposed by hand.

First of all, a limitation must be imposed on the energy that each detector can store. According to Eq. (2.9) a particle localized by a smearing function $f(\mathbf{x})$ have a momentum amplitude $g(\mathbf{k})$. In particular, it can be proved that, if the support of $f(\mathbf{x})$ is confined within a radius ϵ - i.e. the effective size of the particle localization - then the support of $g(\mathbf{k})$ would be confined into a sphere with radius $\sim \epsilon^{-1}$. Therefore, if a detector i has an effective size $\epsilon_{\rm i}$, the maximum energy of a massless particle it can interact with would be of the order $E_c^{\rm i=A,B}\epsilon_{\rm i}^{-1}$. As a consequence, the detector's initial state is expected to not exceed this energy cutoff, noted with $E_c^{\rm i=A,B}$. This immediately gives a bound on the parameters $\mathfrak{n}_{\rm i=A,B}$ and $l_{\rm i=A,B}$ defining the oscillators' initial states (4.83). In particular, the energy of an oscillator i in a state represented by the covariance matrix (4.83) and by a null first momentum vector is

$$E_{\rm i}^0 = \frac{\omega_{\rm i}}{2} {\rm Tr}\sigma_{\rm ii} \,. \quad (4.85)$$

So that the condition $E_{\rm i} < E_{\rm c}^{\rm i}$ must be satisfied for both the detectors A and B. In particular, for the parameters $\mathfrak{n}_{\rm B}$ and $l_{\rm B}$ appearing on the noise W in Eq. (4.84), one has

$$\omega_{\rm B}\left(\frac{1}{2} + \mathfrak{n}_{\rm B}\right) \cosh l_{\rm B} < E_{\rm c}^{\rm B} \,. \quad (4.86)$$

Instead, $E_c^{\rm A}$ simply represents the energy bound E on the constrained classical capacity (3.36).

Once interacting with the field, the detector increases its energy. In particular, the matrix $\mathbb{N}_{\rm B}'$ in Eq. (4.32) gives the contribute on the covariance matrix $\sigma_{\rm BB}$, representing Bob's detector state, given by the interaction with the field. By computing its trace, the energy gained from the interaction with field is obtained, namely

$$\Delta E_{\rm B} := {\rm Tr}\left(\sigma_{\rm BB}(t_{\rm I}^{\rm B+}) - \sigma_{\rm BB}(t_{\rm I}^{\rm B-})\right) = \frac{\lambda_{\rm B}^2}{2m_{\rm B}} J_{\rm B}(t_{\rm I}^{\rm B}) \,. \quad (4.87)$$

Analogously, the energy gained by Alice while interacting with the field is

$$\Delta E_{\rm A} = \frac{\lambda_{\rm A}^2}{2m_{\rm A}} J_{\rm A}(t_{\rm I}^{\rm A}) \,, \quad (4.88)$$

[3]Their relation with $n_{\rm i}$ and $m_{\rm i}$ is $\mathfrak{n}_{\rm i} = -\frac{1}{2} + \sqrt{\left(\frac{1}{2} + n_{\rm i}\right)^2 - |m_{\rm i}|^2}$ and $l_{\rm i} = \frac{1}{2}\cosh^{-1}\left(\frac{\frac{1}{2} + n_{\rm i} + |m_{\rm i}|}{\frac{1}{2} + n_{\rm i} - |m_{\rm i}|}\right)$.

where J_{A} is defined analogously to J_{B} in Eq. (4.82) by exchanging the label B with A. In this way, one has the energetic condition $\Delta E_{\mathrm{i}} < E^{\mathrm{i}}_{\mathrm{c}}$, reading

$$\frac{\lambda_{\mathrm{i}}^2}{2m_{\mathrm{i}}} J(t^{\mathrm{i}}_{\mathrm{I}}) \leq E^{\mathrm{i}}_c \Rightarrow \frac{\lambda_{\mathrm{i}}^2}{m_{\mathrm{i}}} \leq 2\frac{E^{\mathrm{i}}_c}{J_{\mathrm{i}}(t^{\mathrm{i}}_{\mathrm{I}})} \,. \tag{4.89}$$

Eq. (4.89) gives the wanted upper bound on the field-detector interaction strength λ_{i} and a lower bound on the oscillators' mass m_{i}.

Finally, a physical limit is given by the Heisenberg principle, preventing an actual delta-like interaction with the field. In fact, this kind of interaction would assume an infinite precision on time measurements and therefore, an infinite uncertainty on the detectors' energy. The minimum oscillator i energy is provided by $\omega_{\mathrm{i}}/2$, so that the uncertainty on the energy must be much smaller than it. This uncertainty is provided by the inverse of the uncertainty on the interaction time $\Delta t^{\mathrm{i}}_{\mathrm{I}}$. If the window of interaction $\Delta t^{\mathrm{i}}_{\mathrm{I}}$ is much smaller than the time scale when the protocol occurs - corresponding to $d_{\mathrm{i}}(t_{\mathrm{i}})$ - then the delta-like limit is restored, as proved in details in Ref. [P4]. Therefore, the delta-like interaction (4.63) works without violating the uncertainty principle only if the following condition is satisfied

$$\frac{\omega_{\mathrm{i}}}{2} d_{\mathrm{i}}(t_{\mathrm{i}}) \gg 1 \,, \tag{4.90}$$

where d_{i} is the proper distance of the observer i between the two detectors. The condition (4.90) provides then a lower bound on the oscillators' frequencies.

Since $\omega_{\mathrm{i}}/2 < E^{\mathrm{i}}_c$, because the latter is an energy upper bound, it is convenient to write $\omega_{\mathrm{i}} = 2\alpha_{\mathrm{i}} E^{\mathrm{i}}_c$, where α_{i} is upper bounded by 1. The condition (4.90) becomes then

$$\frac{1}{2E^{\mathrm{i}}_c d_{\mathrm{i}}} \ll \alpha_{\mathrm{i}} \leq 1 \,. \tag{4.91}$$

Since E^{i}_c is proportional to ϵ^{-1}, i.e. the inverse of the detector i effective size, then Eq. (4.91) means that $\alpha \gg \frac{\epsilon}{d}$.

At this point, to provide the best protocol, the transmissivity is maximized and the noise minimized while respecting the bounds (4.86) and (4.89). From Eq. (4.84) is can be immediately proved that the parameters minimizing W at each time while respecting the condition (4.86) are $\mathfrak{n}_{\mathrm{B}} = 0$, $l_{\mathrm{B}} = 0$ and $\alpha_{\mathrm{B}} = 1$, leading to

$$W = \frac{1}{4} + \frac{\lambda_{\mathrm{B}}^2}{2m_{\mathrm{B}}\omega_{\mathrm{B}}} J(t^{\mathrm{B}}_{\mathrm{I}}) \,. \tag{4.92}$$

To maximize the classical capacity, the aim is to provide the best ratio $\frac{\tau}{\sqrt{W}}$ and for this purpose, the two couplings must be the largest possible. By imposing, for $\mathrm{i} = \mathrm{A}, \mathrm{B}$

$$\frac{\lambda_{\mathrm{i}}^2}{m_{\mathrm{i}}\omega_{\mathrm{i}}} \equiv \frac{1}{\alpha_{\mathrm{i}} J_i(t^{\mathrm{i}}_{\mathrm{I}})} \,, \quad \text{where} \quad \frac{1}{2E^{\mathrm{i}}_c d_{\mathrm{i}}} \ll \alpha_{\mathrm{i}} \leq 1 \,. \tag{4.93}$$

One has $W = \frac{1}{4} + \frac{1}{2\alpha_{\mathrm{B}}}$ which is minimized for $\alpha_{\mathrm{B}} = 1$, leading simply to

$$W = \frac{3}{4} \,. \tag{4.94}$$

The transmissivity τ from Eq. (4.77) becomes instead

$$\tau = \frac{1}{\alpha_{\mathrm{A}}^2} \frac{E^{\mathrm{B}}_c}{E^{\mathrm{A}}_c} \cdot \frac{I^2(t^{\mathrm{B}}_{\mathrm{I}}, (t^{\mathrm{A}}_{\mathrm{I}})_{\mathrm{B}})}{J_{\mathrm{A}}(t^{\mathrm{A}}_{\mathrm{I}}) J_{\mathrm{B}}(t^{\mathrm{B}}_{\mathrm{I}})} \cdot \frac{\sin^2(\omega_{\mathrm{A}}(t_{\mathrm{A}}(t^{\mathrm{A}}_{\mathrm{I}})_{\mathrm{B}} - t_{\mathrm{A}}(s)))}{\dot{t}^2_{\mathrm{A}}((t^{\mathrm{A}}_{\mathrm{I}})_{\mathrm{B}}) \dot{t}_{\mathrm{A}}(s)} \,. \tag{4.95}$$

Eq. (4.95) provides the maximum transmissivity that the detector protocol can have with a delta-like interaction, providing an upper bound for it. Remarkably, Eq. (4.95) can be written as the product of three different factors, each one representing different features of the protocol, namely:

- $\frac{1}{\alpha_{\mathrm{A}}^2}\frac{E_c^{\mathrm{B}}}{E_c^{\mathrm{A}}}$ depends solely on the detectors energetic setup.
- $\frac{I^2(t_{\mathrm{I}}^{\mathrm{B}},(t_{\mathrm{I}}^{\mathrm{A}})_{\mathrm{B}})}{J_{\mathrm{A}}(t_{\mathrm{I}}^{\mathrm{A}})J_{\mathrm{B}}(t_{\mathrm{I}}^{\mathrm{B}})}$ is the factor depending on the background spacetime the detectors lie on
- $\frac{\sin^2(\omega_{\mathrm{A}}(t_{\mathrm{A}}(t_{\mathrm{I}}^{\mathrm{A}})_{\mathrm{B}}-t_{\mathrm{A}}(s)))}{\dot{t}_{\mathrm{A}}^2((t_{\mathrm{I}}^{\mathrm{A}})_{\mathrm{B}})\dot{t}_{\mathrm{A}}(s)}$ is the trajectory dependent factor.

The maximum classical capacity of the protocol (3.36), bound by the energy E_c^{A}, becomes

$$C = h\left(\frac{\tau}{2\alpha_A}+\sqrt{\frac{3}{4}}\right) - h\left(\frac{\tau}{2}+\sqrt{\frac{3}{4}}\right) . \tag{4.96}$$

For the quantum capacity, the situation is more subtle since $Q^{(1)}$, from Eq. (3.39), is not monotonic with $\frac{\tau}{\sqrt{W}}$. In particular, from Eq. (4.84) one has $W > 1/4$. By considering the limit $W \to 1/4$, then the best quantum capacity is obtained when $\tau = 2$. This situation is reachable in the limit $\lambda_{\mathrm{B}} \to 0$. Therefore, by looking at Eq. (4.77), the parameter τ must be able to be arbitrarily high for finite λ_{B}, so that it can be decreased to reach the ideal transmissivity $\tau = 2$. In this case, the value assumed by the maximized coherent information (3.39), i.e. the quantum capacity, in this limit becomes

$$Q^{(1)} \to 1 . \tag{4.97}$$

As a consequence, regardless the number of qubits encoded in the input state, *no more than one qubit can be reliably sent between two harmonic oscillator detectors*. The reason of this feature relies on the unavoidable noise W which cannot be lower than 1/4. This noise is simply caused by the pre-existing state on the detector B. In other words, the initial state of the detector B must be overwritten to read Alice's detector A signal. This fact causes the aforementioned unavoidable noise, limiting to 1 the number of qubits which can be reliably communicated.

4.2.2.2 Static detectors

The behaviour of the capacities in case of a rapid interaction is now provided for two static detectors, as done in case of a long-term interaction in Sec. 4.2.1. Again, both the detectors work in the proper time t. The following Lorentzian smearing is chosen for both the detectors for the sake of simplicity, namely

$$f_{\mathrm{i}}(\mathbf{x},t) = \frac{1}{\pi^2}\frac{\epsilon}{\left(|\mathbf{x}-\boldsymbol{\xi}_{\mathrm{i}}|^2+\epsilon^2\right)^2} , \tag{4.98}$$

where ϵ is the detector effective size. In this way, the energy cutoffs are the same $E_c^{\mathrm{A}} = E_c^{\mathrm{B}}$.

With this prescription, the integrals $I(t_{\mathrm{I}}^{\mathrm{A}}, t_{\mathrm{I}}^{\mathrm{B}})$ and $J_{\mathrm{i}}(t_{\mathrm{I}}^{\mathrm{i}})$, respectively from Eqs. (4.71) and (4.82), can be analytically computed by using the Minkowski normal modes (2.6) as

$$I(t_{\mathrm{I}}^{\mathrm{A}}, t_{\mathrm{I}}^{\mathrm{B}}) = -\frac{1}{(2\pi)^2}\frac{d}{\epsilon}\frac{1}{d^2+\epsilon^2} ; \tag{4.99}$$

$$J_{\mathrm{i}}(t_{\mathrm{I}}^{\mathrm{i}}) = \frac{1}{16\pi^4\epsilon^2} , \tag{4.100}$$

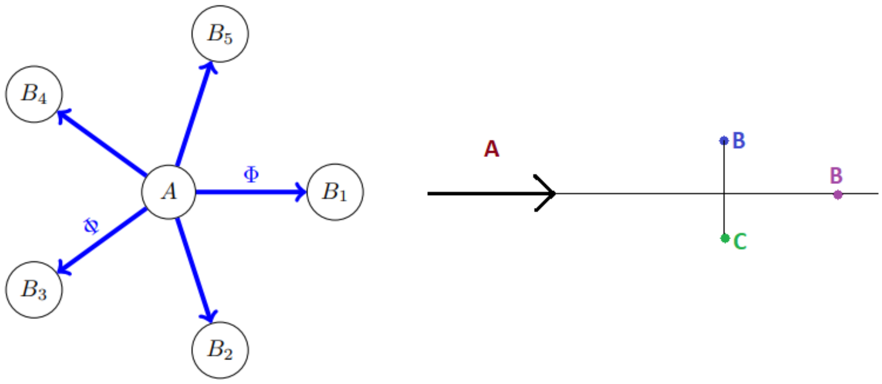

Figure 4.10: This image shows how the no-cloning theorem would prevent the communication of a quantum state between two detectors when spacetime symmetries are present in isotropic spacetimes. The scheme at the left (borrowed by Ref. [45]), shows the static detectors scenario, while the one at the right implies detector A to move with a certain trajectory.

where $d := |\boldsymbol{\xi}_{\mathrm{A}} - \boldsymbol{\xi}_{\mathrm{B}}|$. Therefore, the maximum transmissivity (4.95), called τ_{S} in the static detectors scenario, becomes

$$\tau_{\mathrm{S}} = \frac{16}{\alpha_{\mathrm{A}}^2} \frac{\epsilon^2}{d^2} \sin^2(\omega_{\mathrm{A}}(t_{\mathrm{I}}^{\mathrm{A}} - s)) \,. \tag{4.101}$$

Noticeably, the transmissivity τ_{S} drops as d^{-2} exactly as the amplitude of a spherical wave. This reflects the fact that the detector is effectively behaving as an antenna spreading information to the background field as a spherical wave.

Since $\alpha_{\mathrm{A}} \gg d/\epsilon$, then $\tau_{\mathrm{S}} \ll 1$. In this case, the bounded classical capacity (4.96) becomes

$$C_E \sim \log\left(\frac{\sqrt{3}+1}{\sqrt{3}-1}\right) \frac{\tau}{2} \left(\frac{1}{\alpha_A} - 1\right) \simeq 1.9 \cdot \frac{\tau}{2} \left(\frac{1}{\alpha_A} - 1\right) \tag{4.102}$$

The maximized coherent information (3.39) is clearly negative if $\tau \ll 1$, so that the quantum capacity of the channel is zero.

The quantum capacity of the channel between two oscillators communicating at distance is zero for both a steady and a rapid interaction - as shown also in Sec. (4.2.1). In fact a null quantum capacity is always expected for two static detectors in an isotropic spacetime from the no-cloning theorem [159, 45]. In fact, if Alice, with the detector A communicates reliably a quantum state to Bob, holding the detector B, any other observer - called Charlie, with the detector C - must be prevented to achieve the same signal in a reliable way. In this section and in Sec. 4.2.1, the scenario involves Alice spreading information about her detector to the field with a spherical symmetric, as well represented by the scheme at the left of Fig. 4.10. By looking at this figure, intuition tells that, if a receiver B_1 achieves reliably a quantum state from the detector A, then also the other receivers e.g. B_2 or B_3 would achieve the same quantum state reliably. However, in this case, Alice's initial state would be cloned to all the receivers B_{i} and this clearly violates the no-cloning theorem. Therefore, the fact that the quantum capacity is always zero in the situations considered is consistent with this theorem. Even if the detector A is traveling through a particular direction, a receiver B could easily have its "symmetric respective" C, as shown in the scheme at the right of Fig. (4.10). In this case, the reliable communication of quantum messages is prevented again. The only possibility to have a quantum capacity greater than zero is when the detector B of the receiver is along the line where Alice is traveling. Therefore, these situations are now investigated, hoping to achieve a reliable communication of quantum messages between Unruh-deWitt detectors by playing with their trajectories.

4.2.2.3 Inertial detectors

The situation where Alice travels inertially towards Bob (static), with a speed β, is now addressed. The x-axis is chosen to be the line where the detectors A and B are located. The relation between Alice's proper coordinates $(t_\mathrm{A}, \mathbf{x}_\mathrm{A})$ and Bob ones $(t, \mathbf{x})$ is given by

$$\begin{cases} t = \gamma(t_\mathrm{A} - \beta x_\mathrm{A})\,; \\ x = \gamma(x_\mathrm{A} - \beta t_\mathrm{A}) + d\,; \\ y = y_\mathrm{A}\,; \\ z = z_\mathrm{A}\,, \end{cases} \tag{4.103}$$

where $\gamma := (1-\beta^2)^{-1/2}$. In Bob's frame, the distance between the two detectors is $d(t) = d - \beta t$. The Fermi bound (2.82) is trivially satisfied, since there is no curvature nor acceleration of the detectors. From Eq. (4.68), the relative error achieved by approximating $t_\mathrm{A}(\mathbf{x}, t)$ into $t_\mathrm{A}(t)$ in Eq. (4.66) is $\sim \beta\sqrt{1-\beta^2}$ and therefore negligible when A is non-relativistic and when A has a speed close to the speed of light. In this case, one has $\dot{t}_\mathrm{A}(t) = t/\gamma$. The integral (4.71) is

$$I((t_\mathrm{I}^\mathrm{A})_\mathrm{B}, t_\mathrm{I}^\mathrm{B}) = -\frac{2}{\gamma}\Im \int \frac{\mathrm{d}\mathbf{k}}{(2\pi)^3|\mathbf{k}|} e^{i|\mathbf{k}|((t_\mathrm{I}^\mathrm{A})_\mathrm{B} - t_\mathrm{I}^\mathrm{B}) - ik_x d(t_\mathrm{I}^\mathrm{B}) - \epsilon(|\mathbf{k}| + |\mathbf{k}'|)}\,, \tag{4.104}$$

where $\mathbf{k}' := (\gamma k_x, k_y, k_z)$. The integral (4.104) has not analytic solution. However, since $|\mathbf{k}| \leq |\mathbf{k}'| \leq \gamma|\mathbf{k}|$, one can infer an upper bound (resp. lower bound) for it by considering $|\mathbf{k}|$ (resp. $\gamma|\mathbf{k}|$). In so doing, the parameter μ, such that $1 < \mu < \frac{\gamma+1}{2}$ is introduced. With the mean value theorem, Eq. (4.104) can be rewritten as

$$I((t_\mathrm{I}^\mathrm{A})_\mathrm{B}, t_\mathrm{I}^\mathrm{B}) = -\frac{1}{(2\pi)^2\gamma}\frac{d(t_\mathrm{I}^\mathrm{B})}{\mu\epsilon}\frac{1}{d^2(t_\mathrm{I}^\mathrm{B}) + \mu^2\epsilon^2}\,; \tag{4.105}$$

The integrals $J_{\mathrm{i}=\mathrm{A,B}}(t_\mathrm{I}^\mathrm{i})$ follow again Eq. (4.100). From Eq. (4.95), the transmissivity of the channel, called τ_I can be obtained as

$$\tau_\mathrm{I} = \frac{16}{\alpha_\mathrm{A}^2}\frac{\epsilon^2}{d^2}\frac{\gamma}{\mu^2}\sin^2\left(\omega_\mathrm{A}((t_\mathrm{I}^\mathrm{A})_\mathrm{B} - s)\right)\,. \tag{4.106}$$

By comparing Eq. (4.106) with Eq. (4.101), one has

$$\tau_\mathrm{I} = \frac{\gamma}{\mu^2}\tau_\mathrm{S}\,. \tag{4.107}$$

Since $\tau_\mathrm{S} \ll 1$, the only option for the channel to have a quantum capacity greater than zero is that $\gamma \gg 1$. However, in this limit, it can be easily proved from Eq. (4.104) that μ assumes its maximum value $\frac{1+\gamma}{2}$, so that, when $\gamma \gg 1$

$$\tau_\mathrm{I} = \frac{4}{\gamma}\tau_\mathrm{S}\,. \tag{4.108}$$

Therefore, when $\gamma \gg 1$, i.e. when the detector A is close to the speed of light, the transmissivity of the channel decreases w.r.t. static case. For $\gamma \gtrsim 1$, numerical calculations tell that $\tau_\mathrm{I} \gtrsim \tau_\mathrm{S}$, so that the two detectors communicate better classical information w.r.t. the static case[4]. However, since the increasing on the transmissivity cannot be greater than γ, by considering the minimum value of μ, a value $\gamma \gtrsim 1$ is clearly not enough to obtain quantum capacity greater than zero.

4.2.2.4 Rindler accelerated detectors

In this scenario, the detector A, held by the sender Alice, is Rindler accelerated along the x-axis, while the receiver Bob with the detector B is static. The proper coordinates of Alice and Bob are related through

$$\begin{cases} t = \left(\frac{1}{\alpha} + x_{\mathrm{A}}\right) \sinh(\alpha t_{\mathrm{A}})\,; \\ x = \left(\frac{1}{\alpha} + x_{\mathrm{A}}\right) \cosh(\alpha t_{\mathrm{A}})\,; \\ y = y_{\mathrm{A}}\,; \\ z = z_{\mathrm{A}}\,, \end{cases} \tag{4.109}$$

where α is the proper acceleration of the sender, by following the same notation of Sec. 2.4. The distance between the two detectors, in Bob's frame, is given by

$$d(t) = \sqrt{\frac{1}{\alpha^2} + t^2}\,, \tag{4.110}$$

reaching its minimum at $t_{\mathrm{A}} = t = 0$, reading $d = \alpha^{-1}$. The Fermi bound condition (2.82) reads $\alpha^2\epsilon^2 \ll 1$, which is automatically implied by $\epsilon/d \ll 1$ and also makes valid the condition (4.68). By performing the same analysis of Sec. 4.2.2.3, the integral (4.71) is

$$I((t_{\mathrm{I}}^{\mathrm{A}})_{\mathrm{B}}, t_{\mathrm{I}}^{\mathrm{B}}) = -\frac{1}{(2\pi)^2 \cosh(\alpha (t_{\mathrm{I}}^{\mathrm{A}})_{\mathrm{B}})} \frac{d(t_{\mathrm{I}}^{\mathrm{B}})}{\epsilon\mu'} \frac{1}{\mu'^2\epsilon^2 + d^2(t_{\mathrm{I}}^{\mathrm{B}})}\,, \tag{4.111}$$

where μ' is a parameter upper bounded by $\frac{1+\cosh(\alpha t_{\mathrm{I}}^{\mathrm{A}})}{2}$ and lower bounded by 1. The integral J_{B}, from Eq. (4.82) is the static one (4.100). For J_{A}, instead, one has

$$J_{\mathrm{A}}(t_{\mathrm{I}}^{\mathrm{A}}) = \frac{1 + \alpha^2 (t_{\mathrm{I}}^{\mathrm{A}})^2}{16\pi^4\epsilon^2}\,. \tag{4.112}$$

Notice that $J_{\mathrm{A}} = (1+\alpha^2(t_{\mathrm{I}}^{\mathrm{A}})^2) J_{\mathrm{B}}$. This increasing of the noise achieved by Alice is due to the Unruh radiation absorbed by the detector A. A the peculiar case shown in Fig. 4.11 is now considered. In it, Alice prepares the state of the detector A at a time $s < 0$ and sends it at the time $t_{\mathrm{I}}^{\mathrm{A}} = 0$. In so doing, Eqs. (4.111) and (4.112) become analog to the static one i.e. (4.99) and (4.112), respectively. The transmissivity (4.95), called τ_{R} becomes

$$\tau_{\mathrm{R}} = \frac{16\epsilon^2}{\alpha_{\mathrm{A}}^2 d^2} \sqrt{1 + \alpha^2 s^2} \sin^2(\omega_{\mathrm{A}} s) \sim \sqrt{1 + \alpha^2 s^2}\,\tau_{\mathrm{S}}. \tag{4.113}$$

The parameter $\sqrt{1 + \alpha^2 s^2}$ comes from the factor $\dot{t}_{\mathrm{A}}(s)$ appearing in the denominator on the r.h.s. of Eq. (4.95). As a consequence, the transmissivity of the protocol in Fig. 4.11 can be arbitrarily high by anticipating the time s when the state is prepared. From Ref. [P4], this happens because, in Bob's frame, Alice's initial state is amplified by a factor $\sqrt{\frac{1+\alpha^2 s^2}{1+\alpha^2 t_{\mathrm{I}}^{\mathrm{A}2}}}$ by her motion while waiting to send the state (at the time $t_{\mathrm{I}}^{\mathrm{A}}$) after its preparation (at the time s).

In this protocol, λ_{B} can be arbitrarily low and τ still arbitrarily high. As mentioned at the end of Sec. 4.2.2.1, this allows the quantum capacity to be arbitrarily close to 1. Fig. 4.12 shows how

[4] In particular, for values $d = 1$ and $\epsilon = 0.001$, the transmissivity increases for $1 < \gamma \lesssim 1.054$

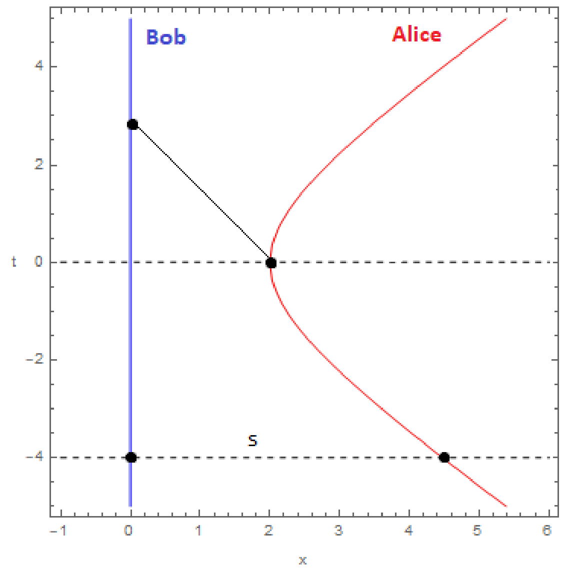

Figure 4.11: Figure showing the protocol considered in Sec. 4.2.2.4, with $s = -4$ and $\alpha = 1/2$.

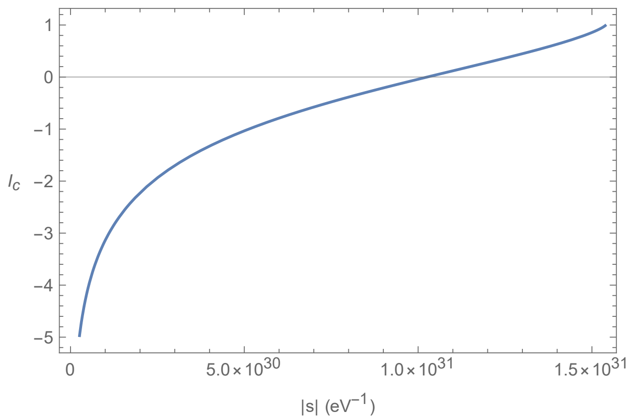

Figure 4.12: Maximized coherent information I_c - giving the one-shot quantum capacity when positive - of the channel depicted in Fig. 4.11, obtained from Eq. (3.39), in terms of s, i.e. the time, in Bob's frame, when Alice prepares the state of the detector A which is then communicated to Bob at $(t_{\mathrm{I}}^{\mathrm{A}})_{\mathrm{B}} = 0$. The parameters chosen are $d = 10^5\, eV^{-1}$, $\epsilon = 10^{-3}\, eV^{-1}$ and $\omega_{\mathrm{A}} = 1\, eV$, so that $\alpha_{\mathrm{A}} = 0.5 \cdot 10^{-3}$.

the quantum capacity of the protocol increases with $|s|$, i.e. the time between the preparation of the state and its communication. The natural units $\hbar = c = 1$ were restored, since no gravitational effects are present. By using atomic quantities (specified in the caption of Fig. 4.12), and a proper acceleration $\alpha = d^{-1}$ giving an Unruh temperature of $\sim 1\,\mathrm{K}$, a quantum capacity greater than zero requires a time $|s|$ excessively high (comparable with the age of the Universe). This obviously makes the protocol impossible to be set up today with actual means. In particular, the quantum capacity is maximized when $\tau \to 2$, and the time needed to reach this value is noted with $|s_\star|$. From Eq. (4.113) it reads

$$|s_\star| \sim \frac{\alpha_{\mathrm{A}}^2}{8} \frac{1}{\epsilon^2 \alpha^3} \tag{4.114}$$

Therefore, to reach an affordable protocol execution time, would be to increase the proper acceleration of the sender, since $|s_\star| \propto \alpha^{-3}$. In this way, the possibility to achieve a reliable communication of quantum messages between detectors is linked with the possibility to see the Unruh effect. The main problem of this observation is on the size of the laboratory needed to reach an observable - i.e. ~ 1 K Unruh temperature, as the one used as reference in Fig. 4.12. To this perspective, detectors with a circular motion have recently proven to provide an analog Unruh effect and potentially reach high accelerations in a limited space [132, 232, 233]. This is believed to be the key to drastically reduce the execution time of the considered communication protocol to reasonable values.

4.3 Role of a cosmological expansion

In Chapter 3, the effects predicted by quantum field theory in curved spacetime have always proved to create further noise to the protocol. In particular, in Sec. 3.4, also the quality of a non-perfect quantum channel was proved to decrease by the evolution of a background spacetime. The intuitive reason behind that is on the spectrum of particles produces, which will always interfere negatively with the communication of one-mode signals.

For localized quantum systems, instead, many factors are expected to contribute to the communication channel such as the structure of the background quantum field and their interaction with locally non-relativistic quantum systems. Therefore, wondering if the communication capabilities of the protocol with quantum antennas - studied in Sec. 4.1 - could increase, the effects of a curved background on it are now explored.

In particular, the detectors are static lying in a cosmological expanding background, characterized by the metric (2.25). Since the detectors are static, the sender Alice and the receiver Bob work with the same proper time t. The spatial Fermi-normal coordinates of the two parts are instead

$$\begin{cases} \mathbf{x}_{\mathrm{A}} = a(t)\,(\mathbf{x} - \mathbf{d})\ ; \\ \mathbf{x}_{\mathrm{B}} = a(t)\mathbf{x}\,, \end{cases} \tag{4.115}$$

where $\mathbf{x} = (x, y, z)$ are the conformal coordinates defined in the metric (2.25) and $|\mathbf{d}| =: d$ is the conformal distance between the detectors.

The two detectors have a Lorentzian smearing function (4.98). Since the detectors themselves experiment a cosmological expansion, their effective size ϵ would scale with $a(t)$. Therefore the smearing function (4.98) is modified to

$$\tilde{f}_i(\mathbf{x}_i, t) = \frac{1}{\pi^2} \frac{a(t)\epsilon}{(\mathbf{x}_i \cdot \mathbf{x}_i + a^2(t)\epsilon^2)^2} = \frac{1}{\pi^2 a^3(t)} \frac{\epsilon}{(|\mathbf{x}|^2 + \epsilon^2)^2}\,. \tag{4.116}$$

The Fermi length (2.82) can be easily computed to be[5]

$$L_{\mathrm{F}} = \sqrt{\frac{6}{R}} = \frac{a}{\dot{a}^2 - \ddot{a}a}\,, \tag{4.117}$$

being R the scalar curvature (2.34). The Fermi bound requires $\epsilon a(t) \ll L_{\mathrm{F}}$ and then, from Eq. (4.117), the following parameter as a relative error given by considering non-relativistic quantum systems in relativistic settings, namely

$$\mathcal{E}_F = a\epsilon\sqrt{\frac{R}{6}}\,. \tag{4.118}$$

Again, since the detectors A and B have the same shape, their cutoff energy is the same, i.e. $E_c^{\mathrm{A}} = E_c^{\mathrm{B}}$. Finally, the detectors interact with the field via the rapid interaction studied in Sec. 4.2.2, i.e. with a switching-in (4.63). For the interaction times $t_{\mathrm{I}}^{\mathrm{i=A,B}}$, by using the conformal coordinates (2.30), one has $\eta_{\mathrm{I}}^{\mathrm{B}} = \eta_{\mathrm{I}}^{\mathrm{A}} + d$.

The integrals $I(t_{\mathrm{I}}^{\mathrm{A}}, t_{\mathrm{I}}^{\mathrm{B}})$, $J_{\mathrm{A}}(t_{\mathrm{I}}^{\mathrm{A}})$ and $J_{\mathrm{B}}(t_{\mathrm{I}}^{\mathrm{B}})$ are now computed. For the normal modes $u_{\mathbf{k}}(t,\mathbf{x})$, the separation of variables in Eq. (2.31) is used. Moreover, the time dependent functions $\chi_k(\eta)$ are found by using the first order perturbative solution presented in Sec. (2.2.2). The relative error expected from this approximation is given by Eq. (2.43) with $n = 1$.

With this method, the integral $I(t_{\mathrm{I}}^{\mathrm{A}}, t_{\mathrm{I}}^{\mathrm{B}})$, from Eq. (4.71) has the form

$$I(t_{\mathrm{I}}^{\mathrm{A}}, t_{\mathrm{I}}^{\mathrm{B}}) = I_0(t_{\mathrm{I}}^{\mathrm{A}}, t_{\mathrm{I}}^{\mathrm{B}}) + I_1(t_{\mathrm{I}}^{\mathrm{A}}, t_{\mathrm{I}}^{\mathrm{B}}) + I_2(t_{\mathrm{I}}^{\mathrm{A}}, t_{\mathrm{I}}^{\mathrm{B}})\,, \tag{4.119}$$

where

$$I_0(t_{\mathrm{I}}^{\mathrm{A}}, t_{\mathrm{I}}^{\mathrm{B}}) = -\frac{1}{(2\pi)^2 a(t_{\mathrm{I}}^{\mathrm{A}}) a(t_{\mathrm{I}}^{\mathrm{B}})}\frac{d}{\epsilon}\frac{1}{d^2+\epsilon^2}\,; \tag{4.120}$$

$$I_1(t_{\mathrm{I}}^{\mathrm{A}}, t_{\mathrm{I}}^{\mathrm{B}}) = -\frac{6\xi - 1}{2(2\pi)^2 a(t_{\mathrm{I}}^{\mathrm{A}}) a(t_{\mathrm{I}}^{\mathrm{B}})}\frac{\arctan(d/\epsilon)}{d}\int_{\eta_{\mathrm{I}}^{\mathrm{A}}}^{\eta_{\mathrm{I}}^{\mathrm{B}}} \mathrm{d}\eta H^2(\eta)\,. \tag{4.121}$$

$$I_2(t_{\mathrm{I}}^{\mathrm{A}}, t_{\mathrm{I}}^{\mathrm{B}}) = \frac{6\xi - 1}{2(2\pi)^2 a(t_{\mathrm{I}}^{\mathrm{A}}) a(t_{\mathrm{I}}^{\mathrm{B}})}\frac{1}{d}\int_{\eta_{\mathrm{I}}^{\mathrm{A}}}^{\eta_{\mathrm{I}}^{\mathrm{B}}} \mathrm{d}\eta H^2(\eta)\left(\arctan\left(\frac{\eta_{\mathrm{I}}^{\mathrm{B}} - \eta}{\epsilon}\right) - \arctan\left(\frac{\eta_{\mathrm{I}}^{\mathrm{A}} - \eta}{\epsilon}\right)\right)\,. \tag{4.122}$$

Since a spatial separation is assumed, then $d \gg \epsilon$, so that $d^2 + \epsilon^2 \sim d^2$ and $\arctan(d/\epsilon) \sim \frac{\pi}{2}$ in Eq. (4.121). For similar reasons, in the integral of Eq. (4.122), the function $\arctan((\eta_{\mathrm{I}}^{\mathrm{B}} - \eta)/\epsilon) - \arctan((\eta_{\mathrm{I}}^{\mathrm{A}} - \eta)/\epsilon)$ can be approximated to π whenever $\eta_{\mathrm{I}}^{\mathrm{B}} - \eta \gg \epsilon$ and $\eta - \eta_{\mathrm{I}}^{\mathrm{A}} \gg \epsilon$. By running η, the range of integration $(\eta_{\mathrm{I}}^{\mathrm{A}}, \eta_{\mathrm{I}}^{\mathrm{B}})$, the conditions for this approximation are true always except where η is close by an order ϵ to the integration bounds. However, since the range of integration is large $d \gg \epsilon$, the range where the approximation $\arctan((\eta_{\mathrm{I}}^{\mathrm{B}} - \eta)/\epsilon) - \arctan((\eta_{\mathrm{I}}^{\mathrm{A}} - \eta)/\epsilon) \sim \pi$ is not valid is negligible w.r.t. the range where it is valid. The integral in equation (4.122) can be approximated to $\pi\int_{\eta_{\mathrm{I}}^{\mathrm{A}}}^{\eta_{\mathrm{I}}^{\mathrm{B}}} H_c^2(\eta)$.

With these approximations, the integral $I(t_{\mathrm{I}}^{\mathrm{A}}, t_{\mathrm{I}}^{\mathrm{B}})$ in Eq. (4.119) can be finally written as

$$I(t_{\mathrm{I}}^{\mathrm{A}}, t_{\mathrm{I}}^{\mathrm{B}}) = -\frac{1}{(2\pi)^2 a(t_{\mathrm{I}}^{\mathrm{A}}) a(t_{\mathrm{I}}^{\mathrm{B}})}\frac{1}{d}\left(\frac{1}{\epsilon} - \frac{\pi}{4}(6\xi - 1)\int_{\eta_{\mathrm{I}}^{\mathrm{A}}}^{\eta_{\mathrm{I}}^{\mathrm{B}}} \mathrm{d}\eta a^2(\eta) H^2(\eta)\right)\,. \tag{4.123}$$

The integrals $J_{\mathrm{i}}(t_{\mathrm{I}}^{\mathrm{i}})$ can be computed as well by putting Eq. (2.42) in Eq. (4.82), getting

$$J_i(\eta_{\mathrm{I}}^{\mathrm{i}}) = \frac{1}{(2\pi)^2 a^2(\eta_{\mathrm{I}}^{\mathrm{i}})}\left(\frac{1}{4\epsilon^2} - (6\xi - 1)\int_{\eta_0}^{\eta_{\mathrm{I}}^{\mathrm{i}}} \mathrm{d}\eta H^2(\eta)\frac{\eta_{\mathrm{I}}^{\mathrm{i}} - \eta}{(\eta_{\mathrm{I}}^{\mathrm{i}} - \eta)^2 + \epsilon^2}\right) \tag{4.124}$$

[5] The matrix $R_{0\mathrm{i}0\mathrm{j}}$ is $\frac{R}{6}\mathbb{I}_{3\times3}$. The result follows.

The focus is now on the ratio $\frac{I^2(t_{\rm I}^{\rm A},t_{\rm I}^{\rm B})}{J_A(t_{\rm I}^{\rm A})J_B(t_{\rm I}^{\rm B})}$, appearing on the transmissivity (4.95), being the only factor dependent on the background spacetime. By using Eqs. (4.123) and (4.124), together with the first order perturbation theory, this ratio, in case of a cosmological expanding background, reads

$$\frac{I^2(t_{\rm I}^{\rm A},t_{\rm I}^{\rm B})}{J_A(t_{\rm I}^{\rm A})J_B(t_{\rm I}^{\rm B})} \sim 16\frac{\epsilon^2}{d^2}\left(1-(6\xi-1)\,F\right) . \tag{4.125}$$

where

$$F=\epsilon\frac{\pi}{2}\int_{\eta_{\rm I}^{\rm A}}^{\eta_{\rm I}^{\rm B}}{\rm d}\eta H^2(\eta)-4\epsilon^2\int_{\eta_0}^{\eta_{\rm I}^{\rm B}}{\rm d}\eta H^2(\eta)\frac{\eta_{\rm I}^{\rm B}-\eta}{(\eta_{\rm I}^{\rm B}-\eta)^2+\epsilon^2}-4\epsilon^2\int_{\eta_0}^{\eta_{\rm I}^{\rm A}}{\rm d}\eta H^2(\eta)\frac{\eta_{\rm I}^{\rm A}-\eta}{(\eta_{\rm I}^{\rm A}-\eta)^2+\epsilon^2} . \tag{4.126}$$

From Eq. (4.95), then

$$\tau_{\rm C}=\frac{16}{\alpha_A^2}\frac{\epsilon^2}{d^2}(1+(1-6\xi)F)\sin^2(\omega_A(t_{\rm I}^{\rm A}-s))=(1+(1-6\xi)F)\,\tau_{\rm S} . \tag{4.127}$$

Since F is a perturbative parameter, then $\tau_{\rm C}\ll 1$ and the quantum capacity of the channel is zero. This is in line with the discussion performed at the end of Sec. 4.2.2.2. In fact, the no-cloning theorem applies to prevent a possible reliable quantum communication, since the universe expansion is isotropic and the detectors are static (the situation is the one at the left of Fig. 4.10).

For the classical capacity of the channel, one has the simplified expression (4.102), for which the relative increasing of the classical capacity - w.r.t. the Minkowski case $F=0$ - is easily obtained as

$$\Delta C := \frac{C_E-C_E(F=0)}{C_E}\sim(1-6\xi)F . \tag{4.128}$$

It is worth understanding whether a cosmological expansion could increase or decrease the communication capabilities of two particle-detectors w.r.t. to the Minkowski case. From Eq. (4.128), a cosmological expansion:

1. increases the classical communication capabilities of two static particle detectors if $\xi<1/6$ and $F>0$ or if $\xi>1/6$ and $F<0$;
2. decreases the classical communication capabilities of them if $\xi<1/6$ and $F<0$ or if $\xi>1/6$ and $F>0$;
3. does not affect the communication capabilities of them in case of *conformal coupling* $\xi=1/6$.

The sign of F is now investigated. At first, the case $\eta_0=\eta_{\rm I}^{\rm A}$ is considered. This means that the spacetime can be approximated as Minkowskian at the time $\eta_{\rm I}^{\rm A}$, i.e. $a(\eta_{\rm I}^{\rm A})=1$ and $\dot a(\eta_{\rm I}^{\rm A})\sim 0$. By doing that, one is basically assuming that any expansion prior to the protocol is ignored, as depicted in Fig. 4.13. In other words, any expansion prior to the time where Alice sends her message is considered to have negligible effects on the protocol. This assumption may be valid only if the Universe is accelerating, i.e. whenever the expansion rate increases[6]. Therefore, the analysis is restricted to such cosmological expansions.

The factor F from (4.126), when $\eta_0\sim\eta_{\rm I}^{\rm A}$, becomes

$$F:=\int_{\eta_{\rm I}^{\rm A}}^{\eta_{\rm I}^{\rm B}}{\rm d}\eta\left(\frac{\pi\epsilon}{2}-\frac{4\epsilon^2(\eta_{\rm I}^{\rm B}-\eta)}{(\eta_{\rm I}^{\rm B}-\eta)^2+\epsilon^2}\right)H^2(\eta) . \tag{4.129}$$

[6]Otherwise, one has $\ddot a<0$ but $\dot a$ negligible before a reference time t_0 and not after, which makes no sense.

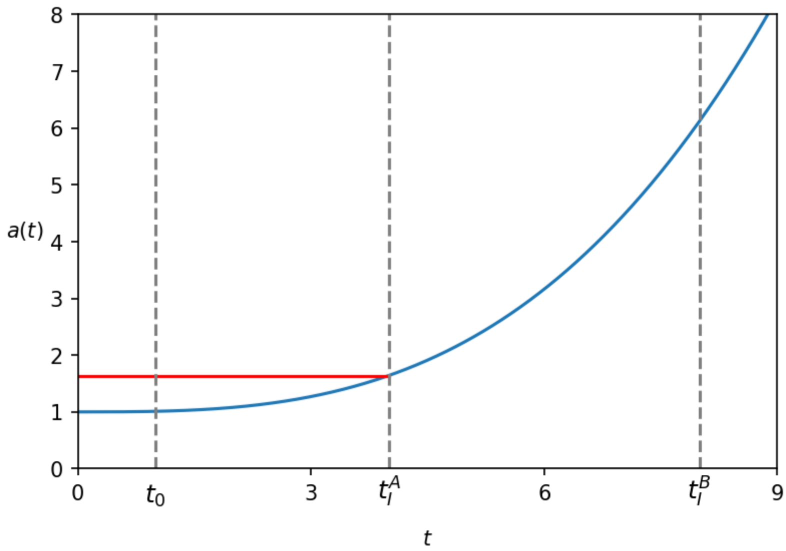

Figure 4.13: In this image, the red line exemplifies a cosmological expansion one effectively considers with the approximation $\eta_0 \sim \eta_{\rm I}^{\rm A}$, i.e. neglecting the effects of any expansion prior to $\eta_{\rm I}^{\rm A}$. The blue line is the cosmological expansion without approximation.

From Eq. (4.129), F turns out to be an integral of a definite-positive function H^2 weighted by a function

$$g(\eta) := \frac{\pi\epsilon}{2} - 4\frac{\epsilon^2(\eta_{\rm I}^{\rm B} - \eta)}{(\eta_{\rm I}^{\rm B} - \eta)^2 + \epsilon^2}\,. \tag{4.130}$$

The plot of $g(\eta)$, in Eq. (4.130) is provided in Fig. 4.14, from which one obtains that $g(\eta)$ is always positive except when

$$\frac{\eta_{\rm I}^{\rm B} - \eta}{\epsilon} \in \left(\frac{4}{\pi} - \sqrt{\frac{16}{\pi^2} - 1}, \frac{4}{\pi} + \sqrt{\frac{16}{\pi^2} - 1}\right) \simeq (0.49, 2.06)\,. \tag{4.131}$$

This interval is much smaller - by a factor $\sim 1.576\frac{\epsilon}{d}$ - than the interval $\left[\eta_{\rm I}^{\rm A}, \eta_{\rm I}^{\rm B}\right]$ where η is integrated in Eq. (4.129). Therefore, the factor F could be negative only in the peculiar situation where $H^2(\eta)$ is really high in the range given by Eq. (4.131) and negligible elsewhere. This occurs when the universe expands sharply right after $\eta_{\rm I}^{\rm A}$ and basically stops its expansion afterwards. Since this situation is very peculiar, and basically never predicted by any cosmological model, one can safely consider $F > 0$.

In this case, one can conclude that a cosmological expansion may increase or decrease the communication capabilities of quantum antennas depending on the value of the coupling with the curvature. In particular, from Eq. (4.127), if $\xi < 1/6$ (resp. $\xi > 1/6$) the quality of the communication of classical messages increases (resp. decreases) due to a cosmological expansion. This result can be briefly explained by considering the effective mass of null-like particles when coupled with the curvature, i.e. $M_{\rm eff}$ given by Eq. (2.33). In fact, when $\xi > 1/6$, $M_{\rm eff}$ is positive and this would hinder the propagation from sender to receiver. On the contrary, if $\xi < 1/6$, $M_{\rm eff}^2$ is negative and the background field assumes a tachyonic behaviour. Therefore, the low frequency modes $|\mathbf{k}| < |M_{\rm eff}|$ amplify exponentially, giving an amplification to the signal which increases the communication capabilities

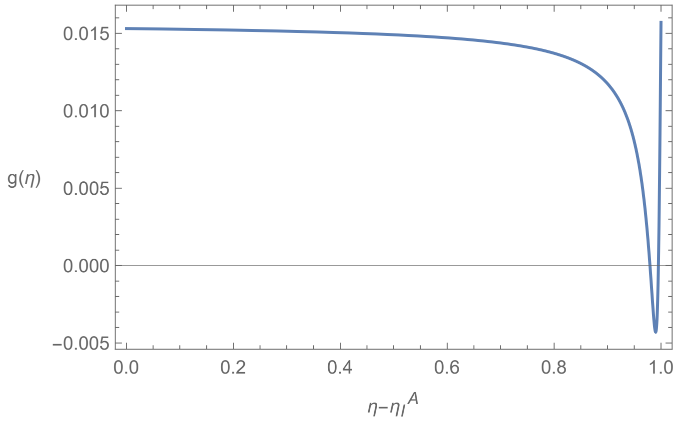

Figure 4.14: Behaviour of the function $g(\eta)$ in confoermal time η (Eq. (4.130)). The parameters $\epsilon = 0.01$ and $d = 1$ were chosen.

of the protocol studied.

From the obtained results, the communication protocol described in Sec. 4.1 may test the value of the coupling field-curvature coupling ξ highly discussed in the literature [234, 235].

4.3.1 Role of an expansion prior to the protocol

With a short analysis, it is now shown how the range $\xi < 1/6$ is more appealing and consistent with the predictions of quantum field theory in curved spacetime. To do that, the approximation $\eta_0 \sim \eta_{\mathrm{I}}^{\mathrm{A}}$ is now relaxed. In this way, the effects of a prior expansion on the communication protocol are now briefly investigated. The factor F obtained when $\eta_0 \sim \eta_{\mathrm{I}}^{\mathrm{A}}$, given by Eq. (4.129) can be easily proved to be always greater than the non-approximated one in Eq. (4.126). As a consequence, from Eq. (4.127) an expansion prior to the start of the protocol decreases (resp. increases) the classical capacity of the channel if $\xi < 1/6$ (resp. $\xi > 1/6$).

As extensively reported in Sec. 2.2, a cosmological expansion produces particles. How the presence of such particles could influence the communication protocol in Sec. 4.1? By changing the initial state of the field, from the vacuum to a whatever particle state, one can easily prove that the integral $I(t_{\mathrm{I}}^{\mathrm{A}}, t_{\mathrm{I}}^{\mathrm{B}})$ from Eq. (4.71) remains unaltered (since it comes from a field commutator), while the integrals (4.82) always increase. Therefore, the transmissivity (4.95) - and therefore the classical capacity - always decreases in presence of cosmological produced particles at the time[7] $t_{\mathrm{I}}^{\mathrm{A}}$.

An expansion prior to the protocol is expected to produce particles. In this way, the contribute of this expansion is supposed to be noisy. This is true, however, only if $\xi < 1/6$. Therefore, values of the parameter ξ are restricted to this range from now on. Before going on, it is worth stressing out that, since an expansion prior to the protocol actually affects it, the communication scheme between quantum antennas is actually able to give information also to the history of our Universe. This possibility would be further explored in the near future.

[7] One can also check that the entanglement between particles with opposite momenta, occurring in the cosmological particle production, only contributes to the integral J with an time oscillating factor, without giving a net contribute.

4.3.2 Einstein-de Sitter expansion

In the specific expansion considered now, there is one background cosmological fluid dominating over the other ones, and this is supposed to have an equation of state is $p = w\varrho$, with a constant barotropic parameter w.

For the sake of simplicity, any effects of expansions prior to the protocol are neglected, i.e. $\eta_{\rm I}^{\rm A} \sim \eta_0$, with $\dot{a}(\eta_{\rm I}^{\rm A}) \sim 0$ and $a(\eta_{\rm I}^{\rm A}) = 1$. By putting this last condition, and the equation of state $p = w\varrho$, into the Friedmann Eqs. (2.27a) and (2.27b) and by solving them, the following scale factor is obtained, i.e.

$$a(t) = \left(\frac{t}{t_{\rm I}^{\rm A}}\right)^{\frac{2}{3w+3}} . \tag{4.132}$$

Since, with the approximation $\eta_{\rm I}^{\rm A} \sim \eta_0$, only accelerated expansions are consistent, then $w < -\frac{1}{3}$ to have $\ddot{a} > 0$. Some manipulations allow to write Eq. (4.132) in conformal time η as

$$a(\eta) = \left(\frac{3w+1}{3w+3}\frac{\eta}{\eta_{\rm I}^{\rm A}} + \frac{2}{3w+3}\right)^{\frac{2}{3w+1}} . \tag{4.133}$$

At this point, the factor F in Eq. (4.129) can be analytically computed. By considering the leading order for ϵ/d, one has

$$F \sim \frac{2\pi d\epsilon}{3\eta_{\rm I}^{\rm A}(1+w)(3\eta_{\rm I}^{\rm A}(1+w)+d(1+3w))} - \frac{16\epsilon^2 \ln\left(\frac{d}{\epsilon}\right)}{(3\eta_{\rm I}^{\rm A}(1+w)+d(1+3w))^2} . \tag{4.134}$$

From Eq. (4.134), as expected from previous discussions, F turns out to be always positive.

The minimal coupling $\xi = 0$ is now considered for the reasons explained in Sec. 4.3.1. In this case, the relative increasing of the classical capacity (4.128) corresponds to F itself. This is shown in terms of w in Fig. 4.15. In it, the dashed lines enclose the possible values of ΔC given by taking into account the relative error $\mathcal{E} = \sqrt{\mathcal{E}_{\rm F}^2 + \mathcal{E}_{\rm P}^2}$, where $\mathcal{E}_{\rm F}$ and $\mathcal{E}_{\rm P}$ are given respectively by Eqs. (4.118) and (2.43), representing the relative error given by the considering non-relativistic quantum systems in relativistic settings and the first order perturbation theory.

Fig. 4.15 shows that the more is the acceleration of the expansion, the better the channel performs. This was expected since the average $|M_{\rm eff}|$ from Eq. (2.33) increases with the universe acceleration and therefore, more background modes are exponentially amplified. Information about the coupling ξ can be achieved as well. If the capacity achieved in an experiment is lower than the one predicted in Fig. 4.15, then the coupling is not minimal, but closer to the conformal one (from below).

More importantly, from Fig. 4.15 and Eq. (4.134), $\Delta C|_{\xi=0} = F$ grows by decreasing w to reach a divergence at $w = -\frac{d+3\eta_{\rm I}^{\rm A}}{3(d+\eta_{\rm I}^{\rm A})}$. In fact, at this point, Bob is at Alice's *comoving horizon* $d_{\rm H}$ at the time $\eta_{\rm I}^{\rm A}$, reading

$$d_{\rm H} = -3\eta_{\rm I}^{\rm A}\left(\frac{1+w}{1+3w}\right) . \tag{4.135}$$

The intuitive meaning of $d_{\rm H}$ is that, since the universe expansion accelerates, if $d > d_{\rm H}$ then the signal sent by Alice would never reach Bob. The factor F is worth being studied with the scaled quantities

$$\tilde{\epsilon} := \frac{\epsilon}{d_{\rm H}} ; \quad \tilde{d} := \frac{d}{d_{\rm H}} , \tag{4.136}$$

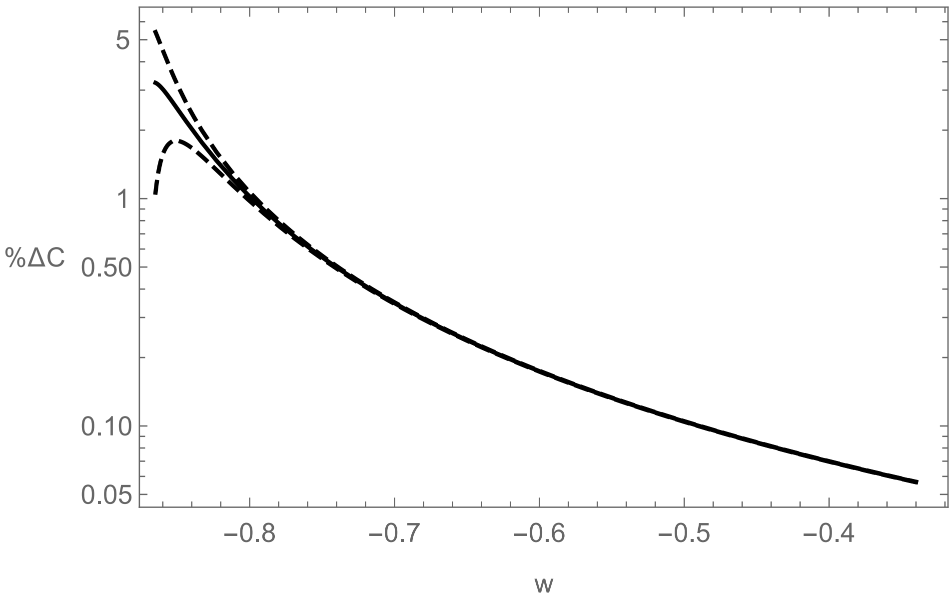

Figure 4.15: The increasing percentage of the classical capacity $\%\Delta C$ from Eq. (4.128) due to a cosmological expansion of an Einstein-de Sitter universe, whose curvature is minimal coupled with the background field $\xi = 0$, for different values of the barotropic index of the fluid w. The other parameters are $\epsilon = 0.01$, $\eta_{\mathrm{I}}^{\mathrm{A}} = 5$ and $d = 1$. The dashed lines represent the minimum and maximum values of $\%\Delta C$ by taking into account the error given by the perturbation theory (2.43) and the Fermi bound (4.118).

where $0<\tilde{\epsilon}<1$, $0<\tilde{d}<1$ and $\tilde{\epsilon}\ll\tilde{d}$. With the adimensional variables (4.136), the factor F in Eq. (4.134) becomes

$$F\sim\frac{2\pi}{(1+3w)^2}\frac{\tilde{\epsilon}\tilde{d}}{1-\tilde{d}}-\frac{16}{(1+3w)^2}\frac{\tilde{\epsilon}^2}{(1-\tilde{d})^2}\ln\left(\frac{\tilde{d}}{\tilde{\epsilon}}\right). \tag{4.137}$$

The errors $\mathcal{E}_P$ and $\mathcal{E}_F$ - from Eqs. (2.43) and (4.118), respectively - can be found as well in terms of $\tilde{\epsilon}$ and $\tilde{d}$ as

$$\mathcal{E}_P=32\frac{6\tilde{d}+2(3-\tilde{d})\ln\left(1-\tilde{d}\right)-\ln^2\left(1-\tilde{d}\right)}{(1+3w)^4}. \tag{4.138}$$

$$\mathcal{E}_F=-\frac{\tilde{\epsilon}}{(1+3w)(1-\tilde{d})}; \tag{4.139}$$

It is worth knowing how the classical capacity increases depending on the scale of the protocol. To study that, the ratio ϵ/d - and so $\frac{\tilde{\epsilon}}{\tilde{d}}$ is fixed and the relative increasing of the classical capacity is shown in terms of $\tilde{d}$ in Fig. 4.16. From it, the relative increase of the capacity grows the larger is the scale of the protocol w.r.t. the covoming horizon d_{H}. In other words, ΔC is higher the more Bob gets close to Alice comoving horizon, i.e. $d\to d_{\mathrm{H}}$ and scaling the effective size of the detector with d. As the detector B approaches Alice's comoving horizon, the error $\mathcal{E}$ diverges, meaning that further order perturbation theory and/or relativistic quantum systems as detectors are required when $d\sim d_{\mathrm{H}}$. Nevertheless, the trend in the range $\mathcal{E}\ll 1$ suggests a significant increasing of the communication qualities of quantum antennas in proximity of horizons. Interestingly, the limit $w\to -1$, involving a de Sitter universe, is not achievable from Eq. (4.134), valid exclusively for the Einstein-de Sitter expansion. Instead, by using the horizon-scaled variables (4.136) (i.e. Eq. (4.137) for F), the limit $w\to -1$ leads to a finite and well-behaved result for the increasing of the classical capacity. A short computation (performed in Ref. [P7]) shows that Eq. (4.137) with $w=-1$, is exactly the result recovered by repeating the computation of F from Eq. (4.129) by starting with the de Sitter scale factor

$$a(t)=e^{H_0(t-t_I^A)}, \tag{4.140}$$

where $H_0=\frac{1}{\eta_0}$. This is important since the de Sitter expansion $w=-1$, represents a very relevant cosmological scenario, typically associated with strongly-accelerated phases of the universe [236]. Principally, at primordial times, inflation represents a phase of de Sitter expansion [237], compatible with $w=-1$.

The factor F, in that case, turns out to be

$$F\sim\frac{\pi}{2}\frac{\tilde{\epsilon}\tilde{d}}{1-\tilde{d}}-\frac{4\tilde{\epsilon}^2}{(1-\tilde{d})^2}\ln(\tilde{d}/\tilde{\epsilon}). \tag{4.141}$$

By comparing the behaviour of ΔC when $w=-1$, shown in Fig. 4.17 with Einstein-de Sitter case $w=-0.7$ in Fig. 4.16, the increment of the classical capacity is slightly lower in the former scenario $w=-1$. Indeed, from Eq. (4.137) $F=\Delta C$ scales as $(1+3w)^{-2}$. However, from Figs. 4.16 and 4.17, the error is lower in the case $w=-1$. In fact, the error $\mathcal{E}_{\mathrm{P}}$ in Eq. (4.138) - expected to be much larger than $\mathcal{E}_{\mathrm{F}}$ when $1-\tilde{d}\gg\tilde{\epsilon}$ - scales as $(1+3w)^{-4}$. Therefore, despite a lower capacity increasing, one can explore more safely the transmission of information in proximity of the sender horizon in de Sitter universes.

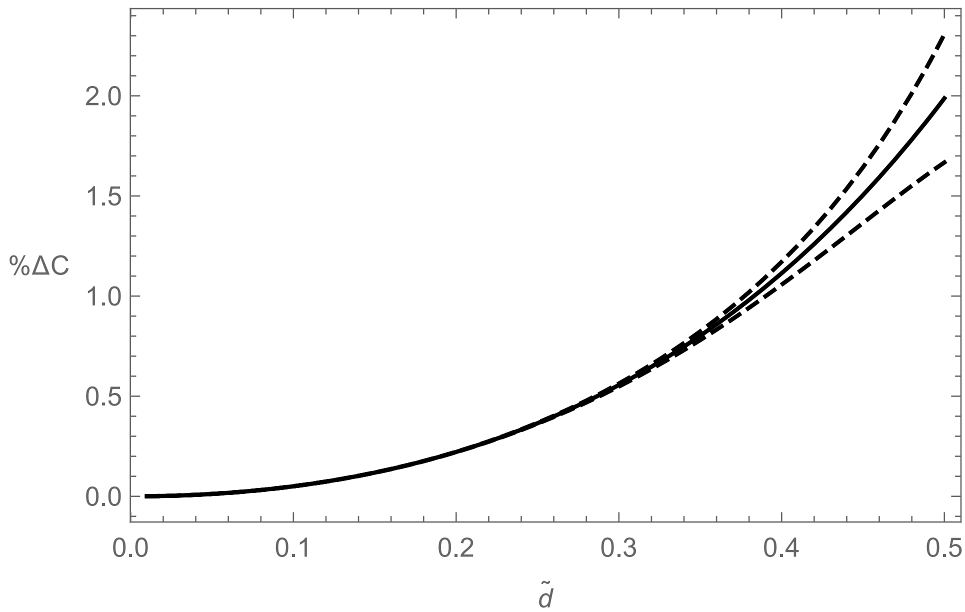

Figure 4.16: The increasing percentage of the classical capacity $\%\Delta C$ from Eq. (4.128) due to a cosmological expansion of an Einstein-de Sitter universe with $w = 0.7$, whose curvature is minimal coupled with the background field $\xi = 0$, for different values $\tilde{d}$ with $\tilde{\epsilon} = \tilde{d}/100$. dashed lines represent the minimum and maximum values of $\%\Delta C$ by taking into account the error given by the perturbation theory (2.43) and the Fermi bound (4.118).

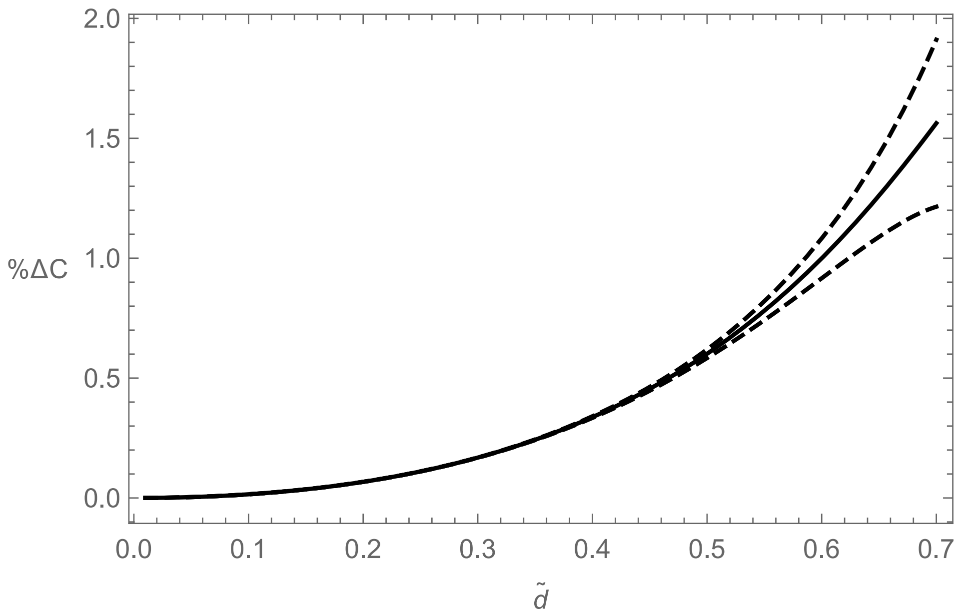

Figure 4.17: The increasing percentage of the classical capacity $\%\Delta C$ from Eq. (4.128) due to a cosmological expansion of a de Sitter universe with, whose curvature is minimal coupled with the background field $\xi = 0$, for different values $\tilde{d}$ with $\tilde{\epsilon} = \tilde{d}/100$. dashed lines represent the minimum and maximum values of $\%\Delta C$ by taking into account the error given by the perturbation theory (2.43) and the Fermi bound (4.118).

4.4 Dephasing and erasure of quantum states due to self-gravity

When undergoing external forces, experimental evidences tell that quantum states lose the property to be in a state superposition - i.e. to be in different states "at the same time" - and tend to assume a classical behaviour [238, 239, 240]. This phenomenon is known as *quantum decoherence* and it is the main responsible to the actual limitations of stable quantum technologies [56].

In line with those predictions, gravity is expected to involve decoherence as well. The *gravitational decoherence*, too weak to be experimentally observed nowadays, is theoretically predicted by many mechanisms predict this phenomenon, both involving a semiclassical gravity theory [219, 220, 48, 221] and a quantum gravity theory [241, 242, 49, 243]. In particular, for the latter scenario, the decoherence occurs because of the interaction of the field with the gravitational environment - having quantum degrees of freedom. Therefore, the decoherence is predicted by a graviton thermal bath, expected from the background noise.

It is interesting to know if an intrinsic decoherence may occur in a quantum gravity setting, as occurs in case of a semiclassical theory of gravity by the Diósi-Penrose mechanism [219, 220]. Motivated by this fact, the evolution of a localized quantum state in the gravitational vacuum is addressed, wondering if a source of decoherence may be given by the gravity the localized state induces to itself - so called "self-gravity". To do that, the linearized quantum gravity theory, discussed in Sec. 2.5, is employed. The interaction with gravitons, supposed initially in the vacuum state, is addressed as a quantum channel whose properties and quantum capacity are investigated, with the hope to find an explicit intrinsic decoherence channel together with other noisy ones.

4.4.1 Initial state

A bosonic scalar particle with mass m is considered to be initially in a generic superposition of two different localizations, centered at $\mathbf{x}_\mathrm{A}$ and $\mathbf{x}_\mathrm{B}$. More precisely, the following ladder operators are defined

$$\hat{a}_\mathrm{A} := \int \mathrm{d}\mathbf{k}\, F^*_{\mathbf{k}_0}(\mathbf{k})\, e^{i\,\mathbf{x}_\mathrm{A}\cdot\mathbf{k}}\, \hat{a}_\mathbf{k}\,; \tag{4.142}$$

$$\hat{a}_\mathrm{B} := \int \mathrm{d}\mathbf{k}\, F^*_{\mathbf{k}_0}(\mathbf{k})\, e^{i\,\mathbf{x}_\mathrm{B}\cdot\mathbf{k}}\, \hat{a}_\mathbf{k}\,, \tag{4.143}$$

so that $\hat{a}^\dagger_{\mathrm{i=A,B}}$ applied to the bosonic field vacuum creates a wave packet localized around the spatial points $\mathbf{x}_\mathrm{i}$ whose momentum amplitude is given by $F_{\mathbf{k}_0}(\mathbf{k})$. The spatial smearing of those wave packets can be obtained from Eq. (2.9) with $g(\mathbf{k}) \equiv F_{\mathbf{k}_0}(\mathbf{k})$.

The two localizations - around $\mathbf{x}_\mathrm{A}$ and $\mathbf{x}_\mathrm{B}$ - must be distinct, so that an observer could tell exactly if the particle is found at the state $|1_\mathrm{A}\rangle := \hat{a}^\dagger_\mathrm{A}|0\rangle$ or $|1_\mathrm{B}\rangle := \hat{a}^\dagger_\mathrm{B}|0\rangle$ (i.e. if it is located at $\mathbf{x}_\mathrm{A}$ or $\mathbf{x}_\mathrm{B}$). Therefore, the two wavepackets cannot superpose, namely $\langle 1_\mathrm{A}|1_\mathrm{B}\rangle = 0$. In this case, the ladder operators (4.142) and (4.143) behave as two bosonic operators of two independent modes, namely A and B. One can go even further and define a set of wavepacket modes, labeled by λ and created by the operators $\{\hat{a}^\dagger_\lambda\}_\lambda$, which, together with the modes A and B, form a complete and independent set of modes - namely $\langle 1_\lambda|1_{\mathrm{i=A,B}}\rangle = 0$ for each mode λ. In this way, the initial state considered involves one particle in generic superposition of the modes $|1_\mathrm{A}\rangle$ and $|1_\mathrm{B}\rangle$ while all the other modes λ are in the vacuum state. With this prescription, by including the gravitational field modes, initially in the vacuum, the initial state of the entire physical system is

$$\hat{\rho}(0) = \hat{\rho}_{\mathrm{S}}(0) \otimes \prod_{\lambda}^{(E)} |0_\lambda\rangle\langle 0_\lambda| \otimes \hat{\rho}_{\mathrm{G}}(0) \equiv \hat{\rho}_{\mathrm{SE}}(0) \otimes \hat{\rho}_{\mathrm{G}}(0)\,, \tag{4.144}$$

where $\hat{\rho}_{\mathrm{S}}$ is the substate focus of interest, which includes the modes A and B, namely

$$\hat{\rho}_{\mathrm{S}}(0) = \alpha\,|1_{\mathrm{A}}\rangle\,\langle 1_{\mathrm{A}}| + \beta\,|1_{\mathrm{A}}\rangle\,\langle 1_{\mathrm{B}}| + \beta^*\,|1_{\mathrm{B}}\rangle\,\langle 1_{\mathrm{A}}| + (1-\alpha)\,|1_{\mathrm{B}}\rangle\,\langle 1_{\mathrm{B}}|\;. \tag{4.145}$$

By following Eq. (4.145), the particle has a probability α (resp. $1-\alpha$) to be found at the position $\mathbf{x}_{\mathrm{A}}$ (resp. $\mathbf{x}_{\mathrm{B}}$). The off-diagonal element β indicates the coherence of the initial state. If $|\beta| = \sqrt{\alpha(1-\alpha)}$, the the state $\hat{\rho}_{\mathrm{S}}$ is in a perfect quantum superposition. If, on the contrary ,$|\beta| = 0$, then the state $\hat{\rho}_{\mathrm{S}}$ is in a classical statistical mixture [243].

To preserve the orthonormality of the modes A, B and λ, the states $|1_{\mathrm{i=A,B}}\rangle$ (and $|1_\lambda\rangle$) are supposed to be the same up to a unitary evolution $\hat{U}_0 = e^{-i\hat{H}_\Phi t}$. The Hamiltonian $\hat{H}_\Phi$, obtained from the Lagrangian density (2.1), reads

$$\hat{H}_0 = \int d\mathbf{k}\sqrt{m^2 + |\mathbf{k}|^2}\hat{a}^\dagger_{\mathbf{k}}\hat{a}_{\mathbf{k}}\,. \tag{4.146}$$

In other words, to preserve the orthogonality of $|1_{\mathrm{A}}\rangle$ and $|1_{\mathrm{B}}\rangle$, one has to assume the wave packets to be *i)* static - i.e. they remain localized around $\mathbf{x}_{\mathrm{i=A,B}}$ - and *ii)* "not spreading" in time.

To satisfy the condition *i)* the amplitude of the momentum distribution $F_{\mathbf{k}_0}(\mathbf{k})$ must have average $\mathbf{0}$ and a standard deviation $k_0 := |\mathbf{k}_0|$ involving a non-relativistic particle, i.e. $k_0 \ll m$. For the condition *ii)* one should have

$$|1_{\mathrm{i=A,B}}(t)\rangle = \int d\mathbf{k}F_{k_0}(\mathbf{k})e^{-i\mathbf{x}_{\mathrm{i}}\cdot\mathbf{k}}e^{-i\sqrt{m^2+|\mathbf{k}|^2}t}\hat{a}^\dagger_{\mathbf{k}}\,|0\rangle \sim e^{-imt}\int d\mathbf{k}F_{k_0}(\mathbf{k})e^{-i\mathbf{x}_{\mathrm{i}}\cdot\mathbf{k}}\hat{a}^\dagger_{\mathbf{k}}\,|0\rangle\;. \tag{4.147}$$

The approximation in Eq. (4.147) is valid as long as

$$e^{-i(m-\sqrt{m^2+|\mathbf{k}|^2})t} \sim 1\,. \tag{4.148}$$

which is true if $\frac{|\mathbf{k}_0|^2}{2m}t \ll 1$. Therefore, the condition *ii)*, requires $k_0^2 \ll \frac{2m}{t}$. A *spreading time* can be associated with $t_{\mathrm{S}} = \frac{2m}{|\mathbf{k}_0|^2}$, so that the condition *ii)* is no more valid[8]. Therefore, to have a wave packet $|1_{\mathrm{i=A,B}}\rangle$ stable in time, the range of times considered must be restricted to $t \ll t_{\mathrm{S}}$.

Finally, by defining $\mathbf{L} := \mathbf{x}_{\mathrm{B}} - \mathbf{x}_{\mathrm{A}}$, then the scalar product $\langle 1_{\mathrm{A}}|1_{\mathrm{B}}\rangle$ is always an order of ϵ/L, where $\epsilon \sim k_0^{-1}$ is the wave packet effective size and $L := |\mathbf{L}|$. Therefore, even if not exactly zero, the orthogonality condition $\langle 1_{\mathrm{A}}|1_{\mathrm{B}}\rangle = 0$ is considered valid as long as $L \gg \epsilon$, or $k_0 \gg L^{-1}$.

4.4.2 Time-evolution

The main goal of the section is to study the evolution of the system without any initial source of gravity. However, for the sake of generality, the presence of a classical source of gravity, i.e. a *planet*, is also considered - which can be easily removed by putting its mass $M_\odot = 0$.

By employing the linearized quantum gravity theory, the Lagrangian expressing the graviton-matter interaction is given by Eq. (2.97), where the presence of the planet gives the classical

[8]the states $|1_{\mathrm{A}}\rangle$ and $|1_{\mathrm{B}}\rangle$ have spread they localization to become no more orthonormal.

contribute $T^{\odot}_{\mu\nu}$ to the normal-ordered stress-energy tensor (2.98). In particular, by considering a static and spherical object of mass $M_\odot$ and radius R one has

$$T^{\odot}_{\mu\nu} = \frac{3M_\odot}{4\pi R^3}\theta(R-r)\delta_{\mu 0}\delta_{\nu 0}\,, \tag{4.149}$$

where r is the radial coordinate from the center of the planet.

From the interaction Lagrangian density (2.97), one can split the stress-energy tensor as in Eq. (2.98) and obtain the interaction Hamiltonian $\hat{H}_{\mathrm{I}} = \hat{H}^{\Phi}_{\mathrm{I}} + \hat{H}^{\odot}_{\mathrm{I}}$, where $\hat{H}^{\Phi}_{\mathrm{I}}$ and $\hat{H}^{\odot}_{\mathrm{I}}$ represent respectively the graviton-field and the graviton-planet interaction. They read respectively

$$\hat{H}^{\Phi}_{\mathrm{I}} =\frac{1}{2}\int \mathrm{d}\mathbf{x}\left(\hat{\gamma}_{\mu\nu} - \frac{1}{2}\gamma\eta_{\mu\nu}\right)\hat{T}^{\mu\nu}_{\Phi}\,, \tag{4.150a}$$

$$\hat{H}^{\odot}_{\mathrm{I}} =\frac{1}{2}\int \mathrm{d}\mathbf{x}\left(\hat{\gamma}_{\mu\nu} - \frac{1}{2}\gamma\eta_{\mu\nu}\right)T^{\mu\nu}_{\odot}\,. \tag{4.150b}$$

Since $m \gg k_0$, the component 00 of the stress energy tensor (2.96) is expected to dominate w.r.t. the other ones [49]. In this way, the Hamiltonian H^{Φ}_{I} expressing the graviton-field interaction, to lowest order becomes

$$\begin{aligned}
\hat{H}^{\Phi}_{\mathrm{I}} &\sim -\frac{m}{2}\int \mathrm{d}\mathbf{x}\int \frac{\mathrm{d}\mathbf{p}\mathrm{d}\mathbf{p}'}{\sqrt{(2\pi)^3}}\left(\hat{\gamma}_{00}(\mathbf{x}) + \frac{1}{2}\hat{\gamma}(\mathbf{x})\right)\hat{a}^{\dagger}_{\mathbf{p}}\hat{a}_{\mathbf{p}'}e^{i(\mathbf{p}'-\mathbf{p})\cdot\mathbf{x}} \\
&= -\sqrt{2\pi}m\int \frac{\mathrm{d}\mathbf{k}}{\sqrt{|\mathbf{k}|}}\int \mathrm{d}\mathbf{x}\int \frac{\mathrm{d}\mathbf{p}\mathrm{d}\mathbf{p}'}{(2\pi)^3}\left[\hat{b}_{\mathbf{k}}e^{i\mathbf{k}\cdot\boldsymbol{x}} + \hat{b}^{\dagger}_{\mathbf{k}}e^{-i\mathbf{k}\cdot\boldsymbol{x}}\right]\hat{a}^{\dagger}_{\mathbf{p}}\hat{a}_{\mathbf{p}'}e^{i(\mathbf{p}'-\mathbf{p})\cdot\mathbf{x}} \\
&= -m\int \frac{\mathrm{d}\mathbf{p}\mathrm{d}\mathbf{p}'}{\sqrt{|\mathbf{p}'-\mathbf{p}|}}\left(\hat{b}_{\mathbf{p}-\mathbf{p}'} + \hat{b}^{\dagger}_{\mathbf{p}'-\mathbf{p}}\right)\hat{a}^{\dagger}_{\mathbf{p}}\hat{a}_{\mathbf{p}'}\,.
\end{aligned} \tag{4.151}$$

where the bosonic operator $\hat{b}_{\mathbf{k}} := \hat{P}_{00}(\mathbf{k}) + \hat{P}(\mathbf{k})$, so that $\hat{b}^{\dagger}_{\mathbf{k}}|0_{\mathrm{G}}\rangle = |1^{\mathrm{G}}_{\mathbf{k}}\rangle$ was introduced - since, from Eq. (2.94), one has $[\hat{P}_{00}(\mathbf{k}) + \hat{P}(\mathbf{k}), \hat{P}_{00}(\mathbf{k}')^{\dagger} + \hat{P}^{\dagger}(\mathbf{k}')] = \delta^3(\mathbf{k}-\mathbf{k}')$.

After some manipulations, the Hamiltonian $\hat{H}_{I,\odot}$ from Eq. (4.150b) can be simplified by using Eq. (4.149). It reads

$$\hat{H}^{\odot}_{\mathrm{I}} = \frac{3}{2}M_\odot\int \mathrm{d}\mathbf{k}\Gamma_{\mathbf{k}}(R)\left(\hat{b}_{\mathbf{k}} + \hat{b}^{\dagger}_{\mathbf{k}}\right)\,, \tag{4.152}$$

where $\Gamma_{\mathbf{k}}(R)$ is called the *form factor* and it reads

$$\Gamma_{\mathbf{k}}(R) := -(\cos(|\mathbf{k}|R) - \mathrm{sinc}(|\mathbf{k}|R))/(R^2|\mathbf{k}|^{5/2})\,. \tag{4.153}$$

The time evolution operator $\hat{U}(t)$ reads

$$\hat{U}(t) = \overleftarrow{\mathcal{T}}\exp\left[-\frac{i}{\hbar}\int_0^t dt'\left(\hat{H}_0(t') + \hat{H}^{\Phi}_{\mathrm{I}}(t') + \hat{H}^{\odot}_{\mathrm{I}}(t')\right)\right], \tag{4.154}$$

where the free Hamiltonian $\hat{H}_0$ is

$$\hat{H}_0(t) \sim \int d\mathbf{k}\left(|\mathbf{k}|\hat{b}^{\dagger}_{\mathbf{k}}\hat{b}_{\mathbf{k}} + m\hat{a}^{\dagger}_{\mathbf{k}}\hat{a}_{\mathbf{k}}\right)\,. \tag{4.155}$$

To study the behaviour of the Hamiltonians $\hat{H}^{\Phi}_{\mathrm{I}}$ and $\hat{H}^{\odot}_{\mathrm{I}}$ in time, a double interaction picture is used. In so doing, the time evolution operator of the system is written as $\hat{U}(t) = \hat{U}_0(t)\hat{U}^{\odot}_{\mathrm{I}}(t)\hat{U}^{\Phi}_{\mathrm{I}}(t)$, where the following are defined

$$\hat{U}_0(t) = e^{-i\hat{H}_0 t}\,; \tag{4.156a}$$

$$\hat{U}^{\odot}_{\mathrm{I}}(t) = e^{-i\int_0^t dt'\hat{U}^{\dagger}_0(t')\hat{H}^{\odot}_{\mathrm{I}}(t')\hat{U}_0(t')}\,; \tag{4.156b}$$

$$\hat{U}_{\mathrm{I},\Phi}(t) = e^{-i\int_0^t dt'\hat{U}^{\odot\dagger}_{\mathrm{I}}(t')\hat{U}^{\dagger}_0(t')\hat{H}^{\Phi}_{\mathrm{I}}(t')\hat{U}_0(t')\hat{U}^{\odot}_{\mathrm{I}}(t')}\,. \tag{4.156c}$$

It is worth remarking that linearized quantum gravity is an effective field theory valid up to the Planck mass cutoff, reading $m_{\mathrm{P}} = 1$ in our units. A quantum particle, e.g. an atom, is supposed to have a mass which is way lower the Planck one, so that, for the mass of the particle in the state (4.145), a value $m \ll 1$ is considered. With this in mind, a perturbative expansion for the operator $\hat{U}_{\mathrm{I},\Phi}$, proportional to m, is employed. In particular, a second order perturbative expansion implies $\hat{U}_{\mathrm{I}}^{\Phi} = \hat{\mathrm{Id}} - i\hat{H}_1(t) - \hat{H}_{2\leftarrow}(t)$, where

$$\hat{H}_1(t) := \int_0^t \mathrm{d}t'\, \hat{U}_{\mathrm{I}}^{\odot\dagger}(t')\hat{U}_0^{\dagger}(t')\, \hat{H}_{\mathrm{I}}^{\Phi}\, \hat{U}_0(t')\hat{U}_{\mathrm{I}}^{\odot}(t')\,, \tag{4.157}$$

$$\hat{H}_{2,\leftarrow}(t) := \int_0^t \mathrm{d}t'\, \hat{U}_{\mathrm{I}}^{\odot\dagger}(t')\hat{U}_0^{\dagger}(t')\, \hat{H}_{\mathrm{I}}^{\Phi}\, \hat{U}_0(t')\hat{U}_{\mathrm{I}}^{\odot}(t') \int_0^{t'} \mathrm{d}t''\, \hat{U}_{\mathrm{I}}^{\odot\dagger}(t'')\hat{U}_0^{\dagger}(t'')\, \hat{H}_{\mathrm{I}}^{\Phi}\, \hat{U}_0(t'')\hat{U}_{\mathrm{I}}^{\odot}(t'')\,. \tag{4.158}$$

By using the second order expansion of $\hat{U}_{\mathrm{I}}^{\Phi}$, the time evolution of the system from $\hat{\rho}(0)$ to $\hat{\rho}(t)$ is given by[9]

$$\begin{aligned}\hat{\rho}(t) =&\hat{U}(t)\,\hat{\rho}(0)\,\hat{U}^{\dagger}(t)\\ =&\hat{U}_0(t)\hat{U}_{\mathrm{I}}^{\odot}(t)\,\left(\hat{\mathrm{Id}} - i\hat{H}_1(t) - \hat{H}_{2,\leftarrow}(t)\right)\,\hat{\rho}(0)\,\left(\hat{\mathrm{Id}} + i\hat{H}_1(t) - \hat{H}_{2,\rightarrow}(t)\right)\,\hat{U}_{\mathrm{I}}^{\odot\dagger}(t)\hat{U}^{(0)\dagger}(t)\\ =&\hat{\rho}(0) + i\left[\hat{\rho}(0), \hat{H}_{1*}(t)\right] - \left(\hat{H}_{2*,\leftarrow}(t)\hat{\rho}(0) + \hat{\rho}(0)\hat{H}_{2*,\rightarrow}(t)\right) + \hat{H}_{1*}(t)\hat{\rho}(0)\hat{H}_{1*}(t),\end{aligned} \tag{4.159}$$

where $\hat{H}_{2,\rightarrow}(t) := \hat{H}_{2,\leftarrow}^{\dagger}(t)$ and the following convenient notation was introduced

$$\hat{H}_{1*}(t) :=\hat{U}_0(t)\hat{U}_{\mathrm{I}}^{\odot}(t)\hat{H}_1(t)\hat{U}_{\mathrm{I}}^{\odot\dagger}(t)\hat{U}_0^{\dagger}(t)\,; \tag{4.160}$$

$$\hat{H}_{2*,\leftrightarrow}(t) :=\hat{U}_0(t)\hat{U}_{\mathrm{I}}^{\odot}(t)\hat{H}_{2,\leftrightarrow}(t)\hat{U}_{\mathrm{I}}^{\odot\dagger}(t)\hat{U}_0^{\dagger}(t)\,. \tag{4.161}$$

A general form for the operators $\hat{H}_{1*}$ and $\hat{H}_{2\leftrightarrow*}$, useful for later computation, can be studied. From Eq. (4.152) one easily obtains

$$\int_0^t \mathrm{d}t'\hat{U}_0^{\dagger}(t')\hat{H}_{I,\odot}\hat{U}_0(t') = -3M_{\odot}\int \mathrm{d}\mathbf{k}\,\left(\alpha_{\mathbf{k}}(t)\hat{b}_{\mathbf{k}} + \alpha_{\mathbf{k}}^{*}(t)\hat{b}_{\mathbf{k}}^{\dagger}\right)\,, \tag{4.162}$$

where $\alpha_{\mathbf{k}}$ is the parameter

$$\alpha_{\mathbf{k}}(t) := -\Gamma_{\mathbf{k}}(R)e^{-\frac{i}{2}|\mathbf{k}|t}\mathrm{sinc}\left(\frac{1}{2}|\mathbf{k}|t\right)\frac{t}{2} = -\frac{i}{2|\mathbf{k}|}\Gamma_{\mathbf{k}}(R)(1-e^{-i|\mathbf{k}|t})\,. \tag{4.163}$$

By putting Eq. (4.162) into Eq. (4.156b), the operator $\hat{U}_{\mathrm{I}}^{\odot}$ becomes a multi-mode displacement operator - with continuous modes. Therefore, it transform a graviton annihilation operator as

$$\hat{U}_{\mathrm{I}}^{\odot\dagger}\hat{b}_{\mathbf{k}}\hat{U}_{\mathrm{I}}^{\odot} = \hat{b}_{\mathbf{k}} - 3iM_{\odot}\alpha_{\mathbf{k}}^{*}\,. \tag{4.164}$$

Therefore, the presence of a classical gravitational source displaces the gravitons' bosonic operators $\hat{b}_{\mathbf{k}}$ by an amount proportional to $M_{\odot}$ - following Eq. (4.164). In General Relativity regimes, the masses of gravitational sources are way higher than the Planck mass, meaning that $M_{\odot} \gg 1$. Therefore, the displacement proportional to $M_{\odot}$ is expected to overcome completely the "quantum

[9] Since $\hat{U}_0\,|1_{\mathrm{i=A,B}}\rangle = e^{-imt}\,|1_{\mathrm{i=A,B}}\rangle$ from the assumption that the wave packet is not spreading (see Sec. 4.4.1), has has $\hat{U}_0\hat{\rho}\hat{U}_0^{\dagger} = \hat{\rho}$.

part" given by $\hat{b}_{\mathbf{k}}$, explaining why quantum features of gravity appear to be hidden in presence of any classical source.

By putting Eq. (4.164) into Eqs. (4.160) and (4.161), after cumbersome calculations, one obtains

$$\hat{H}_{1*}(t) = m \int \mathrm{d}\mathbf{p}\mathrm{d}\mathbf{p}' \left(c_-(\mathbf{p}, \mathbf{p}'; t)\hat{b}_{\mathbf{p}-\mathbf{p}'} + c_+(\mathbf{p}, \mathbf{p}'; t)\hat{b}_{\mathbf{p}'-\mathbf{p}} + M_\odot c_\odot(\mathbf{p}, \mathbf{p}'; t) \right) a^\dagger_{\mathbf{p}} a_{\mathbf{p}'} \,, \tag{4.165}$$

$$\begin{aligned} H_{2\leftarrow*}(t) =& m^2 \int \mathrm{d}\mathbf{p}_1\mathrm{d}\mathbf{p}_2\mathrm{d}\mathbf{p}_3\mathrm{d}\mathbf{p}_4 \\ &\times \Big(c_{--}(\mathbf{p}_1, \mathbf{p}_2, \mathbf{p}_3, \mathbf{p}_4; t)\hat{b}_{\mathbf{p}_1-\mathbf{p}_2}\hat{b}_{\mathbf{p}_3-\mathbf{p}_4} + c_{-+}(\mathbf{p}_1, \mathbf{p}_2, \mathbf{p}_3, \mathbf{p}_4; t)\hat{b}_{\mathbf{p}_1-\mathbf{p}_2}\hat{b}^\dagger_{\mathbf{p}_3-\mathbf{p}_4} \\ &+ c_{+-}(\mathbf{p}_1, \mathbf{p}_2, \mathbf{p}_3, \mathbf{p}_4; t)\hat{b}^\dagger_{\mathbf{p}_1-\mathbf{p}_2}\hat{b}_{\mathbf{p}_3-\mathbf{p}_4} + c_{++}(\mathbf{p}_1, \mathbf{p}_2, \mathbf{p}_3, \mathbf{p}_4; t)\hat{b}^\dagger_{\mathbf{p}_1-\mathbf{p}_2}\hat{b}^\dagger_{\mathbf{p}_3-\mathbf{p}_4} \\ &+ M_\odot c_{\odot-}(\mathbf{p}_1, \mathbf{p}_2, \mathbf{p}_3, \mathbf{p}_4; t)\hat{b}_{\mathbf{p}_3-\mathbf{p}_4} + M_\odot c_{\odot+}(\mathbf{p}_1, \mathbf{p}_2, \mathbf{p}_3, \mathbf{p}_4; t)\hat{b}^\dagger_{\mathbf{p}_3-\mathbf{p}_4} \\ &+ M_\odot c_{-\odot}(\mathbf{p}_1, \mathbf{p}_2, \mathbf{p}_3, \mathbf{p}_4; t)\hat{b}_{\mathbf{p}_1-\mathbf{p}_2} + M_\odot c_{+\odot}(\mathbf{p}_1, \mathbf{p}_2, \mathbf{p}_3, \mathbf{p}_4; t)\hat{b}^\dagger_{\mathbf{p}_1-\mathbf{p}_2} \\ &+ M_\odot^2 c_{\odot\odot}(\mathbf{p}_1, \mathbf{p}_2, \mathbf{p}_3, \mathbf{p}_4; t) \Big) \hat{a}^\dagger_{\mathbf{p}_1}\hat{a}_{\mathbf{p}_2}\hat{a}^\dagger_{\mathbf{p}_3}\hat{a}_{\mathbf{p}_4} \,, \end{aligned} \tag{4.166}$$

where the functions $c_{(\dots)}$ are specified later on.

It is convenient to decompose $\hat{H}_{1*}$ and $\hat{H}_{2\leftarrow*}$ resp. in Eqs. (4.165) and (4.166) into the planet-dependent (i.e. proportional to $M_\odot$) and planet-independent parts. The former is indicated with the apex $\odot$ and the latter with the apex Φ. Therefore

$$\hat{H}_{1*}(t) = \hat{H}^\Phi_{1*}(t) + \hat{H}^\odot_{1*}(t)\,; \quad \hat{H}_{2\leftarrow*}(t) = \hat{H}^\Phi_{2\leftarrow*}(t) + \hat{H}^\odot_{2\leftarrow*}(t)\,. \tag{4.167}$$

4.4.2.1 Tracing out the gravitational sector

To explore the evolution of the state $\hat{\rho}_\mathrm{S}$ one has to evolve the density operator of the entire system with Eq. (4.159) and then trace out the gravitational sector and the λ modes.

In particular, by putting Eq. (4.144) into Eq. (4.159) and tracing out the gravitational field modes, one has

$$\begin{aligned} \hat{\rho}_\mathrm{SE}(t) :=& \sum_{n_\mathbf{k}} {}_\mathrm{G}\langle n_\mathbf{k}| \hat{\rho}(t) |n_\mathbf{k}\rangle_\mathrm{G} = \hat{\rho}_\mathrm{SE}(0) - i \left[\langle 0_\mathrm{G}|\hat{H}^\odot_{1*}(t)|0_\mathrm{G}\rangle, \hat{\rho}_\mathrm{SE}(0) \right] \\ &+ \int d\mathbf{k}\, {}_\mathrm{G}\langle 1_\mathbf{k}|\hat{H}^\Phi_{1*}(t)\hat{\rho}(0)\hat{H}^\Phi_{1*}(t)|1_\mathbf{k}\rangle_\mathrm{G} + \langle 0_\mathrm{G}|\, \hat{H}^\odot_{1*} \,|0_\mathrm{G}\rangle\, \hat{\rho}_\mathrm{SE}(0)\, \langle 0_\mathrm{G}|\, \hat{H}^\odot_{1*} \,|0_\mathrm{G}\rangle \\ &+ \Big(\langle 0_\mathrm{G}|\, \hat{H}^\odot_{2\leftarrow*}(t) \,|0_\mathrm{G}\rangle\, \hat{\rho}_\mathrm{SE}(0) + \hat{\rho}_\mathrm{SE}(0)\, \langle 0_\mathrm{G}|\, \hat{H}^\odot_{2\rightarrow*}(t) \,|0_\mathrm{G}\rangle \Big) \\ &+ \Big(\langle 0_\mathrm{G}|\, \hat{H}^\Phi_{2\leftarrow*}(t) \,|0_\mathrm{G}\rangle\, \hat{\rho}_\mathrm{SE}(0) + \hat{\rho}_\mathrm{SE}(0)\, \langle 0_\mathrm{G}|\, \hat{H}^\Phi_{2\rightarrow*}(t) \,|0_\mathrm{G}\rangle \Big) \,. \end{aligned} \tag{4.168}$$

The operators $\hat{H}^\odot_{1*}$, $\hat{H}^\Phi_{1*}$, $\hat{H}^\odot_{2\leftrightarrow*}$ and $\hat{H}^\Phi_{2\leftrightarrow*}$, simplify inside gravitational state brackets, namely

$$\langle 0_\mathrm{G}|\, \hat{H}^\odot_{1*} \,|0_\mathrm{G}\rangle = mM_\odot \int \mathrm{d}\mathbf{p}\mathrm{d}\mathbf{p}' c_\odot(\mathbf{p}, \mathbf{p}'; t)\hat{a}^\dagger_{\mathbf{p}}\hat{a}_{\mathbf{p}'}\,; \tag{4.169a}$$

$$\langle 1_\mathbf{k}|\, \hat{H}^\Phi_{1*} \,|0_\mathrm{G}\rangle = m \int \mathrm{d}\mathbf{p} c_+(\mathbf{p}, \mathbf{k}-\mathbf{p}; t)\hat{a}^\dagger_{\mathbf{p}}\hat{a}_{\mathbf{k}-\mathbf{p}}\,; \tag{4.169b}$$

$$\langle 0_\mathrm{G}|\, \hat{H}^\Phi_{2\leftarrow*} \,|0_\mathrm{G}\rangle = m^2 \int \mathrm{d}\mathbf{p}_1\mathrm{d}\mathbf{p}_2\mathrm{d}\mathbf{p}_3 c_{-+}(\mathbf{p}_1, \mathbf{p}_2, \mathbf{p}_3, \mathbf{p}_3 + \mathbf{p}_2 - \mathbf{p}_1; t)\hat{a}^\dagger_{\mathbf{p}_1}\hat{a}_{\mathbf{p}_2}\hat{a}^\dagger_{\mathbf{p}_3}\hat{a}_{\mathbf{p}_2+\mathbf{p}_3-\mathbf{p}_1}\,; \tag{4.169c}$$

$$\langle 0_\mathrm{G}|\, \hat{H}^\odot_{2\leftarrow*} \,|0_\mathrm{G}\rangle = m^2 M_\odot^2 \int \mathrm{d}\mathbf{p}_1\mathrm{d}\mathbf{p}_2\mathrm{d}\mathbf{p}_3\mathrm{d}\mathbf{p}_4 c_{\odot\odot}(\mathbf{p}_1, \mathbf{p}_2, \mathbf{p}_3, \mathbf{p}_4; t)\hat{a}^\dagger_{\mathbf{p}_1}\hat{a}_{\mathbf{p}_2}\hat{a}^\dagger_{\mathbf{p}_3}\hat{a}_{\mathbf{p}_4}\,. \tag{4.169d}$$

From Eq. (4.168), the only first order contribute is given by the presence of the planet. Therefore, the "quantum" contributes, occurring with no classical source, are present only at second order perturbation theory.

Moreover, by applying an annihilation operator on the state $|1_{\mathrm{i=A,B}}\rangle$, one has

$$\hat{a}(\mathbf{p})\,|1_{\mathrm{i}}\rangle = \int \mathrm{d}\mathbf{k} F_{\mathbf{k}_0}(\mathbf{k}) e^{-i\mathbf{x}_{\mathrm{A}}\cdot\mathbf{k}} \delta^3(\mathbf{p}-\mathbf{k})\,|0\rangle = F_{\mathbf{k}_0}(\mathbf{p}) e^{-i\mathbf{x}_{\mathrm{A}}\cdot\mathbf{p}}\,|0\rangle \,. \tag{4.170}$$

Since $F_{\mathbf{k}_0}(\mathbf{p})$ is expected to vanish when $|\mathbf{p}| \gtrsim k_0$, and since $k_0 \ll m$, then $\omega_{\mathbf{p}} \sim m$ whenever $\mathbf{p}$ is inside the argument of $F_{\mathbf{k}_0}$.

By taking that into account, with some algebra, the useful functions $c_{\dots}$ are

$$c_{\odot}(\mathbf{p},\mathbf{p}';t) = \frac{3}{2\pi}\frac{\Gamma_{\mathbf{p}-\mathbf{p}'}}{|\mathbf{p}-\mathbf{p}'|^{3/2}}\left(t - \frac{\sin(|\mathbf{p}-\mathbf{p}'|t)}{|\mathbf{p}-\mathbf{p}'|}\right); \tag{4.171a}$$

$$c_{+}(\mathbf{p},\mathbf{p}';t) = \frac{1-e^{-it(|\mathbf{p}-\mathbf{p}'|+\omega_{\mathbf{p}}-\omega_{\mathbf{p}'})}}{2\pi i\sqrt{|\mathbf{p}-\mathbf{p}'|+\omega_{\mathbf{p}}-\omega_{\mathbf{p}'}}}; \tag{4.171b}$$

$$\begin{aligned} c_{-+}(\mathbf{p}_1,\mathbf{p}_2,\mathbf{p}_3,\mathbf{p}_4;t) = &-\frac{1}{4\pi^2|\mathbf{p}_1-\mathbf{p}_2|}\left(\frac{1-e^{-it(\omega_{\mathbf{p}_1}+\omega_{\mathbf{p}_3}-\omega_{\mathbf{p}_2}-\omega_{\mathbf{p}_4})}}{(\omega_{\mathbf{p}_1}+\omega_{\mathbf{p}_3}-\omega_{\mathbf{p}_2}-\omega_{\mathbf{p}_4})(|\mathbf{p}_1-\mathbf{p}_2|+\omega_{\mathbf{p}_3}-\omega_{\mathbf{p}_4})}\right.\\ &\left.-\frac{e^{-it(|\mathbf{p}_1-\mathbf{p}_2|+\omega_{\mathbf{p}_3}-\omega_{\mathbf{p}_4})}-e^{-it(\omega_{\mathbf{p}_1}+\omega_{\mathbf{p}_3}-\omega_{\mathbf{p}_2}-\omega_{\mathbf{p}_4})}}{(|\mathbf{p}_1-\mathbf{p}_2|+\omega_{\mathbf{p}_3}-\omega_{\mathbf{p}_4})(|\mathbf{p}_1-\mathbf{p}_2|-\omega_{\mathbf{p}_1}+\omega_{\mathbf{p}_2})}\right); \end{aligned} \tag{4.171c}$$

$$\begin{aligned} c_{\odot\odot}(\mathbf{p}_1,\mathbf{p}_2,\mathbf{p}_3,\mathbf{p}_4;t) = &\frac{9}{8\pi^2}\frac{\Gamma_{|\mathbf{p}_1-\mathbf{p}_2|}}{|\mathbf{p}_1-\mathbf{p}_2|^{3/2}}\frac{\Gamma_{|\mathbf{p}_3-\mathbf{p}_4|}}{|\mathbf{p}_3-\mathbf{p}_4|^{3/2}}\left\{t^2 + 2\frac{|\mathbf{p}_1-\mathbf{p}_2|^4+|\mathbf{p}_3-\mathbf{p}_4|^4-|\mathbf{p}_1-\mathbf{p}_2|^2|\mathbf{p}_3-\mathbf{p}_4|^2}{|\mathbf{p}_1-\mathbf{p}_2|^2|\mathbf{p}_3-\mathbf{p}_4|^2(|\mathbf{p}_1-\mathbf{p}_2|^2-|\mathbf{p}_3-\mathbf{p}_4|^2)}\right.\\ &-2t\frac{\sin(|\mathbf{p}_3-\mathbf{p}_4|t)}{|\mathbf{p}_3-\mathbf{p}_4|}+2\left[\frac{\cos(|\mathbf{p}_1-\mathbf{p}_2|t)}{|\mathbf{p}_1-\mathbf{p}_2|^2}-\frac{\cos(|\mathbf{p}_3-\mathbf{p}_4|t)}{|\mathbf{p}_3-\mathbf{p}_4|^2}\right]\\ &\left.-\frac{\cos((|\mathbf{p}_1-\mathbf{p}_2|+|\mathbf{p}_3-\mathbf{p}_4|)t)}{|\mathbf{p}_1-\mathbf{p}_2|(|\mathbf{p}_1-\mathbf{p}_2|+|\mathbf{p}_3-\mathbf{p}_4|)}-\frac{\cos((|\mathbf{p}_1-\mathbf{p}_2|-|\mathbf{p}_3-\mathbf{p}_4|)t)}{|\mathbf{p}_1-\mathbf{p}_2|(|\mathbf{p}_1-\mathbf{p}_2|-|\mathbf{p}_3-\mathbf{p}_4|)}\right\}. \end{aligned} \tag{4.171d}$$

4.4.2.2 Tracing out the environment

The degrees of freedom of the environment are now traced out. From the form of the Hamiltonians (4.155), (4.150a) and (4.150b), the number of excitations of the field $\hat{\Phi}$ is conserved. From this fact, by starting with a particle in the superposition of modes A and B and zero particles in the environment modes λ, if a particle is found on an environment mode λ, then one certainly has the vacuum in the modes A and B. In this way, one can write

$$\begin{aligned} \hat{\rho}_{\mathrm{SE}}(t) = &\sum_{\mathrm{i=A,B}}\sum_{m_{\mathrm{i}},n_{\mathrm{i}}} \langle m_{\mathrm{A}} m_{\mathrm{B}} 0_{\mathrm{E}}|\hat{\rho}_{\mathrm{SE}}(t)|n_{\mathrm{A}} n_{\mathrm{B}} 0_{\mathrm{E}}\rangle\,|m_{\mathrm{A}} m_{\mathrm{B}} 0_{\mathrm{E}}\rangle\langle n_{\mathrm{A}} n_{\mathrm{B}} 0_{\mathrm{E}}|\\ &+\sum_{\lambda}^{(E)}\sum_{\{n_\lambda\},\{n'_\lambda\}} \langle 0_{\mathrm{A}} 0_{\mathrm{B}}\{n_\lambda\}|\hat{\rho}_{\mathrm{SE}}(t)|0_{\mathrm{A}} 0_{\mathrm{B}}\{n'_\lambda\}\rangle\,|0_{\mathrm{A}} 0_{\mathrm{A}}\{n_\lambda\}\rangle\langle 0_{\mathrm{B}} 0_{\mathrm{B}}\{n'_\lambda\}|\\ &+\sum_{\lambda}^{(E)}\sum_{\{n_\lambda\}}\sum_{m_{\mathrm{A}},m_{\mathrm{B}}} \langle m_{\mathrm{A}} m_{\mathrm{B}} 0_{\mathrm{E}}|\hat{\rho}_{\mathrm{SE}}(t)|0_{\mathrm{A}} 0_{\mathrm{B}}\{n_\lambda\}\rangle\,|m_{\mathrm{A}} m_{\mathrm{B}} 0_{\mathrm{E}}\rangle\langle 0_{\mathrm{A}} 0_{\mathrm{B}}\{n_\lambda\}| + \text{h.c.}, \end{aligned} \tag{4.172}$$

Tracing over the environment reads

$$\hat{\rho}_{\mathrm{S}} = \mathrm{Tr}_{\mathrm{E}}(\hat{\rho}_{\mathrm{SE}}(t)) = \sum_{\lambda}^{(E)}\sum_{\{n_\lambda\}} \langle\{n_\lambda\}|\hat{\rho}_{\mathrm{SE}}(t)|\{n_\lambda\}\rangle.$$

Using the available expressions, the reduced state of the System $\hat{\rho}_{\rm S}(t)$ reads

$$\hat{\rho}_{\rm S}(t) = \sum_{\lambda}^{(E)} \langle 0_{\rm A}0_{\rm B}1_{\lambda}|\hat{\rho}_{\rm SE}(t)|0_{\rm A}0_{\rm B}1_{\lambda}\rangle \, |0_{\rm A}0_{\rm B}\rangle\langle 0_{\rm A}0_{\rm B}| \\ + \sum_{\rm i=A,B}\sum_{m_{\rm i},n_{\rm i}} \langle m_{\rm A}m_{\rm B}0_{\rm E}|\hat{\rho}_{\rm SE}(t)|n_{\rm A}n_{\rm B}0_{\rm E}\rangle \, |m_{\rm A}m_{\rm B}\rangle\langle n_{\rm A}n_{\rm B}|. \tag{4.173}$$

Eq. (4.173) can be casted in a matrix form $\rho_{\rm S}(t)$. By choosing the basis $|1_{\rm A}\rangle, |1_{\rm B}\rangle, |0\rangle$ one has

$$\rho_{\rm S}(t) = \begin{pmatrix} \rho_{\rm AA}(t) & \rho_{\rm AB}(t) & 0 \\ \rho^*_{\rm AB}(t) & \rho_{\rm BB}(t) & 0 \\ 0 & 0 & \rho_{00}(t) \end{pmatrix} = \left(\begin{array}{c|c} \tilde{\rho}(t) & 0 \\ \hline 0 & \rho_{00}(t) \end{array}\right) . \tag{4.174}$$

where, for simplicity, $\tilde{\rho}$ was defined as the 2×2 matrix whose elements are

$$(\tilde{\rho})_{\rm ij}(t) = \langle 1_{\rm i}0_{\rm E}| \, \hat{\rho}_{\rm SE}(t) \, |1_{\rm j}0_{\rm E}\rangle \ . \tag{4.175}$$

Since $\mathrm{Tr}(\rho_{\rm S}) = 1$, then $\rho_{00}(t) = 1 - \rho_{\rm AA}(t) - \rho_{\rm BB}(t)$. If $p_e := \rho_{00}(t) \neq 0$, there is non-null probability p_e to have the initial state neither localized around $\mathbf{x}_{\rm A}$ nor around $\mathbf{x}_{\rm B}$. Therefore, p_e is an *erasure probability* [52], expressing the possibility that the particle is "erased" from its initial possible locations[10].

In the appendix B, a long calculation is reported to find an expression for $\tilde{\rho}(t)$. After a more general calculation, a specific case is considered. In particular, the radius R of the planet is considered to be very small, so that the form factor (4.153), in the limit $Rk_0 \to 0$, reads

$$\Gamma_{\mathbf{k}}(R\to 0) = -\frac{1}{3\sqrt{|\mathbf{k}|}} \,. \tag{4.176}$$

Moreover, a Gaussian distribution was considered for the momentum amplitude $F_{\mathbf{k}_0}(\mathbf{k})$, i.e.

$$F_{\mathbf{k}_0}(\mathbf{p}) := \frac{e^{-\frac{|\mathbf{p}|^2}{4k_0^2}}}{(2\pi k_0^2)^{3/4}} \,. \tag{4.177}$$

The scalar product between $|1_{\rm A}\rangle$ and $|1_{\rm B}\rangle$ is

$$\langle 1_{\rm A}|1_{\rm B}\rangle = e^{-k_0^2L^2} \,, \tag{4.178}$$

which is practically null as long as $k_0L \gg 1$, i.e. $\epsilon/L \ll 1$.

With this prescription, the Lindblad equation was also employed to discard eventual contributions given by unitary evolutions. In so doing, the evolution of the matrix $\tilde{\rho}$ reads

$$\tilde{\rho}(t) := \begin{pmatrix} \tilde{\rho}_{\rm AA}(t) & \tilde{\rho}_{\rm AB}(t) \\ \tilde{\rho}_{\rm BA}(t) & \tilde{\rho}_{\rm BB}(t) \end{pmatrix} = \begin{pmatrix} \tilde{\rho}_{\rm AA}(0)\,(1-\eta_{\rm AA}) & \tilde{\rho}_{\rm AB}(1-\eta_{\rm AB}) \\ \tilde{\rho}_{\rm BA}(0)(1-\eta_{\rm AB}) & \tilde{\rho}_{\rm BB}(0)(1-\eta_{\rm BB}) \end{pmatrix} . \tag{4.179}$$

where, for $\rm i = A, B$

$$\eta_{\rm ii} = \frac{8m^2}{\pi}\int_0^t dt' \left(\frac{1-\cos(2\Lambda t')}{16\pi t'} - k_0 D_+(t'k_0)\right) + \theta(t-|\mathbf{x}_{\rm i}|)\frac{\pi^2 m^2 M_\odot^2 t^2}{2k_0^2|\mathbf{x}_{\rm i}|^4}\,; \tag{4.180}$$

[10] It does not mean that the state disappears, but that it is just localized elsewhere.

$$\eta_{\rm AB} = \frac{8m^2}{\pi}\int_0^t dt'\left(\frac{1-\cos(2\Lambda t')}{16\pi t'} - \frac{k_0}{4L}\int_0^L dL'\left(|D_+((L'+t')k_0) - D_+((L'-t')k_0)\right)\right)$$
$$+\frac{\pi^2 m^2 M_\odot^2 t^2}{4k_0^2}\left(\frac{\theta(t-|\mathbf{x}_{\rm A}|)}{|\mathbf{x}_{\rm A}|^4} + \frac{\theta(t-|\mathbf{x}_{\rm B}|)}{|\mathbf{x}_{\rm B}|^4}\right), \tag{4.181}$$

where D_+ is the Dawson function and Λ is an energy cut-off, comparable to the Planck mass $\Lambda \sim 1$ in the effective field theory considered.

4.4.3 Quantum channel analysis

The evolution of the state represented by the density operator (4.145) is now casted as a quantum channel $\mathcal{N} : \hat{\rho}_{\rm S}(0) \mapsto \hat{\rho}_{\rm S}(t)$, given by Eqs. (4.145) and (4.174), respectively. The channel maps a qubit state, whose basis is $\{|1_{\rm A}\rangle, |1_{\rm B}\rangle\}$, to a qutrit, whose basis is $\{|1_{\rm A}\rangle, |1_{\rm B}\rangle, |0\rangle\}$, including the erasure flag $|0\rangle$. Therefore, the channel is a map $\mathcal{N} : \mathcal{S}(\mathbb{C}^2) \to \mathcal{S}(\mathbb{C}^3)$ between finite dimensional systems, namely

$$\mathcal{N} : \begin{pmatrix} \alpha & \beta \\ \beta^* & 1-\alpha \end{pmatrix} \mapsto \begin{pmatrix} \alpha(1-\eta_{\rm AA}) & \beta(1-\eta_{\rm AB}) & 0 \\ \beta^*(1-\eta_{\rm AB}) & (1-\alpha)(1-\eta_{\rm BB}) & 0 \\ 0 & 0 & \eta_{\rm AA}\alpha + \eta_{\rm BB}(1-\alpha) \end{pmatrix}, \tag{4.182}$$

Each quantum channel between finite dimensional systems can be written as [244]

$$\mathcal{N}(\hat{\rho}) = \sum_{\rm j} \hat{K}_{\rm j}\hat{\rho}\hat{K}_{\rm j}\,, \tag{4.183}$$

where $\{\hat{K}_{\rm j}\}_{\rm j}$ are a set of operators, called *Kraus operators*. To find these operators, the method presented in Ref. [245] is employed. In particular, the *Choi matrix* is defined as

$$\left(\begin{array}{c|c} \mathcal{N}\begin{pmatrix} 1 & 0 \\ 0 & 0 \end{pmatrix} & \mathcal{N}\begin{pmatrix} 0 & 1 \\ 0 & 0 \end{pmatrix} \\ \hline \mathcal{N}\begin{pmatrix} 0 & 0 \\ 1 & 0 \end{pmatrix} & \mathcal{N}\begin{pmatrix} 0 & 0 \\ 0 & 1 \end{pmatrix} \end{array}\right) = \left(\begin{array}{ccc|ccc} 1-\eta_{\rm AA} & 0 & 0 & 0 & 1-\eta_{\rm AB} & 0 \\ 0 & 0 & 0 & 0 & 0 & 0 \\ 0 & 0 & \eta_{\rm AA} & 0 & 0 & 0 \\ \hline 0 & 0 & 0 & 0 & 0 & 0 \\ 1-\eta_{\rm AB} & 0 & 0 & 0 & 1-\eta_{\rm BB} & 0 \\ 0 & 0 & 0 & 0 & 0 & \eta_{\rm BB} \end{array}\right). \tag{4.184}$$

Notice that $\left(\begin{smallmatrix} 0 & 1 \\ 0 & 0 \end{smallmatrix}\right)$ is not a valid density matrix and then, it is not a proper entry for the channel $\mathcal{N}$ appearing in Eq. (4.184). Despite that, Ref. [245] shows a way to apply $\mathcal{N}$ to such false density matrices as well.

The eigenvectors of the Choi matrix (4.184) are

$$\begin{aligned} \mathbf{a}_1 &= \left(\frac{(1-\eta_{\rm AB})\sqrt{\lambda_+}}{\sqrt{(1-\eta_{\rm AA}-\lambda_+)^2+(1-\eta_{\rm AB})^2}}, 0, 0, 0, \frac{(1-\eta_{\rm AA}-\lambda_+)\sqrt{\lambda_+}}{\sqrt{(1-\eta_{\rm AA}-\lambda_+)^2+(1-\eta_{\rm AB})^2}}\right), \\ \mathbf{a}_2 &= \left(\frac{(1-\eta_{\rm AB})\sqrt{\lambda_-}}{\sqrt{(1-\eta_{\rm AA}-\lambda_-)^2+(1-\eta_{\rm AB})^2}}, 0, 0, 0, \frac{(1-\eta_{\rm AA}-\lambda_-)\sqrt{\lambda_-}}{\sqrt{(1-\eta_{\rm AA}-\lambda_-)^2+(1-\eta_{\rm AB})^2}}\right), \\ \mathbf{a}_3 &= (0, 0, \sqrt{\eta_{\rm AA}}, 0, 0, 0)\ , \\ \mathbf{a}_4 &= (0, 0, 0, 0, 0, \sqrt{\eta_{\rm BB}})\ , \\ \mathbf{a}_5 &= \mathbf{0}\,, \quad \mathbf{a}_6 = \mathbf{0}\,, \end{aligned} \tag{4.185}$$

where

$$\lambda_\pm = \frac{2-\eta_{\mathrm{AA}}-\eta_{\mathrm{BB}} \pm \sqrt{(2-\eta_{\mathrm{AA}}-\eta_{\mathrm{BB}})^2 - 4(1-\eta_{\mathrm{AA}})(1-\eta_{\mathrm{BB}}) + 4(1-\eta_{\mathrm{AB}})^2}}{2} \tag{4.186}$$

Since η_{AA}, η_{BB} and η_{AB} are all second order perturbative parameters, the parameters $\lambda_\pm$ become

$$\lambda_+ = 2 - \frac{\eta_{\mathrm{AA}}}{2} - \frac{\eta_{\mathrm{BB}}}{2} - \eta_{\mathrm{AB}}\,; \quad \lambda_- = \eta_{\mathrm{AB}} - \frac{\eta_{\mathrm{AA}}}{2} - \frac{\eta_{\mathrm{BB}}}{2}\,. \tag{4.187}$$

And the eigenvectors $\mathbf{a}_1$ and $\mathbf{a}_2$ in Eq. (4.185) become

$$\begin{aligned}
\mathbf{a}_1 &= \left(1-\frac{3}{8}\eta_{\mathrm{AA}} + \frac{\eta_{\mathrm{BB}}}{8} - \frac{\eta_{\mathrm{AB}}}{4}, 0, 0, 0, 1-\frac{3}{8}\eta_{\mathrm{BB}} + \frac{\eta_{\mathrm{AA}}}{8} - \frac{\eta_{\mathrm{AB}}}{4}, 0\right)\,; \\
\mathbf{a}_2 &= \left(\sqrt{\frac{\eta_{\mathrm{AB}} - \frac{\eta_{\mathrm{AA}}}{2} - \frac{\eta_{\mathrm{BB}}}{2}}{2}}, 0, 0, 0, -\sqrt{\frac{\eta_{\mathrm{AB}} - \frac{\eta_{\mathrm{AA}}}{2} - \frac{\eta_{\mathrm{BB}}}{2}}{2}}, 0,\right)\,.
\end{aligned} \tag{4.188}$$

From Ref. [245], each Kraus operator $\hat{K}_{\mathrm{j}}$ have the first column made by the first three components of $\mathbf{a}_{\mathrm{i}}$ and the second column made by the last three of them. Therefore, by neglecting the null Kraus operators $K_5 = K_6$, then

$$\begin{aligned}
K_1 &= \begin{pmatrix} \left(1-\frac{3}{4}\eta_{\mathrm{AA}} + \frac{\eta_{\mathrm{BB}}}{4} - \frac{\eta_{\mathrm{AB}}}{2}\right)^{1/2} & 0 \\ 0 & \left(1-\frac{3}{4}\eta_{\mathrm{BB}} + \frac{\eta_{\mathrm{AA}}}{4} - \frac{\eta_{\mathrm{AB}}}{2}\right)^{1/2} \\ 0 & 0 \end{pmatrix}\,; \\
K_2 &= \begin{pmatrix} \sqrt{\frac{\eta_{\mathrm{AB}} - \frac{\eta_{\mathrm{AA}}}{2} - \frac{\eta_{\mathrm{BB}}}{2}}{2}} & 0 \\ 0 & -\sqrt{\frac{\eta_{\mathrm{AB}} - \frac{\eta_{\mathrm{AA}}}{2} - \frac{\eta_{\mathrm{BB}}}{2}}{2}} \\ 0 & 0 \end{pmatrix}\,; \\
K_3 &= \begin{pmatrix} 0 & 0 \\ 0 & 0 \\ \sqrt{\eta_{\mathrm{AA}}} & 0 \end{pmatrix}\,; \quad K_4 = \begin{pmatrix} 0 & 0 \\ 0 & 0 \\ 0 & \sqrt{\eta_{\mathrm{BB}}} \end{pmatrix}\,.
\end{aligned} \tag{4.189}$$

Now, two typical quantum channels are presented, namely

1. $\mathcal{E} : \mathcal{S}(\mathbb{C}^2) \to \mathcal{S}(\mathbb{C}^3)$ is called *asymmetric erasure channel* and it reads

$$\mathcal{E} : \rho \mapsto \left(\begin{array}{c|c} E\rho E^\dagger & 0 \\ \hline 0 & p_e(t) \end{array}\right)\,, \quad \text{where} \quad E = \begin{pmatrix} \sqrt{1-p_e^{\mathrm{A}}} & 0 \\ 0 & \sqrt{1-p_e^{\mathrm{B}}} \end{pmatrix}\,. \tag{4.190}$$

   Basically $\mathcal{E}$ gives a probability of erasure which is different depending on the initial state of the system. In particular, if the particle is localized in $\mathbf{x}_{\mathrm{i=A,B}}$, the probability of erasure is p_e^{i}. The Kraus operators of the channel (4.190) are represented by the matrices

$$E_1 = \begin{pmatrix} \sqrt{1-p_e^{\mathrm{A}}} & 0 \\ 0 & \sqrt{1-p_e^{\mathrm{B}}} \\ 0 & 0 \end{pmatrix}\,, \quad E_2 = \begin{pmatrix} 0 & 0 \\ 0 & 0 \\ \sqrt{p_e^{\mathrm{A}}} & 0 \end{pmatrix}\,, \quad E_3 = \begin{pmatrix} 0 & 0 \\ 0 & 0 \\ 0 & \sqrt{p_e^{\mathrm{B}}} \end{pmatrix}\,. \tag{4.191}$$

2. $\mathcal{D} : \mathcal{S}(\mathbb{C}^2) \to \mathcal{S}(\mathbb{C}^2)$ is a dephasing channel, whose map is

$$\mathcal{D} : \rho = \begin{pmatrix} \rho_{\mathrm{AA}} & \rho_{\mathrm{AB}} \\ \rho_{\mathrm{BA}} & \rho_{\mathrm{BB}} \end{pmatrix} \mapsto \begin{pmatrix} \rho_{\mathrm{AA}} & \rho_{\mathrm{AB}}(1-\varphi) \\ \rho_{\mathrm{BA}}(1-\varphi) & \rho_{\mathrm{BB}} \end{pmatrix}\,. \tag{4.192}$$

The action of $\mathcal{D}$ consists of dropping the off-diagonal elements of a density matrix with a rate given by $\dot{\varphi}$. The Kraus operators of $\mathcal{D}$ are

$$D_1 = \sqrt{\frac{2-\varphi}{2}} \begin{pmatrix} 1 & 0 \\ 0 & 1 \end{pmatrix} , \quad D_2 = \sqrt{\frac{\varphi}{2}} \begin{pmatrix} 1 & 0 \\ 0 & -1 \end{pmatrix} . \tag{4.193}$$

By computing the Kraus operators of the channel $\mathcal{E} \circ \mathcal{D}$ - by putting Eqs. (4.191) and (4.193) into Eq. (4.183) one gets the Kraus operators (4.189) up to second order perturbation theory[11]. In particular, this analogy holds if $\eta_{\rm AA} = p_e^{\rm A}$, $\eta_{\rm BB} = p_e^{\rm B}$ and finally $\varphi = \eta_{\rm AB} - \frac{\eta_{\rm AA}}{2} - \frac{\eta_{\rm BB}}{2}$. Therefore, the conclusion is that

$$\mathcal{N} \equiv \mathcal{E} \circ \mathcal{D} , \tag{4.194}$$

where the the erasure probabilities $p_e^{\rm A}$ and $p_e^{\rm B}$ and the dephasing φ defined repsectively in Eqs. (4.190) (4.192), from Eqs. (4.180) and (4.181), are respectively

$$p_e^{\rm i} = \frac{8m^2}{\pi} \int_0^t dt' \left(\frac{1-\cos(2\Lambda t')}{16\pi t'} - k_0 D_+(t'k_0) \right) + \theta(t - |\mathbf{x}_{\rm i}|) \frac{\pi^2 m^2 M_\odot^2 t^2}{2k_0^2 |\mathbf{x}_{\rm i}|^4} ; \tag{4.195}$$

$$\varphi = \frac{8k_0 m^2}{\pi} \int_0^t dt' \left(D_+(t'k_0) - \frac{1}{4L} \int_0^L dL' \left(D_+((L'+t')k_0) - D_+((L'-t')k_0) \right) \right) . \tag{4.196}$$

Remarkably, the dephasing parameter φ is independent from $M_\odot$, meaning that the dephasing of a particle in a superposition of two spatial location occurs also in absence of an external gravitational source. Moreover, from Eq. (4.192), a dephasing clearly induces a decoherence, making a density operator decrease the absolute value of the off-diagonal elements β which characterize the superposition between two different states in a basis. Therefore, the dephasing φ represents the intrinsic decoherence whose existence was questioned at the beginning of this section. Since this decoherence occurs in absence of initial gravitons or classical sources, this decoherence is not removable and represents a fundamental limit of all particles in a spatial superposition. A plot of the dephasing parameter φ is provided in Fig. 4.18, where natural units $\hbar = c = 1$ are restored by considering *i)* $\Lambda = m_{\rm P} = 1.2209 \cdot 10^{28}$ eV; *ii)* $m/m_{\rm P}$ and $M_\odot/m_{\rm P}$ instead of m and $M_\odot$ in Eqs (4.195) and (4.196). From the atomic scale parameters chosen in Fig. (4.18), the spreading time, defined in Sec. 4.4.1 is $t_{\rm S} \sim 67.248$ eV^{-1}, so that the range of times chosen in Fig. 4.18 satisfies $t \ll t_{\rm S}$.

The results are outstanding. Once the interaction with the gravitons starts, a decoherence takes place by increasing the dephasing parameter. When the two points where the particle is located become causally connected - namely, when $t \sim L$ - after a short oscillation, the dephasing does not increase anymore and remains stable, more or less to the value reached when $t \sim L$. Indeed, one can trivially see that, when $t \gg L$, the argument of the integral in time of Eq. (4.196) nullifies.

The fact that a dephasing occurs even when the two position points are not causally connected is a clear indication of the presence of correlations in the gravitational vacuum. In this range, one can also estimate how φ behaves before the points become causally connected. In fact, when $L \gg t$, the L dependent term vanishes in Eq. (4.196). This leads to

$$\varphi(t \ll L) \approx \frac{m^2}{m_{\rm P}^2} \left(1.2508 + \frac{4}{\pi} \ln(tk_0) \right) \tag{4.197}$$

[11] The Kraus operators whose elements are a square root of orders $\mathcal{O}(m^n)$ with $n > 3$ would give a contribution of order m^n on the channel action (4.182), which are then discarded.

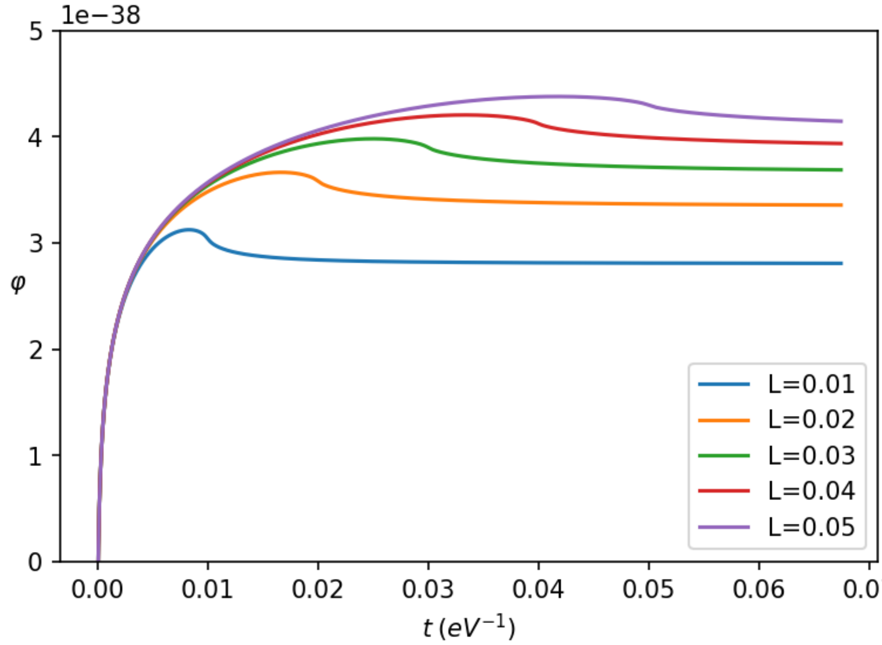

Figure 4.18: Dephasing in time of a particle localized in a quantum superposition of two different space points, distant L (in eV^{-1}) w.r.t. each other. The mass of the particle is the hydrogen mass $m = 9.39 \cdot 10^8\ eV$ while $k_0 = 3.371 \cdot 10^3\ eV$ was chosen as the inverse of the atomic size.

where the parameter 1.2508 departing from the logarithm was numerically estimated.

A rough estimation of the asymptotic value of φ can be done by assuming $\varphi(t \gg L) \sim \varphi(t \sim L)$, namely

$$\varphi(t \gg L) \approx \frac{m^2}{m_{\mathrm{P}}^2}\left(1.2508 + \frac{4}{\pi}\ln(Lk_0)\right) \sim \frac{m^2}{m_{\mathrm{P}}^2}\left(1.2508 + \frac{4}{\pi}\ln\left(\frac{L}{\epsilon}\right)\right). \tag{4.198}$$

Therefore, the dephasing φ experienced by a particle of size ϵ, localized in a superposition of two positions distant L between each other is proportional to the logarithm of the ratio L/ϵ. Eq. (4.198) is consistent when the particle is localized in a single position. In fact, in this case one should have $L \sim \epsilon$, giving $\varphi \sim 0$.

Despite describing an intrinsic dephasing, where there is no need of external gravitons or gravitational sources, quantitatively, the obtained decoherence departs by far from the Diósi-Penrose mechanism, predicting a complete dephasing (with $\varphi = 1$), rather then a partial one.

The properties of the asymmetric erasure channel (4.190) with probabilities given by Eq. (4.195) are now investigated. Firstly, $\mathcal{E}$ is addressed in the absence of the planet, i.e. in the limit $M_\odot \to 0$. In this case, one has $p_e^{\mathrm{A}} = p_e^{\mathrm{B}} = p_e$ and the erasure channel becomes symmetric. In so doing, with the atomic parameters used in Fig. 4.18, the probability of erasure behaves as shown in Fig. 4.19. From it, after an initial bump, occurring at times $t \sim m_{\mathrm{P}}^{-1}$, the erasure probability starts to decrease in time. For t high enough, the erasure probability p_e becomes negative, which is unphysical. However, the time t when this occurs turns out to be of the same order of the spreading time t_G. Therefore, the occurrence of a negative erasure probability corresponds to a failure on the approximation of a static and non-spreading massive particle. Therefore, without a gravitational

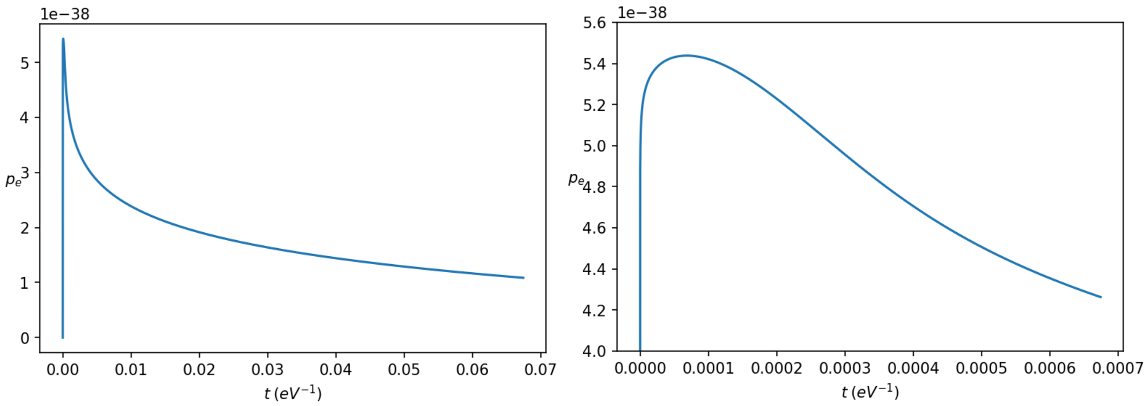

Figure 4.19: Probability of erasure p_e in time with no gravity sources (i.e. $M_\odot = 0$). The parameters used are the ones used in Fig. 4.18. The right plot zooms at the peak of the curve shown in the left plot.

source, the erasure probability p_e plotted in Fig. 4.19 is associated to a temporary instability given by the sharp switching-in of the field-graviton interaction. After this instability, the probability of erasure supposedly drops to zero.

The effects of the presence of a planet are now addressed. The switching-in function $\theta(t - |\mathbf{x}_\mathrm{i}|)$ on the term proportional to $M_\odot$ in Eq. (4.195) comes from the fact that the planet starts to interact with the gravitons at a time $t = 0$. However, in a realistic situation, the planet is not suddenyl created at $t = 0$ but it supposedly already there way before. In this case, the particle "feels" the planet immediately, so that the function $\theta(t - |\mathbf{x}_\mathrm{i}|)$ can be ignored in Eq. (4.195).

When a gravitational source is present, from Eqs. (B.65a) and (B.65b), the erasure rate $-\lambda_{\mathrm{i}=\mathrm{A,B}}$ increases by a factor proportional to $|\mathbf{x}_\mathrm{i}|^{-4}$, making the erasure channel asymmetric. The more the state is positioned near the gravitational well, the more is its erasure probability. This is expected, since the states located near a gravitational source feel more the gravitational force that leads particles to shift their original position.

For the sake on simplicity, the situation where $|\mathbf{x}_\mathrm{A}| = |\mathbf{x}_\mathrm{B}| =: r$ is now considered. In this case, the two points where the particle can be defined are located at the same distance r from the planet. One obviously has $p_e^\mathrm{A} = p_e^\mathrm{B} =: p_e$ and the erasure channel (4.190) is again symmetric. A plot for the erasure probability in time is provided in Fig. 4.20. In it, the quantum state is simulated to be placed in a satellite distant r from the Earth, so that M is the Earth mass $\simeq 5.050 \cdot 10^{60}$ eV and r is expressed in terms of the Earth radius[12] R_E. Since, $p_e \propto |\mathbf{x}_\mathrm{A}|^{-4}$, the increasing of p_e is very sensible from the distance from the planet. Indeed, from Fig. 4.20, while at $r = 10\,R_\mathrm{E}$ the presence of the planet drastically increases immediately the erasure probability, at $r = 30\,R_\mathrm{E}$ this increasing is basically negligible, since the plot is almost identical to the one without the planet in Fig. 4.20 - at least at the range of times $t \ll t_\mathrm{S}$.

In case $p_e \gg \varphi$, then the probability to observe the intrinsic dephasing is completely overcome by the probability of erasure. Therefore, to have the possibility to see the small dephasing given by Eq. (4.196), one has to put the particle very far from each gravitational source[13]. This condition is

[12]To consider a point-like planet, $r \gg R_\mathrm{E}$.

[13]Apart from that, the real experimental challenge would be to bring the two locations of the superposition very

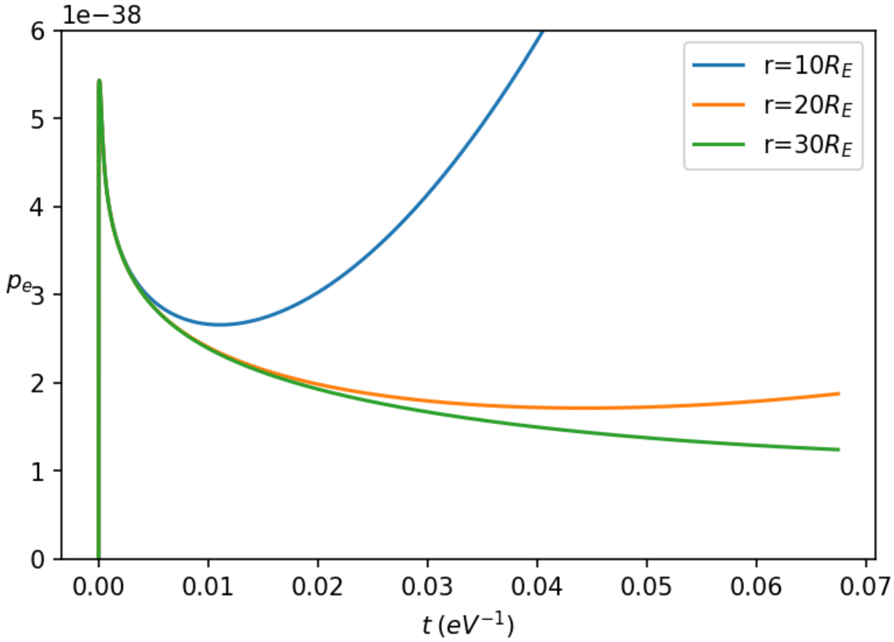

Figure 4.20: Probability of erasure p_e for a quantum state positioned at two points, $\mathbf{x}_\mathrm{A}$ and $\mathbf{x}_\mathrm{B}$ at the same distance $r = |\mathbf{x}_\mathrm{A}| = |\mathbf{x}_\mathrm{B}|$ from a planet with mass $M \simeq 5.050 \cdot 10^{60}\ eV$, corresponding to the mass of the Earth. For the legend, $R_\mathrm{E} \simeq 5.127 \cdot 10^{12}\ eV^{-1}$ is the Earth radius.

now relaxed by the study of the quantum capacity

4.4.4 Quantum capacity of the self-gravity dephasing

From Chapter 3 even a very small variation of the identity channel turned out to compromise the quantum communication capacity of a channel. Motivated by knowing if this is true also for localized systems, the capacities of the channel $\mathcal{N} = \mathcal{E} \circ \mathcal{D}$ studied in Sec. 4.4.3 are now explored, as long as the possibility to retrieve the dephasing φ from Eq. (4.198) via the information loss.

Regarding the classical capacity, it is intuitive, and well-known from the literature [246, 247] that a dephasing channel does not affect the classical information content of a quantum state. Therefore, one has $C(\mathcal{N}) = C(\mathcal{E})$ and then, no dephasing can be seen from a classical information loss. For this reason, the investigation is focus exclusively on the quantum capacity.

First of all, theorem 10 of Ref. [248] is invoked, proving that, a whatever channel $\mathcal{N} : \mathcal{S}(\mathbb{C}^{\otimes 2}) \to \mathcal{S}(\mathbb{C}^{\otimes 3})$ has an additive quantum capacity only if the rank of its Choi matrix is ≤ 3. However, the Choi matrix of the channel $\mathcal{N}$ here investigated, reported in Eq. (4.184), turns out to have rank 4. This is sufficient to say the quantum capacity of our channel is not additive and therefore $Q > Q^{(1)}$.

From this analysis, the restriction to the one shot version of the quantum capacity $Q^{(1)}$ is required for the sake of simplicity. From Sec. 3.1.3.2, this quantity is obtained by maximizing the coherent information (3.37) over all the input states $\hat{\rho}$.

For an identity channel $\hat{\mathrm{Id}}$, the coherent information is trivially maximized when $\rho = \frac{1}{2}\mathbb{I}_{2\times 2}$,

far apart, increasing L and therefore the magnitude of φ.

giving the quantum capacity $Q^{(1)} = 1$. The channel $\mathcal{N}$ studied in Sec. 4.4.3 departs from the identity $\hat{\mathrm{Id}}$ only by a second order perturbative amount. In this way, the maximizing state is expect to depart from $\frac{1}{2}\mathbb{I}_{2\times 2}$ from an analog perturbative amount. Therefore, the state $\hat{\rho}$ maximizing the coherent information (3.37) of the channel $\mathcal{N}$ is represented by a density matrix

$$\rho = \begin{pmatrix} \frac{1}{2} + \epsilon_\alpha & \epsilon_\beta \\ \epsilon_\beta^* & \frac{1}{2} - \epsilon_\alpha \end{pmatrix} , \tag{4.199}$$

where $|\epsilon_\alpha| \ll 1$ and $|\epsilon_\beta| \ll 1$. The Von Neumann entropy of the state (4.199), up to the application of the channel $\mathcal{N}$ in second order perturbation theory, can be computed as

$$S(\mathcal{N}(\hat{\rho})) = 1 - \overline{p}_e + H(\overline{p}_e) , \tag{4.200}$$

where $\overline{p}_e = \frac{p_e^{\mathrm{A}} + p_e^{\mathrm{B}}}{2}$ and $H(x) := -x \log x - (1-x)\log(1-x)$ is the *binary Shannon entropy.*

The purification of the state (4.199) reads

$$|\Psi\rangle = \frac{1}{\sqrt{2}} \left(v_{\mathrm{A}}^{+} |1_{\mathrm{A}}\rangle \otimes |1_{\mathrm{A}}\rangle_{\mathrm{R}} + v_{\mathrm{A}}^{-} |1_{\mathrm{A}}\rangle \otimes |1_{\mathrm{B}}\rangle_{\mathrm{R}} + v_{\mathrm{B}}^{+} |1_{\mathrm{B}}\rangle \otimes |1_{\mathrm{A}}\rangle_{\mathrm{R}} + v_{\mathrm{B}}^{-} |1_{\mathrm{A}}\rangle \otimes |1_{\mathrm{A}}\rangle_{\mathrm{R}} \right) , \tag{4.201}$$

where

$$v_{\mathrm{A}}^{\pm} = \frac{1}{\sqrt{2}} \frac{1}{\sqrt{1 + \frac{\epsilon_\alpha^2}{\epsilon_\beta^2} \mp \frac{\epsilon_\alpha}{\epsilon_\beta}\sqrt{1 + \frac{\epsilon_\alpha^2}{\epsilon_\beta^2}}}} ; \tag{4.202a}$$

$$v_{\mathrm{B}}^{\pm} = \pm v_{\mathrm{A}}^{\mp} , \tag{4.202b}$$

By applying the channel $\mathcal{N} \otimes \mathrm{Id}$ into the purified state $|\Psi\rangle\langle\Psi|$ one gets a state represented by a 6×6 density matrix

$$(\mathcal{N} \otimes \mathrm{Id}) |\Psi\rangle\langle\Psi| \left(\begin{array}{c|c} \tilde{\rho}_{\mathrm{AR}} & \mathbf{0} \\ \hline \mathbf{0}^T & \tilde{\rho}_e \end{array} \right) , \tag{4.203}$$

where

$$\tilde{\rho}_{\mathrm{AR}} = \frac{1}{2} \begin{pmatrix} (v_{\mathrm{A}}^{+})^2 (1 - p_e^{\mathrm{A}}) & v_{\mathrm{A}}^{+} v_{\mathrm{B}}^{+} (1 - \overline{p}_e - \varphi) & v_{\mathrm{A}}^{+} v_{\mathrm{A}}^{-} (1 - p_e^{\mathrm{A}}) & v_{\mathrm{A}}^{+} v_{\mathrm{B}}^{-} (1 - \overline{p}_e - \varphi) \\ v_{\mathrm{A}}^{+} v_{\mathrm{B}}^{+} (1 - \overline{p}_e - \varphi) & (v_{\mathrm{B}}^{+})^2 (1 - p_e^{\mathrm{B}}) & v_{\mathrm{A}}^{-} v_{\mathrm{B}}^{+} (1 - \overline{p}_e - \varphi) & v_{\mathrm{B}}^{+} v_{\mathrm{B}}^{-} (1 - p_e^{\mathrm{B}}) \\ v_{\mathrm{A}}^{+} v_{\mathrm{A}}^{-} (1 - p_e^{\mathrm{A}}) & v_{\mathrm{A}}^{-} v_{\mathrm{B}}^{+} (1 - \overline{p}_e - \varphi) & (v_{\mathrm{A}}^{-})^2 (1 - p_e^{\mathrm{A}}) & v_{\mathrm{A}}^{-} v_{\mathrm{B}}^{-} (1 - \overline{p}_e - \varphi) \\ v_{\mathrm{A}}^{+} v_{\mathrm{B}}^{-} (1 - \overline{p}_e - \varphi) & v_{\mathrm{B}}^{+} v_{\mathrm{B}}^{-} (1 - p_e^{\mathrm{B}}) & v_{\mathrm{A}}^{-} v_{\mathrm{B}}^{-} (1 - \overline{p}_e - \varphi) & (v_{\mathrm{B}}^{-})^2 (1 - p_e^{\mathrm{B}}) \end{pmatrix} ; \tag{4.204}$$

$$\tilde{\rho}_e = \frac{1}{2} \begin{pmatrix} (v_{\mathrm{A}}^{+})^2 p_e^{\mathrm{A}} + (v_{\mathrm{B}}^{+})^2 p_e^{\mathrm{B}} & v_{\mathrm{A}}^{+} v_{\mathrm{A}}^{-} p_e^{\mathrm{A}} + v_{\mathrm{B}}^{+} v_{\mathrm{B}}^{-} p_e^{\mathrm{B}} \\ v_{\mathrm{A}}^{+} v_{\mathrm{A}}^{-} p_e^{\mathrm{A}} + v_{\mathrm{B}}^{+} v_{\mathrm{B}}^{-} p_e^{\mathrm{B}} & (v_{\mathrm{A}}^{-})^2 p_e^{\mathrm{A}} + (v_{\mathrm{B}}^{-})^2 p_e^{\mathrm{B}} \end{pmatrix} , \tag{4.205}$$

The eigenvalues of the matrix (4.203) are

$$\Lambda_1 = \Lambda_2 = 0 , \quad \Lambda_3 = \frac{\varphi}{2} , \quad \Lambda_4 = 1 - \overline{p}_e - \frac{\varphi}{2} , \quad \Lambda_5 = \frac{p_e^{\mathrm{A}}}{2} , \quad \Lambda_6 = \frac{p_e^{\mathrm{B}}}{2} . \tag{4.206}$$

The entropy of $\mathcal{N} \times \mathrm{Id}(|\Psi\rangle\langle\Psi|)$ can be computed from the eigenvalues (4.206). In so doing, both the terms of the coherent information (3.37) turn out to be independent from the parameters ϵ_α and ϵ_β, so that, by putting Eqs. (4.200) and (4.206) into the coherent information (3.37), the quantum capacity is obtained as

$$
\begin{aligned}
Q^{(1)} &= 1 - 2\overline{p}_e + H(\overline{p}_e) + \frac{1}{2}\left(p_e^{\mathrm{A}} \log p_e^{\mathrm{A}} + p_e^{\mathrm{B}} \log p_e^{\mathrm{B}}\right) \\
&+ \left(1 - \overline{p}_e - \frac{\varphi}{2}\right) \log\left(1 - \overline{p}_e - \frac{\varphi}{2}\right) + \frac{\varphi}{2} \log \frac{\varphi}{2} \\
&\sim 1 - 2\overline{p}_e + \frac{1}{2}\overline{p}_e \log\left(1 - \frac{\Delta p_e^2}{\overline{p}_e^2}\right) + \frac{\Delta p_e}{2} \log\left(\frac{\overline{p}_e + \Delta p_e}{\overline{p}_e - \Delta p_e}\right) + \frac{\varphi}{2} \log \frac{\varphi}{2} \,.
\end{aligned} \tag{4.207}
$$

where $\Delta p_e := \frac{p_e^{\mathrm{A}} - p_e^{\mathrm{B}}}{2}$. By analyzing Eq. (4.207), one achieves that $Q^{(1)}$ reaches a minimum when $\Delta p_e = 0$. Therefore, any asymmetry of the erasure channel (4.190) would increase its quantum capacity. By considering $\Delta p_e = 0$, Eq. (4.207) becomes

$$
Q^{(1)} \sim 1 - 2\overline{p}_e + \frac{\varphi}{2} \log \frac{\varphi}{2} \,. \tag{4.208}
$$

In absence of a planet, $\overline{p}_e \equiv p_e$ has the same order of φ - see Figs. 4.18 and 4.19. Since both are very small, the dephasing φ provides a loss on the quantum capacity which is way bigger than the loss provided by $\overline{p}_e$ - in fact, $\log(\varphi/2) \sim 100$ if $\varphi \simeq 10^{-38}$. In presence of an external gravitational field, the erasure probability may easily increase in a short time, completely screening the dephasing if

$$
p_e \gg \frac{\varphi}{4} \log(\varphi/2) \,. \tag{4.209}
$$

In a hypothetical experimental setup where the intrinsic dephasing φ is aimed to be observed, an external gravitational would screen this effect with the erasure probability overcoming the loss of quantum information given by the dephasing. By putting Eq. (4.198) and (4.195) - and considering just the term proportional to $M_\odot$ in the latter - into Eq. (4.209), the condition to have a dephasing effect greater than the erasure is

$$
\left(1.2508 + \frac{4}{\pi} \ln(L/\epsilon)\right) \log(m^2/m_{\mathrm{P}}^2) > \frac{M_\odot^2 t^2 \epsilon}{2 r^4 m_{\mathrm{P}}^2} \,. \tag{4.210}
$$

This gives a restriction on how far one has to be from the planet to observe the dephasing in the range of times $t < t_{\mathrm{S}}$. In Sec. 4.4.3, by looking at Fig. 4.20, to prevent the erasure to affect the probability of dephasing observation, $r = 30R_{\mathrm{E}}$ seemed the required distance from the Earth to perform the experiment. However, the condition for the distance in Eq. (4.210), achieved by studying the information loss, is way less restrictive. In fact, from Eq. (4.210), the l.h.s., i.e. the dephasing, dominates over the r.h.s., i.e. the erasure, just at a distance $r = 3R_{\mathrm{E}}$. Therefore, again, the study of the conserved quantum information proves to be a lens on small quantum effects otherwise irretrievable.

Chapter 5

Conclusion

This thesis aimed to explore the interplay between gravity and quantum information. In particular, by observing what are the effects of gravitational phenomena in quantum communication settings, one may explore whether those can increase or decrease the quality of the communication channel. In a world where space and quantum technologies and rapidly expanding, the prediction of these effects becomes fundamental. In fact, an amplification of the quality of communication may bring to an exploitation of gravity to make more performant quantum communication schemes. On the contrary, eventual gravitational noisy effects must be considered in advance to be able to predict them, finding new solutions for a better protocol.

Two communication protocols were mainly considered. The first one, used in Chapter 3, involved the communication of one-mode bosonic systems. Their states do not lose information in free traveling. In fact, since there is no uncertainty of the bosons' momenta, there is no "spreading" of information, as there is for localized quantum systems (see Chapter 4). This violation of the uncertainty principle makes this protocol realistic only when performed over large time periods. For example, it can be used by studying how information is preserved from remote past [165, P4] or when effects are expected to occur in a finite time period (such as a mirror motion [156, P1] or a black hole evaporation [P3]). Experimentally, this protocol can be reproduced by unidirectional bosonic signals, e.g. lasers, exchanged by two spatial probes at a distance d w.r.t. each other, which must be much greater than the inverse of the frequency uncertainty [249].

The second protocol, considered in Chapter 4, involved two quantum harmonic oscillators communicating via a background field. The field-detector interaction is the one modeled by Unruh-deWitt detectors, which have proved to be an effective mean to "feel" the particles generated by a non-inertial motion in quantum field theory (see Sec. 2.4.1). The protocol emulates two antennas communicating via an electromagnetic field, as occurs in current Wi-Fi communication. However, since the antennas are a quantum system, also the possibility to communicate quantum messages was opened by this protocol.

By applying gravity to these two communication channels, the obtained results have not only the aforementioned experimental implications, but also theoretical ones, shedding light on some phenomena arising from quantum field theory in curved spacetime and on the linearized theory of gravity. This was done with new methods based on the formalization of those phenomena as quantum channels. For example, in Sec. 3.2 a channel was built by a generic Bogoliubov transformation of bosonic single modes. This novel method allows to study the properties of each evolving spacetime to preserve information and entanglement, by simply studying their Bogoliubov coefficients. Moreover, in Secs. 4.1 the Heisenberg evolution of a pair of harmonic oscillator detectors was studied through a quantum Langevin equation. This new approach, as shown in Sec. 4.2, gave the possibility to study communication properties with a non-perturbative field-detector interaction.

By using these methods, many gravitational settings were considered throughout the thesis. Those are listed below, together with their theoretical implications in general relativity and quantum mechanics.

- **Cosmological expansion on single-mode quantum systems.**
  The preservation of information from a single mode and entanglement from two opposite modes were investigated in Sec. 3.3. The cosmological particle production turns out to amplify any pre-existing signal, instead of being simply added to it. Different theories of gravity lead to different results in this context. In particular the focus was on $f(Q)$ non-metric theories of gravity. By adjusting the parameters of a power-law gravity modification (3.86), the amount of preserved quantum information can increase up to 4.23% compared to the prediction of GR - recovered when ($\zeta = 0$). In an analogous way, the evolution of the entanglement between two opposite bosonic modes was studied, generalizing the pre-existing results from the literature [202]. The ability to achieve cosmological particle production, including through analog gravity systems [250], offers a pathway to distinguish between modified theories of gravity and the coupling between fields and curvature (or non-metricity). In conclusion, cosmological particle production can serve as a crucial tool for understanding the evolutionary history of our universe, particularly during the inflationary epoch, which is believed to have generated a substantial quantity of particles [251, 252, 253]. Recent studies have explored models linking dark matter to this particle production process [254, 255, 256]. Within this framework, the reduction in communication capacities due to particle production holds profound implications. It is plausible that the dark particles produced during inflation could obscure information regarding particles from the remote past. As a result, this research, along with related studies focusing on fermions [165], may establish fundamental limits on our ability to recover information about primordial particles.

- **Accelerating mirrors on single-mode quantum systems.**
  The transmission of information through a semitransparent mirror - producing particles while accelerating through the dynamical Casimir effect - was investigated. With respect to the classical scenario, the average transmission coefficient of the mirror decreases in this framework. This means that the particles created by such a mirror create a further noise to the channel, instead of causing an amplification effect. This decreasing of the communication capabilities could be prominent if a mirror accelerates to relativistic speeds. To this perspective, information given by relativistic spatial probes may be severely affected. In view of the new progresses in this sector [257, 85] the prediction of such noisy effects could be pivotal for spatial experiments in a few decades. Moreover, the accelerated boundary correspondence establishes a parallel between the particle production caused by a collapsing black-hole's null shell and that arising from a perfectly reflecting, uniformly accelerating mirror. From this analogy, semitransparency leads to the absorption of radiation given by this shell of light [97]. Therefore, as a future perspective, the protocol used can also be used in the context of gravitational matter,

to study the amount of radiation a collapsing ball should absorb.

- **Black holes on single-mode quantum systems**
Obviously, each quantum signal disappears if sent through a black hole. However, if the black hole evaporates, by using the mirror analogy provided in Sec. 3.5, it was proved that an input signal comes out intact from the black hole after its complete evaporation. By using energy conservation, the mirror-black hole analogy also predicts a new evaporation model involving a sharp transition between a Shwarzschild and a Minkowski spacetime [P3], neglecting any adiabatic approximation. This leads to a complete evaporation time reduced by a factor 3/8 w.r.t. the one obtained adiabatically. At the evaporation time, a huge amount of particles are suddenly released, with a total energy $M_0/\sqrt[3]{2}$, being M_0 the initial black hole mass. These particle would create a noise which will affect the recovery of any input signal in the short term. This model has a lot of implications also on the black hole thermodynamics, predicting an entropy which is $\sim 37\%$ the Beckenstein-Hawking one [P3].
If a signal is sent just in presence of a far black hole, but not through it, then its radiation may be detected due to the high sensibility of the quantum capacity to a slight increment of the background radiation (see Sec. 3.6). To this perspective, a cosmological fluid external pressure on the black hole would change its temperature, leading to different communication capacities. Even if focusing on Anton-Schmidt fluids, it would be interesting to take into account other fluids and show, for instance, how a phase transition could affect these scenarios. Another plausible extension would be to promote our treatment to more general compact objects [258] and/or on accretion disk contexts [259, 260, 261, 262, 263].

- **Cosmological expansion on localized quantum systems.**
When considering a pair of localized quantum systems, a cosmological expansion can increase their capacity to communicate classical messages depending on the coupling between the field and the curvature. The prescription studied in Sec. 4.3 suggests a value for the coupling constant lower than the conformal one. In fact, in this way, an expansion prior to the protocol gives a noisy effect which, in turn, can be associated to a particle production. This opens the possibility to infer a cosmological particle production also when the expansion is still ongoing, giving new possibilities for future predictions on more realistical expansions [60]. By considering an example of cosmological expansion driven by a perfect fluid, the classical capacity enhancement is dependent on the barotropic index w of the fluid. In particular, the classical capacity is proportional to the universe expansion rate. This also suggests a direct connection with the particle production occurring during the communication. In fact, the amplification of the input signal due to the particle production studied in Sec. 3.3 would lead to an increment of the classical capacity for each highly lossy channel. Furthermore, the increase in capacity is larger when the detectors are bigger and farther apart. Consequently, to observe a significant increase in capacity, the physical system might be as large as possible. Naturally, if the oscillator of the receiver is close to the comoving horizon of the sender, the two detectors can no longer be considered non-relativistic.
Future research will address relativistic particle detector models to investigate general communication properties near horizons. As an alternative, one can also consider point-like detectors and drop the hypothesis of a rapid interaction [264]. In addition, detecting the quantum effects here studied would require highly precise instruments or very large experimental setups -

similar to those needed to detect the Unruh effect via particle detectors [233]. However, recent advancements in analog models of cosmological expansion, which predict observable quantum effects, have been developed in laboratory settings [265, 266]. Thus, our communication protocol could be more feasibly implemented in a laboratory using analog gravity systems [34], offering the potential to observe the coupling between the communicated particles and the emulated curvature.

- **Quantum gravity effects on localized quantum systems.**
  By starting the vacuum gravitational state, a bosonic quantum particle would create gravitons which then re-interact with the particle itself. If the initial particle is in a quantum superposition of two different locations, then its self-gravity creates an intrinsic decoherence, which is proportional to the logarithm of the ratio L/ϵ between the size of the particle and the size of the wavepackets where the particle can be localized. This fact puts a fundamental limit on how much we can separate the state localizations to have a quantum superposition, and gives a fundamental reason why superpositions of two distant locations are not possible.

  By considering the evolution of the initial particle as a quantum channel, one has an erasure probability given by the switching-in of the interaction with the gravitational field, expressing how the energy is given to the gravitational sector and then taken back by the particle. Remarkably, in presence of a external source of gravity, the erasure probability increases drastically in short times, meaning that, to experiment the self-induced decoherence studied in Sec. 4.4, one has to put the experiment far enough from any gravitational source. By observing the loss of quantum information, a distance $\gtrsim 3$ times the radius of the earth is sufficient to keep low the erasure probability - provided an observation of the signal enough fast.

Overall, do gravitational effects increase or decrease the communication capabilities of quantum channels? When single-mode signals are communicated, the results provided suggests, in general, a *decreasing* of the communication capabilities. This fact is mostly supported by the examples provided in Sec. 3.4 where an already noisy quantum channel is considered. Indeed, the radiation from a dynamical spacetime appears to be maximally entropic (e.g. for the Unruh and Hawking radiation). Therefore, it is intuitive that this radiation cannot improve the communication of signals, but it provides noise containing no information on the input state.

Regarding the communication between localized quantum systems, the situation is quite different. In fact, in this case, the detectors themselves are affected by the spacetime evolution. The interaction between the background field and the detector would then change its structure in time, leading to possible increasing of the communicate rate. For example, the situation in Sec. 4.3 can be easily seen as the two detectors are communicated through particles which assume a tachyonic behaviour after the expansion. This allows a communication with less inertia and then, a better classical communication quality.

The difference between the communication of classical information and quantum information is remarkable. In particular, while classical communication can be achieved in each situation by amplifying the state in the encoding procedure, quantum communication has more severe limitations, due to the fact that quantum information cannot be arbitrarily amplified and distributed. This thesis addressed, in particular, the possibility to communicate quantum information through localized quantum systems - a fundamental challenge for future reliable quantum key distribution

[267]. Trivially, a detector should send information towards the receiver via a single direction, to prevent loss of information elsewhere (this could be achieved by considering quantum antennas and parabolic mirrors). However, detectors spreading information in a spherically symmetric way, still can communicate quantum information reliably by performing a non-inertial trajectory. Remarkably, with a rapid interaction, no more than one qubit can be reliably communicated, from a limit given by the fact that the receiver should overwrite the sender's state to its detector.

In general, a non-inertial detector undergoes quantum effects (e.g. the Unruh effect) as predicted by quantum field theory in curved spacetimes. These effects could play a crucial role on the possibility to achieve a reliable quantum communication. To this prospect, also entanglement harvesting could be pivotal [268, 269]. Indeed, an arbitrary high entanglement between the detectors always lead to an assisted quantum capacity greater than zero [223]. Future works would try to see in more detail how quantum effects, given by the detectors' non-inertial motion, could affect the possibility of achieving a quantum capacity greater than zero.

Throughout the thesis, a consistent result is recurrent. In several cases, the effects of gravity on quantum field theory are very small -e.g. particle production, decoherence etc. While the classical capacity of quantum channels is basically unaffected by such small effects, the quantum capacity turns out to be very sensible to them even when they are utterly small. For example, a cosmological particle production generating 10^{-30} particles prevents the communication of more than ~ 100 qubits. To date, just a few qubits could be reliably sent over hundred of kilometers of distance. In this way, 100 qubits is still a very high number but nothing in comparison with the amount of classical particles one should use to achieve the aforementioned particle production $\sim 10^{30}$.

Therefore, future quantum technologies [267] may be the key to the detection of these small effects predicted by quantum field theory in curved spacetime, such as Unruh effect, cosmological particle production and Hawking radiation. Moreover, the study of the loss of quantum information in Sec. 4.4 can decrease by some orders the effects of the erasure probability given by gravitational sources, putting a lens on the small decoherence effects. Finally, since the quantum capacity is sensible to many currently unknown gravitational features, one may achieve information on these effects, testing modified gravity theories, cosmological fluids and the nature of gravity itself.

In summary, this thesis has shown that quantum communication protocols offer a powerful operational framework for exploring how gravity shapes the flow of quantum information. By examining their behaviour in curved spacetimes and expanding universes, it is highlighted how effects traditionally studied in cosmology can manifest in information-theoretic quantities such as channel capacity and decoherence. Looking ahead, the convergence between quantum and space technology opens a unique opportunity: the same instruments developed for quantum networks and satellite communication could become experimental platforms to probe the interplay between quantum physics and gravity, bridging the gap between theoretical cosmology and applied quantum science.

Bibliography

[P1] M. R. R. Good, A. Lapponi, O. Luongo, and S. Mancini. Quantum communication through a partially reflecting accelerating mirror. *Phys. Rev. D*, 104(10), November 2021.

[P2] S. Capozziello, R. D'Agostino, A. Lapponi, and O. Luongo. Black hole thermodynamics from logotropic fluids. *Eur. Phys. J. C*, 83(2), February 2023.

[P3] M. R. R. Good, A. Lapponi, O. Luongo, and S. Mancini. Modeling black hole evaporative mass evolution via radiation from moving mirrors. *Phys. Rev. D*, 107(10), May 2023.

[P4] A. Lapponi, D. Moustos, D. E. Bruschi, and S. Mancini. Relativistic quantum communication between harmonic oscillator detectors. *Phys. Rev. D*, 107(12), June 2023.

[P5] A. Lapponi, J. Louko, and S. Mancini. Making two particle detectors in flat spacetime communicate quantumly. *Phys. Rev. D*, 110(2), July 2024.

[P6] S. Capozziello, A. Lapponi, O. Luongo, and S. Mancini. Preserving quantum information in $f(Q)$ non-metric gravity cosmology. *Eur. Phys. J. C*, 84(10), October 2024.

[P7] A. Lapponi, O. Luongo, and S. Mancini. How cosmological expansion affects communication between distant quantum systems. *Phys. Rev. D*, 111:044040, Feb 2025.

[P8] A. Lapponi, A. Ferreri, and D. E. Bruschi. Gravitational redshift via quantized linear gravity. *arXiv:2504.03956*, 2025.

[P9] A. Lapponi, D. E. Bruschi, S. Mancini, and F. Wilhelm-Mauch. Self-gravity affects quantum states. *soon in arXiv*, 2025.

[1] C. W. Misner, K. S. Thorne, and J. A. Wheeler. *Gravitation.* W. H. Freeman, San Francisco, 1973.

[2] R. M. Wald. *General Relativity.* University of Chicago Press, 1984.

[3] A. Einstein. Die feldgleichungen der gravitation. *Sitzungsberichte der Königlich Preußischen Akademie der Wissenschaften zu Berlin*, pages 844–847, 1915.

[4] R. G. Vishwakarma. Einstein and beyond: A critical perspective on general relativity. *Universe*, 2(2), 2016.

[5] S. Weinberg. *Cosmology.* Oxford University Press, 2008.

[6] P. Peter and J.-P. Uzan. *Primordial Cosmology.* Oxford University Press, 2009.

[7] N. Aghanim et al. (Planck Collaboration). Planck 2018 results. VI. Cosmological parameters. *Astronomy & Astrophysics*, 641:A6, 2020.

[8] G. Bertone, D. Hooper, and J. Silk. Particle dark matter: evidence, candidates and constraints. *Phys. Rep.*, 405(5–6):279–390, 2005.

[9] G. L. Klimchitskaya and V. M. Mostepanenko. The nature of dark energy and constraints on its hypothetical constituents from force measurements. *Universe*, 10(3):119, March 2024.

[10] K. Freese, B. Fields, and D. Graff. *Death of Stellar Baryonic Dark Matter*, page 18–23. Springer Berlin Heidelberg, September 2003.

[11] L. Roszkowski, E. M. Sessolo, and S. Trojanowski. Wimp dark matter candidates and searches—current status and future prospects. *Rep. Prog. Phys.*, 81(6):066201, May 2018.

[12] S. Nojiri and S. Odintsov. Introduction to modified gravity and gravitational alternative for dark energy. *Int. J. Geom. Methods Mod. Phys.*, 4(01):115–145, February 2007.

[13] S. Capozziello and M. Francaviglia. Extended theories of gravity and their cosmological and astrophysical applications. *General Relativity and Gravitation*, 40(2-3):357–420, December 2007.

[14] A. Felice and S. Tsujikawa. $f(R)$ theories. *Living Rev. Relativ.*, 13(1), June 2010.

[15] S. Capozziello and M. De Laurentis. Extended theories of gravity. *Phys. Rep.* , 509(4-5):167–321, December 2011.

[16] T. Clifton, P. G. Ferreira, A. Padilla, and C. Skordis. Modified gravity and cosmology. *Phys. Rep.*, 513(1–3):1–189, March 2012.

[17] S. Capozziello, R. D'Agostino, and O. Luongo. Cosmic acceleration from a single fluid description. *Phys. Dark Univ.*, 20:1–12, 2018.

[18] K. Boshkayev, R. D'Agostino, and O. Luongo. Extended logotropic fluids as unified dark energy models. *Eur. Phys. J. C*, 79(4):332, 2019.

[19] K. Boshkayev et al. Testing generalized logotropic models with cosmic growth. *Phys. Rev. D*, 104(2):023520, 2021.

[20] D. O. Sabulsky et al. Experiment to detect dark energy forces using atom interferometry. *Phys. Rev. Lett.*, 123:061102, Aug 2019.

[21] M. Misiaszek and N. Rossi. Direct detection of dark matter: A critical review. *Symmetry*, 16(2):201, February 2024.

[22] DESI Collaboration. Data release 1 of the dark energy spectroscopic instrument. *arXiv:2503.14745*, 2025.

[23] B. Drummond. Understanding quantum mechanics: a review and synthesis in precise language. *Open Physics*, 17(1):390–437, January 2019.

[24] C. Rovelli. Loop quantum gravity. *Living Rev. Relativ. [electronic only]*, 1:1002–, 04 1998.

[25] C. P. Burgess. Quantum gravity in everyday life: General relativity as an effective field theory. *Living Rev. Relativ.*, 7(1):5, April 2004.

[26] S. Hossenfelder. Minimal length scale scenarios for quantum gravity. *Living Rev. Relativ.*, 16(1):2, January 2013.

[27] F. Marchesano, G. Shiu, and T. Weigand. The standard model from string theory: What have we learned? *Annu. Rev. Nucl. Part. S.*, 74(1):113–140, September 2024.

[28] N. D. Birrell and P. C. W. Davies. *Quantum Fields in Curved Space*. Cambridge Monographs on Mathematical Physics. Cambridge University Press, 1982.

[29] S. Hollands and R. M. Wald. Quantum fields in curved spacetime. *Phys. Rep.*, 574:1–35, 2015. Quantum fields in curved spacetime.

[30] D. N. Page. Information in black hole radiation. *Phys. Rev. Lett.*, 71:3743–3746, Dec 1993.

[31] L. Parker. Particle creation and particle number in an expanding universe. *Journal of Physics A: Mathematical and Theoretical*, 45(37):374023, September 2012.

[32] J. Steinhauer. Observation of quantum Hawking radiation and its entanglement in an analogue black hole. *Nature Physics*, 12(10):959–965, 2016.

[33] A. Coutant and S. Weinfurtner. Low-frequency analogue Hawking radiation: The bogoliubov–de gennes model. *Phys. Rev. D*, 97(2):025006, 2018.

[34] M. J. Jacquet, S. Weinfurtner, and F. König. The next generation of analogue gravity experiments. *Philosophical Transactions of the Royal Society A: Mathematical, Physical and Engineering Sciences*, 378(2177):20190239, August 2020.

[35] W. G. Unruh. Notes on black-hole evaporation. *Phys. Rev. D*, 14:870–892, Aug 1976.

[36] K. Collaboration and P. et Al. Constraining Inflation with the BICEP/Keck CMB Polarization Experiments. *arXiv:2405.19469*, July 2024.

[37] S. N. Gupta. Quantization of Einstein's gravitational field: Linear approximation. *Proceedings of the Physical Society. Section A*, 65(3):161, mar 1952.

[38] J. F. Donoghue. General relativity as an effective field theory: The leading quantum corrections. *Phys. Rev. D*, 50(6):3874–3888, September 1994.

[39] R. B. Mann and T. C. Ralph. Relativistic quantum information. *Classical and Quantum Gravity*, 29(22):220301, 2012.

[40] N. Friis, I. Fuentes, et al. Relativistic quantum information. *Journal of Physics A: Mathematical and Theoretical*, 52(13):133001, 2019.

[41] D. E. Bruschi et al. Unruh effect in quantum information beyond the single-mode approximation. *Phys. Rev. A*, 82:042332, 2010.

[42] A. Peres and D. R. Terno. Quantum information and relativity theory. *Rev. Mod. Phys.*, 76:93–123, 2004.

[43] M. Cliche and A. Kempf. Relativistic quantum channel of communication through field quanta. *Phys. Rev. A*, 81(1), January 2010.

[44] B. L. Hu, S.-Y. Lin, and J. Louko. Relativistic quantum information in detectors–field interactions. *Classical and Quantum Gravity*, 29(22):224005, October 2012.

[45] R. H. Jonsson, K. Ried, E. S. Martín-Martinez, and A. Kempf. Transmitting qubits through relativistic fields. *Journal of Physics A: Mathematical and Theoretical*, 51, 2017.

[46] T. R. Perche. Localized nonrelativistic quantum systems in curved spacetimes: A general characterization of particle detector models. *Phys. Rev. D*, 106(2), July 2022.

[47] S. Schlicht. Considerations on the Unruh effect: causality and regularization. *Classical and Quantum Gravity*, 21(19):4647–4660, September 2004.

[48] C. Anastopoulos and B. L. Hu. A master equation for gravitational decoherence: probing the textures of spacetime. *Classical and Quantum Gravity*, 30(16):165007, July 2013.

[49] S. Bose et al. Spin entanglement witness for quantum gravity. *Phys. Rev. Lett.*, 119:240401, Dec 2017.

[50] S. Pirandola, R. Laurenza, C. Ottaviani, and L. Banchi. Fundamental limits of repeaterless quantum communications. *Nat. Commun.*, 8:15043, 2017.

[51] S. Pirandola et al. Advances in quantum cryptography. *Advances in Optics and Photonics*, 12(4):1012, December 2020.

[52] S. Mancini and A. Winter. *A Quantum Leap in Information Theory.* World Scientific Publishing Company Pte Limited, 2020.

[53] P. M. Alsing and G. J. Milburn. Teleportation with a uniformly accelerated partner. *Phys. Rev. Lett.*, 91:180404, 2003.

[54] S. Pirandola, S. L. Braunstein, et al. Quantum communication in networks and technologies: A review. *arXiv preprint*, 2023.

[55] R. Ramya et al. A review of quantum communication and information networks with advanced cryptographic applications using machine learning, deep learning techniques. *Franklin Open*, 10:100223, 2025.

[56] S. Kucera et al. Demonstration of quantum network protocols over a 14-km urban fiber link. *Nat. Phys. J. Quantum Information*, 10:88, 2024.

[57] J. Yin et al. Satellite-based entanglement distribution over 1200 kilometers. *Science*, 356(6343):1140–1144, 2017.

[58] S.-K. Liao et al. Satellite-to-ground quantum key distribution. *Nature*, 549:43–47, 2017.

[59] H. Takenaka et al. Satellite-to-ground quantum-limited communication using a 50-kg-class microsatellite. *Nature Photonics*, 11(8):502–508, July 2017.

[60] L. H. Ford. Cosmological particle production: a review. *Rep. Prog. Phys.*, 84(11):116901, October 2021.

[61] S. W. Hawking. Particle Creation by Black Holes. *Commun. Math. Phys.*, 43:199–220, 1975. [Erratum: Commun.Math.Phys. 46, 206 (1976)].

[62] S. Capozziello, R. D'Agostino, R. Giambò, and O. Luongo. Effective field description of the Anton-Schmidt cosmic fluid. *Phys. Rev. D*, 99(2):023532, 2019.

[63] R. D. Carlitz and R. S. Willey. Reflections on moving mirrors. *Phys. Rev. D*, 36:2327–2335, Oct 1987.

[64] L. H. Ryder. *Quantum Field Theory.* Cambridge University Press, 2 edition, 1996.

[65] V. P. Nair. *Quantum Field Theory: A Modern Perspective.* Graduate Texts in Contemporary Physics. Springer, New York, 2005.

[66] D. Hilbert. Die grundlagen der physik. *Nachrichten von der Gesellschaft der Wissenschaften zu Göttingen, Mathematisch-Physikalische Klasse*, pages 395–407, 1915. Presented on 20 November 1915.

[67] S. Weinberg. The cosmological constant problem. *Rev. Mod. Phys.*, 61:1–23, Jan 1989.

[68] R. M. Wald. The Back Reaction Effect in Particle Creation in Curved Space-Time. *Commun. Math. Phys.*, 54:1–19, 1977.

[69] R. J. Adler, B. Casey, and O. C. Jacob. Vacuum catastrophe: An elementary exposition of the cosmological constant problem. *American Journal of Physics*, 63(7):620–626, July 1995.

[70] O. Luongo and M. Muccino. Speeding up the universe using dust with pressure. *Phys. Rev. D*, 98:103520, Nov 2018.

[71] A. Blanchard et al. λcdm is alive and well. *The Open Journal of Astrophysics*, 7, May 2024.

[72] L. Perivolaropoulos and F. Skara. Challenges for ΛCDM: An update. *New Astronomy Reviews*, 95:101659, December 2022.

[73] S. Capozziello, O. Luongo, and M. Paolella. Bounding f(r) gravity by particle production rate. *International Journal of Modern Physics D*, 25(04):1630010, March 2016.

[74] L. Parker. Thermal radiation produced by the expansion of the Universe. *Nature*, 261(5555):20–23, May 1976.

[75] C. Bernard and A. Duncan. Regularization and renormalization of quantum field theory in curved space-time. *Annals of Physics*, 107(1):201–221, 1977.

[76] Y. Zel'Dovich and A. Starobinsky. Particle production and vacuum polarization in an anisotropic gravitational field. *Soviet Journal of Experimental and Theoretical Physics*, 34:1159, 01 1972.

[77] N. D. Birrell and P. C. W. Davies. Massive particle production in anisotropic space-times. *Journal of Physics A: Mathematical and General*, 13(6):2109, jun 1980.

[78] A. Lapponi, O. Luongo, and S. Mancini. How cosmological expansion affects communication between distant quantum systems. *Phys. Rev. D*, 111:044040, Feb 2025.

[79] N. M. J. Woodhouse. Particle creation by gravitational fields. *Phys. Rev. Lett.*, 36:999–1001, Apr 1976.

[80] S. Winitzki. Cosmological particle production and the precision of the WKB approximation. *Phys. Rev. D*, 72(10), November 2005.

[81] R. Wald. *Quantum Field Theory in Curved Spacetime and Black Hole Thermodynamics.* Chicago Lectures in Physics. University of Chicago Press, 1994.

[82] R. Brunetti, K. Fredenhagen, and R. Verch. The generally covariant locality principle – a new paradigm for local quantum field theory. *Communications in Mathematical Physics*, 237(1):31–68, June 2003.

[83] C. J. Fewster and R. Verch. *Algebraic Quantum Field Theory in Curved Spacetimes*, pages 125–189. Springer International Publishing, Cham, 2015.

[84] L. H. Ford. Gravitational particle creation and inflation. *Phys. Rev. D*, 35:2955–2960, May 1987.

[85] D. J. H. Chung, P. Crotty, E. W. Kolb, and A. Riotto. Gravitational production of superheavy dark matter. *Phys. Rev. D*, 64:043503, Jul 2001.

[86] J. A. Cembranos, L. J. Garay, and J. M. Sánchez Velázquez. Gravitational production of scalar dark matter. *Journal of High Energy Physics*, 2020(6), June 2020.

[87] N. Herring and D. Boyanovsky. Gravitational production of nearly thermal fermionic dark matter. *Phys. Rev. D*, 101(12), June 2020.

[88] V. A. Kuzmin and I. I. Tkachev. Ultrahigh-energy cosmic rays, superheavy long-lived particles, and matter creation after inflation. *Journal of Experimental and Theoretical Physics Letters*, 68:271–275, 1998.

[89] V. Kuzmin and I. Tkachev. Matter creation via vacuum fluctuations in the early universe and observed ultrahigh energy cosmic ray events. *Phys. Rev. D*, 59(12), May 1999.

[90] R. Dick, K. M. Hopp, and K. E. Wunderle. Superheavy dark matter and ultrahigh-energy cosmic rays. *Canadian Journal of Physics*, 84(6–7):537–543, January 2006.

[91] C. Bambi. Astrophysical black holes: A review. In *Proceedings of Multifrequency Behaviour of High Energy Cosmic Sources - XIII — PoS(MULTIF2019)*, MULTIF2019, page 028. Sissa Medialab, November 2020.

[92] N. Kanu, E. Gupta, and V. Gupta. Exploring black holes: From Hawking radiation to quantum hair—insights and challenges in modern astrophysics. *Journal of the Institution of Engineers (India): Series C*, 106:447–461, 2025.

[93] D. N. Page. Particle emission rates from a black hole: Massless particles from an uncharged, nonrotating hole. *Phys. Rev. D*, 13:198–206, Jan 1976.

[94] M. K. Parikh and F. Wilczek. Hawking radiation as tunneling. *Phys. Rev. Lett.*, 85:5042–5045, Dec 2000.

[95] K. Schwarzschild. Über das Gravitationsfeld eines Massenpunktes nach der Einsteinschen Theorie. *Sitzungsberichte der Königlich Preussischen Akademie der Wissenschaften*, 7:189–196, 1916. Translated as: "On the Gravitational Field of a Mass Point According to Einstein's Theory".

[96] S. Massar and R. Parentani. From vacuum fluctuations to radiation. i. accelerated detectors. *Phys. Rev. D*, 54(12):7426–7443, December 1996.

[97] M. R. R. Good, P. R. Anderson, and C. R. Evans. Mirror reflections of a black hole. *Phys. Rev. D*, 94(6), September 2016.

[98] S. W. Hawking. Black holes in general relativity. *Communications in Mathematical Physics*, 25(2):152–166, 1972.

[99] M. Isi et al. Testing the black-hole area law with gw150914. *Phys. Rev. Letters*, 127(1):011103, 2021.

[100] L.-V.-K. Collaboration, M. Isi, et al. Clearest signal yet from colliding black holes yields most precise confirmation of Hawking's area theorem. *Phys. Rev. Letters*, 2025.

[101] J. D. Bekenstein. Black holes and the second law. *Lettere al Nuovo Cimento*, 4:737–740, 1972.

[102] G. W. Gibbons and S. W. Hawking. Cosmological event horizons, thermodynamics, and particle creation. *Phys. Rev. D*, 15:2738–2751, May 1977.

[103] H. Liu and X.-H. Meng. Thermodynamics of Schwarzschild–Beltrami–de Sitter black hole. *Modern Physics Letters A*, 32(27):1750146, 2017.

[104] T. Pappas, P. Kanti, and N. Pappas. Hawking radiation spectra for scalar fields by a higher-dimensional Schwarzschild–de Sitter black hole. *Phys. Rev. D*, 94:024035, Jul 2016.

[105] L. Donnay and G. Giribet. Cosmological horizons, noether charges and entropy. *Classical and Quantum Gravity*, 36, 2019.

[106] E. Witten. Anti de Sitter space and holography. *Adv. Theor. Math. Phys.*, 2:253–291, 1998.

[107] J. Maldacena. The large n limit of superconformal field theories and supergravity. *International Journal of Theoretical Physics*, 38(4):1113–1133, 1999.

[108] S. Ryu and T. Takayanagi. Holographic derivation of entanglement entropy from the anti–de Sitter space/conformal field theory correspondence. *Phys. Rev. Letters*, 96(18), May 2006.

[109] S. W. Hawking and D. N. Page. Thermodynamics of black holes in anti-de Sitter space. *Communications in Mathematical Physics*, 87:577–588, 1983.

[110] O. Lunin and S. D. Mathur. AdS/CFT duality and the black hole information paradox. *Nuclear Physics B*, 623(1–2):342–394, February 2002.

[111] S. Gunasekaran, D. Kubizňák, and R. B. Mann. Extended phase space thermodynamics for charged and rotating black holes and born-infeld vacuum polarization. *Journal of High Energy Physics*, 2012(11), November 2012.

[112] D. Kubizňák and R. B. Mann. P-V criticality of charged AdS black holes. *Journal of High Energy Physics*, 2012(7), July 2012.

[113] G. Montambaux. Generalized Stefan–Boltzmann law. *Foundations of Physics*, 48(4):395–410, March 2018.

[114] A. Fabbri and J. Navarro-Salas. *Modeling Black Hole Evaporation.* 01 2005.

[115] P. C. W. Davies and S. A. Fulling. Radiation from a moving mirror in two-dimensional space-time conformal anomaly. *Proc. Roy. Soc. Lond. A*, 348:393–414, 1976.

[116] N. Obadia and R. Parentani. Uniformly accelerated mirrors. I. Mean fluxes. *Phys. Rev. D*, 67(2), January 2003.

[117] V. V. Dodonov. Current status of the dynamical Casimir effect. *Physica Scripta*, 82(3):038105, aug 2010.

[118] C. M. Wilson et al. Observation of the dynamical Casimir effect in a superconducting circuit. *Nature*, 479(7373):376–379, November 2011.

[119] M. R.R. Good, E. V. Linder, and F. Wilczek. Moving mirror model for quasithermal radiation fields. *Phys. Rev. D*, 101(2):025012, 2020.

[120] D. A. R. Dalvit, P. A. M. Neto, and F. D. Mazzitelli. *Fluctuations, Dissipation and the Dynamical Casimir Effect*, page 419–457. Springer Berlin Heidelberg, 2011.

[121] M. R. R. Good, J. Foo, and E. V. Linder. Accelerating boundary analog of a Kerr black hole. *Classical and Quantum Gravity*, 38(8):085011, March 2021.

[122] M. R. R. Good and Y. C. Ong. Particle spectrum of the Reissner–Nordström black hole. *Eur. Phys. J. C*, 80(12), December 2020.

[123] M. R. R. Good, A. Zhakenuly, and E. V. Linder. Mirror at the edge of the universe: Reflections on an accelerated boundary correspondence with de Sitter cosmology. *Phys. Rev. D*, 102:045020, Aug 2020.

[124] W. Rindler. Hyperbolic motion in curved space time. *Phys. Rev.*, 119:2082–2089, Sep 1960.

[125] L. C. B. Crispino, A. Higuchi, and G. E. A. Matsas. The Unruh effect and its applications. *Rev. Mod. Phys.*, 80:787–838, Jul 2008.

[126] B. S. DeWitt. Quantum gravity: The new synthesis. In S. Hawking and W. Israel, editors, *General Relativity: an Einstein Centenary Survey*. Cambridge University Press, Cambridge, England, 1979.

[127] E. Martín-Martínez, T. R. Perche, and B. de S. L. Torres. General relativistic quantum optics: Finite-size particle detector models in curved spacetimes. *Phys. Rev. D*, 101:045017, Feb 2020.

[128] T. Rick Perche and J. Neuser. A wavefunction description for a localized quantum particle in curved spacetimes. *Classical and Quantum Gravity*, 38(17):175002, aug 2021.

[129] T. R. Perche. General features of the thermalization of particle detectors and the Unruh effect. *Phys. Rev. D*, 104:065001, Sep 2021.

[130] C. J. Fewster, B. A. Juárez-Aubry, and J. Louko. Waiting for Unruh. *Classical and Quantum Gravity*, 33(16):165003, July 2016.

[131] B. A. Juárez-Aubry and J. Louko. Onset and decay of the $1 + 1$ Hawking–Unruh effect: what the derivative-coupling detector saw. *Classical and Quantum Gravity*, 31(24):245007, November 2014.

[132] S. Biermann et al. Unruh and analogue Unruh temperatures for circular motion in $3+1$ and $2+1$ dimensions. *Phys. Rev. D*, 102:085006, Oct 2020.

[133] C. R. D. Bunney et al. Third sound detectors in accelerated motion. *New Journal of Physics*, 26(6):065001, June 2024.

[134] L. J. Parry and J. Louko. Connecting the circular and drifted Rindler Unruh effects. *Phys. Rev. D*, 111(2), January 2025.

[135] S. Bose, A. Mazumdar, M. Schut, and M. Toroš. Mechanism for the quantum natured gravitons to entangle masses. *Phys. Rev. D*, 105:106028, May 2022.

[136] C. H. Bennett and S. J. Wiesner. Communication via one and two particle operators on Einstein-Podolsky-Rosen states. *Phys. Rev. Letters*, 69(20):2881–2884, 1992.

[137] S. Pirandola et al. Advances in quantum teleportation. *Nature Photonics*, 9:641–652, 2015.

[138] M. M. Wilde. *Quantum Information Theory.* Cambridge University Press, 2nd edition, 2017.

[139] S. Lloyd. Capacity of the noisy quantum channel. *Phys. Rev. A*, 55(3):1613–1622, 1997.

[140] A. S. Holevo. The capacity of the quantum channel with general signal states. *IEEE Transactions on Information Theory*, 44(1):269–273, 1998.

[141] A. S. Holevo. One-mode quantum Gaussian channels: Structure and quantum capacity. *Problems of Information Transmission*, 43(1):1–11, 2007.

[142] C. Lupo, S. Pirandola, P. Aniello, and S. Mancini. On the classical capacity of quantum gaussian channels. *Physica Scripta*, T143:014016, February 2011.

[143] O. V. Pilyavets, C. Lupo, and S. Mancini. Methods for estimating capacities and rates of Gaussian quantum channels. *IEEE Transactions on Information Theory*, 58(9):6126–6164, sep 2012.

[144] A. Serafini. *Quantum Continuous Variables: A Primer of Theoretical Methods*. CRC Press, Taylor & Francis Group, Boca Raton, FL, 1st edition, 2017.

[145] S. Ghose and B. C. Sanders. Non-Gaussian ancilla states for continuous variable quantum computation via Gaussian maps. *Journal of Modern Optics*, 54(6):855–869, 2007.

[146] M. Gu et al. Quantum computing with continuous-variable clusters. *Phys. Rev. A*, 79:062318, Jun 2009.

[147] S. Olivares. Quantum optics in the phase space. *Eur. Phys. J. Special Topics*, 203(1):3–24, 2012.

[148] N. Quesada and A. M. Brańczyk. Gaussian functions are optimal for waveguided nonlinear-quantum-optical processes. *Phys. Rev. A*, 98:043813, Oct 2018.

[149] C. Oh, C. Lee, S. H. Lie, and H. Jeong. Optimal distributed quantum sensing using Gaussian states. *Phys. Rev. Res.*, 2:023030, Apr 2020.

[150] V. Giovannetti, A. S. Holevo, and R. García-Patrón. A solution of Gaussian optimizer conjecture for quantum channels. *Communications in Mathematical Physics*, 334(3):1553–1571, August 2014.

[151] J. B. Brask. Gaussian states and operations – a quick reference, 2022.

[152] F. Caruso, V. Giovannetti, and A. S. Holevo. One-mode bosonic Gaussian channels: a full weak-degradability classification. *New Journal of Physics*, 8(12):310, dec 2006.

[153] F. Caruso, J. Eisert, V. Giovannetti, and A. S. Holevo. Multi-mode bosonic Gaussian channels. *New Journal of Physics*, 10(8):083030, August 2008.

[154] G. De Palma. New lower bounds to the output entropy of multi-mode quantum Gaussian channels. *IEEE Transactions on Information Theory*, 65(9):5959–5968, September 2019.

[155] A. Holevo. One-mode quantum Gaussian channels. 08 2006.

[156] G. Gianfelici and S. Mancini. Quantum channels from reflections on moving mirrors. *Scientific Reports*, 7(1), Nov 2017.

[157] J. Williamson. On the algebraic problem concerning the normal forms of linear dynamical systems. *American Journal of Mathematics*, 58(1):141–163, 1936.

[158] K. Brádler. Coherent information of one-mode Gaussian channels—the general case of non-zero added classical noise. *Journal of Physics A: Mathematical and Theoretical*, 48(12):125301, March 2015.

[159] V. Bužek and M. Hillery. Quantum copying: Beyond the no-cloning theorem. *Phys. Rev. A*, 54:1844–1852, Sep 1996.

[160] J. Laurat et al. Entanglement of two-mode Gaussian states: characterization and experimental production and manipulation. *Journal of Optics B: Quantum and Semiclassical Optics*, 7(12):S577–S587, November 2005.

[161] E. Di Valentino et Al. The cosmoverse white paper: Addressing observational tensions in cosmology with systematics and fundamental physics, 2025.

[162] Y. Zhong et al. Deterministic multi-qubit entanglement in a quantum network. *Nature*, 590(7847):571–575, February 2021.

[163] R. Durrer. The cosmic microwave background: The history of its experimental investigation and its significance for cosmology. *Class. Quantum Grav.*, 32(12):124007, June 2015.

[164] M. C. Guzzetti, N. Bartolo, and S. M. Liguori. Gravitational waves from inflation. *Riv. Nuovo Cimento*, 39(9):399–495, August 2016.

[165] S. Mancini, R. Pierini, and M. M. Wilde. Preserving information from the beginning to the end of time in a Robertson–Walker spacetime. *New Journal of Physics*, 16(12):123049, December 2014.

[166] L. et Al. Cluster density profiles as a test of modified gravity. *Phys. Rev. D*, 85(10):102001, May 2012.

[167] M. Reina-Campos, A. Sills, and G. Bichon. Initial sizes of star clusters: implications for cluster dissolution during galaxy evolution. *Mon. Not. R. Astron. Soc.*, 524(1):968–980, September 2023.

[168] S. Nojiri and S. Odintsov. Is the future universe singular: Dark matter versus modified gravity? *Phys. Lett. B*, 686(1):44–48, March 2010.

[169] Z. Davari and S. Rahvar. Testing modified gravity (MOG) theory and dark matter model in Milky Way using the local observables. *Mon. Not. R. Astron. Soc.*, 496(3):3502–3511, August 2020.

[170] M. Adak, Ö. Sert, M. Kalay, and M. Sari. Symmetric teleparallel gravity: some exact solutions and spinor couplings. *Int. J. Mod. Phys. A*, 28(32):1350167, December 2013.

[171] J. Jimenez, L. Heisenberg, and T. Koivisto. The geometrical trinity of gravity. *Universe*, 5(7):173, July 2019.

[172] S. Capozziello, V. De Falco, and C. Ferrara. The role of the boundary term in $f(Q,B)$ symmetric teleparallel gravity. *Eur. Phys. J. C*, 83(10):1–8, October 2023. Published online 10 October 2023.

[173] J. B. Jiménez, L. Heisenberg, and T. S. Koivisto. Teleparallel Palatini theories. *J. Cosmol. Astrop. P.*, 2018(08):039–039, August 2018.

[174] S. Bahamonde and L. Järv. Coincident gauge for static spherical field configurations in symmetric teleparallel gravity. *Eur. Phys. J. C*, 82(10):963, October 2022.

[175] J. B. Jiménez, L. Heisenberg, T. Koivisto, and S. Pekar. Cosmology in $f(Q)$ geometry. *Phys. Rev. D*, 101(10):103507, May 2020.

[176] I. S. Albuquerque and N. Frusciante. A designer approach to $f(Q)$ gravity and cosmological implications. *Phys. Dark Universe*, 35:100980, March 2022.

[177] W. Khyllep, J. Dutta, E. N. Saridakis, and K. Yesmakhanova. Cosmology in $f(Q)$ gravity: A unified dynamical systems analysis of the background and perturbations. *Phys. Rev. D*, 107(4):044022, February 2023.

[178] S. Mandal, D. Wang, and P. Sahoo. Cosmography in $f(Q)$ gravity. *Phys. Rev. D*, 102(12):124029, December 2020.

[179] L. Heisenberg. Review on $f(Q)$ gravity. *Phys. Rept.*, 1066:1–78, May 2024.

[180] S. Maurya, K. Singh, S. Lohakare, and B. Mishra. Anisotropic strange star model beyond standard maximum mass limit by gravitational decoupling in $f(Q)$ gravity. *Fortschritte der Physik*, 70(11):2200061, September 2022.

[181] P. Bhar, S. Pradhan, A. Malik, and P. Sahoo. Physical characteristics and maximum allowable mass of hybrid star in the context of $f(Q)$ gravity. *Eur. Phys. J. C*, 83(7):646, July 2023.

[182] S. Capozziello, M. Capriolo, and S. Nojiri. Gravitational waves in $f(Q)$ non-metric gravity via geodesic deviation. *Phys. Lett. B*, 850:138510, March 2024.

[183] S. Capozziello and M. Capriolo. Gravitational waves in $f(Q)$ non-metric gravity without gauge fixing. *Phys. Dark Univ.*, 45:101548, June 2024.

[184] S. Capozziello and R. D'Agostino. Model-independent reconstruction of $f(Q)$ non-metric gravity. *Phys. Lett. B*, 832:137229, September 2022.

[185] S. Capozziello and M. Shokri. Slow-roll inflation in $f(Q)$ non-metric gravity. *Phys. Dark Univ.*, 37:101113, 2022.

[186] S. Nojiri and S. D. Odintsov. Well-defined $f(Q)$ gravity, reconstruction of FLRW spacetime and unification of inflation with dark energy epoch. *Phys. Dark Univ.*, 45:101538, April 2024.

[187] I. Ayuso, R. Lazkoz, and V. Salzano. Observational constraints on cosmological solutions of $f(Q)$ theories. *Phys. Rev. D*, 103(6):063505, March 2021.

[188] F. Anagnostopoulos, S. Basilakos, and E. Saridakis. First evidence that non-metricity $f(Q)$ gravity could challenge Lambda-CDM. *Phys. Lett. B*, 822(4):136634, November 2021.

[189] F. Anagnostopoulos, V. Gakis, E. Saridakis, and S. Basilakos. New models and big bang nucleosynthesis constraints in $f(Q)$ gravity. *Eur. Phys. J. C*, 83(1), January 2023.

[190] M. Benetti, S. Capozziello, and G. Lambiase. Updating constraints on $f(T)$ teleparallel cosmology and the consistency with Big Bang Nucleosynthesis. *Mon. Not. Roy. Astron. Soc.*, 500(2):1795–1805, June 2020.

[191] S. Capozziello, G. Lambiase, and E. N. Saridakis. Constraining $f(T)$ teleparallel gravity by Big Bang Nucleosynthesis. *Eur. Phys. J. C*, 77(9):576, August 2017.

[192] A. Aviles, C. Gruber, O. Luongo, and H. Quevedo. Cosmography and constraints on the equation of state of the universe in various parametrizations. *Phys. Rev. D*, 86(12):123516, December 2012.

[193] C. Gruber and O. Luongo. Cosmographic analysis of the equation of state of the universe through Padé approximations. *Phys. Rev. D*, 89(10):103506, May 2014.

[194] O. Luongo, G. Pisani, and A. Troisi. Cosmological degeneracy versus cosmography: A cosmographic dark energy model. *Int. J. Mod. Phys. D*, 26(03):1750015, August 2017.

[195] S. Capozziello, P. Dunsby, and O. Luongo. Model-independent reconstruction of cosmological accelerated–decelerated phase. *Mon. Not. R. Astron. Soc.*, 509(4):5399–5415, November 2021.

[196] S. Capozziello, R. D'Agostino, and O. Luongo. Thermodynamic parametrization of dark energy. *Phys. Dark Universe*, 36:101045, June 2022.

[197] M. Muccino et Al. Tracing dark energy history with Gamma-Ray Bursts. *Astrophys. J.*, 908(2):181, February 2021.

[198] O. Luongo and S. Mancini. Entanglement in model-independent cosmological scenario. *Int. J. Geom. Methods Mod. Phys.*, 16(08):1950114, June 2019.

[199] E. W. Kolb and A. J. Long. Cosmological gravitational particle production and its implications for cosmological relics. *Rev. Mod. Phys.*, 96:045005, Nov 2024.

[200] J. L. Ball, I. Fuentes-Schuller, and F. P. Schuller. Entanglement in an expanding spacetime. *Phys. Lett. A*, 359(6):550–554, December 2006.

[201] I. Fuentes, R. B. Mann, E. Martín-Martínez, and S. Moradi. Entanglement of Dirac fields in an expanding spacetime. *Phys. Rev. D*, 82(4):045030, August 2010.

[202] E. Martín-Martínez and N. C. Menicucci. Cosmological quantum entanglement. *Class. Quantum Grav.*, 29(22):224003, October 2012.

[203] J. H. Apfel. Phase retardance of periodic multilayer mirrors. *Appl. Opt.*, 21(4):733–738, Feb 1982.

[204] G. Barton and A. Calogeracos. On the quantum electrodynamics of a dispersive mirror.: I. mass shifts, radiation, and radiative reaction. *Annals of Physics*, 238(2):227 – 267, 1995.

[205] N. Nicolaevici. Semitransparency effects in the moving mirror model for Hawking radiation. *Phys. Rev. D*, 80:125003, Dec 2009.

[206] J. Haro and E. Elizalde. Black hole collapse simulated by vacuum fluctuations with a moving semitransparent mirror. *Phys. Rev. D*, 77(4), February 2008.

[207] R. D. Carlitz and R. S. Willey. Lifetime of a black hole. *Phys. Rev. D*, 36:2336–2341, Oct 1987.

[208] J. Zhang. Black hole quantum tunnelling and black hole entropy correction. *Physics Letters B*, 668(5):353–356, 2008.

[209] S. Capozziello, S. De Bianchi, and E. Battista. Avoiding singularities in Lorentzian-Euclidean black holes: The role of atemporality. *Phys. Rev. D*, 109(10), May 2024.

[210] D. Malyshev, C. Johnson, S. Ritz, and S. Funk. Fermi-LAT limit on individual primordial black holes. page 169, 12 2017.

[211] M. Ackermann et al. Search for gamma-ray emission from local primordial black holes with the Fermi large area telescope. *The Astrophysical Journal*, 857(1):49, apr 2018.

[212] B. Mayer et al. Ab-initio calculation of the elastic constants and thermal expansion coefficients of laves phases. *Intermetallics*, 11(1):23–32, 2003.

[213] S. D. Odintsov, V. K. Oikonomou, A. V. Timoshkin, Emmanuel N. Saridakis, and R. Myrzakulov. Cosmological Fluids with Logarithmic Equation of State. *Annals Phys.*, 398:238–253, 2018.

[214] R. C. Tolman. Static solutions of Einstein's field equations for spheres of fluid. *Phys. Rev.*, 55:364–373, 1939.

[215] J. R. Oppenheimer and G. M. Volkoff. On massive neutron cores. *Phys. Rev.*, 55:374–381, 1939.

[216] S. Capozziello, R. D'Agostino, and D. Gregoris. Black holes and naked singularities from Anton–Schmidt's fluids. *Phys. Dark Univ.*, 28:100513, 2020.

[217] U. Debnath. Thermodynamic Black Hole with Modified Chaplygin Gas as a Heat Engine. *Eur. Phys. J. Plus*, 135(6):424, 2020.

[218] A. Y. Kamenshchik, U. Moschella, and V. Pasquier. An Alternative to quintessence. *Phys. Lett. B*, 511:265–268, 2001.

[219] L. Diósi. A universal master equation for the gravitational violation of quantum mechanics. *Physics Letters A*, 120(8):377–381, 1987.

[220] R. Penrose. On gravity's role in quantum state reduction. *Gen. Rel. Grav*, 28:581–600, 1996.

[221] I. Pikovski, M. Zych, F. Costa, and Časlav Brukner. Universal decoherence due to gravitational time dilation. *Nature Physics*, 11(8):668–672, June 2015.

[222] S. Mikki. Proca metamaterials, massive electromagnetism, and spatial dispersion. *Annalen der Physik*, 533:2000625, 06 2021.

[223] A. G. S. Landulfo. Nonperturbative approach to relativistic quantum communication channels. *Phys. Rev. D*, 93:104019, May 2016.

[224] I. B. Barcellos and A. G. S. Landulfo. Relativistic quantum communication: Energy cost and channel capacities. *Phys. Rev. D*, 104:105018, Nov 2021.

[225] E. Tjoa and K. Gallock-Yoshimura. Channel capacity of relativistic quantum communication with rapid interaction. *Phys. Rev. D*, 105:085011, Apr 2022.

[226] D. J. Raine, D. W. Sciama, and P. G. Grove. Does a uniformly accelerated quantum oscillator radiate? *Proceedings of the Royal Society of London. Series A: Mathematical and Physical Sciences*, 435(1893):205–215, October 1991.

[227] E. G. Brown, E. Martín-Martínez, N. C. Menicucci, and R. B. Mann. Detectors for probing relativistic quantum physics beyond perturbation theory. *Phys. Rev. D*, 87:084062, Apr 2013.

[228] C. Misner, K. Thorne, J. Wheeler, and D. Kaiser. *Gravitation.* Princeton University Press, 2017.

[229] A. Caldeira and A. Leggett. Path integral approach to quantum Brownian motion. *Physica A: Statistical Mechanics and its Applications*, 121(3):587–616, 1983.

[230] H.-P. Breuer and F. Petruccione. *The Theory of Open Quantum Systems*. 01 2006.

[231] L. Buxton, M.-T. Russo, J. Al-Khalili, and A. Rocco. Quantum Brownian motion in the caldeira-leggett model with a damped environment. *arXiv:2303.09516*, 2023.

[232] C. Bunney, L. Parry, T. Perche, and J. Louko. Ambient temperature versus ambient acceleration in the circular motion Unruh effect. *Phys. Rev. D*, 109(6):065001, Mar 2024.

[233] C. Bunney and J. Louko. Circular motion analogue Unruh effect in a 2+1 thermal bath: robbing from the rich and giving to the poor. *Classical and Quantum Gravity*, 40(15):155001, June 2023.

[234] T. Kodama and T. Takahashi. Relaxing inflation models with nonminimal coupling: A general study. *Phys. Rev. D*, 105:063542, Mar 2022.

[235] Q. Gao, Y. Gong, Z. Yi, and F. Zhang. Non-minimal coupling in light of act. *arXiv:2504.15218*, 2025.

[236] P. K. S. Dunsby and O. Luongo. On the theory and applications of modern cosmography. *Int. J. Geom. Meth. Mod. Phys.*, 13(03):1630002, January 2016.

[237] J. Ellis and D. Wands. Inflation (2023). *arXiv:2312.13238*, December 2023.

[238] M. Brune, E. Hagley, J. Dreyer, X. Maître, A. Maali, C. Wunderlich, J. M. Raimond, and S. Haroche. Observing the progressive decoherence of the "meter" in a quantum measurement. *Phys. Rev. Lett.*, 77:4887–4890, Dec 1996.

[239] C. J. Myatt et al. Decoherence of quantum superpositions through coupling to engineered reservoirs. *Nature*, 403(6767):269–273, 2000.

[240] K. Hornberger et al. Collisional decoherence observed in matter wave interferometry. *Phys. Rev. Lett.*, 90:160401, Apr 2003.

[241] G. Cole et al. Phonon-tunnelling dissipation in mechanical resonators. *Nature Communications*, 2:231, 2011.

[242] C. Marletto and V. Vedral. Gravitationally induced entanglement between two massive particles is sufficient evidence of quantum effects in gravity. *Phys. Rev. Letters*, 119(24), December 2017.

[243] M. Schlosshauer. Quantum decoherence. *Phys. Rep.*, 831:1–57, October 2019.

[244] K. Kraus. *States, Effects and Operations: Fundamental Notions of Quantum Theory*, volume 190 of *Lecture Notes in Physics*. Springer-Verlag, Berlin, Heidelberg, 1983.

[245] D. W. Leung. Choi's proof as a recipe for quantum process tomography. *Journal of Mathematical Physics*, 44(2):528–533, January 2003.

[246] A. D'Arrigo, G. Benenti, and G. Falci. Quantum capacity of dephasing channels with memory. *New Journal of Physics*, 9(9):310–310, September 2007.

[247] S. Mancini and A. Winter. *A Quantum Leap in Information Theory*. World Scientific Publishing Company, 2020.

[248] T. S. Cubitt, M. B. Ruskai, and G. Smith. The structure of degradable quantum channels. *Journal of Mathematical Physics*, 49(10), October 2008.

[249] V. Billault et al. Free space optical communication receiver based on a spatial demultiplexer and a photonic integrated coherent combining circuit. *Optics Express*, 29(21):33134, September 2021.

[250] P. Jain, S. Weinfurtner, M. Visser, and C. Gardiner. Analog model of a Friedmann-Robertson-Walker universe in Bose-Einstein condensates: Application of the classical field method. *Phys. Rev. A*, 76(3):033616, September 2007.

[251] N. Barnaby and Z. Huang. Particle production during inflation: Observational constraints and signatures. *Phys. Rev. D*, 80(12), December 2009.

[252] E. W. Kolb, S. Ling, A. J. Long, and R. A. Rosen. Cosmological gravitational particle production of massive spin-2 particles. *J. High Energy Phys.*, 181(5), May 2023.

[253] J. Cembranos, L. Garay, Á. Parra-López, and J. Sánchez Velázquez. Late vacuum choice and slow roll approximation in gravitational particle production during reheating. *J. Cosmol. Astrop. P.*, 2023(08):060, August 2023.

[254] L. Li et al. Gravitational production of superheavy dark matter and associated cosmological signatures. *J. High Energy Phys.*, 2019(67), July 2019.

[255] L. Li, S. Lu, Y. Wang, and S. Zhou. Cosmological signatures of superheavy dark matter. *J. High Energy Phys.*, 2020(231), July 2020.

[256] Z. Safari, K. Rezazadeh, and B. Malekolkalami. Structure formation in dark matter particle production cosmology. *Phys. Dark Universe*, 37:101092, September 2022.

[257] L. Norder et al. Pentagonal photonic crystal mirrors: Scalable lightsails with enhanced acceleration via neural topology optimization. *arXiv:2407.07896*, 2024. Submitted to Phys. Rev. Applied.

[258] V. Cardoso and Paolo Pani. Testing the nature of dark compact objects: a status report. *Living Rev. Rel.*, 22(1):4, 2019.

[259] R. D'Agostino, R. Giambò, and O. Luongo. Constraining primordial black holes as fraction of dark matter through accretion disk luminosity. *arXiv:2204.02098*, 4 2022.

[260] K. Boshkayev, T. Konysbayev, Y. Kurmanov, O. Luongo, and D. Malafarina. Accretion disk luminosity for black holes surrounded by dark matter with tangential pressure. *arXiv:2205.04208*, 5 2022.

[261] E. Kurmanov et al. Accretion Disk Luminosity for Black Holes Surrounded by Dark Matter with Anisotropic Pressure. *Astrophys. J.*, 925(2):210, 2022.

[262] K. Boshkayev et al. Luminosity of accretion disks in compact objects with a quadrupole. *Phys. Rev. D*, 104(8):084009, 2021.

[263] K. Boshkayev, A. Idrissov, O. Luongo, and D. Malafarina. Accretion disc luminosity for black holes surrounded by dark matter. *Mon. Not. Roy. Astron. Soc.*, 496(2):1115–1123, 2020.

[264] J. Louko and A. Satz. How often does the Unruh–DeWitt detector click? Regularization by a spatial profile. *Class. Quant. Grav.*, 23(22):6321–6343, October 2006.

[265] Z. Tian, J. Jing, and A. Dragan. Analog cosmological particle generation in a superconducting circuit. *Phys. Rev. D*, 95(12):125003, June 2017.

[266] J. et Al. Analogue cosmological particle creation in an ultracold quantum fluid of light. *Nat. Comm.*, 13(1), May 2022.

[267] V. Zapatero, T. van Leent, R. Arnon-Friedman, et al. Advances in device-independent quantum key distribution. *npj Quantum Information*, 9(10):1–14, 2023.

[268] B. Reznik. Entanglement from the vacuum. *Foundations of Physics*, 33, 01 2003.

[269] T. R. Perche, J. Polo-Gómez, B. de S. Torres, and E. Martín-Martínez. Fully relativistic entanglement harvesting. *Phys. Rev. D*, 109(4), February 2024.

[270] F. de Felice and C. Clarke. *Relativity on Curved Manifolds.* Cambridge Monographs on Mathematical Physics. Cambridge University Press, 1992.

[271] A. Rajagopal, D. Kubizňák, and R. B. Mann. Van der Waals black hole. *Phys. Lett. B*, 737:277–279, 2014.

[272] M. R. Setare and H. Adami. Polytropic black hole. *Phys. Rev. D*, 91(8):084014, 2015.

[273] L. Perivolaropoulos and F. Skara. Challenges for ΛCDM: An update. *New Astron. Rev.*, 95, 2022.

Appendix A

Calculation for black hole solutions in Anton-Schmidt fluids

Contents

To compute Eq. (3.151), the following form ansatz is assumed for the function h, i.e.

$$h(r,\rho) = \sum_i X_i(r) R_i(\rho) \,. \tag{A.1}$$

By inserting Eq. (A.1) into Eq. (3.151), one has an equation with the following form

$$\sum_j \xi_j(r) F_j(\rho) = 0 \,. \tag{A.2}$$

At this point, the equations $\{\xi_j(r)F_j(\rho) = 0\}_j$ can be separately solved for each j (provided $\{F_j\}_j$ are linear independent) to get the functions $X_i(r)$ from the equations $\{\xi_j(r) = 0\}_j$. Those equations could be algebraic or differential. In particular, $\xi_j = 0$ is differential if $F_j(\rho)$ is present in the third term of the left-hand side of Eq. (3.151) and algebraic otherwise.

To generalize the final solution as much as possible, the number of differential equations on the set $\{\xi_j(r) = 0\}_j$ must be maximized over the algebraic ones - since the former give free integration constants. Therefore, the functions $R_i(\rho)$ are chosen such that all the independent functions of ρ, present in the first and second term of Eq. (3.151) are present in the third term as well. One can check that this condition is verified by choosing $R_1 = 1$, $R_2 = \varrho$, $R_3 = P_1$, $R_4 = P_2$, $R_5 = b(\varrho)$, where $P_1 = \left(\frac{\varrho}{\varrho^\star}\right)^{-n} \ln \varrho$ and $P_2 = \left(\frac{\varrho}{\varrho^\star}\right)^{-n}$ and $b(\varrho)$ is a function satisfying

$$P_\rho b(\rho) = B_1 \rho + B_2 \rho b_\rho + B_3 P b_\rho \,, \tag{A.3}$$

for generic constants B_1, B_2 and B_3. At this point, one has

$$h(r,\rho) = X_1(r) + X_2(r)\rho + X_3(r)P_1 + X_4(r)P_2 + X_5(r)b(\rho) \,. \tag{A.4}$$

By putting Eq. (A.4) into Eq. (3.151), a set of equations for the functions $X_i(r)$ and the parameters B_1, B_2 and B_3 - for the function $b(\rho)$ from Eq. (A.3) - is obtained. They lead to the following results: $X_1 = \frac{c_1}{r}$, $B_1 = 0$, $B_2 = B_3 =: \beta$, $X_2 = 0$, $X_3 = \frac{8}{3}\pi r^2 A$, $X_4 = -\frac{8}{3}\pi r^2 A \ln \varrho^\star$, $X_5 = c_2 r^{\frac{2}{B_2}-1}$, leading to our final solution for $h(r, \varrho)$

$$h(r,\rho) = \frac{c_1}{r} + \frac{8}{3}\pi r^2 P(\rho) + c_2 r^{\frac{2}{\beta}-1}(a(\rho))^{1/\beta}\,. \tag{A.5}$$

where c_1, c_2 and β are free parameters and

$$a(\rho) \equiv \exp\left(\int \frac{P_\rho}{P+\rho}\, d\rho\right). \tag{A.6}$$

A.1 Metric solutions and Energy conditions

By putting $h(r,\rho)$ from Eq. (A.5) into Eq. (A.1), the solutions for $f(r,\rho)$ is finally found as

$$f(r,\rho) = -\frac{2M+c_1}{r} - c_2 r^{\frac{2}{\beta}-1} a(\rho)^{1/\beta}\,. \tag{A.7}$$

The parameters c_1, c_2 are now restricted to have a valid black hole solution and whose induced background satisfies the energy conditions.

c_1 has the only effect to modify the effective value of the black hole mass. Therefore, $c_1 = 0$ can be safely set. In order to obtain an event horizon, the existence of r_h so that $f(r_h,\rho) = 0$ must be imposed, namely

$$r_h = \left(\frac{2M}{-c_2}\right)^{\frac{\beta}{2}} \frac{1}{\sqrt{a(\rho)}}\,, \tag{A.8}$$

which requires $c_2 < 0$. From Eq. (A.8), $|c_2|$ has the only effect to scale the event horizon with the mass. Therefore, for the sake of simplicity $|c_2| = 1$, i.e. $c_2 = -1$ can be considered without loss of generality.

A further condition to have a valid black hole horizon is that $f(r \to r_\mathrm{h}, \rho) \to 0^+$ - giving the metric well-defined outside but not inside. $f(r,\rho)$ is thus required to be positive in the range $r > r_h$. This leads to the following inequality for β

$$\frac{2M}{r_h^2} + r_h^{\frac{2}{\beta}-2}\left(\frac{2}{\beta} - 1\right)(a(\rho))^{1/\beta} > 0\,. \tag{A.9}$$

By putting the value of r_h from Eq. (A.8) into (A.9), one has

$$(2M)^{1-\beta} a(\rho) + (2M)^{1-\beta}\left(\frac{2}{\beta} - 1\right) a(\rho) > 0\,, \tag{A.10}$$

leading to $\beta > 0$.

A.2 Matching the energy conditions

By putting Eq. (A.7) into the Einstein equations (2.12), a stress-energy tensor different from the vacuum is obtained. The matter induced by the black hole solution have to match the energy conditions reported in Sec. 2.2. In the tetrad formalism [270], the stress-energy tensor can be written as

$$T^{\mu\nu} = \rho e_0^\mu e_0^\nu + \sum_{i=1}^{3} p_i e_i^\mu e_i^\nu \,. \tag{A.11}$$

By putting a generic spherical line element (2.56) into the Einstein equations (2.12), one has the following values for ρ, p_1, p_2 and p_3, i.e. [271, 272, 217]

$$\rho_e = -p_1 = \frac{1 - f - rf'}{8\pi r^2} + P \,, \tag{A.12}$$

$$p_2 = p_3 = \frac{rf'' + 2f'}{16\pi r} - P \,. \tag{A.13}$$

Here, p_1 and $p_2 = p_3 = p_{\text{tr}}$ are respectively the longitudinal and transversal pressure. The term P in Eqs. (A.12) and (A.13) is provided by the cosmological constant in Einstein's field equations (2.12).

After simple manipulations, Eqs. (A.12) and (A.13) lead to

$$\rho = P - \frac{a(\varrho)^{1/\beta}}{4\pi\beta} r^{\frac{2}{\beta}-3} + \frac{1}{8\pi r^2} \,, \tag{A.14}$$

$$p_{tr} = \left(\frac{1}{\beta} - \frac{1}{2}\right) \frac{a(\varrho)^{1/\beta}}{4\pi\beta} r^{\frac{2}{\beta}-3} - P \,, \tag{A.15}$$

One can prove that there is only one metric function $f(r, \rho)$ satisfying all of the energy conditions. In particular, the weak energy condition reads

$$P - \frac{a(\rho)^{1/\beta}}{4\pi\beta} r^{\frac{2}{\beta}-3} + \frac{1}{8\pi r^2} \geq 0 \,, \tag{A.16}$$

while the strong one becomes

$$\left(\frac{1}{\beta} - \frac{1}{2}\right) \frac{a(\rho)^{1/\beta}}{4\pi\beta} r^{\frac{2}{\beta}-3} - P \geq 0 \,. \tag{A.17}$$

For the null one

$$\varrho + p_{tr} = \frac{1}{8\pi r^2} + \left(\frac{1}{\beta} - \frac{3}{2}\right) \frac{a(\rho)^{1/\beta}}{4\pi\beta} r^{\frac{2}{\beta}-3} \geq 0 \,. \tag{A.18}$$

Finally, the inequality for the dominant energy condition depends on the sign of the longitudinal and transverse pressures. In the case examined, if Eq. (A.17) is satisfied, then the DEC becomes

$$2P + \frac{1}{8\pi r^2} - \left(\frac{1}{\beta} + \frac{1}{2}\right) \frac{a(\rho)^{1/\beta}}{4\pi\beta} r^{\frac{2}{\beta}-3} \geq 0 \,. \tag{A.19}$$

Different situations arise depending on the values of β.

1. $0 < \beta < 2/3$. In this case, the term $\frac{a(\rho)^{1/\beta}}{4\pi\beta} r^{\frac{2}{\beta}-3}$ in Eq. (A.16) dominates when r is high, since $\frac{2}{\beta} - 3 > 2$. However, this term is also negative, therefore Eq. (A.16) is not satisfied for high radii.

2. $2/3 < \beta \leq 2$. One can easily prove that, is this case, Eq. (A.16) is satisfied when

$$P(\rho) r^2 - \frac{a(\rho)^{1/\beta}}{4\pi\beta} r^{\frac{2}{\beta}-1} + \frac{1}{8\pi} \geq 0 \,. \tag{A.20}$$

Since $0 \leq \frac{2}{\beta} - 1 < 2$, Eq. (A.16) is satisfied both in the limits $r \to 0$ and $r \to \infty$. However, it may happen that Eq. (A.16) is not satisfied in a certain finite range of r. Nevertheless, by ignoring this possibility, Eq. (A.17) is certainly not satisfied for high radii, since the dominant term becomes $-P$.

3. $\beta > 2$. For small radii, a negative term in Eq. (A.16) dominating over the positive ones. Thus, weak energy condition is not satisfied for small radii.

4. $\beta = 2/3$. The weak and the strong energy conditions read, respectively from Eqs. (A.16) and (A.17),

$$P - \frac{3}{8\pi}a(\rho)^{3/2} + \frac{1}{8\pi r^2} \geq 0\,, \tag{A.21}$$

$$\frac{3}{8\pi}a(\rho)^{3/2} - P \geq 0\,. \tag{A.22}$$

Since they must be satisfied for all the radii, then

$$P(\rho) = \frac{3}{8\pi}a(\rho)^{3/2}. \tag{A.23}$$

Thus, $\varrho = -p_1 = \frac{1}{8\pi r^2}$ and $p_{tr} = 0$, which implies that also the null and dominant energy conditions (Eqs. (A.18) and (A.26)) are satisfied. The asymptotic anti-de Sitter spacetime is exactly recovered in this case. Indeed, by inserting Eq. (A.23) into Eq. (A.7), one has

$$f(r,\rho) = -\frac{2M}{r} + \frac{8}{3}\pi P(\rho) r^2\,. \tag{A.24}$$

The parameters of the Anton-Schmidt fluid emulating the situation $\beta = 2/3$ just described are restricted. From Eq. (A.23), since $a(\rho)$ is positive, it is clear that the pressure must be positive. By applying the logarithm on both sides of Eq. (A.23), one has

$$\frac{3}{2}\int \frac{P_\rho}{P+\rho}d\rho = \ln\left(\frac{8\pi}{3}P\right)\,, \tag{A.25}$$

where the definition in Eq. (A.6) has been used.

It is possible to solve Eq. (A.25) by simply computing the derivative w.r.t. ρ, from which one gets:

- a physical solution, namely $P = \text{const}$,
- a unphysical solution, namely $P = 2\rho$.

Even though the first case appears appealing, it just represents the widely-studied trivial cosmological constant case [273].

A.2.1 Relaxing the strong energy condition

In view of the aforementioned considerations, in what follows the strong energy condition (A.17) is relaxed, as often done in cosmological contexts (see the discussion in Sec. 2.2).

The range where the weak energy condition (A.16) is satisfied is $2/3 \leq \beta \leq 2$ previous a previous analysis. The strong energy condition (A.17) is not satisfied in this range, so that the null and dominant energy conditions coincide, both becoming

$$\left(\frac{1}{\beta} - \frac{3}{2}\right)\frac{a(\rho)^{1/\beta}}{4\pi\beta}r^{\frac{2}{\beta}-3} + \frac{1}{8\pi r^2} \geq 0\,. \tag{A.26}$$

The above condition is never satisfied when $2/3 < \beta < 2$, since the first term is negative in this range and it dominates over the second. The only possibilities are then $\beta = 2/3$ or $\beta = 2$. In the first case, the trivial case is recovered. Instead, if $\beta = 2$, Eqs. (A.16) and (A.18) are satisfied when $\frac{a(\rho)^{1/\beta}}{4\pi\beta} \leq \frac{1}{8\pi}$, implying

$$\exp\left(\frac{1}{2}\int \frac{P_\rho}{\rho + P}\, d\rho\right) \leq 1\,. \tag{A.27}$$

Applying the logarithm to both sides, one has

$$\int \frac{P_\rho}{\rho + P}\, d\rho \leq 0\,. \tag{A.28}$$

which is satisfied as long as the integral is upper-bounded.

In the case of the Anton-Schmidt and pure logotropic fluids, one has respectively

$$\frac{P_\rho}{P + \rho} = \frac{\frac{A}{\rho_*}\left(\frac{\rho}{\rho_*}\right)^{-n-1}\left[1 - n\ln\left(\frac{\rho}{\rho_*}\right)\right]}{\rho + A\left(\frac{\rho}{\rho_*}\right)^{-n}\ln\left(\frac{\rho}{\rho_*}\right)}\,, \tag{A.29}$$

and

$$\frac{P_\rho}{P + \rho} = \frac{A}{\rho\left[\rho + A\ln\left(\frac{\rho}{\rho_*}\right)\right]}\,. \tag{A.30}$$

The condition $P = \frac{|\Lambda|}{8\pi}$ ensures the positivity of $P(\rho)$ and, thus, $\rho > \rho_*$. The sign of the right side of Eq. (A.29) depends on the value of n:

- If $n > 0$, the numerator is positive for $\rho < \rho_* e^{1/n}$ and negative for $\rho > \rho_* e^{1/n}$. As a consequence, the function $\ln a(\rho)$ reaches its maximum at $\rho = \rho_*^{1/n}$, being upper-bounded, so that and condition (A.27) is satisfied.

- If $-1 < n \leq 0$, Eq. (A.29) and Eq. (A.30) are both always positive, and a maximum for $\ln a(\rho)$ cannot be found. However, it is easy to show that, when $\rho \gg \rho_*$, $\ln a(\rho)$ behaves as $\alpha - \frac{1}{\rho^{1+n}}$, where α is an integration constant. Since $n > -1$, then $\ln a(\rho)$ has an asymptote identified with α, and thus it is upper-bounded also in this case.

- If $n < -1$, one can easily prove that Eq. (A.29) is always positive. However, in this case, the second term of the denominator dominates over the first and the whole expression behaves as ρ^{-1} for large ρ. This means that $\ln a(\rho)$ increases always as $\ln(\rho)$, so it is not upper-bounded and the condition (A.27) is never satisfied.

Appendix B

Time evolution of a quantum particle in linearized quantum gravity

Contents

The aim is now to compute the matrix $\tilde{\rho}(t)$ by knowing that

$$\tilde{\rho}(0) = \begin{pmatrix} \alpha & \beta \\ \beta^* & 1-\alpha \end{pmatrix} . \tag{B.1}$$

By using the perturbative form for $\hat{\rho}_{\mathrm{SE}}$ from Eq. (4.168), one can write

$$\tilde{\rho}(t) = \tilde{\rho}(0) + \tilde{\rho}^{(1)}(t) + \tilde{\rho}^{(2)}(t) + \tilde{\rho}^{(3)}(t) + \tilde{\rho}^{(4)}(t) + \tilde{\rho}^{(5)}(t)\,, \tag{B.2}$$

where

$$\left(\tilde{\rho}^{(1)}\right)_{\mathrm{ij}}(t) := -\,i\,\langle 1_{\mathrm{i}}0_{\mathrm{E}}|\left[\langle 0_{\mathrm{G}}|\hat{H}^{\odot}_{1*}(t)|0_{\mathrm{G}}\rangle, \hat{\rho}_{\mathrm{SE}}(0)\right]|1_{\mathrm{j}}0_{\mathrm{E}}\rangle\ ; \tag{B.3a}$$

$$\left(\tilde{\rho}^{(2)}\right)_{\mathrm{ij}}(t) := \langle 1_{\mathrm{i}}0_{\mathrm{E}}|\int d^3k\ {}_{\mathrm{G}}\langle 1_{\mathbf{k}}|\hat{H}_{1*}(t)\hat{\rho}(0)\hat{H}^{\Phi}_{1*}(t)|1_{\mathbf{k}}\rangle_{\mathrm{G}}\,|1_{\mathrm{j}}0_{\mathrm{E}}\rangle\ ; \tag{B.3b}$$

$$\left(\tilde{\rho}^{(3)}\right)_{\mathrm{ij}}(t) := \langle 1_{\mathrm{i}}0_{\mathrm{E}}|\,\langle 0_{\mathrm{G}}|\,\hat{H}^{\odot}_{1*}\,|0_{\mathrm{G}}\rangle\,\hat{\rho}_{\mathrm{SE}}(0)\,\langle 0_{\mathrm{G}}|\,\hat{H}^{\odot}_{1*}\,|0_{\mathrm{G}}\rangle\,|1_{\mathrm{j}}0_{\mathrm{E}}\rangle\ ; \tag{B.3c}$$

$$\left(\tilde{\rho}^{(4)}\right)_{\mathrm{ij}}(t) := -\,\langle 1_{\mathrm{i}}0_{\mathrm{E}}|\left(\langle 0_{\mathrm{G}}|\,\hat{H}^{\odot}_{2\leftarrow *}(t)\,|0_{\mathrm{G}}\rangle\,\hat{\rho}_{\mathrm{SE}}(0) + \hat{\rho}_{\mathrm{SE}}(0)\,\langle 0_{\mathrm{G}}|\,\hat{H}^{\odot}_{2\to *}(t)\,|0_{\mathrm{G}}\rangle\right)|1_{\mathrm{j}}0_{\mathrm{E}}\rangle \tag{B.3d}$$

$$\left(\tilde{\rho}^{(5)}\right)_{\mathrm{ij}}(t) := -\,\langle 1_{\mathrm{i}}0_{\mathrm{E}}|\left(\langle 0_{\mathrm{G}}|\,\hat{H}^{\Phi}_{2\leftarrow *}(t)\,|0_{\mathrm{G}}\rangle\,\hat{\rho}_{\mathrm{SE}}(0) + \hat{\rho}_{\mathrm{SE}}(0)\,\langle 0_{\mathrm{G}}|\,\hat{H}^{\Phi}_{2\to *}(t)\,|0_{\mathrm{G}}\rangle\right)|1_{\mathrm{j}}0_{\mathrm{E}}\rangle \tag{B.3e}$$

To proceed with the computation the natural units ($c = \hbar = 1$) are restored by dividing the masses m and $M_{\odot}$ by the Planck mass m_{P} (to restore the Planck units, one can simply put $m_{\mathrm{P}} = 1$).

The matrix $\tilde{\rho}^{(1)}$ is firstly computed from Eq. (B.3a). To this aim, the following is defined

$$h_{\mathrm{ij}} := \langle 1_{\mathrm{i}}0_{\mathrm{G}}|\,H_{1*}(t)\,|1_{\mathrm{j}}0_{\mathrm{G}}\rangle \tag{B.4}$$

$$\begin{aligned} &= \frac{3mM_{\odot}}{2\pi m_P^2}t\int\frac{\mathrm{d}\mathbf{p}\mathrm{d}\mathbf{p}'}{|\mathbf{p}-\mathbf{p}'|^{3/2}}\Gamma_{\mathbf{p}-\mathbf{p}'}(R)F^*_{\mathbf{k}_0}(\mathbf{p})F_{\mathbf{k}_0}(\mathbf{p}')e^{i\mathbf{x}_{\mathrm{i}}\cdot\mathbf{p}'-i\mathbf{x}_{\mathrm{j}}\cdot\mathbf{p}} \\ &+ \frac{3mM_{\odot}}{2\pi m_{\mathrm{P}}}\int\mathrm{d}\mathbf{p}\mathrm{d}\mathbf{p}'\frac{\sin(t|\mathbf{p}-\mathbf{p}'|)}{|\mathbf{p}-\mathbf{p}'|^{5/2}}\Gamma_{\mathbf{p}-\mathbf{p}'}(R)F^*_{\mathbf{k}_0}(\mathbf{p})F_{\mathbf{k}_0}(\mathbf{p}')e^{i\mathbf{x}_{\mathrm{i}}\cdot\mathbf{p}'-i\mathbf{x}_{\mathrm{j}}\cdot\mathbf{p}}\,. \end{aligned} \tag{B.5}$$

At this point, from Eq. (B.3a) one can write

$$\tilde{\rho}^{(1)} = \begin{pmatrix} -2\Im(\beta h_{\mathrm{BA}}) & -i\beta(h_{\mathrm{AA}} - h_{\mathrm{BB}}) - i(1-2\alpha)h_{\mathrm{AB}} \\ i\beta^*(h_{\mathrm{AA}} - h_{\mathrm{BB}}) + i\xi(1-2\alpha)h_{\mathrm{BA}} & 2\Im(\beta h_{\mathrm{BA}}) \end{pmatrix} . \tag{B.6}$$

Regarding $\tilde{\rho}^{(2)}$, since its contribution is independent from the presence of the planet, the only relevant distance is $\mathbf{L} := \mathbf{x}_{\mathrm{B}} - \mathbf{x}_{\mathrm{A}}$. In this way, algebraic calculations lead to

$$\begin{aligned}\tilde{\rho}^{(2)} = \int d\mathbf{q}d\mathbf{p}d\mathbf{p}'\mathfrak{F}(\mathbf{q},\mathbf{p},\mathbf{p}';t)\Bigg(\alpha\begin{pmatrix} 1 & e^{i\mathbf{L}\cdot\mathbf{p}'} \\ e^{-i\mathbf{L}\cdot\mathbf{p}} & e^{i\mathbf{L}\cdot(\mathbf{p}'-\mathbf{p})}\end{pmatrix} + \beta e^{-i\mathbf{L}\cdot\mathbf{q}}\begin{pmatrix} e^{-i\mathbf{L}\cdot\mathbf{p}'} & 1 \\ e^{i\mathbf{L}\cdot(\mathbf{p}'-\mathbf{p})} & e^{-i\mathbf{L}\cdot\mathbf{p}}\end{pmatrix} \\ +\beta^* e^{i\mathbf{L}\cdot\mathbf{q}}\begin{pmatrix} e^{i\mathbf{L}\cdot\mathbf{p}} & e^{i\mathbf{L}\cdot(\mathbf{p}-\mathbf{p}')} \\ 1 & e^{i\mathbf{L}\cdot\mathbf{p}'}\end{pmatrix} + (1-\alpha)\begin{pmatrix} e^{i\mathbf{L}\cdot(\mathbf{p}-\mathbf{p}')} & e^{i\mathbf{L}\cdot\mathbf{p}} \\ e^{-i\mathbf{L}\cdot\mathbf{p}'} & 1\end{pmatrix}\Bigg) ,\end{aligned} \tag{B.7}$$

where

$$\mathfrak{F}(\mathbf{q},\mathbf{p},\mathbf{p}';t) := \frac{m^2}{m_{\mathrm{P}}^2}\frac{1-\cos(|\mathbf{q}|t)}{2\pi^2|\mathbf{q}|^3}F^*_{\mathbf{k}_0}(\mathbf{p}')F_{\mathbf{k}_0}(\mathbf{p})F_{\mathbf{k}_0}(\mathbf{p}+\mathbf{q})F^*_{\mathbf{k}_0}(\mathbf{p}'+\mathbf{q}) . \tag{B.8}$$

The calculation of $\tilde{\rho}^{(3)}$ is straightforward from Eq. (B.5), giving

$$\tilde{\rho}^{(3)} = \begin{pmatrix} \alpha h_{AA}^2 + \beta h_{AA}h_{BA} + \beta^* h_{AA}h_{AB} + (1-\alpha)|h_{AB}|^2 & \alpha h_{AA}h_{AB} + \beta h_{AA}h_{BB} + \beta^*|h_{AB}|^2 + (1-\alpha)h_{AB}h_{BB} \\ \alpha h_{AA}h_{BA} + \beta^* h_{AA}h_{BB} + \beta|h_{AB}|^2 + (1-\alpha)h_{BA}h_{BB} & \alpha|h_{AB}|^2 + \beta h_{AB}h_{BB} + \beta^* h_{BA}h_{BB} + (1-\alpha)h_{BB}^2 \end{pmatrix} . \tag{B.9}$$

The matrix $\rho^{(4)}$ from Eq. (B.3d) is now studied. By defining the following two

$$g_{\mathrm{ij}\leftarrow} := \frac{m^2 M_\odot^2}{m_{\mathrm{P}}^4}\int d\mathbf{p}_1 d\mathbf{p}_2 d\mathbf{p}_3 F^*_{\mathbf{k}_0}(\mathbf{p}_1)F_{\mathbf{k}_0}(\mathbf{p}_2)e^{i\mathbf{x}_i\cdot\mathbf{p}_1 - i\mathbf{x}_j\cdot\mathbf{p}_2}c_{\odot\odot}(\mathbf{p}_3,\mathbf{p}_1,\mathbf{p}_2,\mathbf{p}_3;t) ; \tag{B.10a}$$

$$g_{\mathrm{ij}\rightarrow} := \frac{m^2 M_\odot^2}{m_{\mathrm{P}}^4}\int d\mathbf{p}_1 d\mathbf{p}_2 d\mathbf{p}_3 F^*_{\mathbf{k}_0}(\mathbf{p}_1)F_{\mathbf{k}_0}(\mathbf{p}_2)e^{i\mathbf{x}_i\cdot\mathbf{p}_1 - i\mathbf{x}_j\cdot\mathbf{p}_2}c^*_{\odot\odot}(\mathbf{p}_3,\mathbf{p}_2,\mathbf{p}_1,\mathbf{p}_3;t) , \tag{B.10b}$$

one has

$$\tilde{\rho}^{(4)} = -\begin{pmatrix} \alpha(g_{AA\leftarrow} + g_{AA\rightarrow}) + \beta g_{BA\rightarrow} + \beta^* g_{AB\leftarrow} & \alpha g_{AB\rightarrow} + \beta(g_{AA\leftarrow} + g_{BB\rightarrow}) + (1-\alpha)g_{AB\leftarrow} \\ \alpha g_{BA\leftarrow} + \beta^*(g_{AA\rightarrow} + g_{BB\leftarrow}) + (1-\alpha)g_{BA\rightarrow} & \beta g_{BA\leftarrow} + \beta^* g_{AB\rightarrow} + (1-\alpha)(g_{BB\leftarrow} + g_{BB\rightarrow}) \end{pmatrix} . \tag{B.11}$$

The calculation of $\rho^{(5)}$ from Eq. (B.3e), is more subtle and requires a deeper study than the previous contributions' computation.

First of all, $\hat{H}^{\Phi}_{2*} := -i\left(\hat{H}^{\Phi}_{2\rightarrow*} - \hat{H}^{\Phi}_{2\leftarrow*}\right)$ is defined. Then, by using the property $\hat{H}^{\Phi}_{2\rightarrow*} + \hat{H}^{\Phi}_{2\leftarrow*} = \hat{H}^{\Phi\,2}_{1*}$, Eq. (B.3e) can be rewritten as

$$\left(\tilde{\rho}^{(5)}\right)_{\mathrm{ij}}(t) := \frac{i}{2}\langle 1_{\mathrm{i}}0_{\mathrm{G}}|\left[\hat{H}^{\Phi}_{2*}(t), \hat{\rho}_{\mathrm{SE}}(0)\right]|1_{\mathrm{j}}0_{\mathrm{G}}\rangle - \frac{1}{2}\langle 1_{\mathrm{i}}0_{\mathrm{G}}|\left\{\hat{H}^{\Phi\,2}_{1*}(t), \hat{\rho}_{\mathrm{SE}}(0)\right\}|1_{\mathrm{j}}0_{\mathrm{G}}\rangle \tag{B.12}$$

The two terms at the r.h.s. of Eq. (B.12) are now called σ_1 and σ_2, for brevity. Moreover, following functions are defined

$$C^+(\mathbf{k},\mathbf{p};t) := \Re c_{-+}(\mathbf{k},\mathbf{p},\mathbf{p},\mathbf{k};t) = \frac{1}{4\pi^2|\mathbf{p}-\mathbf{k}|}\frac{1-\cos(t(|\mathbf{k}-\mathbf{p}| - \omega_{\mathbf{k}} + \omega_{\mathbf{p}}))}{(|\mathbf{k}-\mathbf{p}| - \omega_{\mathbf{k}} + \omega_{\mathbf{p}})^2} ; \tag{B.13a}$$

$$C^-(\mathbf{k},\mathbf{p};t) := \Im c_{-+}(\mathbf{k},\mathbf{p},\mathbf{p},\mathbf{k};t) = \frac{1}{4\pi^2|\mathbf{p}-\mathbf{k}|}\left(\frac{t}{|\mathbf{k}-\mathbf{p}| - \omega_{\mathbf{k}} + \omega_{\mathbf{p}}} + \frac{\sin(t(|\mathbf{k}-\mathbf{p}| - \omega_{\mathbf{k}} + \omega_{\mathbf{p}}))}{(|\mathbf{k}-\mathbf{p}| - \omega_{\mathbf{k}} + \omega_{\mathbf{p}})^2}\right) . \tag{B.13b}$$

The commutator between $\langle 0_G| H_{2*} |0_G\rangle$ and $|1_\pm\rangle\langle 1_\pm|$ trivially vanishes. Therefore, one can easily get

$$\sigma_1 = \begin{pmatrix} \Im(\beta f_1) & \frac{i}{2} f_1^*(1-2\alpha) \\ -\frac{i}{2} f_1^*(1-2\alpha) & -\Im(\beta f_1) \end{pmatrix}, \tag{B.14}$$

where

$$f_1 := \langle 1_{\mathrm{B}}| \langle 0_G| \hat{H}_{2*}(t) |0_G\rangle |1_{\mathrm{A}}\rangle = \frac{m^2}{m_{\mathrm{P}}^2} \int d\mathbf{k} d\mathbf{p} C^-(\mathbf{k},\mathbf{p},\mathbf{p},\mathbf{k};t) |F_{\mathbf{k_0}}(\mathbf{k})| e^{-i\mathbf{L}\cdot\mathbf{k}}. \tag{B.15}$$

Finally, for σ_2 one gets

$$\begin{aligned} \sigma_2 = -\frac{m^2}{m_{\mathrm{P}}} \int d\mathbf{k} d\mathbf{p} C^+(\mathbf{k},\mathbf{p},\mathbf{p},\mathbf{k};t) |F_{\mathbf{k}_0}(\mathbf{k})|^2 &\left(\alpha \begin{pmatrix} 2 & e^{i\mathbf{L}\cdot\mathbf{k}} \\ e^{-i\mathbf{L}\cdot\mathbf{k}} & 0 \end{pmatrix} + \beta \begin{pmatrix} e^{i\mathbf{L}\cdot\mathbf{k}} & 2 \\ 0 & e^{-i\mathbf{L}\cdot\mathbf{k}} \end{pmatrix} \right. \\ &\left. +\beta^* \begin{pmatrix} e^{-i\mathbf{L}\cdot\mathbf{k}} & 0 \\ 2 & e^{i\mathbf{L}\cdot\mathbf{k}} \end{pmatrix} + (1-\alpha) \begin{pmatrix} 0 & e^{i\mathbf{L}\cdot\mathbf{k}} \\ e^{-i\mathbf{L}\cdot\mathbf{k}} & 2 \end{pmatrix} \right). \end{aligned} \tag{B.16}$$

Notice that, since $\mathbf{k}$ is inside the argument of $F_{\mathbf{k_0}}$, in the functions C^+ and C^- (Eqs. (B.13a) and (B.13b)) one can approximate $\omega_{\mathbf{k}} \sim m$ for the argument presented below Eq. (4.170).

The matrices σ_1 and σ_2, from Eqs. (B.14) and (B.16) can be compared and analyzed to get a good approximation for $\rho^{(5)}$ in Eq. (B.12). To begin, the function C^+ in Eq. (B.13a) can be manipulated as

$$\begin{aligned} C^+(\mathbf{k},\mathbf{p};t) =& \frac{1-\cos(t(|\mathbf{p}|+\omega_{\mathbf{p}}-m))}{4\pi^2|\mathbf{p}|(|\mathbf{p}|+\omega_{\mathbf{p}}-m)^2} \\ &- \left(\frac{1-\cos(t(|\mathbf{p}|+\omega_{\mathbf{p}}-m))}{4\pi^2|\mathbf{p}|(|\mathbf{p}|+\omega_{\mathbf{p}}-m)^2} - \frac{1-\cos(t(|\mathbf{p}-\mathbf{k}|+\omega_{\mathbf{p}}-m))}{4\pi^2|\mathbf{p}-\mathbf{k}|(|\mathbf{p}-\mathbf{k}|+\omega_{\mathbf{p}}-m)^2} \right). \end{aligned} \tag{B.17}$$

The first term of Eq. (B.17) is called T_1 and the second one T_2. Therefore, by putting Eq. (B.17) in Eq. (B.16) one ends up with the sum of two integrals, i.e.

$$\begin{aligned} \sigma_2 =& -\frac{m^2}{m_{\mathrm{P}}^2} \int d\mathbf{k} d\mathbf{p} T_1(\mathbf{p}) |F_{\mathbf{k}_0}(\mathbf{k})|^2 \left[\alpha \begin{pmatrix} 2 & e^{2i\mathbf{L}\cdot\mathbf{k}} \\ e^{-2i\mathbf{L}\cdot\mathbf{k}} & 0 \end{pmatrix} + \beta \begin{pmatrix} e^{2i\mathbf{L}\cdot\mathbf{k}} & 2 \\ 0 & e^{-2i\mathbf{L}\cdot\mathbf{k}} \end{pmatrix} + \right. \\ &\left. +\beta^* \begin{pmatrix} e^{-2i\mathbf{L}\cdot\mathbf{k}} & 0 \\ 2 & e^{2i\mathbf{L}\cdot\mathbf{k}} \end{pmatrix} + (1-\alpha) \begin{pmatrix} 0 & e^{2i\mathbf{L}\cdot\mathbf{k}} \\ e^{-2i\mathbf{L}\cdot\mathbf{k}} & 2 \end{pmatrix} \right] \\ & -\frac{m^2}{m_{\mathrm{P}}^2} \int d\mathbf{k} d\mathbf{p} T_2(\mathbf{p},\mathbf{k}) |F_{\mathbf{k}_0}(\mathbf{k})|^2 \left[\alpha \begin{pmatrix} 2 & e^{2i\mathbf{L}\cdot\mathbf{k}} \\ e^{-2i\mathbf{L}\cdot\mathbf{k}} & 0 \end{pmatrix} + \beta \begin{pmatrix} e^{2i\mathbf{L}\cdot\mathbf{k}} & 2 \\ 0 & e^{-2i\mathbf{L}\cdot\mathbf{k}} \end{pmatrix} \right. \\ &\left. +\beta^* \begin{pmatrix} e^{-2i\mathbf{L}\cdot\mathbf{k}} & 0 \\ 2 & e^{2i\mathbf{L}\cdot\mathbf{k}} \end{pmatrix} + (1-\alpha) \begin{pmatrix} 0 & e^{2i\mathbf{L}\cdot\mathbf{k}} \\ e^{-2i\mathbf{L}\cdot\mathbf{k}} & 2 \end{pmatrix} \right]. \end{aligned} \tag{B.18}$$

Because of the orthonormality condition $\int d\mathbf{k}|F_{\mathbf{k_0}}|^2 = 1$ and $\int d\mathbf{k}|F_{\mathbf{k_0}}|^2 e^{2i\mathbf{L}\cdot\mathbf{k}} = 0$, since T_1 is independent on $\mathbf{k}$, the first integral of σ_2 at the r.h.s. of Eq. (B.18), called I_1, reduces to

$$I_1 = 2\rho_{\mathrm{S}}(0) \int d\mathbf{p} C^+(\mathbf{0},\mathbf{p};t) = 2\rho_{\mathrm{S}}(0) \int d\mathbf{p} \frac{1-\cos(t(|\mathbf{p}|+\omega_{\mathbf{p}}-m))}{4\pi^2|\mathbf{p}|(|\mathbf{p}|+\omega_{\mathbf{p}}-m)^2}. \tag{B.19}$$

Notice that the integral in Eq. (B.19) presents a logarithmic ultraviolet divergence when integrating in $d|\mathbf{p}|$. However, m_P is a natural ultraviolet cutoff for this divergence, so that one can consider $\int_0^\infty d|\mathbf{p}|(\dots) = \int_0^{m_P} d|\mathbf{p}|(\dots)$.

Regarding the second integral in Eq. (B.18), called I_2 from now on, one can safely integrate the variable $\mathbf{p}$ in $\mathbb{R}^3$ without divergences. In this way, also $\mathbf{p}' := \mathbf{p} - \mathbf{k}$ can be integrated in $\mathbf{R}^3$. Therefore, one can manipulate the integral as

$$\begin{aligned} I_2 &= -\int d\mathbf{p}d\mathbf{k}\left(\frac{1-\cos(t(|\mathbf{p}|+\omega_{\mathbf{p}}-m))}{4\pi^2|\mathbf{p}|(|\mathbf{p}|+\omega_{\mathbf{p}}-m)^2} - \frac{1-\cos(t(|\mathbf{p}-\mathbf{k}|+\omega_{\mathbf{p}}-m))}{4\pi^2|\mathbf{p}-\mathbf{k}|(|\mathbf{p}-\mathbf{k}|+\omega_{\mathbf{p}}-m)^2}\right)(\dots) \\ &= -\int d\mathbf{k}(\dots)\left(\int_{\mathbb{R}^3} d\mathbf{p}\frac{1-\cos(t(|\mathbf{p}|+\omega_{\mathbf{p}}-m))}{4\pi^2|\mathbf{p}|(|\mathbf{p}|+\omega_{\mathbf{p}}-m)^2} - \int_{\mathbb{R}^3} d\mathbf{p}'\frac{1-\cos(t(|\mathbf{p}'|+\omega_{\mathbf{p}'+\mathbf{k}}-m))}{4\pi^2|\mathbf{p}'|(|\mathbf{p}'|+\omega_{\mathbf{p}'+\mathbf{k}}-m)^2}\right). \end{aligned} \tag{B.20}$$

The difference between the two integrals in Eq. (B.20) gives a term of the order $|\mathbf{k}|^2/m^2$, which is clearly negligible since $\mathbf{k}$ is confined in a range with length $\sim k_0$, which must be much smaller than m to prevent the particle to travel in time. Therefore, one has

$$\sigma_2 = -\rho_{\mathrm{S}}(0)\frac{m^2}{m_{\mathrm{P}}}\int d\mathbf{p}\frac{1-\cos(t(|\mathbf{p}|+\omega_{\mathbf{p}}-m))}{2\pi^2|\mathbf{p}|(|\mathbf{p}|+\omega_{\mathbf{p}}-m)^2} + \mathcal{O}\left(\frac{k_0}{m}\right). \tag{B.21}$$

Conveniently, $\sigma_2 \sim -f_2\rho_{SE}(0)$, where

$$f_2 := \frac{m^2}{m_{\mathrm{P}}^2}\int d\mathbf{p}\frac{1-\cos(t(|\mathbf{p}|+\omega_{\mathbf{p}}-m))}{2\pi^2|\mathbf{p}|(|\mathbf{p}|+\omega_{\mathbf{p}}-m)^2} = \frac{2}{\pi}\frac{m^2}{m_{\mathrm{P}}^2}\int_0^\infty d|\mathbf{p}|\frac{|\mathbf{p}|}{(|\mathbf{p}|+\omega_{\mathbf{p}}-m)^2}(1-\cos(t(|\mathbf{p}|+\omega_{\mathrm{p}}-m))). \tag{B.22}$$

The integral in f_2 from Eq. (B.22) has an ultraviolet logarithmic divergence, which regularized with a cutoff Λ, so that[1]

$$f_2 \sim \frac{2}{\pi}\frac{m^2}{m_{\mathrm{P}}^2}\int_0^\Lambda d|\mathbf{p}|\frac{|\mathbf{p}|}{(|\mathbf{p}|+\omega_{\mathbf{p}}-m)^2}(1-\cos(t(|\mathbf{p}|+\omega_{\mathrm{p}}-m))). \tag{B.23}$$

By coming back to σ_1 from Eq. (B.14), f_1 is now attempted to be computed, which explicitly reads

$$f_1 = \frac{t}{2\pi^2}\frac{m^2}{m_{\mathrm{P}}^2}\int\frac{d\mathbf{k}d\mathbf{p}|F_{\mathbf{k}_0}(\mathbf{k})|^2e^{-i\mathbf{L}\cdot\mathbf{k}}}{|\mathbf{p}-\mathbf{k}|(|\mathbf{p}-\mathbf{k}|-m+\omega_{\mathbf{p}})} + \frac{m^2}{m_{\mathrm{P}}^2}\int d\mathbf{k}d\mathbf{p}\frac{\sin(t(|\mathbf{p}-\mathbf{k}|-m+\omega_{\mathbf{p}}))}{4\pi^2|\mathbf{p}-\mathbf{k}|(|\mathbf{p}-\mathbf{k}|-m+\omega_{\mathbf{p}})^2}|F_{\mathbf{k}_0}(\mathbf{k})|^2e^{-i\mathbf{L}\cdot\mathbf{k}}. \tag{B.24}$$

The second integral of Eq. (B.24) can be manipulated as done before for σ_2, giving as result an order of k_0/m, multiplied by a finite integral. Therefore, the second term of Eq. (B.18) can be neglected. By substituting $\mathbf{p}' = \mathbf{p} - \mathbf{k}$ and by integrating over the solid angle between $\mathbf{p}'$ and $\mathbf{k}$, one has

$$f_1 \sim \frac{t}{\pi}\frac{m^2}{m_{\mathrm{P}}^2}\int d\mathbf{k}|F_{\mathbf{k}_0}(\mathbf{k})|^2e^{-i\mathbf{L}\cdot\mathbf{k}}g(m,|\mathbf{k}|) \tag{B.25}$$

where

$$g(m,|\mathbf{k}|) := \frac{1}{|\mathbf{k}|}\int_0^\infty d|\mathbf{p}'|\left(\sqrt{m^2+(|\mathbf{p}'|+|\mathbf{k}|)^2} - \sqrt{m^2+(|\mathbf{p}'|-|\mathbf{k}|)^2}\right. \tag{B.26}$$

$$\left. -(|\mathbf{p}'|-m)\ln\left(\frac{|\mathbf{p}'|-m+\sqrt{m^2+(|\mathbf{p}'|+|\mathbf{k}|)^2}}{|\mathbf{p}'|-m+\sqrt{m^2+(|\mathbf{p}'|-|\mathbf{k}|)^2}}\right)\right). \tag{B.27}$$

By expanding $g(m,|\mathbf{k}|)$ as $|\mathbf{k}|/m \ll 1$, since $\mathbf{k}$ is confined to the support of $F_{\mathbf{k}_0}$, one obtains

$$g(m,|\mathbf{k}|) = 2\int_0^\infty\frac{|\mathbf{p}'|}{\sqrt{|\mathbf{p}'|^2+m^2}+|\mathbf{p}'|-m} + \mathcal{O}\left(\frac{k_0^2}{m^2}\right). \tag{B.28}$$

[1] Since linearized quantum gravity is an effective field theory valid at energies $\ll m_{\mathrm{P}}$, Λ is naturally defined to be at the order of m_{P}.

The first integral in Eq. (B.28) has an ultraviolet divergence, which can be regularized, as done before, by considering a cutoff Λ for the momentum of the graviton. In this way, since the first term of Eq. (B.28) is independent from $\mathbf{k}$, and since $\int d\mathbf{k}|F_{\mathbf{k}_0}(\mathbf{k})|^2 e^{-i\mathbf{L}\cdot\mathbf{k}}$ is identically zero, then Eq. (B.27) becomes

$$f_1 = \mathcal{O}\left(\frac{k_0^2}{m^2}\right) . \tag{B.29}$$

Therefore, one can safely consider σ_1 to be negligible w.r.t. σ_2. By doing that, finally

$$\tilde{\rho}^{(5)} \sim -\frac{2}{\pi}\frac{m^2}{m_{\mathrm{P}}^2}\rho_{\mathrm{S}}(0)\int_0^{\Lambda} d|\mathbf{p}|\frac{|\mathbf{p}|}{(|\mathbf{p}|+\omega_{\mathbf{p}}-m)^2}(1-\cos(t(|\mathbf{p}|+\omega_{\mathrm{p}}-m))) . \tag{B.30}$$

B.1 Gaussian momentum distribution

The following Gaussian form for $F_{\mathbf{k}_0}$ is imposed to obtain analytic solutions, i.e.

$$F_{\mathbf{k}_0}(\mathbf{p}) := \frac{e^{-\frac{|\mathbf{p}|^2}{4k_0^2}}}{(2\pi k_0^2)^{3/4}} . \tag{B.31}$$

Moreover, the radius of the planet is put to zero, so that $\Gamma_{\mathbf{p}}(R) = \frac{1}{3\sqrt{|\mathbf{p}|}}$.

In this way, the elements h_{ij} from Eq. (B.5) are explicitly computed. By starting with the diagonal elements, the two terms at the r.h.s. of Eq. (B.5) are computed separately. For the first, called $h_{\mathrm{ii}}^{(1)}$, one has

$$h_{\mathrm{ii}}^{(1)} = \frac{mM_{\odot}}{m_{\mathrm{P}}^2}\frac{t}{2\pi}\int\frac{d\mathbf{p}d\mathbf{p}'}{|\mathbf{p}-\mathbf{p}'|^2}\frac{e^{-\frac{|\mathbf{p}|^2+|\mathbf{p}'|^2}{4k_0^2}}}{(2\pi k_0^2)^{3/2}}e^{i\mathbf{x}_{\mathrm{i}}\cdot(\mathbf{p}'-\mathbf{p})} . \tag{B.32}$$

By performing a change of variables, i.e. from $\mathbf{p}'$ to $\mathbf{p}_1 = \mathbf{p}' - \mathbf{p}$, one has

$$\begin{aligned}
h_{\mathrm{ii}}^{(1)} &= \frac{mM_{\odot}t}{2\pi m_{\mathrm{P}}^2}\int \mathrm{d}\mathbf{p}_1\frac{e^{-\frac{|\mathbf{p}_1|^2}{4k_0^2}}}{|\mathbf{p}_1|^2}e^{i\mathbf{x}_{\mathrm{i}}\cdot\mathbf{p}_1}\int d\mathbf{p}\frac{e^{-\frac{|\mathbf{p}|^2}{2k_0^2}-\frac{-\mathbf{p}\cdot\mathbf{p}_1}{2k_0^2}}}{(2\pi k_0^2)^{3/2}} = \frac{mM_{\odot}t}{2\pi m_{\mathrm{P}}^2}\int d\mathbf{p}_1\frac{e^{-\frac{|\mathbf{p}_1|^2}{8k_0^2}+i\mathbf{x}_A\cdot\mathbf{p}_1}}{|\mathbf{p}_1|^2} \\
&= 2\frac{mM_{\odot}}{m_{\mathrm{P}}^2}t\int_0^{\infty} d|\mathbf{p}_1|e^{-\frac{|\mathbf{p}_1|^2}{8k_0^2}}\int_{-1}^{+1} d\cos\theta e^{i|\mathbf{x}_{\mathrm{i}}||\mathbf{p}_1|\cos\theta} = 2\frac{mM_{\odot}}{m_{\mathrm{P}}^2}\frac{t}{|\mathbf{x}_{\mathrm{i}}|}\int_0^{\infty} d|\mathbf{p}_1|\frac{e^{-\frac{|\mathbf{p}_1|^2}{8k_0^2}}\sin(|\mathbf{x}_{\mathrm{i}}||\mathbf{p}_1|)}{|\mathbf{p}_1|} \\
&= 2\frac{mM_{\odot}}{m_{\mathrm{P}}^2}\frac{t}{|\mathbf{x}_{\mathrm{i}}|}\int_0^{|\mathbf{x}_{\mathrm{i}}|} dy\int_0^{\infty} d|\mathbf{p}_1|e^{-\frac{|\mathbf{p}_1|^2}{8k_0^2}}\cos(y|\mathbf{p}_1|) = \frac{mM_{\odot}}{m_{\mathrm{P}}^2}\frac{t}{|\mathbf{x}_{\mathrm{i}}|}\int_0^{|\mathbf{x}_{\mathrm{i}}|} dy\int_{-\infty}^{+\infty} d|\mathbf{p}_1|e^{-\frac{|\mathbf{p}_1|^2}{8k_0^2}}\cos(y|\mathbf{p}_1|) \\
&= \frac{mM_{\odot}}{m_{\mathrm{P}}^2}\frac{t}{|\mathbf{x}_{\mathrm{i}}|}\sqrt{8\pi}k_0\int_0^{|\mathbf{x}_{\mathrm{i}}|} dy e^{-2k_0^2y^2} = \pi\frac{mM_{\odot}}{m_{\mathrm{P}}^2}\frac{t}{|\mathbf{x}_{\mathrm{i}}|}\mathrm{erf}\left(\sqrt{2}k_0|\mathbf{x}_{\mathrm{i}}|\right) .
\end{aligned} \tag{B.33}$$

For the second term at the r.h.s. of Eq. (B.5), by performing a similar calculation, one obtains

$$\begin{aligned}
h_{\mathrm{ii}}^{(2)} &:= -\frac{mM_{\odot}}{2\pi m_{\mathrm{P}}^2}\int \mathrm{d}\mathbf{p}\mathrm{d}\mathbf{p}'\frac{\sin(t|\mathbf{p}-\mathbf{p}'|)}{|\mathbf{p}-\mathbf{p}'|^3}\frac{e^{-\frac{|\mathbf{p}|^2}{4k_0^2}-\frac{|\mathbf{p}'|^2}{4k_0^2}-i\mathbf{x}_{\mathrm{i}}\cdot(\mathbf{p}-\mathbf{p}')}}{(2\pi k_0^2)^{3/2}} \\
&= -2\frac{mM_{\odot}}{m_{\mathrm{P}}^2}\int_0^{\infty} \mathrm{d}|\mathbf{p}_1|\frac{\sin(|\mathbf{p}_1|t)\sin(|\mathbf{p}_1||\mathbf{x}_{\mathrm{i}}|)}{|\mathbf{p}_1|^2|\mathbf{x}_{\mathrm{i}}|}e^{-\frac{|\mathbf{p}_1|^2}{8k_0^2}} \\
&= -\frac{mM_{\odot}}{m_{\mathrm{P}}^2}\int_0^t \mathrm{d}t'\int_0^{|\mathbf{x}_{\mathrm{i}}|} dy\int_{-\infty}^{+\infty}\cos(|\mathbf{p}_1|t')\cos(|\mathbf{p}_1|y)e^{-\frac{|\mathbf{p}_1|^2}{8k_0^2}} \\
&= -\frac{\pi}{2}\frac{mM_{\odot}|\mathbf{x}_{\mathrm{i}}|}{m_{\mathrm{P}}^2}\int_0^t dt'\left(\mathrm{erf}(\sqrt{2}k_0t'+\sqrt{2}k_0|\mathbf{x}_{\mathrm{i}}|)-\mathrm{erf}(\sqrt{2}k_0t'-\sqrt{2}k_0|\mathbf{x}_{\mathrm{i}}|)\right) .
\end{aligned} \tag{B.34}$$

One can simplify Eqs. (B.33) and (B.34) by using the fact that $k_0|\mathbf{x}_\mathrm{i}| \gg 1$ and $\mathrm{erf}(x \to \pm\infty) \sim \pm 1 - \mathcal{O}(e^{-x^2})$. Then,

$$\begin{aligned} h_\mathrm{ii} &\sim \frac{\pi}{2}\frac{mM_\odot}{m_\mathrm{P}^2}\frac{1}{|\mathbf{x}_i|}\left(t - \int_0^t dt' \mathrm{erf}(\sqrt{2}k_0(|\mathbf{x}_i| - t'))\right) \\ &= \frac{\pi}{2}\frac{mM_\odot}{m_\mathrm{P}^2}\frac{t-|\mathbf{x}_i|}{|\mathbf{x}_i|}\left(1 - \mathrm{erf}(\sqrt{2}k_0(|\mathbf{x}_\mathrm{i}| - t))\right) - \frac{\pi}{2}\frac{mM_\odot}{m_\mathrm{P}^2}\frac{e^{-2k_0^2(|\mathbf{x}_i|-t)^2)}}{\sqrt{2\pi}k_0|\mathbf{x}_\mathrm{i}|}\,. \end{aligned} \tag{B.35}$$

By performing a similar calculation, h_AB becomes

$$h_\mathrm{AB} \sim \pi\frac{mM_\odot}{m_\mathrm{P}^2}\frac{t}{\left|\mathbf{x}_\mathrm{A} + \frac{\mathbf{L}}{2}\right|}e^{-\frac{k_0^2|\mathbf{L}|^2}{2}}\mathrm{erf}\left(\sqrt{2}k_0\left|\mathbf{x}_\mathrm{A} + \frac{\mathbf{L}}{2}\right|\right)\,, \tag{B.36}$$

which can be considered negligible since $|\mathbf{L}|k_0 \gg 1$.

By studying the behaviour of h_ii from Eq. (B.35), for $t \ll |\mathbf{x}_\mathrm{i}$, $h_\mathrm{ii} = \mathcal{O}\left(e^{-2k_0^2(|\mathbf{x}_\mathrm{i}|-t)^2}\right)$ which is effectively zero. On the contrary, for $t \gg |\mathbf{x}_\mathrm{i}|$, one has

$$h_\mathrm{ii} \sim \pi\frac{mM_\odot}{m_\mathrm{P}^2}\frac{t}{|\mathbf{x}_i|} = \pi E_\odot(\mathbf{x}_i)t\,, \tag{B.37}$$

where $E_\odot(\mathbf{x}_i) := \frac{GmM_\odot}{|\mathbf{x}_i|}$ is the Newton's gravitational potential energy. Therefore, h_ii/t is Newton's gravitational energy that switches in when $t = |\mathbf{x}_i|$, i.e. when the gravitons driven by the planet reach the quantum state. Therefore, one can effectively write

$$h_\mathrm{ii} = \theta(t - |\mathbf{x}_i|)\pi\frac{mM_\odot}{m_\mathrm{P}^2}\frac{t}{|\mathbf{x}_i|}\,, \tag{B.38}$$

where $k_0 \neq 0$ has the only effect to smooth the step function θ in time, with no other quantitative effects - except for a small "bump" occurring at $t \sim |\mathbf{x}_i|$ given by the second term of Eq. (B.35).

The expression (B.38) for h_ii and the fact that $h_{\mathrm{i}\neq\mathrm{j}} \sim 0$ provides an effective expression for $\tilde{\rho}^{(1)}$ and $\tilde{\rho}^{(3)}$ from Eqs. (B.6) and (B.9), respectively. In particular, the only first order contribute, given by the presence of the planet, is

$$\tilde{\rho}^{(1)} \sim \begin{pmatrix} 0 & -i\pi\beta(\theta(t-|\mathbf{x}_\mathrm{A}|)E_\odot(\mathbf{x}_\mathrm{A}) - \theta(t-|\mathbf{x}_\mathrm{B}|)E_\odot(\mathbf{x}_\mathrm{B}))t \\ i\pi\beta^*(\theta(t-|\mathbf{x}_\mathrm{A}|)E_\odot(\mathbf{x}_\mathrm{A}) - \theta(t-|\mathbf{x}_\mathrm{B}|)E_\odot(\mathbf{x}_\mathrm{B}))t & 0 \end{pmatrix} \tag{B.39}$$

To study the second order contribute given by the planet, the matrix $\tilde{\rho}^{(4)}$ from Eq. (B.11) has to be studied as well. In particular, expressions for $g_{\mathrm{ij}\leftrightarrow}$ with i,j = A,B have to be found from Eqs. (B.10a) and (B.10b). In the calculation of h_ii, by starting from Eq. (B.5), the only net contribute was given by the first term of h_ii, i.e. the non-oscillating function (B.33). The oscillating part of h_ii, i.e. Eq. (B.34), gives instead the switching-in of the term when t reaches $|\mathbf{x}_i|$. One can prove that the same occurs for the functions $g_{\mathrm{ij}\leftrightarrow}$, so that only the non-oscillating terms of the function $c_{\odot\odot}(\mathbf{p}_3, \mathbf{p}_1, \mathbf{p}_2, \mathbf{p}_3)$ can be considered, keeping in mind that a switching-in $\theta(t - |\mathbf{x}_i|)$ occurs.

Since $tk_0 \gg 1$ is employed, only the non-oscillating terms of are expected to give a net contribute to the g functions. Therefore, one has

$$c_{\odot\odot}(\mathbf{p}_3, \mathbf{p}_1, \mathbf{p}_2, \mathbf{p}_3) \sim \frac{m^2M_\odot^2}{8\pi^2 m_\mathrm{P}^4}\frac{t^2}{|\mathbf{p}_1 - \mathbf{p}_3|^2|\mathbf{p}_2 - \mathbf{p}_3|^2}\,. \tag{B.40}$$

Therefore, in this case, one has

$$g_\mathrm{ii} := g_{\mathrm{ii}\rightarrow} = g_{\mathrm{ii}\leftarrow} \sim \theta(t - |\mathbf{x}_\mathrm{i}|)\frac{m^2M_\odot^2}{8\pi^2 m_\mathrm{P}^4}t^2\int\frac{d\mathbf{p}_1 d\mathbf{p}_2 d\mathbf{p}_3}{|\mathbf{p}_1 - \mathbf{p}_3|^2|\mathbf{p}_2 - \mathbf{p}_3|^2}F_{\mathbf{k}_0}(\mathbf{p}_1)F_{\mathbf{k}_0}(\mathbf{p}_2)e^{i\mathbf{x}_\mathrm{i}\cdot(\mathbf{p}_1 - \mathbf{p}_2)}\,. \tag{B.41}$$

First of all, the integral in d$\mathbf{p}_3$ is analytically computed, namely

$$\int \frac{d\mathbf{p}_3}{|\mathbf{p}_1-\mathbf{p}_3|^2|\mathbf{p}_2-\mathbf{p}_3|^2} = \frac{\pi^3}{|\mathbf{p}_1-\mathbf{p}_2|}\,. \tag{B.42}$$

By considering the Gaussian functions for $F_{\mathbf{k}_0}$ and performing similar calculations as done for h_{ii}, one has

$$\begin{aligned}
g_{ii} &= \theta(t-|\mathbf{x}_\mathrm{i}|)\frac{m^2M_\odot^2}{8m_\mathrm{P}^4}\pi t^2\int \mathrm{d}\mathbf{p}\frac{e^{-\frac{|\mathbf{p}|^2}{8k_0^2}+i\mathbf{x}_\mathrm{i}\cdot\mathbf{p}}}{|\mathbf{p}|}\\
&= \theta(t-|\mathbf{x}_\mathrm{i}|)\frac{m^2M_\odot^2}{4m_\mathrm{P}^4}\pi^2 t^2\int_0^\infty \mathrm{d}|\mathbf{p}||\mathbf{p}|e^{-\frac{|\mathbf{p}|^2}{8k_0^2}}\int_{-1}^{+1}\mathrm{d}\cos\theta e^{i|\mathbf{x}_\mathrm{i}||\mathbf{p}|\cos\theta}\\
&= \theta(t-|\mathbf{x}_\mathrm{i}|)\frac{m^2M_\odot^2}{2m_\mathrm{P}^4}\pi^2 \frac{t^2}{|\mathbf{x}_\mathrm{i}|}\int_0^\infty \mathrm{d}|\mathbf{p}|e^{-\frac{|\mathbf{p}|^2}{8k_0^2}}\sin(|\mathbf{x}_i||\mathbf{p}|)\\
&= \theta(t-|\mathbf{x}_\mathrm{i}|)\frac{m^2M_\odot^2}{4m_\mathrm{P}^4}\pi^2 \frac{t^2}{|\mathbf{x}_\mathrm{i}|}\sqrt{8\pi}k_0 e^{-2|\mathbf{x}_\mathrm{i}|^2k_0^2}\mathrm{erfi}\left(\sqrt{2}k_0|\mathbf{x}_\mathrm{i}|\right)\,.
\end{aligned} \tag{B.43}$$

One can easily prove that $g_{\mathrm{AB}\rightarrow}$ and $g_{\mathrm{AB}\leftarrow}$ are smaller than g_{AA} and g_{BB} by a factor $e^{-k_0|\mathbf{L}|}$, so that they can be considered negligible as well.

The second order contribute given by the presence of the planet is then

$$\tilde{\rho}^{(3)}+\tilde{\rho}^{(4)} \sim \begin{pmatrix} \alpha(h_{\mathrm{AA}}^2-2g_{\mathrm{AA}}) & \beta(h_{\mathrm{AA}}h_{\mathrm{BB}}-g_{\mathrm{AA}}-g_{\mathrm{BB}}) \\ \beta^*(h_{\mathrm{AA}}h_{\mathrm{BB}}-g_{\mathrm{AA}}-g_{\mathrm{BB}}) & (1-\alpha)h_{\mathrm{BB}}^2-2g_{\mathrm{BB}} \end{pmatrix}\,. \tag{B.44}$$

For large arguments, the function erfi(x) approximates as

$$\mathrm{erfi}(x) \sim \frac{e^{x^2}}{\sqrt{\pi}}\left(\frac{1}{x}+\frac{1}{2x^3}+\mathcal{O}(x^{-5})\right)\,. \tag{B.45}$$

In this way,

$$h_{\mathrm{ii}}^2-2g_{\mathrm{ii}} = -\theta(t-|\mathbf{x}_\mathrm{i}|)\frac{\pi^2}{2}\frac{m^2M_\odot^2}{m_\mathrm{P}^4}\frac{t^2}{k_0^2|\mathbf{x}_\mathrm{i}|^4}\,; \tag{B.46}$$

$$\begin{aligned}
&h_{\mathrm{AA}}h_{\mathrm{BB}}-g_{\mathrm{AA}}-g_{\mathrm{BB}} = -\frac{\pi^2}{2}\frac{m^2M_\odot^2}{m_\mathrm{P}^4}t^2\left(\frac{\theta(t-|\mathbf{x}_\mathrm{A}|)}{|\mathbf{x}_\mathrm{A}|}-\frac{\theta(t-|\mathbf{x}_\mathrm{B}|)}{|\mathbf{x}_\mathrm{B}|}\right)^2\\
&-\frac{\pi^2}{4}\frac{m^2M_\odot^2t^2}{m_\mathrm{P}^4k_0^2}\left(\frac{\theta(t-|\mathbf{x}_\mathrm{A}|)}{|\mathbf{x}_\mathrm{A}|^4}+\frac{\theta(t-|\mathbf{x}_\mathrm{B}|)}{|\mathbf{x}_\mathrm{B}|^4}\right)\\
&= -\frac{\pi^2}{2}(\theta(t-|\mathbf{x}_A|)E_\odot(\mathbf{x}_A)-\theta(t-|\mathbf{x}_B|)E_\odot(\mathbf{x}_B))^2-\frac{\pi^2}{4}\frac{m^2M_\odot^2t^2}{m_\mathrm{P}^4k_0^2}\left(\frac{\theta(t-|\mathbf{x}_\mathrm{A}|)}{|\mathbf{x}_\mathrm{A}|^4}+\frac{\theta(t-|\mathbf{x}_\mathrm{B}|)}{|\mathbf{x}_\mathrm{B}|^4}\right)\,.
\end{aligned} \tag{B.47}$$

Let us now study the contributes $\tilde{\rho}^{(2)}$ and $\tilde{\rho}^{(5)}$ coming from the interaction with the gravitons and present independently from the planet.

The matrix $\tilde{\rho}^{(5)}$ follows Eq. (B.30) and it is independent from the wave packet shape. Regarding $\tilde{\rho}^{(2)}$, one can compute it from Eq. (B.7). It is easy to check that

$$F_{\mathbf{k}_0}(\mathbf{p})e^{i\mathbf{p}\cdot\mathbf{L}} \propto e^{-|\mathbf{L}|^2k_0^2}\,. \tag{B.48}$$

Therefore, since $k_0|\mathbf{L}| \gg 1$, only few terms survive in Eq. (B.7). This leads to the following simplified expression

$$\tilde{\rho}^{(2)} \sim \frac{m^2}{m_{\mathrm{P}}} \int \mathrm{d}\mathbf{q}\mathrm{d}\mathbf{p}\mathrm{d}\mathbf{p}' \frac{1-\cos(|\mathbf{q}|t)}{2\pi^2|\mathbf{q}|^3} F^*_{\mathbf{k}_0}(\mathbf{p}')F_{\mathbf{k}_0}(\mathbf{p})F^*_{\mathbf{k}_0}(\mathbf{p}'+\mathbf{q})F_{\mathbf{k}_0}(\mathbf{p}+\mathbf{q}) \begin{pmatrix} \alpha & \beta e^{-i\mathbf{L}\cdot\mathbf{q}} \\ \beta^* e^{i\mathbf{L}\cdot\mathbf{q}} & 1-\alpha \end{pmatrix} . \tag{B.49}$$

By using Gaussian momentum distribution (B.31), the element $\left(\tilde{\rho}^{(2)}\right)_{\mathrm{AA}}$, can be written as

$$\begin{aligned} \left(\tilde{\rho}^{(2)}\right)_{\mathrm{AA}} &\sim \frac{m^2}{m_{\mathrm{P}}^2} \frac{\alpha}{(2\pi k_0^2)^3} \int \mathrm{d}\mathbf{q}\mathrm{d}\mathbf{p}\mathrm{d}\mathbf{p}' \frac{1-\cos(|\mathbf{q}|t)}{2\pi^2|\mathbf{q}|^3} \exp\left(-\frac{|\mathbf{p}|^2+|\mathbf{p}'|^2+|\mathbf{p}+\mathbf{q}|^2+|\mathbf{p}'+\mathbf{q}|^2}{4k_0^2}\right) \\ &= \alpha\frac{m^2}{m_P^2}\frac{4}{\pi}\int_0^\infty \mathrm{d}|\mathbf{q}| \frac{1-\cos(|\mathbf{q}|t)}{|\mathbf{q}|} e^{-\frac{|\mathbf{q}|^2}{4k_0^2}} = \frac{8}{\pi}\int_0^{tk_0} d\tilde{t} D_+(\tilde{t}) , \end{aligned} \tag{B.50}$$

where $D_+(x) := e^{-x^2}\int_0^x dx' e^{x'^2}$ is called Dawson function. The integral of the Dawson function increases logarithmically for large arguments. In particular, for large x, one gets

$$\int_0^x dx' D_+(x') \sim 0.4896 + \frac{1}{2}\ln(tk_0) . \tag{B.51}$$

Therefore, if $k_0 t \gg 1$, then

$$\left(\tilde{\rho}^{(2)}\right)_{\mathrm{AA}} = \alpha\left(\frac{4}{\pi}\ln(tk_0) + 1.2468\right) . \tag{B.52}$$

An analog thing occurs for $\left(\tilde{\rho}^{(2)}\right)_{\mathrm{BB}}$ by using $1-\alpha$ instead of α. From a similar calculation, the off-diagonal elements of $\tilde{\rho}^{(2)}$ read

$$\left(\tilde{\rho}^{(2)}\right)_{\mathrm{AB}} = \frac{2\beta}{\pi|\mathbf{L}|k_0}\int_0^{|\mathbf{L}|k_0} d\tilde{L} \int_0^{tk_0} d\tilde{t}(D_+(\tilde{L}+\tilde{t}) - D_+(\tilde{L}-\tilde{t})) . \tag{B.53}$$

From Eq. (B.30), $\tilde{\rho}^{(5)}$ is independent from the shape of the wave packet. Therefore, one can define $\tilde{p} := |\mathbf{p}| + \sqrt{|\mathbf{p}| + m^2} - m$ to have

$$\tilde{\rho}^{(5)}(t) = -\frac{m^2}{2\pi m_{\mathrm{P}}}\tilde{\rho}(0)\int_0^{\tilde{\Lambda}} \frac{1-\cos(t\tilde{p})}{\tilde{p}}\left(1+\frac{2m^2}{(\tilde{p}+m)^2}\right)\frac{\tilde{p}+2m}{\tilde{p}+m} d\tilde{p} , \tag{B.54}$$

where $\Lambda' := \Lambda - m + \sqrt{\Lambda^2+m^2}$. Notice that the integrand in Eq. (B.54) is zero for $\tilde{p}\to 0$. By increasing $\tilde{\mathbf{p}}$, this integrand oscillates from 0 to an amplitude increasing logarithmically for $\tilde{p}\to\infty$. From this fact, by considering the ultraviolet cutoff Λ to be many orders higher than m, then

$$\tilde{\rho}^{(5)}(t) \sim -\frac{m^2}{2\pi m_{\mathrm{P}}}\tilde{\rho}(0)\int_0^{\tilde{\Lambda}} \frac{1-\cos(t\tilde{p})}{\tilde{p}} d\tilde{p} = -\frac{m^2}{2\pi m_{\mathrm{P}}}\tilde{\rho}(0)\left(\gamma + \ln(2\Lambda t) - \mathrm{Ci}(2\Lambda t)\right) , \tag{B.55}$$

where $\gamma \simeq 0.57721$ is the Euler-Mascheroni constant and Ci the cosine integral function.

B.2 Lindbladian

All the ingredients to write the matrix $\tilde{\rho}(t)$ evolved to second order perturbation theory are provided. In particular, the diagonal elements are

$$\tilde{\rho}_{\mathrm{ii}}(t) = \tilde{\rho}_{\mathrm{ii}}(0)\left[1 - \frac{m^2}{m_{\mathrm{P}}^2}\frac{8}{\pi}\int_0^t dt'\left(\frac{1-\cos(2\Lambda t')}{16\pi t'} - k_0 D_+(t'k_0)\right) - \theta(t-|\mathbf{x}_i|)\frac{\pi^2 m^2 M^2}{2m_{\mathrm{p}}^2}\frac{t^2}{k_0^2|\mathbf{x}_i|^4}\right] . \tag{B.56}$$

Instead, the off-diagonal ones are

$$\tilde{\rho}_{\mathrm{AB}}(t) = \tilde{\rho}_{\mathrm{AB}}(0)\left(1 - i\pi t\Theta(t) - t^2\frac{\pi^2}{2}\Theta^2(t)\right)$$
$$+\,\tilde{\rho}_{\mathrm{AB}}(0)\left[\frac{m^2}{m_{\mathrm{P}}^2}\frac{2}{\pi}\int_0^t dt'\left(\frac{k_0}{|\mathbf{L}|}\int_0^{|\mathbf{L}|} dL'\left(|D_+((L'+t')k_0) - D_+((L'-t')k_0)\right) - \frac{1-\cos(2\Lambda t')}{4\pi t'}\right)\right.$$
$$\left. - \frac{\pi^2}{4}\frac{m^2 M_\odot^2 t^2}{m_{\mathrm{P}}^4 k_0^2}\left(\frac{\theta(t-|\mathbf{x}_{\mathrm{A}}|)}{|\mathbf{x}_{\mathrm{A}}|^4} + \frac{\theta(t-|\mathbf{x}_{\mathrm{B}}|)}{|\mathbf{x}_{\mathrm{B}}|^4}\right)\right] \tag{B.57}$$

The first bracket on the r.h.s. of Eq. (B.57) can be recast as the exponential $\exp\left(-i\pi t\Theta(t)\right)$, where $\Theta(t) := \theta(t-|\mathbf{x}_{\mathrm{A}}|)E_\odot(\mathbf{x}_{\mathrm{A}}) + \theta(t-|\mathbf{x}_{\mathrm{B}}|)E_\odot(\mathbf{x}_{\mathrm{B}})$ expanded to second order for m/m_{P}. This exponential is the same one occurring from a unitary time-evolution of a two-level density matrix when there is an energy gap between these two levels.

Therefore, it is intuitive to associate the evolution expressed by the first line in Eq. (B.57) to a unitary evolution and all the other terms as a non-unitary evolution. To verify this assumption, the following effective Hamiltonian $\hat{H}_{\mathrm{eff}}^{\mathrm{SE}}$, acting on the system and on the environment, is ansatzed as

$$\hat{H}_{\mathrm{eff}}^{\mathrm{SE}}\left|1_{\mathrm{i=A,B}}\right\rangle = \pi E_\odot(\mathbf{x}_{\mathrm{i}})\left|1_{\mathrm{i=A,B}}\right\rangle \;;\quad \hat{H}_{\mathrm{eff}}^{\mathrm{SE}}\left|e\right\rangle = E_e\left|e\right\rangle \,. \tag{B.58}$$

For our purposes, the value of E_e is irrelevant. If the ansatz is correct, then the state should evolve, at least perturbatively, according to the Lindblad equation

$$\frac{d\hat{\rho}_{\mathrm{SE}}}{dt} = -i\left[\hat{H}_{\mathrm{eff}}^{\mathrm{SE}}, \hat{\rho}_{\mathrm{SE}}(t)\right] + \mathcal{L}_t\left[\hat{\rho}_{\mathrm{SE}}(t)\right] \,, \tag{B.59}$$

where the Lindbladian $\mathcal{L}_t$ must have the form

$$\mathcal{L}_t\left[\hat{\rho}\right] = \sum_k \lambda_k\left(\hat{L}_k\hat{\rho}\hat{L}_k^\dagger - \frac{1}{2}\left\{\hat{L}_k^\dagger\hat{L}_k, \hat{\rho}\right\}\right) \,. \tag{B.60}$$

In other words, to prove that our guess that the unitary part is given by $\hat{H}_{\mathrm{eff}}^{\mathrm{SE}}(t)$ is correct, the existence of the operators $\hat{L}_k$ have to be proved.

It is now convenient to write

$$\hat{\rho}_{\mathrm{S}}(t) = \sum_{\mathrm{ij}}\tilde{\rho}_{\mathrm{ij}}(t)\left|i\right\rangle\left\langle j\right| + p_e(t)\left|e\right\rangle\left\langle e\right| \,. \tag{B.61}$$

In so doing, Eq. (B.61) is put into Eq. (B.59) to obtain

$$\mathcal{L}_t[\hat{\rho}_{\mathrm{S}}] = \sum_{\mathrm{ij}}\dot{\tilde{\rho}}_{\mathrm{ij}}\left|1_{\mathrm{i}}\right\rangle\left\langle 1_{\mathrm{j}}\right| + \dot{p}_e(t)\left|e\right\rangle\left\langle e\right| + i\pi\Theta(t)(\tilde{\rho}_{\mathrm{AB}}\left|1_{\mathrm{A}}\right\rangle\left\langle 1_{\mathrm{B}}\right| - \tilde{\rho}_{\mathrm{BA}}\left|1_{\mathrm{B}}\right\rangle\left\langle 1_{\mathrm{A}}\right|) \,. \tag{B.62}$$

Notice that, from trace conservation, $\dot{p}_e = -\dot{\tilde{\rho}}_{\mathrm{AA}} - \dot{\tilde{\rho}}_{\mathrm{BB}}$ as well as $\rho_{\mathrm{AB}} = \rho_{\mathrm{BA}}$.

The following Lindblad operators are then chosen by ansatz

$$\hat{L}_{\mathrm{A}} = \left|e\right\rangle\left\langle 1_{\mathrm{A}}\right| \;;\quad \hat{L}_{\mathrm{B}} = \left|e\right\rangle\left\langle 1_{\mathrm{B}}\right| \;;\quad \hat{L}_\chi = \left|1_{\mathrm{A}}\right\rangle\left\langle 1_{\mathrm{A}}\right| - \left|1_{\mathrm{B}}\right\rangle\left\langle 1_{\mathrm{B}}\right| \,. \tag{B.63}$$

By putting Eq. (B.63) into Eq. (B.60) and by comparing it with Eq. (B.62), one ends up with the following equations for λ_{A}, λ_{B} and λ_χ, namely

$$\begin{cases} \dot{\tilde{\rho}}_{\mathrm{AA}} = -\lambda_{\mathrm{A}}\tilde{\rho}_{\mathrm{AA}} \,; \\ \dot{\tilde{\rho}}_{\mathrm{BB}} = -\lambda_{\mathrm{B}}\tilde{\rho}_{\mathrm{BB}} \,; \\ \dot{\tilde{\rho}}_{\mathrm{AB}} + i\pi\Theta(t) = -\left(2\lambda_\chi + \frac{\lambda_{\mathrm{A}}}{2} + \frac{\lambda_{\mathrm{B}}}{2}\right)\tilde{\rho}_{\mathrm{AB}} \,, \end{cases} \tag{B.64}$$

from which, by considering only the perturbative leading order, then

$$\lambda_{\mathrm{A}} = \frac{m^2}{m_{\mathrm{P}}^2}\left(\frac{1-\cos(2\Lambda t)}{2\pi t} - \frac{8k_0}{\pi}D_+(tk_0) + \theta(t-|\mathbf{x}_{\mathrm{A}}|)\frac{M^2}{m_{\mathrm{P}}^2}\frac{\pi^2 t}{k_0^2|\mathbf{x}_{\mathrm{A}}|^4}\right) . \tag{B.65a}$$

$$\lambda_{\mathrm{B}} = \frac{m^2}{m_{\mathrm{P}}^2}\left(\frac{1-\cos(2\Lambda t)}{2\pi t} - \frac{8k_0}{\pi}D_+(tk_0) + \theta(t-|\mathbf{x}_{\mathrm{B}}|)\frac{M^2}{m_{\mathrm{P}}^2}\frac{\pi^2 t}{k_0^2|\mathbf{x}_{\mathrm{B}}|^4}\right) ; \tag{B.65b}$$

$$\lambda_{\chi} = \frac{4k_0}{\pi}\frac{m^2}{m_{\mathrm{P}}^2}\left(D_+(tk_0) - \frac{1}{4|\mathbf{L}|}\int_0^{|\mathbf{L}|} dL'\left(D_+((L'+t)k_0) - D_+((L'-t)|k_0)\right)\right) . \tag{B.65c}$$

Therefore, the ansatz to associate the first line of Eq. (B.57) as given by a unitary transformation $U = \exp(-i\hat{H}_{\mathrm{eff}}t)$ - where $\hat{H}_{\mathrm{eff}}$ is given by Eq. (B.58) - turns out to be correct. In this way, one can compactly write Eqs. (B.56) and (B.57) as

$$\tilde{\rho}_{\mathrm{ii}}(t) = \tilde{\rho}_{\mathrm{ii}}(0)\left(1 - \int_0^t dt'\lambda_{\mathrm{i}}(t')\right) ; \tag{B.66a}$$

$$\tilde{\rho}_{\mathrm{AB}}(t) = \tilde{\rho}_{\mathrm{AB}}(0)e^{-i\pi t\Theta(t)}\left(1 - \int_0^t dt'\left(\frac{\lambda_{\mathrm{A}}(t')}{2} + \frac{\lambda_{\mathrm{B}}(t')}{2} + 2\lambda_{\chi}(t')\right)\right) . \tag{B.66b}$$

which is recasted to Eq. (4.179) by neglecting the complex exponential, giving just a unitary evolution.